

第15回呼吸機能イメージング研究会 第11回国際ワークショップ

合同開催

第15回呼吸機能イメージング研究会 第11回国際ワークショップ

Joint Meeting of JSPFI and IWPMFI 2024

The 15th meeting of the Japanese Society of Pulmonary Functional Imaging
The 11th International Workshop on Pulmonary Functional Imaging

呼吸機能イメージング：
現在と未来

Pulmonary functional imaging:
present and future

大会長
President

中野 恭幸 Yasutaka Nakano, MD, PhD.

滋賀医科大学 内科学講座 呼吸器内科 教授
Professor and Chairman, Division of Respiratory Medicine,
Department of Internal Medicine, Shiga University of Medical Science



2024.

8/23 (金) Fri. → 8/25 (日) Sun.

会場
Venue

大津市民会館
Otsu Civic Hall

〒520-0042 滋賀県大津市島の関14-1
14-1 Shimanoseki, Otsu City, Shiga Prefecture 520-0042 Japan



Abstract Book



神経内分泌腫瘍(NET)には
ソマトスタチン受容体
シンチグラフィを

放射性医薬品/神経内分泌腫瘍診断薬 処方箋医薬品[※] 薬価基準収載

オクトレオスキャン[®] 静注用セット

Octreoscan[®] Injection

インジウムペンテトレオチド (¹¹¹In) 注射液 調製用

[※]注意—医師等の処方箋により使用すること。

2. 禁忌(次の患者には投与しないこと)

本剤の成分に対し過敏症の既往歴のある患者

4. 効能又は効果
神経内分泌腫瘍の診断におけるソマトスタチン受容体シンチグラフィ
5. 効能又は効果に関連する注意
神経内分泌腫瘍(NET)であってもソマトスタチン受容体(SSTR)を発現していない場合は検出できないことに留意すること。また、インスリノーマについてはSSTRの発現が他のNETに比べて少ないため、本剤により検出できない場合があることに留意すること。[17.1.1, 17.1.2参照]
6. 用法及び用量
(インジウムペンテトレオチド(¹¹¹In)注射液の調製)
バイアルAの全量をバイアルBに加えて振り混ぜた後、常温で30分開放置する。
(ソマトスタチン受容体シンチグラフィ)
通常、成人には本品111MBqを静脈内投与し、4時間後及び24時間後にガンマカメラを用いてシンチグラムを得る。必要に応じて、48時間後にもシンチグラムを得る。投与量は、患者の状態により適宜増減する。
必要に応じて、断層像を追加する。
8. 重要な基本的注意
診断上の有益性が被曝による不利益を上回ると判断される場合にのみ投与することとし、投与量は最小限度にとどめること。
9. 特定の背景を有する患者に関する注意
- 9.2 腎機能障害患者
本剤は主に尿中に排泄されるため、被曝線量が増加する可能性がある。[16.5参照]
- 9.5 妊婦
妊婦又は妊娠している可能性のある女性には、診断上の有益性が被曝による不利益を上回ると判断される場合にのみ投与すること。
- 9.6 授乳婦
診断上の有益性及び母乳栄養の有益性を考慮し、授乳の継続又は中止を検討すること。
- 9.7 小児等
小児等を対象とした臨床試験は実施していない。
- 9.8 高齢者
患者の状態を十分に観察しながら慎重に投与すること。一般に生理機能が低下している。
10. 相互作用

10.2 併用注意(併用に注意すること)

薬剤名等	臨床症状・措置方法	機序・危険因子
ソマトスタチンアナログ製剤 オクトレオチド チド酢酸塩 ランレオチド酢酸塩等	本剤の腫瘍への集積が抑制され、診断能に影響を及ぼす可能性が考えられるため、オクトレオチド酢酸塩等の休薬を検討することが望ましい。なお、休薬することにより離脱症状が発現する可能性があるため、休薬の要否及び休薬期間は、患者の状態及び使用製剤を考慮して決めること。休薬する場合は、患者の症状の変化に十分注意すること。	本剤のソマトスタチン受容体(SSTR)との結合を阻害する可能性がある。

11. 副作用

次の副作用があらわれることがあるので、観察を十分に行い、異常が認められた場合には適切な処置を行うこと。

11.2 その他の副作用

		0.1~5%
精神・神経系	頭痛	
血管障害	潮紅、ほてり	
その他	熱感、ALT増加、AST増加	

14. 適用上の注意

- 14.1 薬剤調製時の注意
- 14.1.1 調製にあたっては、バイアルA以外の塩化インジウム(¹¹¹In)を使用しないこと。
- 14.1.2 本品の調製は無菌的に行い、また適当な鉛容器で遮蔽して行うこと。
- 14.1.3 本品の調製の際、バイアル内に空気を入れないこと、またバイアル内を確圧にしないこと。
- 14.1.4 調製後の注射液は25℃以下で保存し、6時間以内に投与すること。
- 14.2 薬剤投与時の注意
膀胱部の被曝を軽減させるため、投与後できるだけ患者に水分を摂取させ、排尿させることが望ましい。
20. 取扱上の注意
放射線を安全に遮蔽できる貯蔵設備(貯蔵箱)に保存すること。
21. 承認条件
医薬品リスク管理計画を策定の上、適切に実施すること。

*その他の使用上の注意等は電子添文をご参照ください。

製造販売元
PDRファーマ株式会社
文献請求先及び問い合わせ先 TEL 03-3538-3624
〒104-0031 東京都中央区京橋2-14-1 兼松ビルディング
輸入先: Mellinckrodt Medical B.V.(オランダ)

2022年3月作成

The 15th Meeting of the Japanese Society of Pulmonary Functional Imaging
and the 11th International Workshop on Pulmonary Functional Imaging

Joint Meeting of JSPFI and IWPMI 2024

Pulmonary functional imaging: present and future

Date: August. 23(Fri.) - 25(Sun.), 2024

Venue: Otsu Civic Hall, Shiga, Japan

President

Yasutaka Nakano, MD, PhD.

Professor and Chairman,
Division of Respiratory Medicine,
Department of Internal Medicine,
Shiga University of Medical Science

■ Welcome Message

Dear Colleagues and Friends,

It is my great pleasure to welcome you to the joint meeting of the 15th Meeting of the Japanese Society of Pulmonary Functional Imaging and the 11th International Workshop on Pulmonary Functional Imaging in Otsu City. The main theme of this meeting is "Pulmonary Functional Imaging: present and future". The organizing committee hopes that this meeting will summarize the past in this field and show the future direction of this field.

The Japanese Society of Pulmonary Functional Imaging was founded in 2009 with the aim to promote and develop the knowledge in this field and to contribute to the patients with respiratory diseases. Starting with the first meeting in Kyoto in 2009, the annual meeting has been held every year except 2021 when it was postponed due to COVID-19, and this year is the 15th anniversary meeting. The International Workshop on Pulmonary Functional Imaging was first held in Philadelphia, USA in 2002 and has been held in cities in North America, Europe and Asia. This meeting in Otsu is the 11th workshop, and it has been 13 years since the 5th workshop was held in Japan in 2011.

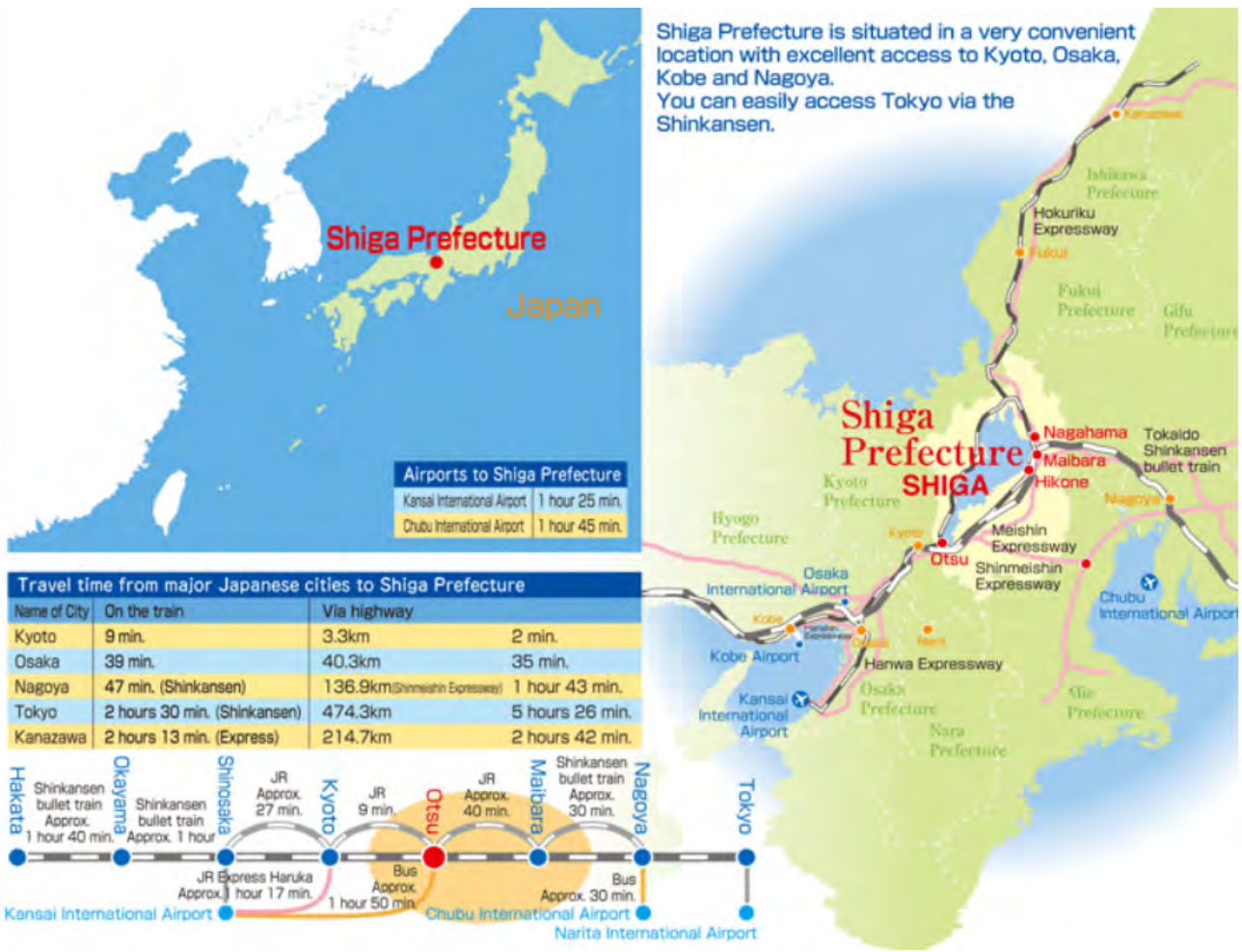
A key feature of the Japanese Society of Pulmonary Functional Imaging and the International Workshop on Pulmonary Functional Imaging is that clinicians and radiologists, as well as engineering researchers, meet and exchange ideas. Many of the world's leading clinicians and researchers in this field from North America, Europe, Oceania and Asia will be attending this joint meeting. I am looking forward to meeting and discussing with you at this joint meeting.



Yasutaka Nakano, MD, PhD.

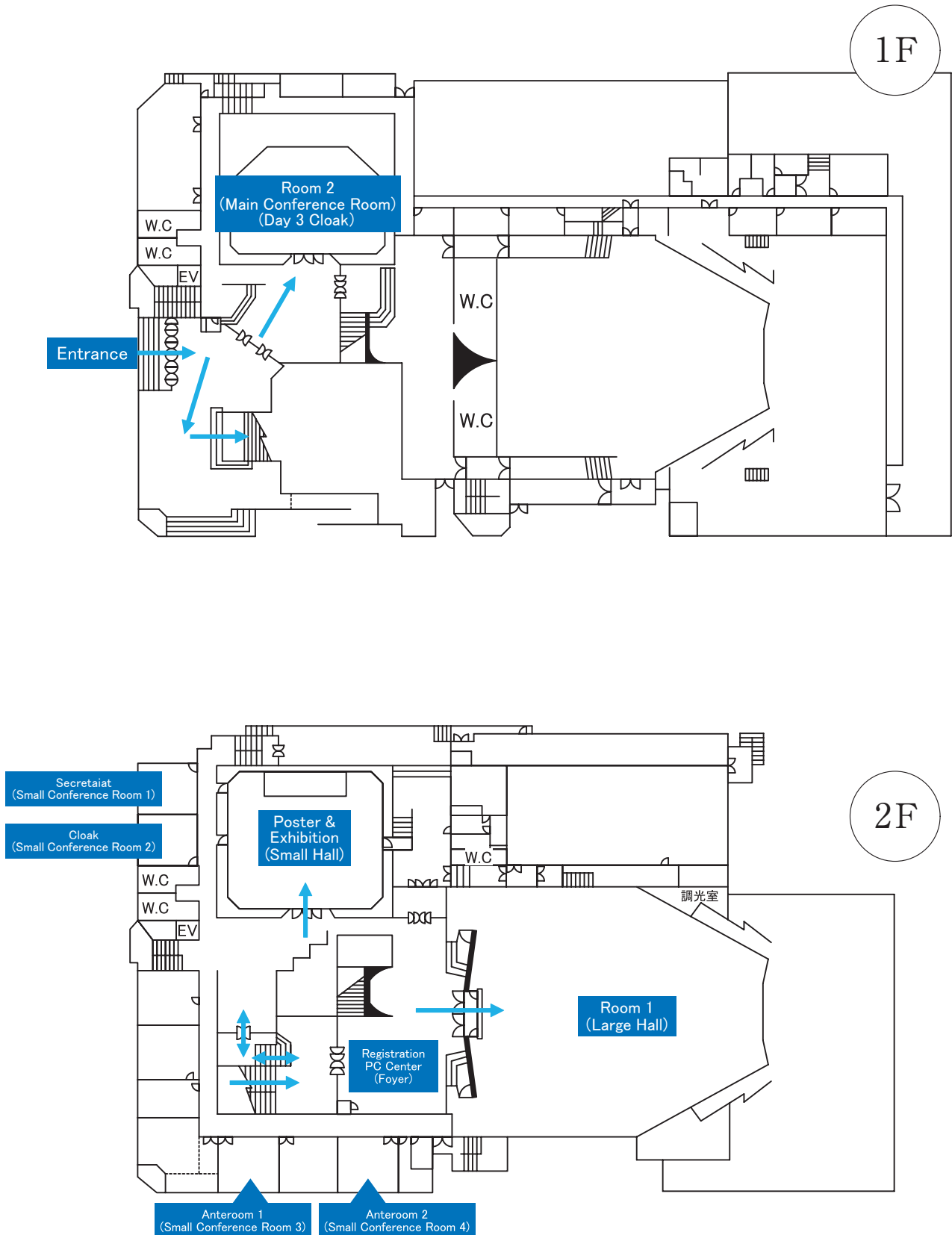
Professor and Chairman,
Division of Respiratory Medicine,
Department of Internal Medicine,
Shiga University of Medical Science

Access & Map



Floor Guide

Otsu Civic Hall



Program at a Glance

[Day-1] Friday, August 23, 2024

	Room 1	Room 2	Poster & Exhibition Room	
	Otsu Civic Hall			
	2F Large Hall	1F Main Conference Room	2F Small Hall	
8:00				
	8:50-9:00 Opening Ceremony			
9:00	9:00-11:00 Session 1 Lung Cancer		8:00-11:00 Poster Setting	
10:00	Chair : Hidetake Yabuuchi, Koichi Takayama, Jin Mo Goo			
11:00				
	11:20-12:20 Luncheon Seminar 1 State of the Art CT and MRI for Pulmonary Functional Imaging	11:20-12:20 Luncheon Seminar 2 COPDとACO ~最新のガイドライン・ 手引きを踏まえた治療介入		
12:00	Chair : Takatoshi Aoki Speaker : Yoshiharu Ohno Sponsored by CANON MEDICAL SYSTEMS CORPORATION	Chair : 中野 恭幸 Speaker : 室 繁郎 *Japanese Sponsored by AstraZeneca K.K.		
13:00	12:40-14:20 Session 2 COPD/Airway Disease			9:00-17:00 Exhibition
14:00	Chair : Shigeo Muro, Tsuneo Yamashiro, Hans-Ulrich Kauczor Sponsored by FUJIFILM Medical Co.,Ltd.		11:00-17:00 Poster Viewing	
15:00	14:40-16:30 Session 3 Vascular Diseases			
16:00	Chair : Nobuhiro Tanabe, Shuji Sakai, Ki Yeol Lee			
17:00			17:00-17:50 Poster Session (English)	
18:00				
19:00				
20:00				

[Day-2] Saturday, August 24, 2024

	Room 1	Room 2	Poster & Exhibition Room	
	Otsu Civic Hall			
	2F Large Hall	1F Main Conference Room	2F Small Hall	
8:00	8:00-9:40 Session 4 Interstitial Pneumonia			
9:00	Chair : Takeshi Johkoh, Takafumi Suda, Pim de Jong			
10:00	10:00-11:40 Session 5 New Modality			
11:00	Chair : Masashi Takahashi, Jens Vogel-Claussen Chang Hyun Lee			
12:00	12:00-13:00 Luncheon Seminar 3 AI in Lung Health: From Early Detection to Advanced Treatment Chair : Ki Yeol Lee, Sang Hyun Paik Speaker : Jens Vogel-Claussen, Gong Yong Jin Sponsored by Corelinesoft Co., Ltd.	12:00-13:00 Luncheon Seminar 4 Advancing Pulmonary CT Imaging: AI Integration with the uCT 960+ System Chair : Yoshiharu Ohno Speaker : Adam G. CHANDLER Sponsored by United Imaging Healthcare Japan K.K.	8:00-17:00 Poster Viewing	9:00-17:00 Exhibition
13:00	13:20-14:50 Session 6 Special Session			
14:00	Chair : Yasutaka Nakano, Sadayuki Murayama, Yeun-Chung Chang			
15:00	15:00-15:30 JSPFI General Assembly			
16:00	15:40-16:40 Young Investigator Award Session			
	16:40-17:00 IWPF Closing Ceremony			
17:00				
18:00				
19:00	18:30-20:30 Gala Dinner (RURI, BIWAKO HOTEL)			
20:00				

[Day-3] Sunday, August 25, 2024

	Room 1	Poster & Exhibition Room	
	Otsu Civic Hall		
	2F Large Hall	2F Small Hall	
8:00	<p>8:00-9:00 Morning Seminar 間質性肺疾患診療における AI 応用の現状と可能性 Chair : 井上 義一 Speaker : 半田 知宏 *Japanese Sponsored by Nippon Boehringer Ingelheim Co., Ltd.</p>		
9:00		<p>8:00-13:20 Poster Viewing</p>	<p>9:00-14:20 Exhibition</p>
10:00	<p>9:10-11:45 Session 7 How to apply AI to lung diseases Chair : 木戸 尚治 Shoji Kido 羽石 秀昭 Hideaki Haneishi 平井 豊博 Toyohiro Hirai *Japanese</p>		
11:00			
12:00	<p>12:00-13:00 Luncheon Seminar 5 多角的に捉える閉塞性肺疾患の治療 Chair : 中野 恭幸 Speaker : 福永 興彦 *Japanese Sponsored by Sanofi K.K. / Regeneron Japan KK</p>		
13:00		<p>13:20-14:20 Poster Session (Japanese)</p>	
14:00		<p>14:20-15:00 Poster Removal</p>	
15:00			

Information for Participants

1. Registration Desk

Registration desk will be opened on the 2F.

Open Hours:

Date	Time
Day 1: August 23	8:00-18:00
Day 2: August 24	7:30-17:30
Day 3: August 25	7:30-15:00

2. Registration Fee

The all type of registration fee includes:

1. Admission to scientific programs.
2. Admission to the exhibition
3. Documentation including a book of abstracts.

JSPFI: Japanese Society for Pulmonary Functional Imaging
All dates and times are Japan Standard Time.(GMT+9)

Category		Early Bird Noon, May. 10 - Jul. 31, 2024	Standard Noon, Aug. 1 - Aug. 15, 2024	On-site Aug. 23 - Aug. 25, 2024	Tax
JSPFI Member (Local Only)	MD	JPY 30,000	JPY 35,000	JPY 40,000	Tax exemption
	Non-MD	JPY 20,000	JPY 25,000	JPY 30,000	Tax exemption
	Undergraduate Student	JPY 10,000	JPY 10,000	JPY 10,000	Tax exemption
Non-JSPFI Member	MD/Non-MD	JPY 65,000	JPY 75,000	JPY 80,000	Tax exemption
	Undergraduate Student	JPY 20,000	JPY 20,000	JPY 20,000	Tax exemption
Accompanying Person		JPY 10,000	JPY 10,000	JPY 10,000	Tax exemption

MD: Medical Doctor

*Student: Please upload your student ID onto the registration system.

3. Payment Method (Only Japanese Yen)

Payment must be made in Japanese Yen, by cash or with a credit card at Registration Desk. Please note that neither personal checks nor any other currencies will be accepted.

Credit card: American Express, Visa, MasterCard, Diners Club, and JCB are acceptable.

4. Name Badges

Please wear your name badges at all times during the meeting for identification and security purposes.

Only registered participants wearing a name badge will be allowed access to the session rooms, exhibition.

5. Exhibition

Exhibition will be held at Smal Hall on the 2F during the meeting.

Exhibitors will be eager to demonstrate and explain their latest products and answer your question.

6. Internet Access Service & Drink Service

Wi-Fi access is available only in the Poster & Exhibition Room(Small Hall) and the registration on the 2F.

If you need a secure network environment, please make your own arrangements with rental services, etc.

Kansai International Airport (KIX)

<https://www.kansai-airport.or.jp/en/service/internet/03.html>



Narita International Airport (NRT)

<https://www.narita-airport.jp/en/service/internet/rental/>



Haneda Airport (HND)

<https://tokyo-haneda.com/en/index.html>



Drink service is available at Poster & Exhibition Room (Small Hall).

7. Travel Desk

Travel Desk will be opened next to the registration desk.

8. Mobile Phone

During the session, you are prohibited from using a mobile phone. Please turn off or switch to the silent mode.

9. Cloakroom

The Cloakroom is at Small Conference Room 2 on the 2F. Please keep valuables in your possession at all times. The organizing committee cannot responsible for lost or stolen items.

※ On Day 3, the cloakroom will be moved to the Main Conference Room on the 1F.

10. Regarding parking.

There is no parking for participants. Please use public transportation or pay parking near the venue if you are coming by private car.

11. Social Events

The organizing committee takes pleasure in presenting the following social event that offer all participants and accompanying persons.

Gala Dinner

Date & Time: 18:30-20:30, Saturday, August 24, 2024

Venue: RURI, BIWAKO HOTEL

※ YIA Award ceremony will be held during the Gala Dinner.

Information for Presenters & Chairpersons

Presentation Time and Language

Speaker	Presentation	Q&A	Abstract	Presentation	Slide
Invited Speakers (Session1-5)	15 min	5 min	English		
Invited Speakers (Session 6)	25 min	5 min	English		
Invited Speakers (Session 7)	20 min	5 min	English & Japanese	English & Japanese	English
YIA Session Speakers	7 min	3 min	English		
Scientific Presentations* (Session 1-5)	7 min	3 min	English		
Scientific Presentations* (Session 7)	7 min	3 min	English & Japanese	Japanese	English
Poster Presenters (English/Aug. 23)	6 min	4 min	English		
Poster Presenters (Japanese/Aug. 25)	6 min	4 min	English & Japanese	Japanese	English

* Scientific presentations are presentations of open abstracts accepted for oral sessions.

Instructions for Chairpersons

All chairpersons are asked to ensure that each session start on time and finish punctually as scheduled.

Oral Sessions

Please come to the Next Chairperson's seat of the session room (the front row on your right side) no later than **15 minutes** prior to the beginning of the session and identify yourself to the staff.

Poster Sessions

All chairpersons for poster session are requested to come to the Poster Reception Desk near by Poster Session Area no later than **15 minutes** prior to the beginning of the session. Please select the best poster presentation of the session (one person per session) and tell the staff of Poster Reception Desk.

Instruction for Oral Presenters

All Oral presentation must be made in the form of PC presentation in English.

All Oral Presenters are requested to come to the PC Preview Center at least **30 minutes** in

advance of their presentations to verify that the data functions properly on the equipment provided.

If you bring your own laptop PC, after checking-in at the PC Preview Center, please come to the PC operation desk near the podium located at the left-front in the session room by **15 minutes** prior to your presentation and hand your PC to the staff. (You can come to the PC operation desk while the previous session is in progress.)

PC Preview Center

PC Preview Center will be located on the 2F.

Open Hours:

Date	Time
Day 1: August 23	8:00-18:00
Day 2: August 24	7:30-17:30
Day 3: August 25	7:30-15:00

Preparing Presentation Data

Application software for preparing presentation data should be PowerPoint 365.

Aspect ratio of your presentation should be 16:9.

The name of the presentation file should include the presenter's name and the presentation title. If you have prepared your presentation data on a Macintosh PowerPoint, please check that your presentation functions correctly in a windows-based environment or bring your own PC in order to avoid display problems.

Use standard font (e.g. Arial, Helvetica, Times, Times New Roman) in preparing your presentation to avoid conversion errors.

Bringing Laptop

Macintosh users are requested to bring your own laptop.

Please turn off any sleep functions and screen savers beforehand.

Cable connector used at the venue for image output is D-sub 15 pin connector or HDMI. Please bring your own connector conversion adapter if necessary.

After checking-in at the PC Preview Center, please come to the PC operation desk near the podium located at the left-front in the session room by **15 minutes** prior to your presentation and hand your PC to the staff. (You can come to the PC operation desk while the previous session is in progress.)

Please pick up your PC at the PC operation desk after your presentation.

Presenter view not available.

COI disclosure

All presenters required to disclose any conflict of interest with sponsoring companies. Please include the slide disclosing the state of COI in your PowerPoint presentation after your title slide.

Instruction for Poster Presenters

For poster presenters on Day1

Please prepare your poster and give your presentation in English.

For poster presenters on Day 3

Please prepare your poster in English and give your presentation in Japanese.

Presenters are requested to follow the schedule below in mounting poster on their assigned board.

The poster number for your presentation can be found in the program book.

Please make sure to arrive at your poster panel at least **10 minutes** prior to the poster session.

Schedule

Date	Time	
August 23	8:00-17:00	Poster Mounting* & Viewing
	17:00-17:50	Poster Session (English)
August 24	8:00-17:00	Poster Viewing
August 25	8:00-13:20	
	13:20-14:20	Poster Session (Japanese)
	14:20-15:00	Poster Removal**

* All posters should be mounted on August 23.

** Posters must be removed during the Poster Removal hours. Any poster remaining after the designated removal period will be discarded by the Organizers.

Venue

Poster Room Small Hall, 2F, Otsu Civic Hall

Presentation Time

6 min. for Presentation + 3 min. for Q&A

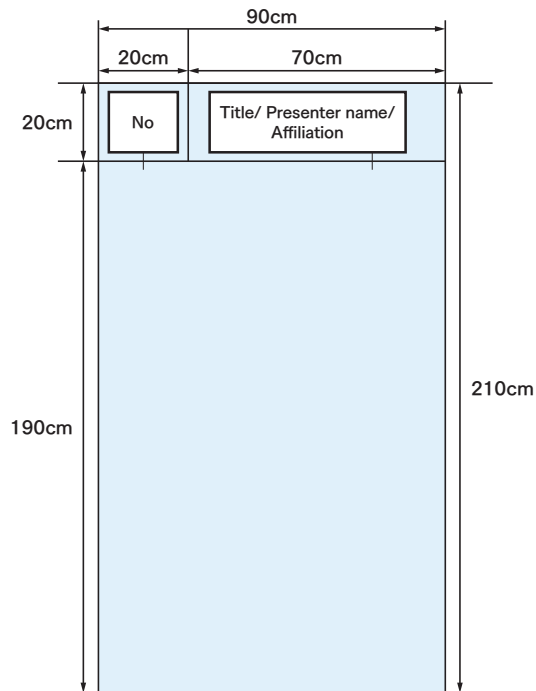
Poster Size

Poster board size: H210cm × W90cm

Presenters should prepare a title section (H20cm × W70cm) including a title, presenter's name(s), and affiliation(s).

Poster number (H20cm × W20cm) will be prepared by the secretariat.

The size of the poster is as described the following.



COI disclosure

All presenters required to disclose any conflict of interest with sponsoring companies.

For Poster presentations, please display at the end of the poster.

Program

Program

Session

August 23 (Fri) 9:00-11:00 **Session 1 Lung Cancer**

[Chair] Hidetake Yabuuchi (Department of Health Sciences, Graduate School of Medical Sciences, Kyushu University)

Koichi Takayama (Department of Pulmonary Medicine, Kyoto Prefectural University of Medicine)

Jin Mo Goo (Department of Radiology, Seoul National University College of Medicine)

S1-1 New Era of Lung Cancer Treatment

Takashi Kijima (Department of Respiratory Medicine and Hematology, Hyogo Medical University, School of Medicine)

S1-2 Basics and clinical applications of CT-based Radiomics for lung cancer

Motohiko Yamazaki (Department of Radiology and Radiation Oncology, Niigata University Graduate School of Medical and Dental Sciences)

S1-3 AI applications in lung cancer imaging

Jin Mo Goo (Department of Radiology, Seoul National University College of Medicine)

S1-4 MRI for Lung Cancer Imaging

Jürgen Biederer (Diagnostic and interventional Radiology, University Hospital Heidelberg)

S1-5 FDG PET in lung cancer: the role of PET/CT and the potential of PET/MRI

Munenobu Nogami (Department of Radiology, Kobe University Hospital/ Biomedical Imaging Research Center, University of Fukui)

S1-6 Development of multimodal fully automated ensembled model to predict EGFR-mutation in NSCLC

Taichi Miyawaki (Department of Respiratory Medicine, Juntendo University Graduate School of Medicine)

S1-7 Predictive modeling for airway geometry analysis on navigation CT for peripheral pulmonary nodules

Jonghoon Kim (Department of Health Sciences and Technology, SAIHST, Sungkyunkwan University)

August 23 (Fri) 12:40-14:20 **Session 2 COPD/Airway Disease**

Sponsored by FUJIFILM Medical Co.,Ltd.

[Chair] Shigeo Muro (Department of Respiratory Medicine, Nara Medical University)

Tsuneo Yamashiro (Department of Radiology, Yokohama City University)

Hans-Ulrich Kauczor (Department Diagnostic and Interventional Radiology, Heidelberg University/ German Center for Lung Research)

S2-1 Quantitative CT

Naoya Tanabe (Department of Respiratory Medicine, Kyoto University)

- S2-2 Quantitative Dual Energy CT for COPD**
Sang Min Lee (Department of Radiology, Ulsan University Asan Medical Center)
- S2-3 Proton MRI for COPD**
Mark Oliver Wielpütz (Department of Diagnostic and Interventional Radiology, Heidelberg University Hospital)
- S2-4 Pulmonary Imaging of Airway Remodeling in Asthma and response to therapy**
Grace Parraga (Robarts Research Institute, Western University)
- S2-5 Reversibility study in healthy, COPD, and asthma subjects with 3D MR spirometry**
Ithar Gharmaoui (Université Paris-Saclay, CEA, CNRS, Inserm, BioMaps)
- S2-6 Data Homogenization with Sequence-to-Sequence GAN Mapping improves Comparability of PREFUL MRI**
Andreas Voskrebenezv (Institute of Diagnostic and Interventional Radiology, Hannover Medical School, Biomedical Research in Endstage and Obstructive Lung Disease (BREATH), Member of the German Center for Lung Research (DZL))

August 23 (Fri) 14:40-16:30 Session 3 Vascular Diseases

- [Chair] Nobuhiro Tanabe (Pulmonary Hypertension Center, Chibaken Saiseikai Narashino Hospital)
Shuji Sakai (Department of Diagnostic Imaging and Nuclear Medicine, Tokyo Woman's Medical University)
Ki Yeol Lee (Department of Radiology, College of Medicine, Korea University)
- S3-1 Current management and molecular basis of pulmonary hypertension due to lung disease**
Seiichiro Sakao (Department of Pulmonary Medicine, IUHW Narita Hospital/Department of Pulmonary Medicine, International University of Health and Welfare (IUHW), School of Medicine)
- S3-2 Dynamic Chest Radiography for vascular diseases**
Yuzo Yamasaki (Department of clinical radiology, Graduate School of Medical Sciences, Kyushu University)
- S3-3 Dual-Energy CT imaging for vascular diseases**
Yoshiyuki Ozawa (Department of Diagnostic Radiology, Fujita Health University School of Medicine)
- S3-4 Advanced MRI methods for the diagnosis of Pulmonary Hypertension**
Mark L. Schiebler (Department of Radiology, University of Wisconsin School of Medicine and Public Health School of Medicine)
- S3-5 Pulmonary function evaluation using non-contrast-enhanced 3D ultrashort echo-time MRI**
Jang-Yeon Park (Department of Biomedical Engineering, Sungkyunkwan University)
- S3-6 the usefulness of Volume Helical Shuttle Scan for whole lung dynamic study in hemoptysis patients**
Toshihiko Sugiura (Department of Respiriology, Graduate School of Medicine, Chiba University, . , Department of Respiratory Medicine, Chibaken Saiseikai Narashino Hospital)

August 24 (Sat) 8:00-9:40

Session 4 Interstitial Pneumonia

- [Chair] Takeshi Johkoh (Department of Radiology, Kansai Rosai Hospital)
Takafumi Suda (2nd Division, Department of Internal Medicine, Hamamatsu University School of Medicine)
Pim de Jong (Department of Radiology, UMC Utrecht)
- S4-1 Recent Topics and Perspectives in the Clinical Practice of Interstitial Lung Disease**
Tomohiro Handa (Department of Advanced Medicine for Respiratory Failure, Graduate School of Medicine, Kyoto University)
- S4-2 Quantitative CT evaluation for interstitial lung disease**
Jooae Choe (Department of Radiology, Asan Medical Center, University of Ulsan College of Medicine)
- S4-3 Update on Diagnostic Imaging of Fibrotic Interstitial Lung Diseases**
Ryoko Egashira (Department of Radiology, Faculty of Medicine, Saga University)
- S4-4 Interstitial Pneumonia and PET: Potential and Pitfalls**
Munenobu Nogami (Department of Radiology, Kobe University Hospital/ Biomedical Imaging Research Center, University of Fukui)
- S4-5 Regional lung structure and function associated with 1-year decline in DLCO in IPF**
Hongseok Ko (Kangwon National University Hospital)
- S4-6 Projected lung area on dynamic chest radiography as an index of lung fibrosis**
Takeshi Kubo (Department of Radiology, Tenri Hospital)

August 24 (Sat) 10:00-11:40

Session 5 New Modality

- [Chair] Masashi Takahashi (Department of Radiology, Yujin-Yamazaki hospital)
Jens Vogel-Claussen (Institute of Diagnostic and Interventional Radiology, Hannover Medical School)
Chang Hyun Lee (Department of Radiology, Seoul National University)
- S5-1 Upright Area-Detector CT: Initial Experience and Potentials for Pulmonary Functional Imaging**
Yoshiharu Ohno (Department of Diagnostic Radiology, Fujita Health University School of Medicine)
- S5-2 Comprehensive assessment of pulmonary morphology and function with Photon counting CT**
Hoen-Oh Shin (Institute of Diagnostic and Interventional Radiology, Hannover Medical School)
- S5-3 High-Spatial-Resolution CT with Energy Integrated Detector**
Ho Yun Lee (Department of Radiology, Samsung Medical Center, Sungkyunkwan University School of Medicine)
- S5-4 Low-Field MRI**
Jens Vogel-Claussen (Institute of Diagnostic and Interventional Radiology, Hannover Medical School)

S5-5 Dark-field Radiographs for the Detection of Pneumothoraces

Henriette Bast (Department of Physics - TUM School of Natural Sciences - Technical University of Munich, Munich Institute of Biomedical Engineering - Technical University of Munich, Department of Diagnostic and Interventional Radiology - Klinikum Rechts der Isar - Technical University of Munich)

S5-6 Synchrotron radiation-based CT for Ultra-High Resolution and Multiscale Lung Imaging

Willi L Wagner (Department of Diagnostic and Interventional Radiology, University Hospital Heidelberg, Translational Lung Research Center)

August 24 (Sat) 13:20-14:50 Session 6 Special Session

[Chair] Yasutaka Nakano (Division of Respiratory Medicine, Department of Internal Medicine, Shiga University of Medical Science)
Sadayuki Murayama (Department of Radiology, University of the Ryukyus Hospital)
Yeun-Chung Chang (Department of Radiology, National Taiwan University College of Medicine)

S6-1 Basics of Pulmonary Physiologic Imaging

Eric A. Hoffman (Department of Radiology, University of Iowa Carver College of Medicine)

S6-2 Pulmonary Functional CT

Hans-Ulrich Kauczor (Department Diagnostic and Interventional Radiology, Heidelberg University/German Center for Lung Research)

S6-3 Artificial Intelligence for Pulmonary Functional Imaging

Edwin J.R. van Beek (Edinburgh Imaging QMRI, University of Edinburgh)

August 25 (Sun) 9:10-11:45 Session 7 How to apply AI to lung diseases

[Chair] Shoji Kido (Department of Artificial Intelligence Diagnostic Radiology, Osaka University Graduate School of Medicine)
木戸 尚治 (大阪大学大学院医学系研究科人工知能画像診断学共同研究講座)
Hideaki Haneishi (Center for Frontier Medical Engineering, Chiba University)
羽石 秀昭 (千葉大学フロンティア医工学センター)
Toyohiro Hirai (Department of Respiratory Medicine, Kyoto University)
平井 豊博 (京都大学大学院医学研究科 呼吸器内科学)

S7-1 Fundamentals of Artificial Technology and Its Application to Pulmonary Imaging

Atsushi Teramoto (Faculty of Information Engineering, Meijo University)

AIの基礎と呼吸機能イメージングへの応用

寺本 篤志 (名城大学 情報工学部 情報工学科)

S7-2 Towards routine quantitative lung imaging with artificial intelligence

Joon Beom Seo (Department of Radiology, University of Ulsan College of Medicine, Asan Medical Center)

- S7-3 Current Situation and Future Direction of CAD and AI in Pulmonary Diseases**
Yoshiharu Ohno (Department of Diagnostic Radiology, Fujita Health University School of Medicine)
呼吸器疾患における CAD および AI の現状と将来展望
大野 良治 (藤田医科大学 医学部 放射線診断学・先端画像診断共同研究講座)
- S7-4 Potential and Prospects of Chest Imaging using AI from Respiratory Physician's Perspective**
Toyohiro Hirai (Department of Respiratory Medicine, Kyoto University)
呼吸器内科医から見た AI による胸部画像診断の可能性と展望
平井 豊博 (京都大学大学院医学研究科 呼吸器内科学)
- S7-5 Quantitative CT Evaluation of Diffuse Lung Disease Using Artificial Intelligence**
Tae Iwasawa (Department of Radiology, Kanagawa Cardiovascular and Respiratory Center)
AI によるびまん性肺疾患の CT 定量評価
岩澤 多恵 (神奈川県立循環器呼吸器病センター放射線科)
- S7-6 Implementation and Evaluation of a DLAD Chest X-ray Analysis System in University Health Screenings**
Yunosuke Kumazawa (Department Of Radiology, Fujita Health University School Of Medicine)
大学生検診における DLAD 胸部 X 線解析システムの評価
熊澤 佑之介 (藤田医科大学医学部放射線医学講座)
- S7-7 Generation of short-term follow-up chest CT images using a latent diffusion model in COVID-19**
Naoko Kawata (Department of Respirology, Graduate School of Medicine, Chiba University ,
Graduate School of Science and Engineering, Chiba University)
COVID-19 における拡散モデルを用いた短期経過予測画像の作成
川田 奈緒子 (千葉大学大学院医学研究院 呼吸器内科学 / 千葉大学大学院融合理工学府 基幹工学専攻
医工学コース)

Young Investigator Award

August 24 (Sat) 15:40-16:40

- [Chair] Satoshi Konno (Department of Respiratory Medicine, Faculty of Medicine, Hokkaido University)
Joon B. Seo (Department of Radiology, University of Ulsan College of Medicine, Asan Medical Center)
David Lewis Levin (Department of Radiology, Stanford University School of Medicine)
- YIA-1 Fibrotic interstitial lung abnormalities in smokers are an independent risk factor for mortality**
Esther Pompe (University Medical Center Utrecht)

- YIA-2 Predictive Value of Oxygen-enhanced MRI T1 Mapping after Lung Transplantation**
Milan Speth (Institute for Diagnostic and Interventional Radiology, Hannover Medical School, Biomedical Research in Endstage and Obstructive Lung Disease (BREATH), German Center for Lung Research)
- YIA-3 High volume ratio of airway to lung blood vessel on exacerbations in COPD**
Nobuyasu Wakazono (Department of Respiratory Medicine, Faculty of Medicine, Hokkaido University)
- YIA-4 Small pulmonary vein volume is associated with a lower saturation and more supplemental oxygen use**
Natascha Kwee (University Medical Center Utrecht - Department of radiology)
- YIA-5 High-resolution 4D pulmonary ventilation MRI correlates strongly to Xe MRI**
Filip Klimes (Institute of Diagnostic and Interventional Radiology, Hannover Medical School, Biomedical Research in Endstage and Obstructive Lung Disease Hannover (BREATH), German Center for Lung Research (DZL))
- YIA-6 Volume doubling time of solid components in lung cancer: distinct implications vs. whole tumor**
Yura Ahn (Asan Medical Center)

Poster (English)

August 23 (Fri) 17:00-17:50 COPD-1

- [Chair] David Lewis Levin (Department of Radiology, Stanford University School of Medicine)
Hoehn-Oh Shin (Institute of Diagnostic and Interventional Radiology, Hannover Medical School)
- PE1-1 Hybrid Evaluation with MRI Series of Multi-direction Diaphragm Motion and CT Images on COPD Patients**
Xingyu Zhou (Graduate School of Science and Engineering, Chiba University, Chiba, Japan)
- PE1-2 Comparison Of Ventilation Imaging Threshold Techniques For Determining Non-Ventilated Volume**
Edward Moon Kyu Jeagal (Airway Physiology and Imaging Group, The Woolcock Institute of Medical Research, Macquarie University and The University of Sydney, Faculty of Life Sciences, University of Technology Sydney)
- PE1-3 Estimating Small Airways Disease from a Single Inspiratory Chest Computed Tomography Scan**
Joseph M Reinhardt (The University of Iowa)
- PE1-4 Determination of sound source of wheezes in COPD based on 4D-CT images and CFD simulation study**
Hiroko Kitaoka (Dept. of Biomedical Engineering, Tokyo University of Agriculture and Technology)
- PE1-5 4D-CT images have solved the mystery of hilar hot spots in COPD on aerosol inhalation scintigraphy**
Hiroko Kitaoka (Dept. of Biomedical Engineering, Tokyo University of Agriculture and Technology)

August 23 (Fri) 17:00-17:50 **COPD-2/Airway Diseases**

[Chair] Sang Min Lee (Department of Radiology, Ulsan University Asan Medical Center)
Noboru Niki (Tokushima University)

PE2-1 AI-based quantification of small pulmonary artery and vein volume on CT and mortality in smokers

Natascha Kwee (University Medical Center Utrecht - Department of Radiology)

PE2-2 Quantitative CT Analysis based on Smoking and COPD in Normal Looking Chest CT

Gong Yong Jin (Chonbuk National University Medical School and Hospital)

PE2-3 NOVAA-CT: a novel artificial intelligence-driven volumetric CT outcome score for airway diseases

Gael Dournes (University Hospital of Bordeaux)

PE2-4 Respiratory function evaluation using CT airway analysis in thoracic scoliosis surgery

Nanae Tsuchiya (University of the Ryukyus)

PE2-5 Correlation of dynamic chest radiograph (DCR) with respiratory function: a study of asthma cases

Masahiro Kaneko (Kobe City West Hospital)

August 23 (Fri) 17:00-17:50 **Lung Cancer**

[Chair] Ho Yun Lee (Department of Radiology, Samsung Medical Center, Sungkyunkwan University School of Medicine)

Hiroyuki Isihikawa (Department of Radiology and Radiation Oncology, Niigata University)

PE3-1 Incidental Findings in the HANSE LCS Trial - Preliminary Report

Rimma Kondrashova (Institute of Diagnostic and Interventional Radiology, Hannover Medical School, Biomedical Research in Endstage and Obstructive Lung Disease Hannover (BREATH), German Center for Lung Research (DZL))

PE3-2 Characteristics of Ground-Glass Nodules in Female Never-Smokers with a Family History of Lung Cancer

Soon Ho Yoon (Department of Radiology, Seoul National University Hospital)

PE3-3 Interobserver Variability in Lung-RADS Categorization: Tertiary Hospital vs. Non-tertiary Hospitals

You Na Kim (Ajou University School of Medicine)

PE3-4 Real world impact of DL supported CAD for routine chest CT on management of incidental lung nodules

Edwin J.R. van Beek (University of Edinburgh)

PE3-5 Application of Fractal Analysis to Chest CT of NSCLC Patients Undergoing Radiotherapy for Prognosis

Jeongeun Hwang (Soonchunhyang University)

August 23 (Fri) 17:00-17:50 **Interstitial Pneumonia**

- [Chair] Jürgen Biederer (Department of Diagnostic and interventional Radiology, University Hospital Heidelberg)
Jooae Choe (Department of Radiology, Asan Medical Center, University of Ulsan College of Medicine)
- PE4-1 Quantitative computed tomography assessment of lung volumes in interstitial lung diseases**
Yi Xian Cassandra Yang (Sengkang General Hospital)
- PE4-2 Automated Quantification of ILA and emphysema on CT: A Predictive Marker for PPC after Esophagectomy**
You Jin Oh (Department of Health Sciences and Technology, SAIHST, Sungkyunkwan University, Department of Radiology and Center for Imaging Science, Samsung Medical Center, Sungkyunkwan University School of Medicine)
- PE4-3 Temporal volumetric concordance between bronchi and lung field on dynamic ventilation CT**
Yukihiro Nagatani (Shiga University of Medical Science)
- PE4-4 Prediction of antifibrotic therapy response for idiopathic pulmonary fibrosis by quantitative CT**
Hidetake Yabuuchi (Department of Health Sciences, Graduate School of Medical Sciences, Kyushu University)
- PE4-5 Quantitative Risk Thresholds for Interstitial Lung Abnormalities and Prognostic Associations**
Yeon Joo Jeong (Pusan National University Yangsan Hospital)

August 23 (Fri) 17:00-17:50 **CT**

- [Chair] Pim de Jong (Department of Radiology, UMC Utrecht)
Chang Hyun Lee (Department of Radiology, Seoul National University)
- PE5-1 Pulmonary small vessel dimensions on CT in pulmonary hypertension: association with ^{99m}Tc-MAA uptake**
Yukihiro Nagatani (Shiga University of Medical Science)
- PE5-2 Association between low-attenuation area on computed tomography and severity of COVID-19**
Sadatomo Tasaka (Hiroshima University Graduate School of Medicine, Murakami Shinmachi Hospital)
- PE5-3 Analysis of alveolar walls in 3D lung micro images from large-field synchrotron radiation CT**
Ryuki Ono (Program of Science and Technology, Graduate School of Creative Science, Tokushima University)
- PE5-4 Increased adiposity to muscle ratio and sinusitis affect quality of life in asthma—CT analysis—**
Kaoruko Shimizu (Division of Emergent Respiratory and Cardiovascular Medicine, Hokkaido University Hospital, Department of Respiratory Medicine, Faculty of Medicine)

PE5-5 Evaluations of pulmonary function for the separated right/left lungs and five lobes by dynamic-ventilation CT

Tsuneo Yamashiro (Department of Radiology, Yokohama City University Graduate School of Medicine)

August 23 (Fri) 17:00-17:50 MRI/AI

[Chair] Mark Oliver Wielpütz (Department of Diagnostic and Interventional Radiology, Heidelberg University Hospital)

Grace Parraga (Robarts Research Institute, Western University)

PE6-1 Estimating Physiological Values of Membrane and RBC Conductance Using ^{129}Xe Gas Exchange MRI

David Mummy (Duke University)

PE6-2 Lung normal strains in free, diaphragmatic, and thoracic breathing using 3D MR Spirometry

Adrien Duwat (Université Paris-Saclay, CEA, CNRS, Inserm, BioMaps)

PE6-3 Vendor-Independent Simultaneous Multislice sequence for accelerated PREFUL MRI – A Proof of Concept

Sonja Luediger (Institute of Diagnostic and Interventional Radiology, Hannover Medical School, Biomedical Research in Endstage and Obstructive Lung Disease (BREATH), Member of the German Center for Lung Research (DZL))

PE6-4 Coronary Artery Calcification on Low-Dose Lung Cancer Screening CT in South Korea

Won Gi Jeong (Department of Radiology, Chonnam National University Hwasun Hospital and Chonnam National University Medical School)

PE6-5 Deep learning-based CAD for pulmonary nodule detection in the coronary artery calcium-scoring CT

Jung Im Jung (Department of Radiology, Seoul St. Mary's Hospital, College of Medicine, The Catholic University of Korea)

PE6-6 Octafluorocyclobutane: A new Fluorine-19 MRI agent for Pulmonary Imaging

Mitchell Albert (Lakehead University/Thunder Bay Regional Research Institute)

Poster (Japanese)

August 25 (Sun) 13:20-14:20 COPD-1

- [Chair] Kenichi Takahashi (Kishiwada City Hospital)
高橋 憲一 (市立岸和田市民病院呼吸器内科)
Yoshiki Kawata (Institute of Post-LED Photonics, Tokushima University)
河田 佳樹 (徳島大学ポスト LED フォトニクス研究所)
- PJI-1 Diaphragm dome height on chest radiography as a predictor of dynamic lung hyperinflation in COPD**
Masashi Shiraishi (Department of Rehabilitation Medicine, Kindai University School of Medicine)
慢性閉塞性肺疾患患者における動的肺過膨張と胸部単純 X 線による横隔膜ドーム高との関連
白石 匡 (近畿大学病院 リハビリテーション部)
- PJI-2 Correlation of DCR with symptoms, physical function, and respiratory function: A Study of COPD cases**
Masahiro Kaneko (Kobe City West Hospital)
胸部 X 線動態画像 (DCR) と症状, 運動耐用能・身体機能, 呼吸機能の相関: COPD 症例における検討
金子 正博 (神戸市立医療センター西市民病院 呼吸器内科)
- PJI-3 CT imaging indices to predict COPD in smokers**
Fumi Mochizuki (Department of Respiratory Medicine, Tsukuba Medical Center Hospital)
健診受診喫煙者における COPD 診断と関連する CT 指標の検討
望月 芙美 (筑波メディカルセンター病院呼吸器内科)
- PJI-4 Association of gut microbiome and CT measured indices in patients with COPD**
Daisuke Kinose (Division of Respiratory Medicine, Department of Internal Medicine, Shiga University of Medical Science)
COPD 患者における腸内細菌叢と CT 指標の関連について
黄瀬 大輔 (滋賀医科大学 呼吸器内科)
- PJI-5 Longitudinal analysis of fibrotic lesions in COPD using Persistent Homology**
Yusuke Shiraishi (Department of Respiratory Medicine, Kyoto University)
パーシステントホモロジーを用いた COPD における線維化病変の評価
白石 祐介 (京都大学大学院医学研究科呼吸器内科学)

August 25 (Sun) 13:20-14:20 COPD-2/Airway-CT

[Chair] Tsuneo Yamashiro (Department of Radiology, Yokohama City University)
山城 恒雄 (横浜市立大学放射線診断学)
Tsuyoshi Oguma (Pulmonology, Kyoto City Hospital)
小熊 毅 (京都市立病院 呼吸器内科)

PJ2-1 Examination of the effects of smoking in healthy subjects using medical examination images

Takahiro Ibaraki (Respiratory Medicine, Osaka Saiseikai Suita Hospital)

健診画像を用いた健常者における喫煙の影響の検討

茨木 敬博 (大阪府済生会吹田病院 呼吸器内科)

PJ2-2 The relationships between FEV1 and inspiratory and expiratory CT measurements

Emiko Ogawa (Health Administration Center, Shiga University of Medical Science, Division of Respiratory Medicine, Department of Medicine, Shiga University of Medical Science)

一秒量と吸気・呼気 CT 測定の関係

小川 恵美子 (滋賀医科大学保健管理センター / 滋賀医科大学内科学講座呼吸器内科)

PJ2-3 Clinical significance of airway to lung ratio in asthma patients

Takafumi Shimada (Department of Respiratory Medicine, Tsukuba Medical Center Hospital, Tsukuba, Japan)

喘息患者における Airway to lung ratio の臨床的意義

嶋田 貴文 (筑波メディカルセンター病院)

PJ2-4 Development of the method for CT imaging evaluation of the airways in bronchiectasis

Tomoki Maetani (Department of Respiratory Medicine, Graduate School of Medicine, Kyoto University)

気管支拡張症における気道の画像的評価手法の開発

前谷 知毅 (京都大学大学院医学研究科 呼吸器内科学)

PJ2-5 Clinical Remission and Chest Computed Tomography Findings with Biologics in Severe Asthma

Shinya Tsukamoto (Department of Respiratory Medicine, Graduate school of Medicine Kyoto University)

重症喘息に対する生物学的製剤による Clinical Remission と胸部 CT 所見の検討

塚本 信哉 (京都大学大学院医学研究科呼吸器内科学)

August 25 (Sun) 13:20-14:20 **Interstitial Pneumonia/Vascular Diseases**

- [Chair] Yukihiro Nagatani (Division of Radiology, Shiga University of Medical Science)
永谷 幸裕 (滋賀医科大学 放射線医学講座)
Kiminobu Tanizawa (Kyoto Medical Center)
谷澤 公伸 (京都医療センター 呼吸器内科)
- PJ3-1 4DCT study of regional lung mobility in patients with interstitial lung disease**
Yoko Tsunoda (Division of Respiratory Medicine, Department of Internal Medicine, Shiga University of Medical Science)
4DCT を用いた間質性肺炎患者における肺局所の可動性についての検討
角田 陽子 (滋賀医科大学医学部附属病院呼吸器内科)
- PJ3-2 Factors in lung volume reduction in RA-related ILD by quantitative chest CT**
Masahiro Tahara (Department of Respiratory Medicine, University of Occupational and Environmental Health)
関節リウマチ関連間質性肺疾患における胸部 CT 定量評価での肺容積減少因子の解析
田原 正浩 (産業医科大学 医学部 呼吸器内科学)
- PJ3-3 Lung volume changes by lung lobe in patients with interstitial lung disease**
Masashi Zenta (Department of Rehabilitation, International University of Health and Welfare (IUHW) Ichikawa Hospital, Department of Health and Social Services, Course of Health and Social Services, Graduate School of Saitama Prefectural University)
間質性肺疾患患者における肺葉別の肺容積の変化
善田 督史 (国際医療福祉大学市川病院リハビリテーション室/埼玉県立大学大学院保健医療福祉学研究所)
- PJ3-4 Pulmonary hypertension associated with systemic sclerosis: utility of pulmonary artery volume ratio**
Hidetake Yabuuchi (Department of Health Sciences, Graduate School of Medical Sciences, Kyushu University)
全身性強皮症合併肺高血圧症：3D-CT 肺動脈容積比の有用性
藪内 英剛 (九州大学大学院医学研究院保健学部)
- PJ3-5 Quantitative assessment of heterogeneity of lung density in patients with CTEPH**
Naoko Kawata (Department of Respiratory, Graduate School of Medicine, Chiba University, Graduate School of Science and Engineering, Chiba University)
慢性血栓塞栓性肺高血圧症患者における肺野濃度の不均一性の評価
川田 奈緒子 (千葉大学大学院医学研究院 呼吸器内科学 / 千葉大学大学院融合理工学府 基幹工学専攻 医工学コース)
- PJ3-6 Dual-Energy CT Thoracic Imaging: Late-Phase Can Replace Unenhanced and Early-Phase Scans.**
Shuhei Doi (Osaka University Graduate School of Medicine)
デュアルエネルギー CT による胸部画像の後期相の検討：単純および早期相の代替可能性の評価
土居 秀平 (大阪大学大学院医学系研究科放射線統合医学講座放射線医学教室)

August 25 (Sun) 13:20-14:20 CT

- [Chair] Yoshiyuki Ozawa (Department of Diagnostic Radiology, Fujita Medical University)
小澤 良之 (藤田医科大学 医学部 放射線診断学)
Hidekazu Hattori (Department of Clinical Pathophysiology, Fujita Health University Graduate School of Health Sciences)
服部 秀計 (藤田医科大学医療科学部臨床病態解析学)
- PJ4-1 Micro-nodule analysis of pneumoconiosis using 3D CT images**
Rento Nii (Tokushima University)
3次元CT画像によるじん肺の粒状影解析
新居 蓮叶 (徳島大学)
- PJ4-2 Lung and airway dynamics using respiratory 4DCT including the whole respiratory system**
Hiroshi Moriya (Ohara general hospital)
呼吸器系全体を含む呼吸動態4DCTによる肺・気道動態の可視化 一定量化と技術的課題一
森谷 浩史 (大原総合病院)
- PJ4-3 Association Between The Cross-sectional Area Of Erector Spinae Muscles And Mortality inCPFE Patients**
Tatsuhiko Furuyama (Department of Respiratory Medicine, Nara Medical University)
気腫合併肺線維症患者における脊柱起立筋横断面積と臨床パラメータや予後との関連
古山 達大 (奈良県立医科大学附属病院呼吸器内科)
- PJ4-4 Experimental analysis of usefulness of ultra-high-resolution scanning on dynamic ventilation CT**
Ryo Uemura (Department of Radiology, Shiga University of Medical Science)
動態CTにおける超高精細スキャンの有用性の実験的解析
上村 諒 (滋賀医科大学 放射線科)
- PJ4-5 Correlation between CT findings and pulmonary function parameters in NTM disease**
Nobuyoshi Hamao (Department of Respiratory Medicine, Graduate School of Medicine, Kyoto University)
肺非結核性抗酸菌症における画像所見と呼吸機能検査の相関について
濱尾 信叔 (京都大学大学院医学研究科 呼吸器内科学)

August 25 (Sun) 13:20-14:20 **Nuclear/AI**

- [Chair] Takeshi Kubo (Department of Radiology, Tenri Hospital)
久保 武 (天理よろづ相談所病院 放射線科)
Nanae Tsuchiya (Department of Radiology, University of the Ryukyus)
土屋 奈々絵 (琉球大学大学院医学研究科 放射線診断治療学講座)
- PJ5-1 A case of Sjögren's syndrome in whom thymic MALT lymphoma was detected by gallium scintigraphy**
Nanae Tsuchiya (University of the Ryukyus)
ガリウムシンチにて胸腺 MALT リンパ腫を指摘出来たシェーグレン症候群の一例
土屋 奈々絵 (琉球大学病院放射線科)
- PJ5-2 Effectiveness of prior PET/CT fusion imaging using CT-guided trans thoracic biopsy**
Fumiyasu Tsushima (Hirosaki University School of Medicine & Hospital)
胸部 CT ガイド下生検における術前 PET の有用性
対馬 史泰 (弘前大学医学部放射線診断学講座)
- PJ5-3 A Case of Pulmonary MALT Lymphoma that was Difficult to Differentiate from Inflammatory Changes**
Tsuyoshi Komori (Osaka Medical and Pharmaceutical University)
FDG-PET で炎症性変化と鑑別困難であった肺 MALT リンパ腫の一例
小森 剛 (大阪医科薬科大学)
- PJ5-4 Automatic extraction of PA and PV in the mediastinum / pulmonary hilum from non-contrast 3DCT images**
Manato Akatsuka (Graduate School of Integrated Science and Technology, Department of Engineering, University of Tokushima)
非造影 3 次元 CT 画像の縦隔部・肺門部の肺動脈・肺静脈の自動抽出
赤塚 真人 (徳島大学大学院 創成科学研究科 理工学専攻)

Sponsored Seminar

August 23 (Fri) 11:20-12:20 Luncheon Seminar 1

Sponsored by CANON MEDICAL SYSTEMS CORPORATION

State of the Art CT and MRI for Pulmonary Functional Imaging

- [Chair] Takatoshi Aoki (Department of Radiology, University of Occupational and Environmental Health)
- [Speaker] Yoshiharu Ohno (Department of Diagnostic Radiology, Fujita Health University School of Medicine / Joint Research Laboratory of Advanced Medical Imaging, Fujita Health University School of Medicine)

August 23 (Fri) 11:20-12:20 Luncheon Seminar 2

共催：アストラゼネカ株式会社

COPD と ACO ～最新のガイドライン・手引きを踏まえた治療介入

- [Chair] 中野 恭幸 (滋賀医科大学 内科学講座 呼吸器内科 教授)
- [Speaker] 室 繁郎 (奈良県立医科大学 呼吸器内科学講座 教授)

August 24 (Sat) 12:00-13:00 Luncheon Seminar 3

Sponsored by Corelinesoft Co., Ltd.

AI in Lung Health: From Early Detection to Advanced Treatment

- [Chair] Ki Yeol Lee (Department of Radiology, College of Medicine, Korea University)
Sang Hyun Paik (Chief Medical Office of Coreline)
- [Speaker] Jens Vogel-Claussen (Hannover Medical School)
- Implementation of Artificial Intelligence in LDCT lung cancer screening - the HANSE Study**
- [Speaker] Gong Yong Jin (Jeonbuk National University Medical School and Hospital)
- Role of artificial intelligence in the clinical practice of interstitial lung disease**

August 24 (Sat) 12:00-13:00 Luncheon Seminar 4

Sponsored by United Imaging Healthcare Japan K.K.

Advancing Pulmonary CT Imaging: AI Integration with the uCT 960+ System

- [Chair] Yoshiharu Ohno (Department of Diagnostic Radiology, Fujita Health University School of Medicine)
- [Speaker] Adam G. CHANDLER (UIH America, Inc., Houston, TX, USA)

August 25 (Sun) 8:00-9:00

Morning Seminar

共催：日本ベーリンガーインゲルハイム株式会社

間質性肺疾患診療における AI 応用の現状と可能性

[Chair] 井上 義一 (大阪府結核予防会・大阪複十字病院 内科・近畿中央呼吸器センター臨床研究センター)

[Speaker] 半田 知宏 (京都大学大学院医学研究科 呼吸不全先進医療講座)

August 25 (Sun) 12:00-13:00

Luncheon Seminar 5

共催：サノフィ株式会社 / リジェネロン・ジャパン株式会社

多角的に捉える閉塞性肺疾患の治療

[Chair] 中野 恭幸 (滋賀医科大学 内科学講座 呼吸器内科 教授)

[Speaker] 福永 興壱 (慶應義塾大学医学部 呼吸器内科 教授)

Abstracts

〈Session 1〉 Lung Cancer

S1-1 New Era of Lung Cancer Treatment

Takashi Kijima

Department of Respiratory Medicine and Hematology, Hyogo Medical University, School of Medicine

Lung cancer is the leading cause of cancer-related deaths worldwide. As of 2022, WHO reports that approximately 2.5 million patients are newly diagnosed and 1.8 million patients die every year. The median overall survival of unresectable and metastatic lung cancer was around one year because chemotherapeutic regimens were limited and the concept of evidence-based medicine had not been established by the end of the 20th century. However, entering the 21st century, both diagnostic method and treatment strategy have been developed with rapid progress and the prognosis has improved dramatically. In this quarter century, two major paradigm shifts have occurred in terms of diagnosis and treatment of lung cancer.

The first one is the discovery of driver oncogenes and the development of molecular-target drugs for individual oncogenes especially in non-small cell lung cancer (NSCLC). Nowadays, the multi-gene panel testing is carried out before starting treatment and the most suitable molecular-target drug is selected for each driver oncogene profile, which is so-called biomarker-based medicine. Moreover, the comprehensive genomic profiling test can be conducted after standard treatments were completed for the purpose of finding targetable gene alterations and candidate drug expected to be effective. Thus, the genomic medicine has become popular and the prognosis of driver oncogene-positive unresectable and metastatic NSCLC has extended to around 5 years in Japan.

The second one is the clinical application of immune checkpoint inhibitors (ICIs). Immunotherapy has brought about the 5-year survival rate of approximately 20% especially in driver oncogene-negative unresectable and metastatic NSCLC. The most promising benefit of immunotherapy is being able to make patients even with advanced stage NSCLC achieve cure as well as live out the natural life while coexisting with the disease. More recently, the survival benefits of ICIs in patients with earlier stage NSCLC have also been established, such as the consolidation use after chemo and radical radiation therapy as well as the perioperative period use. Furthermore, combined use of ICIs with chemotherapy has been shown to prolong overall survival with the 3-year survival rate of nearly 20% in patients with extensive-stage SCLC, which has the poorest prognosis among all histological types and has no reported targetable driver oncogenes so far.

Continuous and further discovery of targetable genomic alterations and development of new promising drugs are expected in the next decade.

S1-2 Basics and clinical applications of CT-based Radiomics for lung cancer

Motohiko Yamazaki

Department of Radiology and Radiation Oncology, Niigata University Graduate School of Medical and Dental Sciences

Radiomics is a methodology for extracting numerous quantitative features from medical images using computer software. These features, called radiomics features, contain voxel-level information that cannot be captured by human eyes, thereby enabling a more detailed and objective image evaluation than would be obtained through conventional visual assessment.

Lung cancer is a disease that has garnered significant attention in radiomics analysis. Studies on lung cancer have reported that intra-tumoral radiomics on CT images provides useful insights for predicting patient prognosis, histology, gene mutations, and response to drug therapy. It has also been suggested that the addition of peri-tumoral radiomics to intra-tumoral radiomics provides a more comprehensive lung cancer profile.

In this lecture, I will first explain the basic workflow for radiomics analysis, including image segmentation, feature extraction, and prediction. Next, I will present previous radiomics research and mention the potential of radiomics in clinical applications. Finally, I will introduce how artificial intelligence (AI) technology has been used in radiomics analysis.

Radiomics, together with AI, will play an important role in the realization of precision medicine.

S1-3 AI applications in lung cancer imaging

Jin Mo Goo

Department of Radiology, Seoul National University College of Medicine

Artificial intelligence (AI) is a broad concept that refers to the capacity to simulate intelligent behavior. AI can be applied in various segments of lung cancer imaging, including test selection, image generation, image triage, image analysis, and image reporting. Many studies have been focused on detection, classification, quantification, segmentation, registration, response evaluation, and predicting prognosis. Radiomics and deep-learning approach based on data-driven technology have shown their potential in these tasks, but still, there are many challenges and limitations. This lecture will deal with the current status of AI applications in lung cancer imaging.

S1-4 MRI for Lung Cancer Imaging

Jürgen Biederer

Diagnostic and interventional Radiology, University Hospital Heidelberg

MRI offers unique imaging capacities for screening, staging and therapy of lung cancer (LC).

In LC screening, MRI has the potential to be cost-effective and reduce overdiagnosis due to its higher sensitivity for malignant lesions compared to benign. Meta-analyses show a sensitivity of 0.81 for nodules of 4-8mm (0.99 for >8mm) with a low false positive rate of 0.09. Alternatively, multi-parametric imaging with dynamic contrast enhanced (DCE-) and diffusion weighted (DW-)MRI could serve as onsite test for immediate characterization of nodules detected with CT. Clinical trials evaluating these potential benefits are desperately needed.

For LC staging, whole body MRI challenges the current practice using MDCT (morphology), PET (metabolism), scintigraphy (ventilation/perfusion/bone metastases) and MRI (brain). For T-staging, superior soft tissue contrast allows differentiation of tumour/atelectasis, mediastinal involvement, chest wall invasion and may identify vital tumour for guided biopsy. Mediastinal N-staging is often decisive for prognosis and therapy of LC. Here contrast-/non-contrast-enhanced MRI as well as DCE- and DW-MRI reach a high sensitivity/specificity. In dedicated studies, M-staging with whole-body MRI equals the diagnostic accuracy of PET-CT. Whole body PET/MRI combining the excellent functional imaging capacities of both modalities appears very promising.

Recent studies show that early response to systemic therapy of LC can be monitored with DCE- and DWI-MRI. In radiotherapy, regional lung tissue characterization with functional MRI can help to refine target definition and dose delivery. Fast 4D-MRI for detection of lung motion and tumour displacement without radiation exposure can provide key information for patient selection and planning motion adapted radiotherapy.

S1-5 FDG PET in lung cancer: the role of PET/CT and the potential of PET/MRI

Munenobu Nogami

Department of Radiology, Kobe University Hospital/ Biomedical Imaging Research Center, University of Fukui

Regarding lung cancer and FDG PET/CT, the following points are discussed:

1. Physiological Uptake & Non-tumor Uptake

In the thoracic region, physiological uptake in multiple organs or uptake suggestive of pathologies other than lung cancer can be observed. It is important to differentiate these from lesions related to lung cancer.

2. Differentiation of Lung Nodules

Malignant lesions that can exhibit low uptake include tumors with low cell density or low glucose metabolism, ground-glass opacity components, mucin production, well-differentiated tumors, some malignant lymphomas, and some metastatic tumors. Conversely, inflammatory nodules, tumors associated with inflammation, some benign tumors, thrombi, etc., can show high uptake.

3. Staging of Lung Cancer

CT during shallow breath-holding or free breathing, as obtained in PET/CT imaging, is inappropriate for diagnosis of the T factor in the TNM classification. FDG PET is useful in diagnosing lymph node and distant metastases. Important points to evaluate in lymph node metastasis include the presence of metastasis (N0 or not), ipsilateral or contralateral, hilar or mediastinal, or beyond. Care must be taken to avoid false negatives due to small lesions or false positives due to inflammation in lymph node metastasis diagnosis.

4. Assessment of Treatment Efficacy and Prognostic Prediction

Although not covered by insurance in Japan, the usefulness of quantitative indicators using PERCIST and similar methods has been demonstrated. Criteria based on the use of immune checkpoint inhibitors (imPERCIST) have also been proposed.

Finally, the potential of integrated PET/MRI in lung cancer is discussed.

S1-6 Development of multimodal fully automated ensembled model to predict EGFR-mutation in NSCLC

Taichi Miyawaki¹⁾, Takehito Shukuya¹⁾, Kazuhiro Szuki²⁾, Shiting XU¹⁾, Yusuke Nakamura³⁾, Yoshika Koinuma¹⁾, Tetsuhiko Asao¹⁾, Ryota Kanemaru¹⁾, Shoko Shimamura¹⁾, Yoichiro Mitsuishi¹⁾, Rina Shibayama¹⁾, Ken Tajima¹⁾, Naoko Shimada¹⁾, Yujiro Otsuka³⁾, Kazuhisa Takahashi¹⁾

1) Department of Respiratory Medicine, Juntendo University Graduate School of Medicine

2) Department of Radiology, Juntendo University Graduate School of Medicine

3) Plusman LLC

Backgrounds

Systemic therapy to patients with advanced or recurrent non-small cell lung cancer (NSCLC) are determined by the type of driver oncogenes and PD-L1 immunostaining. In this study, we investigated the potential for artificial intelligence to assist in detecting *EGFR*-mutation and predicting the efficacy of EGFR-TKI in patients with NSCLC.

Methods

We built an ensemble model which combined two machine learning models (logistic regression and Bernoulli naive Bayes) analyzing clinical information and tumor characteristics, and deep convolutional neural network analyzing CT image. Each sub-model was independent, could be adjusted individually, attached and detached. The models were trained for predicting EGFR-mutation of EGFR-TKI using cross-entropy loss. The performance of the proposed model was evaluated by 5-fold cross-validation. The final performance metric was the average of the area under the curve (AUC) computed across all folds.

Results

One-hundred-and-fifty consecutive evaluable patients were included in this study. Among them, 89 patients without *EGFR*-mutation, 59 patients with common *EGFR*-mutation and 2 patients with uncommon *EGFR*-mutation. The ensemble model was possible to predict *EGFR*-mutation with AUC of 0.87 (95% CI: 0.77 – 0.96). Each sub-model integrated in the ensemble model predicted *EGFR*-mutation in AUC of 0.83 (95% CI: 0.71 – 0.95), 0.88 (95% CI: 0.79 – 0.97), and 0.87 (95% CI: 0.79 – 0.96) for logistic regression, Bernoulli naive Bayes and deep neural network respectively.

Conclusions

The results suggest that there was sufficient potential for the use of deep learning to assist in predicting *EGFR*-mutation.

S1-7 Predictive modeling for airway geometry analysis on navigation CT for peripheral pulmonary nodules

Jonghoon Kim¹⁾, Byeong-Ho Jeong²⁾, Hwanho Cho³⁾, Sung Goo Park⁴⁾, Yoojin Oh^{1,4)}, Ho Yun Lee^{1,4)}

1) Department of Health Sciences and Technology, SAIHST, Sungkyunkwan University

2) Division of Pulmonary and Critical Care Medicine, Department of Medicine, Samsung Medical Center, Sungkyunkwan University School of Medicine

3) Department of Electronics Engineering, Incheon National University, Incheon

4) Department of Radiology and Center for Imaging Science, Samsung Medical Center, Sungkyunkwan University School of Medicine

Objectives: To investigate the 3D geometric airway analysis on navigation CT for peripheral pulmonary nodules (PPNs) during radial probe endobronchial ultrasound-guided transbronchial lung biopsies (R-EBUS-TBLB) and to identify the clinical feasibility of prediction model for CT-guided intervention

Methods: We prospectively collected from patients who underwent R-EBUS-TBLB between December 2021 and February 2023. The navigation approach for the PPNS was manually performed on the chest navigation CT by an expert bronchoscopist, where the operators examined the accessibility in reaching the targeted lesion. The 3D geometric analysis was conducted by automatically tracing from main bronchus to PPNS and quantifying airway geometric characteristics using in-house software. We developed predictive models to identify the potential factors for lesion accessibility by integrating airway geometric characteristics and clinical variables. The proposed models were evaluated by the area under the curve (AUC).

Results: Of the 219 cases who were eligible for analysis (mean age, 68.61 years \pm 9.97 [standard deviation]; 118 male), thirty-seven cases were not accessible in bronchus sign before intervention on CT. For the proposed models, the composite model integrating clinical variables with airway geometrical variables showed better performance than the clinical model or the airway geometrical model (AUC, 95% CI; the integrated model: 0.84, 0.76-0.92; the clinical model: 0.68, 0.56-0.81; airway geometrical model: 0.79, 0.74-0.84, respectively).

Conclusion: 3D airway geometric analysis might have the potential to reveal factors that examine accessibility for endobronchial airway navigation. The proposed models, developed by integrating quantitative CT scan with clinical variables, could provide feasibility for CT-guided navigation interventions.

Tables

Table 1. Baseline characteristics

Variables	Total case (N=219)	Easily accessible (N=182)	Difficult or not accessible (N=37)	P
Age, year	61.61 \pm 9.97	68.69 \pm 9.91	68.22 \pm 10.49	0.792
Sex, male	118 (59.3%)	106 (58.2%)	20 (54.1%)	0.639
Lesion size, mm	24.54 \pm 16.01	24.44 \pm 17.25	20.10 \pm 6.28	0.065
Lesion depth from pleural surface, mm	10.78 \pm 12.42	11.56 \pm 13.01	6.99 \pm 8.34	0.008
Solidity				0.911
Solid	150 (68.49%)	124 (68.13%)	26 (70.27%)	
Sub-solid	47 (21.46%)	39 (21.43%)	8 (21.62%)	
Cavitary	22 (10.05%)	19 (10.44%)	3 (8.11%)	
The number of branch level	7.17 \pm 1.75	7.15 \pm 1.79	7.27 \pm 1.57	0.7
Lesion location				0.124
Right upper	47 (21.46%)	37 (20.33%)	10 (27.03%)	
Right middle	16 (7.31%)	16 (8.79%)	0	
Right lower	47 (21.46%)	35 (19.23%)	12 (32.43%)	
Left upper	69 (31.51%)	59 (32.42%)	10 (27.03%)	
Left lower	40 (18.26%)	35 (19.23%)	5 (13.51%)	
Bronchus clustering				0.059
RB1, LB1, RB6, LB6	97 (44.29%)	155 (85.16%)	27 (72.97%)	
RB 8-10, LB8-10	57 (26.03%)	21 (11.54%)	4 (10.81%)	
Others	65 (29.68%)	6 (3.30%)	6 (16.22%)	
Bronchus sign on CT				0.007
Within	182 (83.10%)	155 (85.16%)	27 (72.97%)	
Adjacent	25 (11.42%)	21 (11.54%)	4 (10.81%)	
Invisible	12 (5.48%)	6 (3.30%)	6 (16.22%)	

Note—Data are reported as mean \pm standard deviation, and numbers (%). We confirmed that among the 199 patients, nineteen have multiple lesions, for which R-EBUS-TBLB were performed. This study analyzed all available cases, including those with multiple lesions.

Abbreviations: R-EBUS-TBLB, radial probe endobronchial ultrasound-guided transbronchial lung biopsy

Table 2. Procedure results

Variables	Total case (N=219)	Easily accessible (N=182)	Difficult or not accessible (N=37)	p
Procedure time, min	10.48 \pm 6.21	25.44 \pm 9.45	15.78 \pm 8.73	<0.001
Radial probe positioning during the procedure				<0.001
Within	179 (81.74%)	162 (89.01%)	17 (45.95%)	
Adjacent	29 (13.24%)	20 (10.99%)	9 (24.32%)	
Invisible	11 (5.02%)	0	11 (27.73%)	
Pathologic diagnosis				<0.001
Malignancy	126 (57.53%)	119 (65.38%)	7 (18.92%)	
Benignancy	20 (9.13%)	17 (9.34%)	3 (8.11%)	
Non-diagnostic	57 (26.03%)	46 (25.27%)	11 (29.73%)	
Fail to obtain the tissue	16 (7.31%)	0	16 (43.24%)	

Table 3. Univariable analysis for clinical variables

Variables	Odds ratio (95% confidence interval)	P
Age	0.995 (0.961 – 1.031)	0.791
Sex	1.219 (0.596 – 2.494)	0.588
Lesion size, mm	0.931 (0.883 – 0.981)	0.007
Lesion depth from pleural surface, mm	0.963 (0.927 – 0.999)	0.046
Solidity		
Sub-solid (vs. Solid)	0.978 (0.041 – 2.336)	0.961
Cavitary (vs. Solid)	0.753 (0.208 – 2.733)	0.666
The number of branch level	1.04 (0.853 – 1.269)	0.699
Lesion location		
Right middle (vs. Right upper)	0	0.998
Right lower (vs. Right upper)	1.269 (0.487 – 3.307)	0.626
Left upper (vs. Right upper)	0.627 (0.238 – 1.651)	0.345
Left lower (vs. Right upper)	0.529 (0.164 – 1.701)	0.285
Bronchus clustering		
RB8-10, LB8-10 (vs. Others)	0.905 (0.338 – 2.418)	0.842
RB1, LB1, RB6, LB6 (vs. Others)	2.288 (1.024 – 5.116)	0.044
Radial probe positioning during the procedure		
Adjacent (vs. Within)	1.093 (0.348 – 3.435)	0.878
Invisible (vs. Within)	5.741 (1.724 – 19.120)	0.004
Procedure time, min	1.156 (1.090 – 1.226)	<0.001

Table 4. Univariable analysis for airway geometrical features

Variables	Odds ratio (95% confidence interval)	P
Total sectional length	0.820 (0.569 – 1.182)	0.284
Total Sum of bifurcation angle-in	1.505 (1.057 – 2.145)	0.023
Total Min of bifurcation angle-in	1.223 (0.862 – 1.736)	0.257
Total Max of bifurcation angle-in	1.595 (1.086 – 2.344)	0.017
Total Mean of bifurcation angle-in	1.636 (1.147 – 2.333)	0.006
Total Std of bifurcation angle-in	1.362 (0.968 – 1.916)	0.075
Sectional length	0.708 (0.467 – 1.072)	0.101
Bifurcation angle-in	1.304 (0.925 – 1.836)	0.127
Min sectional area	1.090 (0.782 – 1.520)	0.608
Max sectional area	1.163 (0.870 – 1.555)	0.305
Average sectional area	1.043 (0.739 – 1.472)	0.809
Min of max inscribed sphere R	0.887 (0.607 – 1.297)	0.534
Max of max inscribed sphere R	0.794 (0.522 – 1.208)	0.278
Max of min diameter	0.975 (0.678 – 1.403)	0.891
Max of Max diameter	1.223 (0.893 – 1.675)	0.208
Min of min-max diameter ratio	0.641 (0.435 – 0.943)	0.023
Max of min-max diameter ratio	0.931 (0.660 – 1.313)	0.684
Average of min-max diameter ratio	0.850 (0.600 – 1.205)	0.359
Max curvature	0.951 (0.663 – 1.364)	0.786
Average curvature	1.033 (0.723 – 1.475)	0.858
Min torsion	1.133 (0.745 – 1.727)	0.556
Max torsion	0.966 (0.664 – 1.406)	0.856
Average torsion	1.084 (0.754 – 1.506)	0.716
Min perimeter	0.974 (0.678 – 1.400)	0.888
Max perimeter	1.066 (0.754 – 1.506)	0.716
Min luminal circularity	0.867 (0.614 – 1.225)	0.417
Max luminal circularity	0.972 (0.676 – 1.399)	0.879
Average luminal circularity	0.949 (0.661 – 1.363)	0.777
Max hydraulic luminal diameter	1.013 (0.713 – 1.439)	0.942
Average hydraulic luminal diameter	0.987 (0.688 – 1.416)	0.944

Sectional length	1.259 (0.896 – 1.767)	0.182
Bifurcation angle-in	1.358 (0.979 – 1.885)	0.065
Min sectional area	0.653 (0.364 – 1.172)	0.151
Max sectional area	1.017 (0.716 – 1.444)	0.924
Average sectional area	0.696 (0.411 – 1.177)	0.174
Min of max inscribed sphere R	0.697 (0.477 – 1.017)	0.060
Average of max inscribed sphere R	0.623 (0.419 – 0.928)	0.019
Max of min diameter	0.896 (0.615 – 1.306)	0.565
Min of min-max diameter ratio	0.966 (0.676 – 1.380)	0.848
Max of min-max diameter ratio	1.218 (0.789 – 1.882)	0.371
Average of min-max diameter ratio	1.308 (0.887 – 1.931)	0.173
Max curvature	1.512 (1.068 – 2.141)	0.019
Average curvature	1.474 (1.027 – 2.115)	0.034
Min torsion	0.976 (0.693 – 1.376)	0.891
Max torsion	1.061 (0.777 – 1.449)	0.708
Average torsion	1.226 (0.858 – 1.754)	0.261
Min perimeter	1.667 (0.876 – 1.554)	0.290
Max perimeter	0.889 (0.633 – 1.250)	0.497
Min luminal circularity	0.388 (0.127 – 1.182)	0.094
Max luminal circularity	1.132 (0.787 – 1.629)	0.501
Average luminal circularity	0.712 (0.483 – 1.051)	0.086
Max hydraulic luminal diameter	0.349 (1.270 – 0.960)	0.040
Average hydraulic luminal diameter	0.496 (0.294 – 0.834)	0.008

Note—Univariable analysis was conducted by using the selected airway geometrical features, assessed for multicollinearity through VIF. Our study defined the term “final branch” as the branch that contacts or is adjacent to the PPNs on navigation CT.

Abbreviation: VIF, variance inflation factor, PPNs, peripheral pulmonary nodules

Table 5. Contributions for variables to the three predictive models using logistic-LASSO analysis

Proposed model	Variables	Odds ratio (95% confidence interval)
Clinical model	Lesion size	0.2803 (0.2311 – 0.3401)
	Lesion depth from pleural surface	0.4674 (0.4388 – 0.4978)
	Bronchus clustering (RB1, RB6, LB1, LB6)	1.3718 (1.2944 – 1.4537)
	Bronchus sign (Invisible)	1.3471 (1.3083 – 1.3869)
Airway geometrical model	Sum of bifurcation angle-in	1.1945 (1.1175 – 1.2769)
	Total branch Max of bifurcation angle-in	1.6209 (1.4904 – 1.7628)
	Mean of bifurcation angle-in	1.0732 (1.0219 – 1.1270)
	Previous branch to final branch Min of min-max diameter ratio	0.6339 (0.5910 – 0.6800)
Final branch	Average of max inscribed sphere R	0.7889 (0.7320 – 0.8502)
	Max curvature	1.5852 (1.4742 – 1.7044)
	Max hydraulic luminal diameter	0.5283 (0.8458 – 0.5745)
	Composite model	Lesion size
Lesion depth from pleural surface		0.4706 (0.4153 – 0.5333)
Bronchus clustering (RB1, RB6, LB1, LB6)		1.2782 (1.1831 – 1.3808)
Bronchus sign (Invisible)		1.3550 (1.2881 – 1.4254)
Total branch	Sum of bifurcation angle-in	1.2136 (1.1311 – 1.3022)
	Max of bifurcation angle-in	1.4356 (1.3129 – 1.5698)
Previous branch to final branch	Min of min-max diameter ratio	0.5628 (0.5184 – 0.6109)
	Max curvature	1.3765 (1.2944 – 1.4638)
Final branch	Average curvature	1.1045 (1.0435 – 1.1691)
	Max hydraulic luminal diameter	0.4805 (0.4167 – 0.5540)

Abbreviation: LASSO, least absolute shrinkage and selection operator

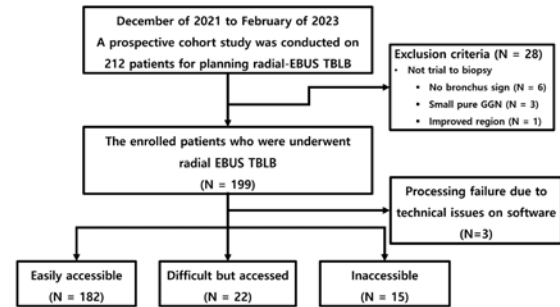
Table 6. Performance evaluation and statistics for three proposed models

Models	Performance and statistics			
	AUC	Sensitivity	Specificity	Delong test
Clinical	0.68	0.15	0.99	ref
	(0.60 – 0.81)	(0.02 – 0.28)	(0.98 – 1.00)	N/A
Airway geometrical	0.79	0.36	0.97	0.43
	(0.74 – 0.84)	(0.22 – 0.50)	(0.97 – 1.00)	ref
Composite	0.84	0.51	0.98	0.05
	(0.76 – 0.92)	(0.28 – 0.74)	(0.96 – 1.00)	0.28

Note—Performance metrics such as AUC, sensitivity and specificity are represented as mean (95% confidence interval). Model’s performance was evaluated by using 10-fold cross validation. The Delong test was performed to compare the model performance values (e.g., AUC).

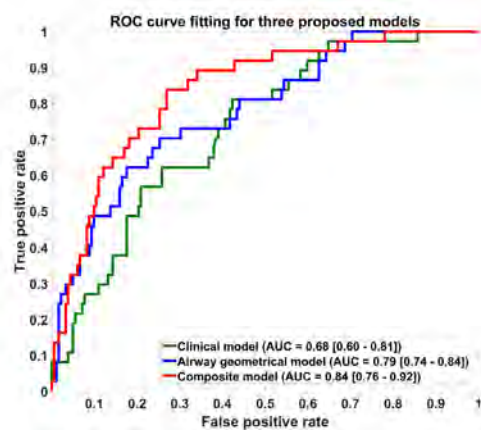
Abbreviations: AUC, area under the curve, NA, not available

Figure 1. Flow chart of patient



Note—We confirmed that among the 199 patients, nineteen have multiple lesions, for which R-EBUS TBLB were performed. This study analyzed all available cases, including those with multiple lesions (N=219).

Figure 2. Receiver operating curve for three proposed models



〈Session 2〉 COPD/Airway Disease

S2-1 Quantitative CT

Naoya Tanabe

Department of Respiratory Medicine, Kyoto University

Chronic obstructive pulmonary disease (COPD) and asthma are major chronic airway diseases with heterogeneous clinical manifestations and outcomes. Chest computed tomography (CT) can be used to evaluate the underlying pathophysiological changes and to perform more individualized managements of the diseases. While visual CT assessments of lung parenchyma and airways are central in clinical practice, recent advances in image analyses have allowed for the detailed structural assessment of the airway tree and lung parenchyma on CT. In addition to local measurements of airway lumen and wall size, the global feature of the airway tree can be quantified using novel parameters, such as airway fractal dimension representing the complexity of airway branching pattern, total airway count, and airway-to-lung size ratio representing dysanapsis. The percentage of low attenuation areas in lung parenchyma as well as exponent D for the cumulative size distribution of low attenuation clusters can be used to evaluate the parenchymal destruction in patients with COPD and even in subgroup of patients with asthma. In this presentation, focus will be mainly placed on what we have found using these airway and lung parenchymal parameters and how this progress should be applied to next research and clinical practice.

S2-2 Quantitative Dual Energy CT for COPD

Sang Min Lee

Department of Radiology, Ulsan University Asan Medical Center

Quantitative imaging was defined as “the extraction of quantifiable features from medical images for the assessment of normal or the severity, degree of change, or status of a disease, injury, or chronic condition relative to normal.” by Quantitative Imaging Biomarker Analysis (QIBA).

Quantitative analysis of chest CT is being increasingly used in clinical practice of COPD and asthma patients. Several quantitative analyzes derived from chest CT including inspiration/expiration scan, dual energy CT or photon counting CT can provide functional indicators. These functional analysis offers regional measures of lung dynamics, assessment of functional small airways disease, and regional ventilation-perfusion matching (V/Q).

In the near future, quantitative dual energy CT imaging may become a practical tool in clinical settings for assessing COPD and asthma, assessing disease progression and predicting treatment response.

S2-3 Proton MRI for COPD

Mark Oliver Wielpütz

Department of Diagnostic and Interventional Radiology, Heidelberg University Hospital

Magnetic resonance imaging (MRI) has emerged as a new modality for lung imaging recently, with airway diseases such as cystic fibrosis being the most accepted indications for clinical routine imaging. Beyond being a substitute for X-ray and computed tomography (CT), MRI combines morphologic and functional information more consequentially than any other technologies. Morphological sequences for proton MRI suitable for airways disease are available, but the focus will be on functional techniques that have been introduced into clinical routine imaging, or are most advanced in scientific studies. These are dynamic contrast-enhanced perfusion MRI, T1-mapping, and non-contrast ventilation and perfusion MRI, which allow for a regional analysis of lung function. Recently, MRI angiography complements these techniques for detection of bronchial artery dilatation. It has been shown that MRI may sensitively detect changes in lung morphology related to large airways disease such as airway wall thickening, bronchiectasis, mucus plugging or tracheobronchomalacia with lower resolution than CT, but with similar clinical impact. Ventilation abnormalities attributable to small airways disease are closely linked to subsequent perfusion changes, which can be sensitively detected by dynamic contrast-enhanced perfusion MRI. By a combination of morphological with functional techniques, MRI has the potential to specifically differentiate reversible from irreversible lung changes especially in airway diseases such as COPD and cystic fibrosis. This makes MRI an important modality for non-irradiating regional disease monitoring and therapy follow-up. Subsequently, it has now been used as an endpoint in pioneer clinical trials.

S2-4 Pulmonary Imaging of Airway Remodeling in Asthma and response to therapy

Grace Parraga

Robarts Research Institute, Western University

Despite inhaled corticosteroid/long-acting beta-2-agonist (ICS/LABA) therapy, 30-50% of participants with asthma remain poorly controlled. Inhaled ICS/LABA in combination with a long-acting muscarinic antagonist (LAMA) was demonstrated to significantly improve forced expiratory volume in 1-second (FEV1) and disease-control after 24 weeks of treatment, compared to ICS/LABA alone. Whilst the addition of LAMA to ICS/LABA is known to target the smooth muscle, the influence of once daily combined ICS/LABA/LAMA on small-airways dysfunction and its relationship to pathologies downstream from type-2 airway inflammation, like airway functional abnormalities and occlusions, has not been definitively ascertained. Imaging biomarkers including those provided by computed tomography (CT) and pulmonary functional magnetic resonance imaging (MRI) using inhaled hyperpolarized ¹²⁹Xe gas, have emerged in small focused studies of asthma patients and asthma therapy studies. Recently, CT-measured airway mucus-occlusions have been linked to asthma severity and MRI ventilation defects. In patients with asthma, pulmonary functional MRI detects and quantifies airway dysfunction as MRI ventilation defect percent (VDP) which is spatially and quantitatively related to CT airway abnormalities, biomarkers of type-2 inflammation, mucus-occlusions and poor disease control. To provide mechanistic insights on the effect of ICS/LABA/LAMA on small-airways dysfunction, we quantified ¹²⁹Xe MRI ventilation defects following 6- and 12-weeks fluticasone-furoate/umeclidinium/vilanterol (FF/UMEC/VI 200/62.5/25µg) treatment. We also examined whether type-2 inflammation measured using fraction of exhaled nitric oxide (FeNO), blood eosinophils and CT airway mucus-occlusions, influenced treatment response.

S2-5 Reversibility study in healthy, COPD, and asthma subjects with 3D MR spirometry

Ithar Gharmaoui¹⁾, Nathalie Barrau¹⁾, Adrien Duwat¹⁾, Angeline Nemeth¹⁾, Antoine Beurnier²⁾, Anna Reitmann¹⁾, Claire Pellot-Barakat¹⁾, Vincent Lebon¹⁾, Xavier Maitre¹⁾

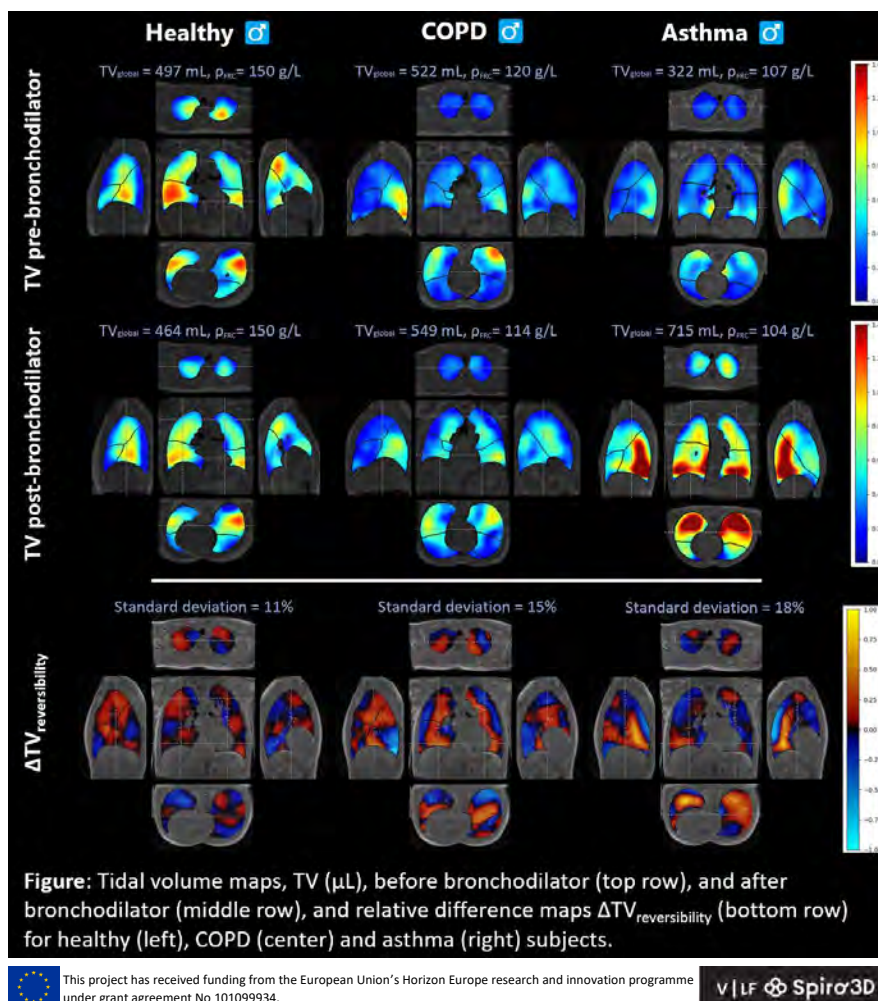
1) Université Paris-Saclay, CEA, CNRS, Inserm, BioMaps, Orsay, France

2) Department of Physiology and Functional Explorations, Hôpital Bicêtre, APHP Paris, Kremlin-Bicêtre, France

Three-dimensional MR spirometry produces voxel-wise flow-volume loops, allowing the assessment of local ventilation in the lung over a 10-minute 3D UTE MRI acquisition while the patient is lying in supine position and freely breathing. The bronchodilator reversibility was assessed regionally in one healthy, COPD, and asthma subject.

Lung density, ρ_{FRC} , was estimated from the MR magnitude images normalized over the segmented lung volume at the end of expiration. nnUNet segmentation was performed to the lobar level. Tidal volume maps, TV, were extracted and mean lobar and integrated lung TV values were computed. After morphological and feature scaling normalization, relative difference maps $\Delta \text{TV}_{\text{reversibility}}$ were computed before and after bronchodilator administration to highlight gas redistribution.

The global ρ_{FRC} was found rather constant for each subject over acquisitions: $155 \pm 2 \text{g}\cdot\text{L}^{-1}$ in healthy, and lower values, $117 \pm 4 \text{g}\cdot\text{L}^{-1}$ in COPD, and $104 \pm 3 \text{g}\cdot\text{L}^{-1}$ in asthma, reflecting possible gas trapping in patients. After bronchodilator, $\text{TV}_{\text{global}}$ barely changes for healthy (-6.6%) and COPD (+5.2%) whereas it increases significantly for asthma (+121.7%). $\Delta \text{TV}_{\text{reversibility}}$ maps show greater gas redistribution in asthma and in COPD than in healthy: standard deviations in the left and right inferior lobes reach 27% and 19% in asthma, 21% and 13% in COPD, and 11% and 12% in healthy subjects. $\text{TV}_{\text{global}}$ increased in asthma and remained constant in COPD as expected in reversibility test. Locally, larger lobar TVs were found with enhanced values in the inferior lobes in asthma and COPD. In COPD, bronchodilator response seems to be positive at lobar level with large gas redistribution.



This project has received funding from the European Union's Horizon Europe research and innovation programme under grant agreement No 101099934.

v|f Spiro3D

S2-6 Data Homogenization with Sequence-to-Sequence GAN Mapping improves Comparability of PREFUL MRI

Andreas Voskrebenzev^{1,2)}, Jonah Hahn¹⁾, Maximilian Zubke^{1,2)}, Filip Klimes^{1,2)}, Marius Wernz^{1,2)}, Robin Mueller^{1,2)}, Frank Wacker^{1,2)}, Jens Vogel-Claussen^{1,2)}

1) Institute of Diagnostic and Interventional Radiology, Hannover Medical School, Hannover, Germany

2) Biomedical Research in Endstage and Obstructive Lung Disease (BREATH), Member of the German Center for Lung Research (DZL), Hannover, Germany

Introduction

Free-breathing acquisition with proton MRI has gained popularity for assessing ventilation and perfusion without ionizing radiation, contrast media, or additional equipment. Typically, this involves either a balanced steady-state free precession (bSSFP) or spoiled gradient echo (SPGRE) sequence. While bSSFP offers superior signal-to-noise ratio (SNR) and strong perfusion contrast, SPGRE is less prone to artifacts and is suitable for field strengths beyond 1.5T. This study evaluates using generative adversarial networks (GAN) to convert perfusion results acquired with SPGRE to bSSFP-like results.

Methods

Retrospective analysis of 31 healthy volunteers scanned at 1.5T with lung-optimized bSSFP and conventional SPGRE was performed. Images were evaluated with Phase-Resolved functional lung (PREFUL) pipeline. 2D Perfusion maps (n=186) were assigned to training, validation or test (60/20/20%). GANs were trained following the Pix2Pix approach with additional structural similarity (SSIM) and edge loss functions.

Results

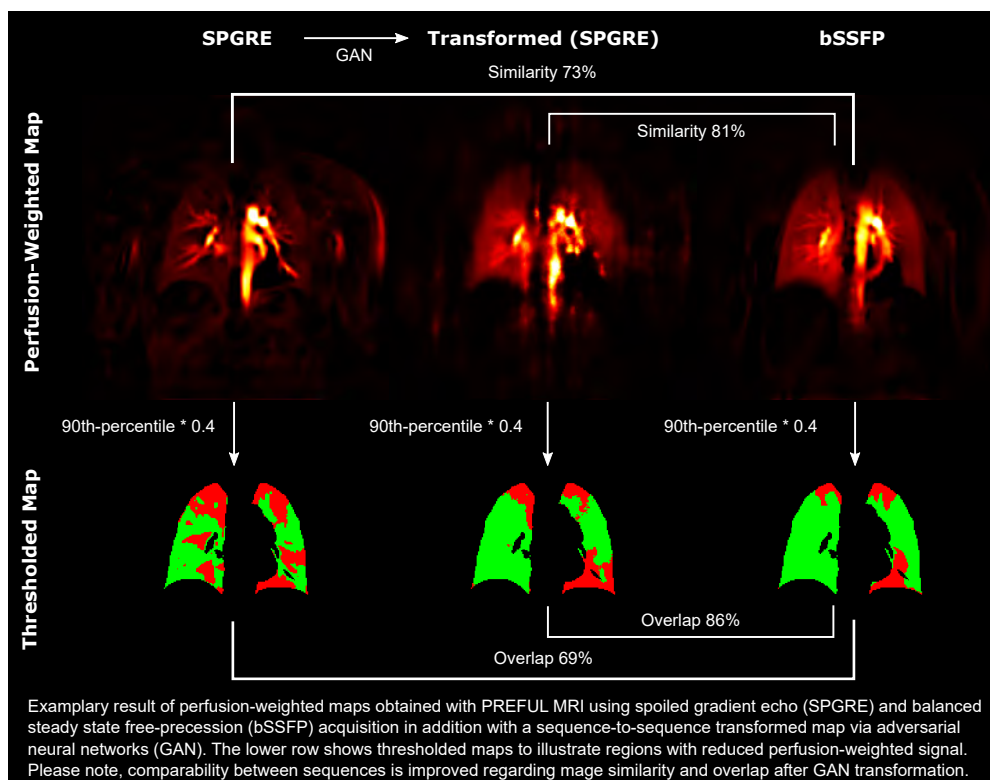
After sequence-to-sequence transformation, SSIM improved from 68% to 76% ($P < 0.001$) and total-overlap of perfusion defect maps from 79% to 84% ($P < 0.001$).

Discussion

Multi-center studies require delicate hardware and sequence protocols tuning, limiting technique dissemination. The lung-optimized bSSFP sequence, despite providing strong perfusion-weighted contrast at 1.5T, is not feasible at 3T. The presented results indicate that combining SPGRE acquisition with sequence-to-sequence transformation to bSSFP may mitigate these challenges. Further validation in patient data is necessary. Additionally, optimization of the training procedure (e.g. including cardiac-cycle phases) can be explored to further improve the transformation.

Conclusion

Homogenizing differently acquired free-breathing data with GANs can potentially yield more comparable results and combine the advantages of different sequences.



〈Session 3〉 Vascular Diseases

S3-1 Current management and molecular basis of pulmonary hypertension due to lung disease

Seiichiro Sakao

Department of Pulmonary Medicine, IUHW Narita Hospital/Department of Pulmonary Medicine, International University of Health and Welfare (IUHW), School of Medicine

The prognosis of pulmonary arterial hypertension (PAH) improved after the introduction of the current pulmonary vasodilator drugs. However, survival of patients with pulmonary hypertension (PH) due to lung disease remains poor despite advance in the vasodilator drug development, especially because there is no evidence from RCTs indicating that these drugs can improve symptoms or outcomes in patients with PH of this kind. Actually, the use of current vasodilator drugs is not approved for this PH. As is generally known, however, there should be patients with suspected PAH in addition to lung disease. These patients are probably diagnosed as PH which is attributable to lung disease. It is possible that current vasodilator drugs have an effect on suspected PAH with lung disease. Unfortunately, there is no way to make a distinction between patients with suspected PAH in addition to lung disease and with PH due to lung disease. For further improvement in mortality rate of PH of this kind, the understanding of more details of molecular basis is required. I am afraid that there should be the completely different basis between PH related idiopathic pulmonary fibrosis (IPF) and chronic obstructive pulmonary disease (COPD). Moreover, the development of method to differentiate patients to whom current vasodilator drugs are effective or ineffective is also required. Here we review the recent molecular and pathological concepts of PH due to lung disease and latest clinical trials. Subsequently, we explore the possibility of the differentiation strategies in accordance with hypoxic pulmonary vasoconstriction (HPV) and diffusion lung capacity for carbon monoxide (DLco).

S3-2 Dynamic Chest Radiography for vascular diseases

Yuzo Yamasaki

Department of clinical radiology, Graduate School of Medical Sciences, Kyushu University

The assessment of pulmonary perfusion is essential for many pulmonary diseases. Lung perfusion scintigraphy and contrast-enhanced computed tomography (CT) play important roles in these evaluations in clinical practice. However, the use of scintigraphy may be restricted owing to the prerequisite such as large sized facilities and equipment, or the difficulties in managing urgent examinations. Contrast-enhanced CT is a widely available and reliable method for most pulmonary vascular diseases; however, its use is occasionally limited because of the requirement of contrast media or high radiation doses. Dynamic chest radiography (DCR) is a novel imaging technique based on conventional X-ray technology that visualizes pulmonary perfusion without contrast media or radionuclides and requires a small space for installation and short examination time. At times, these benefits of DCR exert compelling effects. The utility of this promising technique has been demonstrated in phantoms, animals, and humans with various pulmonary diseases. Thus, evidence regarding DCR perfusion imaging has accumulated. This presentation aims to 1) explain the basic principles of lung perfusion assessment using DCR, 2) discuss the advantages of DCR over other imaging modalities, and 3) review multiple specific clinical applications of DCR for pulmonary vascular diseases and compare them with other imaging modalities.

S3-3 Dual-Energy CT imaging for vascular diseases

Yoshiyuki Ozawa

Department of Diagnostic Radiology, Fujita Health University

Dual-energy computed tomography (DECT) can differentiate materials by using two different X-ray energy spectra, and provide new imaging techniques to diagnostic radiology to overcome the limitations of conventional CT in characterizing tissue. Some techniques have used dual-energy imaging, including dual-source, rapid kVp switching, dual-layer detectors, and split-filter imaging. In iodine images, images of the lung's perfused blood volume (PBV) based on DECT have been applied in patients with pulmonary embolism (PE) to obtain both images of the PE occluding the pulmonary artery and the consequent perfusion defects in the lung's parenchyma. Lung PBV images also have the potential to indicate the severity of PE, including chronic thromboembolic pulmonary hypertension. Virtual monochromatic imaging, as another DECT-based application, can improve the accuracy of diagnosing pulmonary vascular diseases by optimizing kiloelectronvolt settings for various purposes.

S3-4 Advanced MRI methods for the diagnosis of Pulmonary Hypertension

Mark L. Schiebler

Department of Radiology, University of Wisconsin School of Medicine and Public Health School of Medicine

The role of MRA, MRI, MRS with Hyperpolarized Xenon ventilation will be discussed with respect to their roles in the workup of pulmonary hypertension. The follow-up after the initiation of therapy is also very important, as the return of right ventricular functional metrics is associated with longer survival.

S3-5 Pulmonary function evaluation using non-contrast-enhanced 3D ultrashort echo-time MRI

Jang-Yeon Park

Department of Biomedical Engineering, Sungkyunkwan University

Pulmonary function information including ventilation and perfusion are important for accurate assessment of the lungs, especially in the case of diffuse lung disease such as chronic obstructive pulmonary disease (COPD), asthma, and interstitial lung disease (ILD), which often develop into cardiopulmonary dysfunction. While pulmonary function test (PFT) is the most widely used test of the respiratory system and provides valuable measurements of ventilation, image-based pulmonary function evaluation using CT and SPECT has recently been proposed to provide regional information about ventilation and/or perfusion of the lungs. In particular, MRI is receiving increasing attention in pulmonary function assessment due to versatility in image contrast and no risk of radiation exposure. In this talk, I will first briefly review some of the existing MRI methods for evaluating pulmonary function, mainly those that do not use any exogenous contrast agents, including Fourier decomposition, PREFUL (Phase Resolved Functional Lung), and SENCEFUL (Self-gated Non-contrast-enhanced Functional Lung) imaging techniques. Then, I will introduce pulmonary function MRI methods using 3D perfusion-weighted mapping as well as 3D ventilation-weighted and ventilation flow capacity-weighted mapping, all of which can be obtained simultaneously from free-breathing non-contrast-enhanced 3D ultrashort-echo time (UTE) imaging.

S3-6 the usefulness of Volume Helical Shuttle Scan for whole lung dynamic study in hemoptysis patients

Toshihiko Sugiura^{1,2)}, Nobuhiro Tanabe^{1,2)}, Shun Imai¹⁾, Jun Nagata²⁾, Naoko Kawata¹⁾, Akira Nishiyama³⁾, Takuji Suzuki¹⁾

1) Department of Respiriology, Graduate School of Medicine, Chiba University.

2) Department of Respiratory Medicine, Chibaken Saiseikai Narashino Hospital

3) Department of Radiology, Chiba University Hospital

Purpose: To evaluate the usefulness of Volume Helical Shuttle Scan (VHSS) using 64-slice CT for whole lung dynamic study (4D study) in patients with hemoptysis.

Methods: This study included 13 patients (6 females, aged 33-84 years) who underwent a 4D study using VHSS with 64-slice CT, followed by angiography and embolization. We examined whether the diagnostic capability of CT for responsible vessels and bronchial artery-pulmonary artery (BA-PA) shunts matched the diagnosis by angiography.

Results: The underlying diseases included bronchiectasis in 7 cases, nontuberculous mycobacterial infection in 2 cases, aspergilloma in 1 case, and idiopathic in 3 cases. In all 13 cases, the bronchial artery (right in 6 cases, left in 7 cases) was identified as the responsible vessel. Additionally, the internal thoracic artery in 4 cases and the inferior phrenic artery in 2 cases were also identified as responsible vessels. All responsible vessels were diagnosed by CT. Furthermore, the shunt flow causing hemoptysis was confirmed by CT in all cases.

Conclusion: We previously reported the usefulness of 4D studies using 320-slice CT for patients with hemoptysis. VHSS showed no significant difference in the diagnostic capability for BA-PA shunts compared to 320-slice CT. While the 320-slice CT can capture only a 16 cm width, VHSS allows for whole lung imaging, enabling the diagnosis of responsible vessels other than bronchial arteries.

〈Session 4〉 Interstitial Pneumonia

S4-1 Recent Topics and Perspectives in the Clinical Practice of Interstitial Lung Disease

Tomohiro Handa

Department of Advanced Medicine for Respiratory Failure, Graduate School of Medicine, Kyoto University

In the diagnostic process of ILD, the importance of multidisciplinary discussion (MDD) has been recognized, and its methodology is being discussed. Cryobiopsy has become widespread and suggested in the official ATS/ERS/JRS/ALAT Clinical Practice Guideline on IPF as an alternative to surgical lung biopsy in experienced medical centers. Artificial intelligence (AI) is being incorporated into clinical practice, particularly in the areas of imaging and histological diagnosis based on gene expression patterns. Regarding the drug treatment of IPF, some recent clinical trials for novel drugs have failed to show their efficacy, but several clinical trials for promising drugs are now ongoing. The importance of family history, genetic background, and telomere length in ILD has been increasingly recognized in recent years. Familial pulmonary fibrosis generally has a poor prognosis and its clinical significance has been recognized. Recent studies have shown that shortened leukocyte telomere length is associated with poor prognosis in ILDs, and that immunosuppressive treatment worsens prognosis in patients with short telomeres. Accordingly, clinical significance of genetic testing and peripheral blood telomere length in ILD is increasing. In the future, AI technology is expected to contribute to personalized medicine and drug discovery by integrating data on clinical information, genetics, morphology, environmental factors, and lifestyle.

S4-2 Quantitative CT evaluation for interstitial lung disease

Jooae Choe

Department of Radiology, Asan Medical Center, University of Ulsan College of Medicine

Interstitial lung disease (ILD) includes a variety of lung disorders with different degrees of inflammation or fibrosis, requiring a combination of clinical, imaging, and pathologic data for evaluation. CT scans not only enable a noninvasive diagnosis of ILD but are also crucial for evaluating disease severity, tracking its progression, and observing treatment responses. However, traditional visual assessments of ILD with CT suffer from reader variability and quantitative analysis of chest CT has a growing role in the clinical evaluation and management of ILD. Automated quantitative CT (QCT) provides a more objective method by utilizing computer-based analysis to consistently assess and measure ILD. Technological advancements have markedly enhanced the accuracy and reliability of these measurements. This lecture will focus on the current status of CT quantification in ILD, tackle differences in clinical and research applications which makes the challenges for its implementation in clinical practice, and underline how machine learning and deep learning in quantitative imaging can enhance diagnosis and management of ILD by providing more accurate assessments. Finally, future directions for QCT in this field will be discussed.

S4-3 Update on Diagnostic Imaging of Fibrotic Interstitial Lung Diseases

Ryoko Egashira

Department of Radiology, Faculty of Medicine, Saga University

Guideline updates and current research topics on issues related to visual imaging assessment of interstitial pneumonia will be presented.

In 2022, new international guideline for IPF (an update) /Progressive Pulmonary Fibrosis (PPF) was published. While the IPF guideline were not expected to change drastically, the HRCT diagnosis added a confidence level in the prediction of a histological UIP pattern, and contents for "indeterminate for UIP" was modified. For the diagnosis of PPF, six findings are listed as 'radiological evidence of disease progression' and are part of the 'Definition of PPF'. Although the same criteria are proposed to assess the fibrotic progression beyond the etiological background, fibrosis tends to progress differently by the morphological pattern.

The trend towards higher resolution has been seen in clinical machines, with the introduction of ultra-high-resolution CT and photon-counting CT in recent years, enabling the clear evaluation of submillimetre structures. At the research level, a micro-CT has been used to evaluate frozen lungs extracted for transplantation with a spatial resolution of 0.08 mm for the whole lung, enabling the detection of early fibrosis that is not depicted by clinical CT. Hierarchical Phase-Contrast Tomography, a synchrotron radiation CT, was also developed, which enables to evaluate fibroblastic foci and the layered structure of the vascular wall with a spatial resolution of 0.020 mm for whole lungs and 0.002-0.005 mm for the selected zoomed areas.

S4-4 Interstitial Pneumonia and PET: Potential and Pitfalls

Munenobu Nogami

Department of Radiology, Kobe University Hospital/ Biomedical Imaging Research Center, University of Fukui

Positron emission tomography (PET), as an imaging biomarker, has been long studied as a tool for pathophysiological assessment and prediction of interstitial pneumonia. Fluorodeoxyglucose (FDG), a glucose metabolism imaging agent, has been the most extensively researched due to its accumulation in inflammatory cells. Several reports exist on predicting the risk of radiation pneumonitis by quantitatively evaluating FDG uptake in normal lungs. Other imaging modalities using different radiopharmaceuticals have also been studied, with recent reports highlighting the utility of FAPI (fibroblast activation protein inhibitor) PET for imaging fibroblasts. Since PET imaging is performed by respiratory-gating or respiratory-triggered acquisition, there are distinct pitfalls compared to CT imaging performed under inspiratory breath-hold conditions. Particularly, caution is needed in evaluating the posterior regions of lung fields, where gravitational effects may prominently coincide with sites of interstitial pneumonia lesions. While many studies evaluating interstitial pneumonia have utilized PET/CT systems, PET/MRI systems, which allow simultaneous acquisition under respiratory synchronization, also hold potential for assessing interstitial pneumonia. This presentation provides an overview of the utility of PET in interstitial pneumonia while also addressing pitfalls.

S4-5 Regional lung structure and function associated with 1-year decline in DLCO in IPF

Hongseok Ko¹, Jiwoong Choi², Sun Mi Choi³, Chang-Hoon Lee³, Kum Ju Chae⁴, Chang Hyun Lee³

- 1) Kangwon National University Hospital, Chuncheon
- 2) University of Kansas School of Medicine, Kansas City
- 3) Seoul National University Hospital, Seoul
- 4) Jeonbuk National University Hospital, Jeonju

Purpose

We characterized regional lung structure and function in idiopathic pulmonary fibrosis (IPF) patients with 1-year decline of diffusing capacity of carbon monoxide (DLCO) using quantitative inspiratory and expiratory computed tomography (CT) analysis.

Methods

Baseline and 1-year follow-up pulmonary function tests (PFTs) and baseline inspiratory and expiratory chest CT scans were collected from 51 IPF patients (71.5 ± 5.9 years) and 30 healthy controls (70.2 ± 5.2 years). Commercial and *in-house* quantitative CT (qCT) software provided segmentation and 113 quantitative regional lung structural-functional features. qCT features were compared between patients with 5% or more percent-predicted DLCO decline (IPF-A) and the rest (IPF-B). We evaluated severity and extent of pulmonary fibrosis in a subset of 38 patients, using a recently introduced four-point scale traction bronchiectasis honeycombing index (TBHI) on CT.

Results

Compared to IPF-B (n=25, 1 female), IPF-A (n=26, 4 females) had moderately greater normalized hydraulic diameter (D_h^*) at right lower lobe (RLL) segmental airways (9.3%, p=0.038). Interestingly, IPF-A had less baseline high attenuation area percent (HAA%) in the RUL (-5.8%p, p=0.004) and RLL (-9.2%p, p=0.013) and greater anisotropic deformation index (ADI, 31.2%, p=0.045) and relative displacement (26.2%, p=0.046) in LLL, indicating relatively preserved lung motion. Demographics, PFTs and TBHI were not significantly different at baseline.

Conclusion

IPF patients with a 1-year decline in DLCO had right lower lobe segmental airway dilatation at baseline and greater relative motion in the LLL. RLL segmental airway diameter may be a potential imaging biomarker for rapid decline in gas exchange, possibly indicating fibrosis near proximal airways.

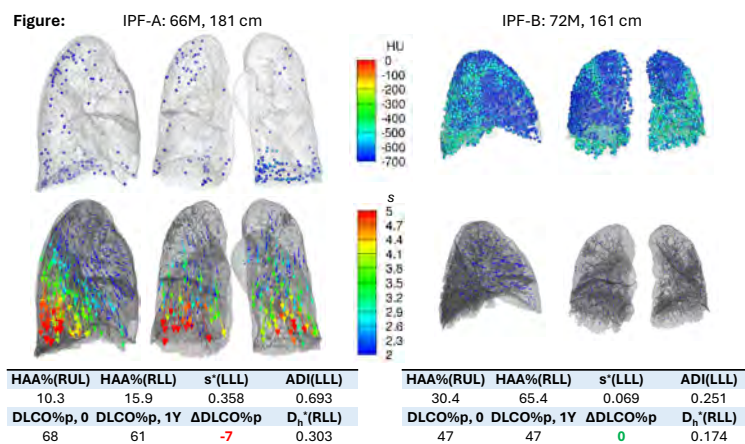


Table: Differences between IPF-A (5% or more DLCO decline) and IPF-B

Variables	Total (n = 51)	IPF-A (n = 26)	IPF-B (n = 25)	p-value	Normal (n=30)
Change in DLCO, % pred, 1-yr	-4.5 ± 7.4	-9.8 ± 5.1	1.1 ± 7.4	<0.001	
HAA% in RUL	14.6 ± 7.0	11.9 ± 3.9	17.5 ± 8.3	0.004	8.3 ± 5.1
HAA% in RLL	28.8 ± 14.1	24.0 ± 9.6	33.8 ± 16.4	0.013	13.9 ± 14.8
ADI in LLL (anisotropic deformation index)	0.51 ± 0.25	0.57 ± 0.27	0.44 ± 0.20	0.045	0.48 ± 0.19
s* in LLL (normalized 3D local lung displacement)	0.263 ± 0.109	0.294 ± 0.116	0.232 ± 0.095	0.046	0.280 ± 0.105
D _h * in sRLL (normalized hydraulic diameter)	0.248 ± 0.037	0.259 ± 0.037	0.237 ± 0.033	0.038	0.219 ± 0.034
TBHI (traction bronchiectasis honeycombing index)	TBHI-1: n = 5, 13% TBHI-2: n = 16, 42% TBHI-3: n = 17, 45%	TBHI-1: n = 2, 11% TBHI-2: n = 7, 37% TBHI-3: n = 10, 53%	TBHI-1: n = 3, 16% TBHI-2: n = 9, 47% TBHI-3: n = 7, 37%	0.402	
FVC, % predicted	82.7 ± 19.0	84.3 ± 15.5	80.9 ± 22.2	0.528	
Age, years	71.5 ± 5.9	70.1 ± 5.5	72.8 ± 6.0	0.102	70.2 ± 5.2
Height, cm	164 ± 6.3	163 ± 6.5	165 ± 6.2	0.269	162 ± 9.8
Body weight, kg	68.1 ± 9.7	67.0 ± 10.1	69.2 ± 9.3	0.419	67.6 ± 11.0

S4-6 Projected lung area on dynamic chest radiography as an index of lung fibrosis

Takeshi Kubo¹⁾, Takuya Hino²⁾, Akinori Tsunomori³⁾, Akinori Hata⁴⁾, Noriaki Wada^{2,5)}, Vladimir Valtchinov⁵⁾, Yusuke Yokota¹⁾, Seishu Hashimoto⁶⁾, Masakuni Ueyama⁶⁾, Masako Ueyama⁷⁾, Atsuko Kurosaki⁸⁾, Hiroto Hatabu⁵⁾, Shoji Kudoh⁹⁾, Takashi Hajiro⁶⁾, Yoshio Taguchi⁶⁾, Satoshi Noma¹⁾

- 1) Department of Radiology, Tenri Hospital
- 2) Department of Clinical Radiology, Graduate School of Medical Sciences, Kyushu University
- 3) Medical Imaging R&D Center, Healthcare Business Headquarters, KONICA MINOLTA, INC.
- 4) Department of Radiology, Graduate School of Medicine, Osaka University
- 5) Center for Pulmonary Functional Imaging, Department of Radiology, Brigham and Women's Hospital and Harvard Medical School
- 6) Department of Respiratory Medicine, Tenri Hospital
- 7) Department of Health Care, Fukujuji Hospital, Japan Anti-Tuberculosis Association
- 8) Department of Diagnostic Radiology, Fukujuji Hospital, Japan Anti-Tuberculosis Association
- 9) Department of Respiratory Medicine, Fukujuji Hospital, Japan Anti-Tuberculosis Association

Objectives: To evaluate the correlation between the projected lung area (PLA) using dynamic chest X-ray (DCR) and pulmonary function and determine if we can use DCR as an index of lung volume.

Materials and Methods: This retrospective study included 149 interstitial pneumonia patients and 149 sex-matched healthy volunteers who underwent posteroanterior chest DCR examination. IP patients were divided into two classes (percent predicted vital capacity $\geq 80\%$, and percent predicted vital capacity $< 80\%$). DCR acquisition sequences included a full expiratory motion from maximal inspiration at 0.667 seconds/frame. PLA was defined as an area within the contour of the automatically segmented lungs. Δ PLA was defined as the difference in PLA between full inspiration and expiration. Slope and intercept were calculated with an expiratory time-PLA curve by linear approximation. The Spearman's correlation coefficients of PLA, Δ PLA, slope, and intercept with demographics and pulmonary function test values were calculated.

Results: PLA at the full inspiration and expiration, Δ PLA, slope, and intercept differed among volunteers, normal VC patients, and abnormal VC patients ($p < .001$). Vital capacity had a strong positive correlation with intercept and PLA of both lungs at full inspiration ($p < .001$; correlation coefficients, .738 and .739. PLA in the left and right lungs strongly correlated with inspiration and expiration ($p < .001$; correlation coefficients, .804 and .838).

Conclusions: PLA demonstrated a strong positive correlation with vital capacity in a combined population of normal volunteers and interstitial pneumonia patients, suggesting the feasibility of PLA-based estimation of lung fibrosis severity.

〈Session 5〉 New Modality

S5-1 Upright Area-Detector CT: Initial Experience and Potentials for Pulmonary Functional Imaging

Yoshiharu Ohno

Department of Diagnostic Radiology, Fujita Health University School of Medicine

Since clinical setting of computed tomography (CT), several vendors had been tried to apply upright CT with sitting position as well as conventional supine CT. However, whole-body imaging has been difficult to perform by previously reported upright CT until 2017. Then, Canon Medical Systems has been introduced commercially available upright CT, and Fujita Health University Hospital has installed it and fully applied in not only routine clinical practice, but also CT screening for various academic and clinical aims since 2023. The upright CT was developed based on 3rd generation of area-detector CT (ADCT: Aquilion ONE/ Genesis Edition) and obtain routine CT images with similar noise characteristics and spatial resolution of upright ADCT and considered as comparable to those of conventional supine ADCT. On this upright CT, patients has no need to lie on the patient table of CT and access to CT system similar to chest radiograph. Moreover, patient's organs as well as different body compositions are physiologically moved or have influence of gravity. Furthermore, all subjects can fully inspire or expire to obtain CT images. In this lecture, we present 1) preliminary experience of upright ADCT in different chest diseases, 2) influence of gravity to lung and mediastinal structures, and 3) differences of quantitatively assessed chest motion from paired inspiratory-expiratory ADCT between upright and conventional supine ADCT in patients with different chest diseases.

S5-2 Comprehensive assessment of pulmonary morphology and function with Photon counting CT

Hoehn-Oh Shin

Institute of Diagnostic and Interventional Radiology, Hannover Medical School

A photon-counting CT protocol will be presented that allows for a dose-efficient and robust simultaneous assessment of lung morphology, ventilation, vasculature and parenchymal perfusion. The protocol includes a paired inspiration/expiration scan with the administration of an intravenous contrast agent in the inspiration scan and a delay of 5 minutes in the expiration scan. Spectral post-processing generates 6 additional data sets: ventilation, perfusion, late contrast enhancement, CT angiography and virtual non-contrast images in inspiration and expiration for CT densitometry. The protocol is applicable in a routine clinical setting without the need for additional hardware.

The proposed protocol is dose efficient (mean CT dose index for inspiration / expiration: 3.22 mGy / 3.09 mGy), and robust with a > 92% success rate. Its application in routine clinical practice in patients with interstitial lung disease and chronic thromboembolic pulmonary hypertension will be demonstrated and initial results discussed.

S5-3 High-Spatial-Resolution CT with Energy Integrated Detector

Ho Yun Lee

Department of Radiology, Samsung Medical Center, Sungkyunkwan University School of Medicine

High-spatial resolution (HSR) CT has the potential to narrow the gap between conventional CT and histologic examination with better visualization of the secondary pulmonary lobule and the in vivo changes of various pathologies such as interstitial lung disease or lung cancer. However, the improved spatial resolution comes at the cost of increased radiation dose, and the question remains whether that cost is justified by the added value provided by this technologic advancement. In this regard, software-based approaches, such as image filtering and iterative reconstruction algorithms, to reduce radiation dose without affecting image quality and interpretation should be coupled with implementation of this technology. This talk will review the current status of HSR CT, thereby highlighting its potential for providing more opportunity for this technology and its true value.

S5-4 Low-Field MRI

Jens Vogel-Claussen

Institute of Diagnostic and Interventional Radiology, Hannover Medical School

High-performance low-field MRI systems will enable sophisticated diagnostic exams that have previously been difficult to perform. This new technology has important implications for the diagnosis and monitoring of pulmonary diseases, as well as our understanding of these diseases. Because MRI is free of ionizing radiation, the ability to obtain high-quality MR images of the lung could be particularly important for pediatric lung imaging.

S5-5 Dark-field Radiographs for the Detection of Pneumothoraces

Henriette Bast^{1,2,3}, Florian T. Gassert³, Lennard Kaster^{1,2,3}, Maximilian Lochschmidt^{1,2,3}, Thomas Koehler^{4,5}, Ariane Keppler³, Alexander W. Marka³, Manuel Steinhardt^{3,6}, Andreas Sauter³, Daniela Pfeiffer^{3,4}, Franz Pfeiffer^{1,2,3,4}

- 1) Department of Physics - TUM School of Natural Sciences - Technical University of Munich
- 2) Munich Institute of Biomedical Engineering - Technical University of Munich
- 3) Department of Diagnostic and Interventional Radiology - Klinikum Rechts der Isar - Technical University of Munich
- 4) Institute of Advanced Study - Technical University of Munich
- 5) Philips Innovative Technologies
- 6) MVZ Neumaier & Kollegen

Introduction

X-ray dark-field imaging is an imaging technology that uses small-angle scattering to visualize the structural integrity of human lungs.

Methods

In this prospective study, participants were included if they were diagnosed with a pneumothorax or if they had no pathologic lung changes according to their chest CT. All participants were imaged at a clinical prototype for dark-field chest radiography that provides both attenuation and dark-field images of the human chest. Both image contrasts were fused to create an overlay image. In a reader study, three radiologists assessed the attenuation images individually and in random order. They were asked if a pneumothorax was present and if yes, to specify its location. Multiple weeks later, this study was repeated: this time, the readers could switch the overlaid dark-field signal on and off to see additional image contrast. In both cases, the reading time per patient was measured.

Results

The study group consisted of a total of 100 patients (61 men), including 36 pneumothorax patients. When the overlay images were available, the radiologists needed 1.5 to 3 times less time to assess the 100 patients than when they only saw the attenuation images. Due to the overlays, the time for the image assessment dropped significantly for each reader, while the reader's sensitivity and specificity remained either constant or improved.

Conclusion

Dark-field images can improve and accelerate the diagnosis of pneumothoraces.

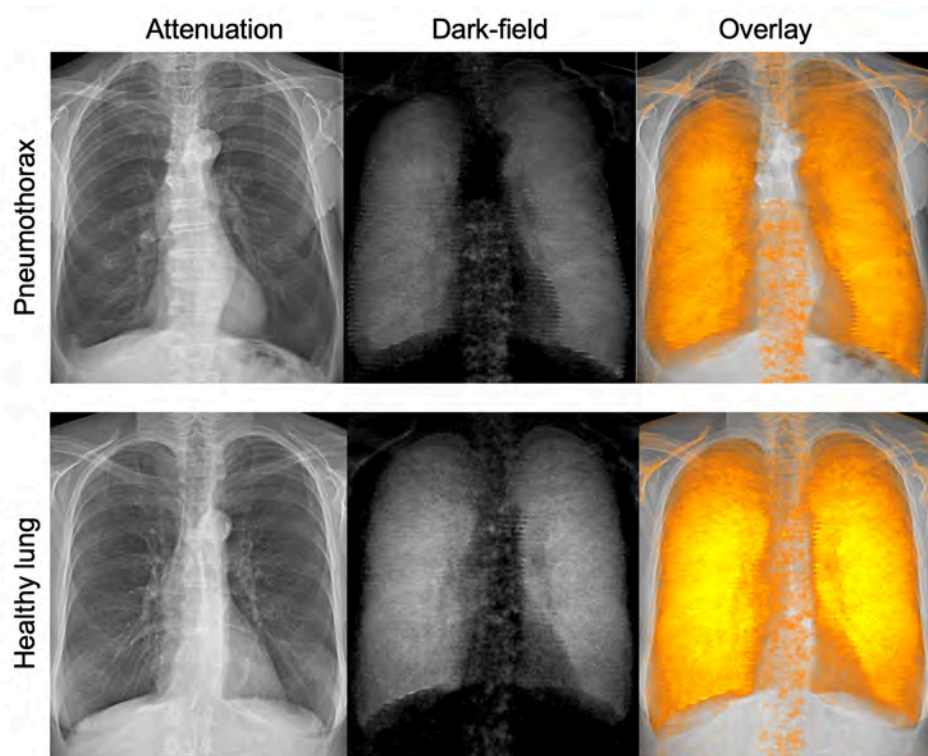


Fig. 1: Attenuation, dark-field, and overlay images for a patient with pneumothorax and without. The overlay was created by combining the attenuation and a colored version of the dark-field image.

S5-6 Synchrotron radiation-based CT for Ultra-High Resolution and Multiscale Lung Imaging

Willi L Wagner^{1,2)}, Christian Dullin^{1,2)}, Giuliana Tromba³⁾, Marco Confalonieri⁴⁾, Mark O Wielpuetz^{1,2)}, Juergen Biederer^{1,2)}, Hans-Ulrich Kauczor^{1,2)}

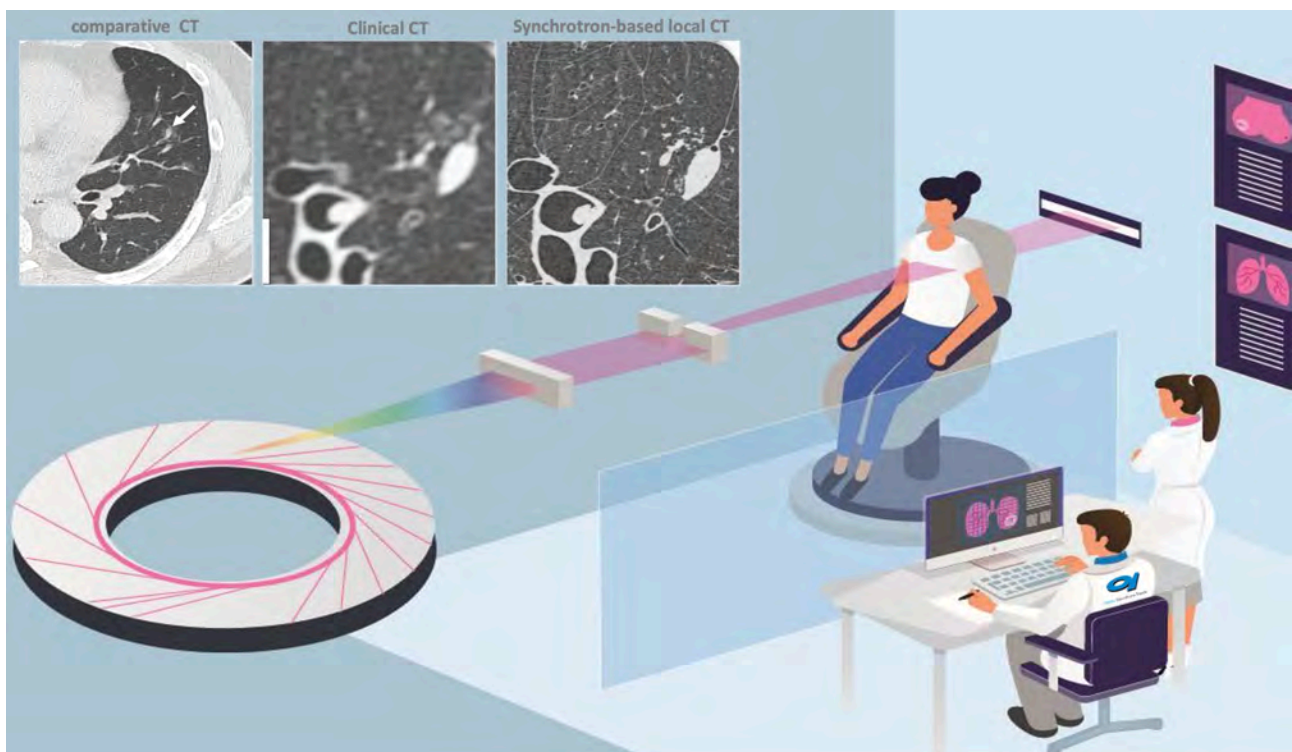
1) Department of Diagnostic and Interventional Radiology, University Hospital Heidelberg, Germany

2) Translational Lung Research Center, Heidelberg, Germany

3) Elettra-Sincrotrone Trieste, Trieste, Italy

4) Pulmonology Unit, University Hospital of Cattinara, Trieste, Italy

Synchrotron radiation-based Computed Tomography (SR-CT) has emerged as a powerful tool for achieving ultra-high resolution and multiscale imaging of lung structures. This advanced imaging technique utilizes synchrotron radiation, generated by high-energy particle accelerators, to produce X-rays of exceptional intensity and coherence. Through innovative imaging algorithms and specialized detectors, SR-CT offers unprecedented spatial resolution, enabling the visualization of intricate details within lung tissues at the micron scale, holding promise for diagnostic applications in patients. This talk explores the advancements and applications of SR-CT in lung imaging, emphasizing its ability to provide ultra-high spatial resolution and contrast sensitivity, crucial for visualizing intricate pulmonary structures at various scales. By leveraging the unique properties of synchrotron radiation, SR-CT surpasses the limitations of conventional CT imaging, particularly in differentiating soft tissues and elucidating subtle structural variations associated with lung diseases. Synchrotron radiation-based CT represents a transformative approach to lung imaging, offering unparalleled resolution and sensitivity for the comprehensive assessment of pulmonary structure and pathologies that affect lung structure, such as emphysema, fibrosis, and lung cancer. Despite notable progress, challenges remain in translating SR-CT from research laboratories to clinical settings, including accessibility, radiation dose considerations, and workflow integration. Nevertheless, ongoing developments in synchrotron facilities, imaging algorithms, and international collaboration between multidisciplinary teams hold promise for realizing the diagnostic potential of SR-CT in patient care.



〈Session 6〉 Special Session

S6-1 Basics of Pulmonary Physiologic Imaging

Eric A. Hoffman

Department of Radiology, University of Iowa Carver College of Medicine

Functional CT of the lung has emerged from quantitative CT (qCT). Structural details extracted at multiple lung volumes offer indices of function. With the emergence of dual energy CT (DECT), function is tagged via use of contrast agents. Lung disease phenotypes have previously been lumped together by the limitations of spirometry and plethysmography. Functional CT offers regional measures of lung mechanics, the assessment of functional small airways disease, as well as regional ventilation-perfusion matching (V/Q) and more. Reductions in radiation dose by an order of magnitude or more have been achieved. At the same time, we have seen significant increases in spatial and density resolution. Together, these have allowed attention to turn towards more mild forms of disease and younger populations. Recently, it has been demonstrated that risk of COPD is associated with airway branching patterns and airway dysanapsis. Additionally, there are hints that airway dysanapsis may be accompanied by pulmonary vascular dysanapsis. Metrics used to characterize the lungs in more advanced COPD (texture assessed broncho-vascular prominence, DPM-based (image matching) air trapping and small-vessel-to-total-vessel volume) have now been shown to correlate with early lung function decline. DECT methods for assessing ventilation/perfusion (V/Q) allow for the regional quantitation of shunt and functional dead space which are increased in smokers and reduced via a single dose of sildenafil. Through examples, this talk will focus on the use of quantitative/functional CT for the non-invasive exploration of the lung within the unique negative pressure intrathoracic environment of the closed chest.

Expanded from: Hoffman EA. Origins of and lessons from quantitative functional X-ray computed tomography of the lung. *Br J Radiol.* 2022 PMID: PMC9153696.

S6-2 Pulmonary Functional CT

Hans-Ulrich Kauczor

Department Diagnostic and Interventional Radiology, Heidelberg University/ German Center for Lung Research

Current developments and expected innovations in CT are huge. They facilitate many applications of quantitative, ultra-high resolution, ultra-low dose and dynamic CT, and thus functional CT. Reduction of noise using iterative reconstructions and AI are providing a much better basis for (AI-enhanced) software aiming at segmentation of the tracheobronchial tree as well as quantitation of emphysema and interstitial lung abnormalities and fibrotic disease. Additionally, the new generation of CT scanners allow for the acquisition of ultra-high resolution images (higher matrix size). Multi-energy (spectral) and photon counting CT offer many more opportunities for functional CT, esp. with regard to ventilation / perfusion imaging by using paired inspiratory/expiratory acquisitions. Tools for rigid and non-rigid registration are a prerequisite for many of these applications. The wish to investigate lung function in the physiological erect position will be met by the first upright CT scanners. Furthermore, darkfield radiography holds a lot of promise. This technology is already available in the micro-CT avenue and might become available on human CT scanners in the near future. Synchrotron CT offers unique potential with regard to ultra-high resolution. Currently it is restricted to phantoms and small samples. However, extension to human size and human application is expected in the future.

S6-3 Artificial Intelligence for Pulmonary Functional Imaging

Edwin J.R. van Beek

Edinburgh Imaging QMRI, University of Edinburgh

Artificial Intelligence (AI) is making rapid inroads in the field of Radiology, and more so in Thoracic imaging than in any other field. Most of the tools developed thus far have focused on three main topics: chest radiography detection of abnormalities and triage of normal; chest CT diagnosis of lung nodules, as well as associated clinical support using volume and guidelines; chest CT diagnosis of pulmonary embolism. We should recognise that NONE of these tools currently are cleared to work independently and these applications are all used as a secondary viewer (although the chest radiography triage system is closest to independent review by selecting out normal cases).

As we are moving forward, there are several options that are coming into view for functional lung imaging, which will be a significantly more challenging area to develop given the complexities that will be inherent into this.

Many options are at an exploratory phase, but may be grouped according to the following: Anatomical analysis (segmentation of organs, bolus passing through heart/lungs/blood vessels); Functional (tracking of moving organs, e.g. lungs/heart/diaphragm/chest wall) and Quantification (automated volumetry of chest/native lungs/perfused lungs/ventilated lungs).

Last but not least, we should not underestimate the potential of AI as a background support, for instance helping with scheduling, preprocedural patient set-up and positioning, postprocessing, administrative tasks, and workflow management.

Clearly, the road for AI development into the domain of functional lung imaging is still a long way one, but experience with previous developments will surely add to the speed with which these systems can be developed. The ultimate aim will be to develop, validate and prospectively assess the value of such tools.

〈Session 7〉 How to apply AI to lung diseases

S7-1 Fundamentals of Artificial Technology and Its Application to Pulmonary Imaging

Atsushi Teramoto

Faculty of Information Engineering, Meijo University

Artificial intelligence (AI) has made rapid strides in recent years, becoming an indispensable technology in our daily lives. Its significance in the medical field is particularly notable, with applications featuring high performance in pulmonary imaging, including imaging techniques, lesion detection, and classification techniques. The algorithms used in them have evolved from artificial neural networks based on the structure of our biological neural networks to convolutional neural networks that mimic the functionality of our vision, thus enhancing image recognition capabilities. In addition, technologies based on attention mechanisms have been developed. It has not only had great success in natural language processing, but has also been found to perform well when incorporated into image recognition. Also, image generation technology is one of the most successful AI applications for image processing in recent years, with the emergence of generative adversarial networks (GANs) enabling image generation and transformation. Recently, diffusion models inspired by diffusion phenomena in gases and liquids have been introduced, demonstrating the production of higher-quality images compared to GANs. In this presentation, I will share some fundamental technologies and progresses in AI, followed by several AI research case studies in respiratory imaging.

AIの基礎と呼吸機能イメージングへの応用

寺本 篤司

名城大学 情報工学部 情報工学科

人工知能は近年急速に進歩を遂げ、現在では日常生活の中で欠かせない要素技術となっている。医療分野でもその有用性は高く、呼吸器のイメージングに関しても撮像技術、病変検出技術、鑑別技術について高い性能を有するアプリケーションが登場している。それらの技術で利用されているアルゴリズムは、我々の神経回路網の構造に基づき作られた人工ニューラルネットワークから始まり、我々の視覚のはたらきを模した畳み込みニューラルネットワークが登場して画像認識能力が高まった。さらに2020年代からは Attention 機構をベースとした技術が自然言語処理を中心に開発され、画像認識にも取り入れられた。画像生成技術は最近の AI 特有のアプリケーションであるが、敵対的生成ネットワークが登場して画像生成や画像変換が可能となった。最近は気体や液体の拡散現象をヒントにして作成した拡散モデルが登場し、GAN に比べて高品位な画像が得られることが示された。本講義では、これら AI の基礎的技術やその変遷を解説したあと、その呼吸器イメージングへの応用事例について私の研究グループの成果を中心に紹介する。

S7-2 Towards routine quantitative lung imaging with artificial intelligence

Joon Beom Seo

Department of Radiology, University of Ulsan College of Medicine, Asan Medical Center

Although many research papers showed that quantitative lung imaging of lung cancer, COPD, ILD is useful in the diagnosis and management of diseases, implementation of quantification in real clinical practice is limited. It is caused by several technical factors such as long procession time, requirement of human interaction, and measurement variations. These technical issued can be solved at least partly by the applying deep learning-based algorithms. AI algorithms can remove the human interaction steps, so that quantification can be done in the background automatically. AI based image conversion can reduce the measurement variation significantly. The application of these quantification methods will lead us to the era of thoracic imaging bigdata. One of potential new application will be content-based image retrieval, which is searching for the case of similar disease patten in the imaging bigdata. Initial study showed the providing the confirmed casred of similar disease pattern increase the initial diagnosis of IIP.

S7-3 Current Situation and Future Direction of CAD and AI in Pulmonary Diseases

Yoshiharu Ohno

Department of Diagnostic Radiology, Fujita Health University School of Medicine

Many investigators have suggested that artificial intelligence (AI) for pulmonary diseases is as useful as well as computer-aided diagnosis (CAD) including computer-aided detection (CADE), computer-aided diagnosis (CADx), computer-aided volumetry (CADv) or computer-aided simple triage (CAST). Since 2004, Canon Medical Systems Corporation and we are developing and providing academically or commercially available CADE for CT lung cancer screening and CADx for COVID-19 pneumonia, CADv for lung nodule management and CAST for management of interstitial lung diseases as well as other parenchymal diseases based on glossary of terms for thoracic radiology recommended from the Nomenclature Committee of the Fleischner Society. In this lecture, I will present 1) state of the art CAD and AI systems for pulmonary diseases developed and provided with Canon Medical Systems and 2) future direction of CAD and AI for pulmonary diseases.

呼吸器疾患における CAD および AI の現状と将来展望

大野 良治^{1,2)}

- 1) 藤田医科大学 医学部 放射線診断学
- 2) 藤田医科大学 医学部 先端画像診断共同研究講座

呼吸器疾患におけるコンピュータ支援診断 (Computer-Aided Diagnosis: 以下 CAD) には Computer-Aided Detection (以下: CADE)、Computer-Aided Diagnosis (以下 CADx) と Computer-Aided Volumetry (以下: CADv) が提唱されてきたが、近年 Computer-Aided Simple Triage (以下 CAST) が新たに加えられた。同様の目的で CT などの画像診断を目的にした人工知能 (Artificial Intelligence: 以下 AI) に関しては同様の CADE, CADx, CADv や CAST を目的としたものと生成系 AI を用いたものが近年様々な領域で開発及び応用が試みられている。

我々はキヤノンメディカルシステムズ株式会社と 2004 年以来 CAD の開発を肺結節などを皮切りに開始し、2023 年に欧州での認証を得て販売開始するとともに、2022 年には COVID-19 診断用 CADx としての AI ソフトを国内で承認を得て販売し、臨床応用を行った。あわせて、肺結節診断および経過観察用の CADv およびその発展形である AI 併用 CADv や肺野における CT 所見を The Fleischner Society の CT 所見用語に基づき分類し、様々な呼吸器疾患の診断および患者マネージメントに応用可能な基本 AI ソフトも開発し、今後 CADx や CAST として臨床応用を試みている。本講演では呼吸器疾患の CT 検査における CAD および AI の現状と将来展望に関して述べる。

S7-4 Potential and Prospects of Chest Imaging using AI from Respiratory Physician's Perspective

Toyohiro Hirai

Department of Respiratory Medicine, Kyoto University

AI technology has advantages in recognizing and discriminating forms that are difficult to verbalize and has been applied to image analysis in the field of medicine. Especially in chest imaging, chest X-ray and CT examinations are often performed in medical examinations, requiring diagnosis of a large number of images in a limited time. In addition, it is also an essential part of respiratory medicine, including diagnosis and treatment evaluation of pulmonary diseases. Thus, clinical application of image analysis using AI technology is expected to assist physicians in diagnosis, equalize medical care, avoid diagnostic errors, and reduce the workload of medical staff. Moreover, the possibility of recognizing differences in shadow patterns that cannot be distinguished visually may lead to the proposal of new disease classifications based on image findings. In this presentation, the possibilities and prospects of AI technology for thoracic imaging diagnosis will be discussed using the example of automatic recognition and quantification of various parenchymal patterns in CT chest images of interstitial lung diseases, which were developed in collaboration with industry.

呼吸器内科医から見た AI による胸部画像診断の可能性と展望

平井 豊博

京都大学大学院医学研究科 呼吸器内科学

AI 技術は言語化が困難な形態の認識や弁別に利点を持ち、医療の分野でも画像解析に応用されている。特に胸部画像においては、検診で胸部 X 線や CT 検査が行われ、限られた時間で多数例の画像診断を要する機会も多く、また、呼吸器診療においても、疾患の診断や治療評価など不可欠な検査の一つとなっている。日々の診断における問題として、結節影の良悪の判断に迷う例や細かな陰影の見落としがちなかへの注意などもあるが、特に間質性肺疾患においては多彩な陰影がさまざまな分布を示し、疾患の分類も多様で複雑であることから、専門医間でも診断の不一致がみられるという課題もある。このような背景から、AI による画像解析の臨床応用は、医師の診断支援、医療の均霑化、診断エラーの回避や医療従事者の負担軽減などの点で期待されるところであり、さらには、ヒトでは弁別できない陰影の相違を認識できる可能性から、画像所見から見た新しい疾患分類の提案などにも発展する将来性も考えられる。本講演では、産学共同で開発した間質性肺疾患の胸部 CT 画像における各種陰影の自動認識と定量化を例にあげて、AI による胸部画像診断の可能性や展望について考察したい。

S7-5 Quantitative CT Evaluation of Diffuse Lung Disease Using Artificial Intelligence

Tae Iwasawa

Department of Radiology, Kanagawa Cardiovascular and Respiratory Center

Quantitative evaluation of CT is essential to assess the severity of interstitial lung diseases (ILDs). In this presentation, we will introduce a quantitative analysis system (QZIP-ILD) for lung CT with ILDs, which we are currently developing with Ziosoft, Inc. The system is deep-learning-based lung analysis, and it is able to classify the lungs with diffuse lung disease into eight patterns: normal, emphysema, ground glass opacities, reticulation, consolidation, consolidation with traction bronchiectasis, traction bronchiectasis, and honeycombing (Aoki R, et al, 2022, Diagnostics). Consolidation with traction bronchiectasis is a classification based on the lesions of pleuroparenchymal fibroelastosis (PPFE). It has been reported that PPFE-like lesion is a common finding in a variety of ILDs, and that the patients with idiopathic pulmonary fibrosis with PPFE-like fibrosis is known to have a particularly poor prognosis (Sumikawa H, Eur J Radiol Open 2020). QZIP-ILD can measure lung lesion distribution by lung lobe. It can also display the percentage of lesions on the lung surface. The percentage of fibrotic lesions on the lung surface is related to the patient's prognosis (Iwasawa T, Radiology, 2019).

The QZIP-ILD is also applicable to COVID-19 pneumonia, and we used it as an indicator of the severity of COVID-19 pneumonia during the COVID-19 pandemic (Aoki R, JJR, 2021). Quantitative evaluation with QZIP-ILD allows more objective assessment of fibrosis progression on CT in IPF patients.

AIによるびまん性肺疾患のCT定量評価

岩澤 多恵

神奈川県立循環器呼吸器病センター放射線科

本発表では、現在我々がザイオソフト社と共同で開発を進めているCTの定量解析システム(QZIP-ILD)について紹介する。QZIP-ILDは、AIを利用したシステムであり、胸部CTで、びまん性肺疾患の肺を、肺気腫、正常、すりガラス影、網状影、牽引性気管支拡張、蜂巣肺、consolidation、牽引性気管支拡張を伴うconsolidationに分類する。また、肺の各葉を区別し、それぞれの葉ごとに病変を定量できる。

このうち、牽引性気管支拡張を伴うconsolidationはPleuroparenchymal fibroelastosis (PPFE)の病変を主な教師画像として作成した分類である。PPFE様の線維化は様々な間質性肺炎で見られる所見であり、PPFE様の線維化を伴う特発性肺線維症はとくに予後不良であることが知られている。

QZIP-ILDはCOVID-19肺炎にも応用可能であり、我々は、COVID-19パンデミックの際に、COVID-19肺炎の重症度の目安として利用した。

本発表ではQZIP-ILDの有用性について、解説する。

S7-6 Implementation and Evaluation of a DLAD Chest X-ray Analysis System in University Health Screenings

Yunosuke Kumazawa¹⁾, Hidekazu Hattori²⁾, Yuhei Nakagaki¹⁾, Yui Takagi¹⁾, Yurika Shimamura¹⁾, Ryo Izuno³⁾, Eirin Sakaguchi²⁾, Hiroyuki Naruse²⁾, Yoshiharu Ohno⁴⁾, Masanori Inoue¹⁾

- 1) Department Of Radiology, Fujita Health University School Of Medicine
- 2) Department Of Medical Laboratory Science, Fujita Health University School Of Health Sciences
- 3) FUJIFILM Corporation
- 4) Department Of Diagnostic Radiology, Fujita Health University School Of Medicine

Objective: From September 2021 to August 2023, we trialed DLAD (Deep Learning-Based Automatic Detection) algorithms (CXR-AID, Fujifilm, Japan) to analyze chest radiographs. The DLAD algorithm could detect lung nodules, consolidation, and pneumothorax. This study assesses the frequency and imaging patterns of false positives and false negatives, providing insights into interpreting chest radiographs with DLAD support. Methods: The study included 9841 chest radiographs from 4380 students (male: female = 3745:6096, average age 20.7 ± 2.7 years) taken during the trial period. All chest radiographs were initially reviewed by a radiologist and then by a diagnostic radiologist, with DLAD analysis conducted as a secondary reading for final reports. Results: A total of 237 false positives were identified in 205 exams from 187 students. False negatives were found in 37 of 74 exams with abnormalities in 64 students by the DLAD. Follow-up or further observation was required in 18 cases, all of which were detected by the DLAD. Discussion: It is important to understand the characteristics of DLAD systems and the tendency for false positives and false negatives. This study, along with a comprehensive literature review, seeks to elucidate the role of DLAD in the interpretation of chest radiographs.

大学生検診における DLAD 胸部 X 線解析システムの評価

熊澤 佑之介¹⁾, 服部 秀計²⁾, 中垣 勇平¹⁾, 高木 悠衣¹⁾, 島村 宥里佳¹⁾, 伊津野 諒³⁾, 坂口 英林²⁾, 成瀬 寛之²⁾, 大野 良治⁴⁾, 井上 政則¹⁾

- 1) 藤田医科大学医学部放射線医学講座
- 2) 藤田医科大学医療科学部臨床病態解析学
- 3) 富士フィルム
- 4) 藤田医科大学医学部放射線診断学講座

目的

当大学では、2021年9月から2023年8月の間に、胸部X線画像を自動的に解析するシステム（CXR-AID: 富士フィルム社製）を試用する機会を得た。これは、結節、浸潤影および気胸が疑われる領域を検出し、見落としを防止することが可能である。AI併用による胸部X線の読影は、偽陽性の多さが指摘されているものの、偽陰性の有無は見落としにもつながるため重要である。当大学学生検診で、AI併用読影による偽陽性、偽陰性の頻度と画像上の傾向を調べ、読影上の留意点を明らかにする。方法対象は、試用期間内に撮影された9841症例（4380人、男：女=3745:6096、年齢 20.7 ± 2.7 ）である。放射線科医および放射線診断専門医が二重読影した後に、CXR-AIDによる解析結果を参照し、最終的な読影結果とした。結果187名474検査中の205検査において偽陽性が確認された。対象疾患について、74検査において異常が指摘されたが、うち37検査でCXR-AIDによる偽陰性が確認された。2次検診後の介入が必要とされたのは18例で、すべてCXR-AIDによる指摘があった。

考察

CADの特徴や偽陽性の傾向について利用者自身が詳しく把握することは重要と考えられるため、文献的考察を加え報告する。

S7-7 Generation of short-term follow-up chest CT images using a latent diffusion model in COVID-19

Naoko Kawata^{1,2)}, Yuma Iwao^{3,4)}, Yukiko Matsuura⁵⁾, Takashi Higashide^{6,7)}, Takayuki Okamoto³⁾, Yuki Sekiguchi²⁾, Masaru Nagayoshi⁵⁾, Yasuo Takiguchi⁵⁾, Takuji Suzuki¹⁾, Hideaki Haneishi³⁾

- 1) Department of Respiriology, Graduate School of Medicine, Chiba University
- 2) Graduate School of Science and Engineering, Chiba University
- 3) Center for Frontier Medical Engineering, Chiba University
- 4) Institute for Quantum Medical Science, National Institutes for Quantum Science and Technology
- 5) Department of Respiratory Medicine, Chiba Aoba Municipal Hospital
- 6) Department of Radiology, Chiba University Hospital
- 7) Department of Radiology, Japanese Red Cross Narita Hospital

Purpose: Despite a global decrease in the number of COVID-19 patients, early prediction of the clinical course for optimal patient care remains challenging. Recently, the utility of image generation for medical imaging has been investigated. This study aimed to generate short-term follow-up chest CT images using a latent diffusion model.

Materials and Methods: We retrospectively enrolled 505 patients with COVID-19 for whom clinical parameters were available at admission and who underwent chest CT imaging. Subject datasets were divided into training (n = 403) and evaluation (n = 102) datasets. The images underwent variational autoencoder (VAE) encoding, resulting in latent vectors. The information, consisting of initial clinical parameters and radiomic features, was formatted as a tabular data encoder. The initial and follow-up latent vectors and the initial table data encoders were used to train the diffusion model. The evaluation data were used to generate prognostic images. The similarity between the prognostic images (generated images) and the follow-up images (real images) was then assessed by zero-mean normalized cross-correlation (ZNCC), peak signal-to-noise ratio (PSNR) and structural similarity (SSIM). Visual evaluation was also performed.

Results: Image similarity showed reasonable values of 0.973 for ZNCC, 24.48 for PSNR and 0.844 for SSIM. Visual assessment by two pulmonologists and one radiologist showed reasonable agreement between the images.

Conclusions: The similarity and validity of the generated prognostic images were reasonable. The generation of prognostic images may suggest a potential utility for early prediction of clinical course in COVID-19 associated pneumonia and other respiratory diseases.

COVID-19における拡散モデルを用いた短期経過予測画像の作成

川田 奈緒子^{1,2)}, 岩男 悠真^{3,4)}, 松浦 有紀子⁵⁾, 東出 高至^{6,7)}, 岡本 尚之³⁾, 関口 結貴²⁾, 永吉 優⁵⁾, 瀧口 恭男⁵⁾, 鈴木 拓児¹⁾, 羽石 秀昭³⁾

- 1) 千葉大学大学院医学研究院 呼吸器内科学
- 2) 千葉大学大学院融合理工学府 基幹工学専攻 医工学コース
- 3) 千葉大学フロンティア医工学センター
- 4) 量子科学技術研究開発機構
- 5) 千葉市立青葉病院 呼吸器内科
- 6) 千葉大学大学院医学研究院画像診断・放射線腫瘍学
- 7) 成田赤十字病院 放射線科

目的：COVID-19の患者数は減少傾向だが、最適な患者ケアのための臨床経過の早期予測は未だ困難である。近年、医用画像における画像生成の有用性が報告されてきた。本研究では、拡散モデルを用いて短期経過予測画像を生成することを目的とした。

対象と方法：入院時に臨床検査、および入院時と経過時に複数回の胸部CTを施行したCOVID-19患者505例を後方視的に登録した。画像は変分オートエンコーダ（VAE）を用いて潜在ベクトルとした。入院時検査と放射線学的特徴量（Radiomics）は表形式のデータエンコーダとした。入院時および経過時の潜在ベクトル、入院時データエンコーダからなる学習用データ（n = 403）を用いて拡散モデルを学習させ、評価データ（n = 102）を用いて予測画像を生成した。その後、正規化相互相関（ZNCC）、ピーク信号対雑音比（PSNR）、構造的類似度（SSIM）による予測画像（生成画像）と経過画像（実画像）の類似度を評価した。更に、3名の専門医による肉眼評価を行った。

結果：画像の類似度はZNCC=0.973、PSNR=24.48、SSIM=0.844と妥当な値を示した。肉眼評価でも、検者間の妥当な一致を認めた。

結論：予後予測画像の生成は、COVID-19関連肺炎やその他の呼吸器疾患における臨床経過の早期予測に有用である可能性がある。

Young Investigator Award

YIA-1 Fibrotic interstitial lung abnormalities in smokers are an independent risk factor for mortality

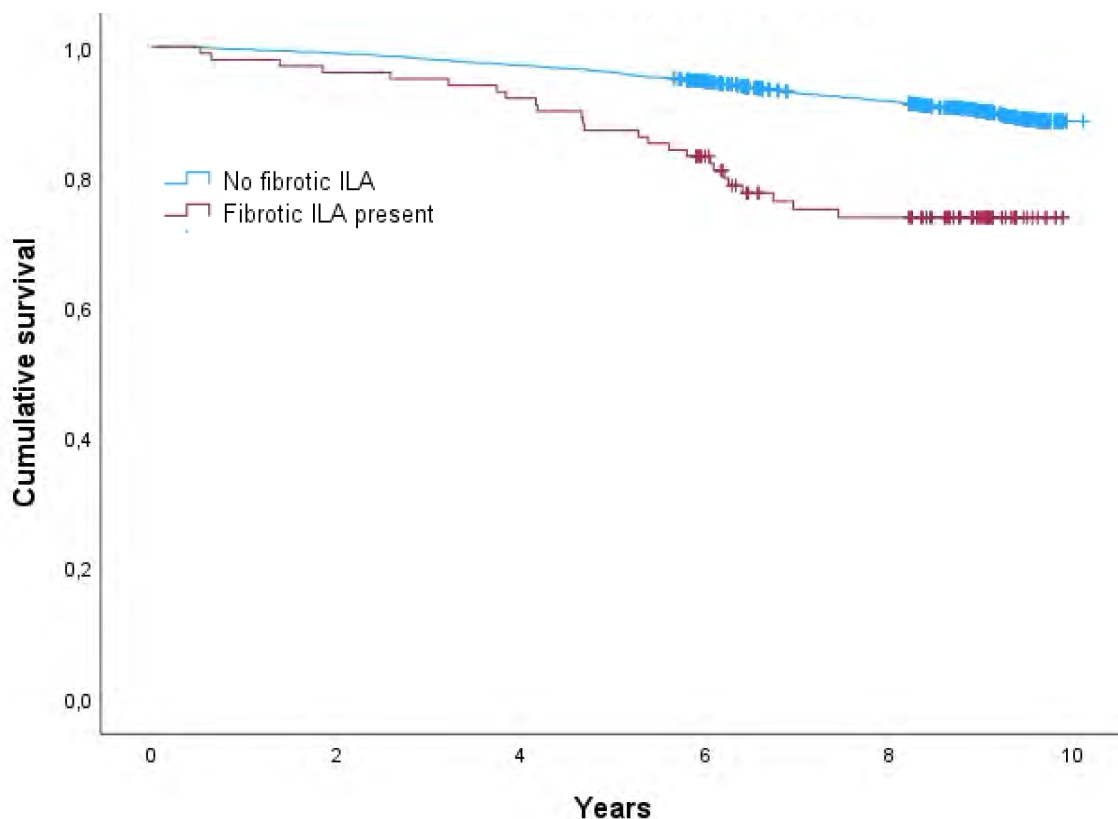
Esther Pompe, Natascha Kwee, Pim A de Jong

University Medical Center Utrecht

Interstitial lung abnormalities (ILA) are a common incidental finding in smokers. We aimed to investigate the association between fibrotic and non-fibrotic ILA and all-cause mortality, independent of lung function, emphysema and bronchitis. The Dutch-Belgian lung cancer screening trial is a population-based prospective study that included current and former smokers aged 50-75 years old with a smoking history of >15 cigarettes/day during > 25 years or >10 cigarettes/day during >30 years. This side study included participants who underwent additional lung function testing. Computed tomography (CT) quantification methods were used to evaluate emphysema (LAA-950) and airway wall thickness (Pi10). ILA was visually evaluated according to Fleischner Society definitions. Probable usual interstitial pneumonitis pattern (UIP) and UIP were grouped as fibrotic. Indeterminate UIP and inconsistent UIP patterns were grouped as non-fibrotic ILA. Cox proportional hazard analyses were utilized to calculate the hazard ratio (HR) for all-cause mortality of ILA with a correction for age, sex, pack-years, smoking status, FEV₁, emphysema and Pi10.

We followed 3221 participants for 8.2 ± 1.7 years during which 319 (9.9%) died. The age was 60.3 ± 5.4 years, smoking intensity was 40.5 ± 17.7 years and 52.2% were current smokers. Mortality was 281/3020 (9.3%) without ILA, 13/100 (13.0%) with non-fibrotic ILA and 25/101 (24.8%) with fibrotic ILA. After adjustment for covariates, fibrotic ILA (HR = 2.14, 95% CI: 1.37-3.30) was significantly associated with mortality, non-fibrotic ILA was not (HR = 1.14, 95% CI: 0.63-2.10).

CT-detected fibrotic ILA could provide prognostically important information for current and former smokers participating in lung cancer screening.



YIA-2 Predictive Value of Oxygen-enhanced MRI T1 Mapping after Lung Transplantation

Milan Speth^{1,2)}, Till Frederik Kaireit^{1,2)}, Marcel Gutberlet^{1,2)}, Filip Klimes^{1,2)}, Lea Behrendt^{1,2)},
Andreas Voskrebenezv^{1,2)}, Frank Wacker^{1,2)}, Tobias Welte^{2,3,4)}, Jens Gottlieb^{2,3)}, Jens Vogel-Claussen^{1,2)}

1) Institute for Diagnostic and Interventional Radiology, Hannover Medical School, Hannover, Germany

2) Biomedical Research in Endstage and Obstructive Lung Disease (BREATH), German Center for Lung Research, Hannover, Germany

3) Department of Respiratory Medicine, Hannover Medical School, Hannover, Germany

4) Posthumous

Background:

Chronic lung allograft dysfunction (CLAD) related graft loss (death, re-do transplantation) is a major long-term post-pulmonary transplant complication. Biomarkers are currently being explored in their predictive value for graft loss.

Aim:

To explore the value of Oxygen-enhanced MRI (OE-MRI) T1 mapping in predicting CLAD-related graft loss.

Methods

After including 141 double lung transplanted patients, OE-MRI T1 mapping biomarkers and same-day spirometry were explored, all acquired single-centric after 6-12 months (baseline) and 2.5 years (follow-up) post-transplantation over 6.1 years. For imaging, six coronal sections were scanned at 1.5 T with spoiled gradient echo sequences, taken under breath hold. Registered, calculated, and segmented T1 maps after oxygen wash-in were subtracted from room air maps (Delta T1). Survival was analyzed applying ROC, Kaplan-Meier, and Cox analysis, with graft loss as the primary endpoint. Biomarkers from OE-MRI were compared with same-day PREFUL MRI biomarkers using Spearman's correlation.

Results:

24 from 132 participants screened at baseline developed graft loss, and OE-MRI-derived Delta T1 median (hazard ratio for graft loss (HR) 3.5, 95%CI 1.01-9.40, P=.048), Quartile Coefficient of Dispersion (HR 3.43, 1.12-8.70, P=.03), and threshold-driven Oxygenated Volume (HR 3.07, 1.18-7.22, P=.02) predicted CLAD-related graft loss, when FEV₁ from spirometry was unable to predict (P=.32). At follow-up, 11 from 103 patients met the endpoint; all biomarkers predicted graft loss. PREFUL did not correlate with OE-MRI parameters (P>.05 each), and compound biomarkers also predicted graft loss.

Conclusion:

T1 mapping parameters from pulmonary OE-MRI predicted future CLAD-related graft loss, potentially adding value after lung transplantation.

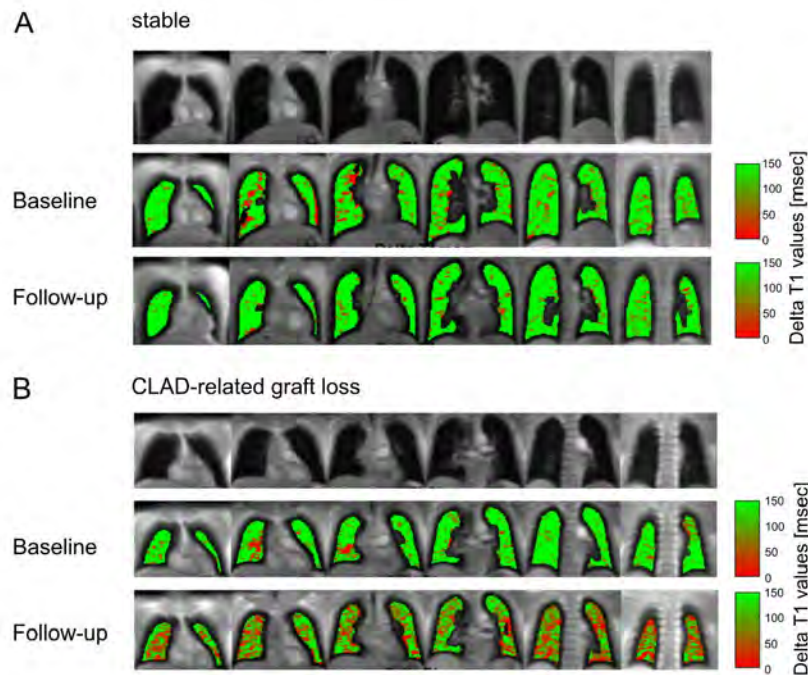


Figure: Exemplary coronal slices of oxygen-enhanced MRI. First row: morphology of baseline examination. Second and third row: Delta T1 maps of baseline and follow-up MRI. (A) Clinical stable patient (end of observation 42 months after follow-up MRI). (B) Patient with progressive CLAD (CLAD-related death 11 months after follow-up MRI).

YIA-3 High volume ratio of airway to lung blood vessel on exacerbations in COPD

Nobuyasu Wakazono¹, Kaoruko Shimizu¹, Naoya Tanabe², Akira Oguma¹, Hironi Makita³, Kazufumi Okada⁴, Miho Wakazono¹, Hiroki Nishimura¹, Yuichi Kojima¹, Michiko Takimito-Sato¹, Munehiro Matsumoto¹, Yuki Abe¹, Nozomu Takei¹, Hirokazu Kimura¹, Houman Goudarzi¹, Ichizo Tsujino¹, Susumu Sato², Shigeo Muro⁵, Masaharu Nishimura³, Toyohiro Hirai², Satoshi Konno¹

- 1) Department of Respiratory Medicine, Faculty of Medicine, Hokkaido University
- 2) Department of Respiratory Medicine, Graduate School of Medicine, Kyoto University
- 3) Hokkaido Medical Research Institute of Respiratory Diseases
- 4) Data Science Center, Promotion Unit, Institute of Health Science Innovation for Medical Care, Hokkaido University Hospital
- 5) Department of Respiratory Medicine, Nara Medical University

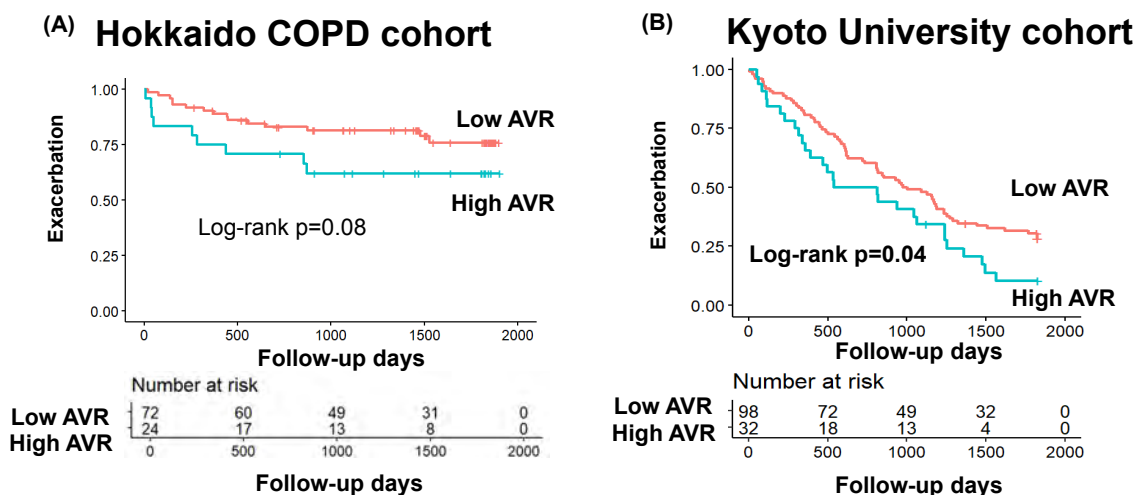
RATIONALE AND AIM: The impact of unbalanced morphology of total airway luminal volume (TAV) and total blood vessel volume (TBV) on COPD exacerbation has not been explored. This study aimed to examine the association between increased Airway to Vessel ratio in the lungs (AVR) and exacerbations in Japanese patients with COPD.

METHODS: Participants were recruited from the Hokkaido COPD Cohort Study (original, N = 96) and the Kyoto University cohort (validation, N=130). CT-derived indices on TAV and TBV at baseline were assessed using the A-VIEW software (Coreline, Korea) . The time to the first exacerbation was examined during the five years of follow-up, compared using the Kaplan-Meier method with the log-rank tests between high (the highest quartile) and low (the other quartiles) groups. Multivariable Cox proportional hazard models were performed to determine the association between high/low AVR and exacerbation.

RESULTS: In two cohorts, high AVR group showed the shorter time to the first exacerbations than low AVR group, the association with exacerbations, after adjusting for smoking status, pack-years of tobacco, the percent predicted of FEV₁ and transfer coefficients (Kco), visual bronchiectasis score (modified Reiff score) and the ratio of pulmonary artery to aorta in diameter (PA/Ao). Whereas either TAV corrected for Lung Volume (LV) or TBV/LV was not associated with exacerbations.

CONCLUSIONS: High AVR was associated with the shorter time to the first exacerbation during the 5-year follow-up period, complementary to mReiff and PA/Ao, indicating that AVR would be a potential novel CT derived predictor for exacerbation in patients with COPD.

Time to first exacerbation in high and low AVR groups



YIA-4 Small pulmonary vein volume is associated with a lower saturation and more supplemental oxygen use

Natascha Kwee¹⁾, Wouter A. C. van Amsterdam²⁾, Leticia Gallardo-Estrella³⁾, Jean-Paul Charbonnier³⁾, Stephen M. Humphries⁴⁾, Harm A. W. M. Tiddens³⁾, James Crapo⁵⁾, Richard Casaburi⁶⁾, Pim A. de Jong⁶⁾, David A. Lynch⁴⁾, Esther Pompe^{1,7)}

- 1) University Medical Center Utrecht - Department of radiology
- 2) University Medical Center Utrecht - Department of data science and biostatistics
- 3) Thirona
- 4) National Jewish Health - Department of radiology
- 5) National Jewish Health - Department of pulmonology
- 6) The Lundquist Institute at Harbor-UCLA Medical Center
- 7) Meander Medical Center - Department of radiology

Background

Hypoxia can have multiple causes in chronic obstructive pulmonary disease (COPD), including airflow limitation, emphysema and pulmonary vascular remodeling. In this study, the independent contribution of small pulmonary veins to hypoxia was evaluated.

Methods

Small pulmonary vein dimensions (<1mm \varnothing) were quantified on computed tomography (CT) down to approximately 0.2mm, with artificial intelligence based software (LungQ, Thirona). In 7903 current and former smokers from the COPD Gene study, we used regression models corrected for clinical (e.g. FEV1%predicted, emphysema) and technical covariates, to determine if small vein volume corrected for body surface area was independently associated with resting oxygen saturation and supplemental oxygen use.

Results

7903 subjects were included, mean age was 60.1 \pm 9.0 years. 53.2% were male. Half were current smokers (50.8%); mean number of packyears was 44.7 \pm 25.2. Median resting saturation was 97% (IQR 95-98%); 882 (11.2%) subjects used supplemental oxygen. Range of small vein volume was 0.28 - 6.07 mL/m² (IQR 2.32-2.99). Multivariable regression showed that for each 1 mL/m² increase in small vein volume, saturation decreased significantly by 0.23% [0.11%, 0.35%]. Oxygen users had higher mean small vein volumes (2.98 \pm 0.59 mL/m²) compared to those without supplemental oxygen (2.65 \pm 0.51 mL/m²); each 1 mL/m² increase in small vein volume was significantly associated with more oxygen use (adjusted OR 1.70 [1.35, 2.14]).

Conclusion

In current and former smokers, higher small pulmonary vein volume was associated with lower resting saturation and more supplemental oxygen use, independent of lung disease or technical CT parameters. This suggests a role for venous remodeling in hypoxia.

YIA-5 High-resolution 4D pulmonary ventilation MRI correlates strongly to Xe MRI

Filip Klimes^{1,2}, Joseph W Plummer^{3,4}, Matthew M Wilmering³, Alexander M Matheson³,
Abdullah S Bdaiwi^{3,4}, Marcel Gutberlet^{1,2}, Andreas Voskrebenezv^{1,2}, Marius M Wernz^{1,2},
Frank Wacker^{1,2}, Zackary I Cleveland^{3,4,5,6}, Laura L Walkup^{3,4,5,6}, Jens Vogel-Claussen^{1,2}

- 1) Institute of Diagnostic and Interventional Radiology, Hannover Medical School, Hannover, Germany
- 2) Biomedical Research in Endstage and Obstructive Lung Disease Hannover (BREATH), German Center for Lung Research (DZL), Hannover, Germany
- 3) Center for Pulmonary Imaging Research, Cincinnati Children's Hospital Medical Center, Cincinnati, Ohio, USA
- 4) Department of Biomedical Engineering, University of Cincinnati, Cincinnati, Ohio, USA
- 5) Imaging Research Center, Department of Radiology, Cincinnati Children's Hospital Medical Center, Cincinnati, Ohio, USA
- 6) Department of Pediatrics, University of Cincinnati Medical Center, Cincinnati, Ohio, USA

Background

Hyperpolarized xenon gas MRI (Xe MRI) effectively assesses regional ventilation heterogeneity in a single breath-hold but lacks sensitivity to dynamic ventilation abnormalities. Here, we introduce a complementary technique using a novel proton MRI sequence with Fermat Looped, ORthogonally Encoded Trajectories (FLORET) to enhance lung parenchymal signal, coupled with phase-resolved functional lung (PREFUL) postprocessing to reveal dynamic ventilation abnormalities.

Methods

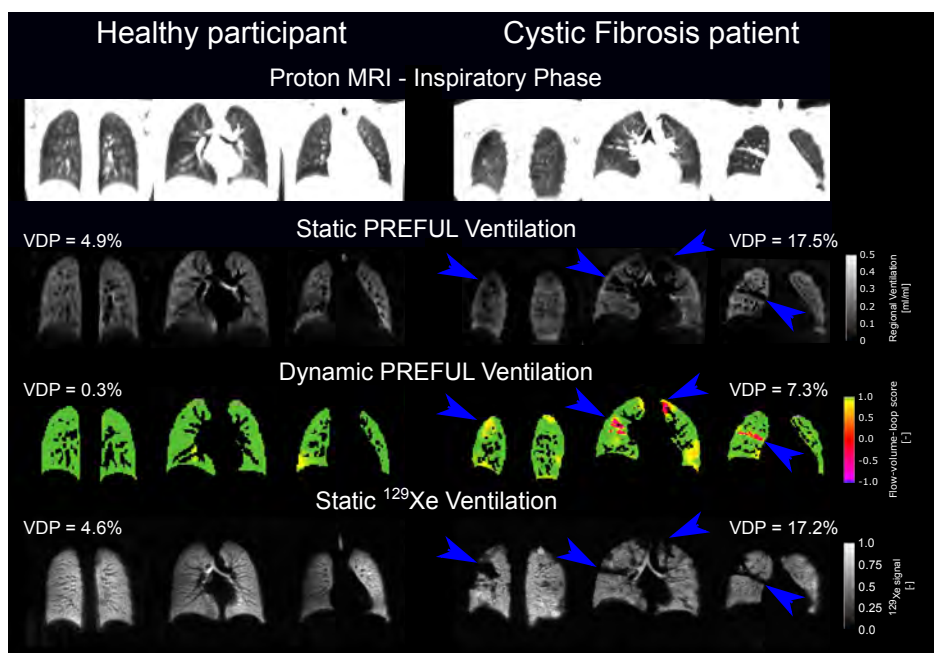
29 participants with pulmonary diseases (13-female, 16-male, aged [5-59]) and 7 healthy participants (2-female, 5-male, aged [8-26]) underwent imaging on a Philips 3T scanner. Xe ventilation images ($3 \times 3 \times 15 \text{ mm}^3$) were obtained with a <16-second breath-hold, while proton images were acquired using a FLORET sequence within a <10-minute free-breathing window (reconstructed to $3 \times 3 \times 3 \text{ mm}^3$). PREFUL ventilation images were generated from 24 respiratory phases and aligned spatially to the inspiratory phase, to calculate static and dynamic ventilation parameters. Xe ventilation-defect-percentage (VDP) and two PREFUL VDPs (static and dynamic) were compared using Pearson correlations and Bland-Altman analysis.

Results

Both static and dynamic PREFUL VDP measurements significantly correlated with Xe VDP ($p < 0.0001$). Static PREFUL VDP showed stronger correlation ($r = 0.76$) compared to dynamic PREFUL ventilation ($r = 0.61$). While dynamic PREFUL VDP values did not differ significantly from Xe VDP (mean bias = 1.38%, $p = 0.26$), static PREFUL VDP values were notably higher (mean bias = 10.09%, $p < 0.0001$).

Conclusions

PREFUL-derived VDPs using the high-resolution FLORET acquisition correlate strongly with static Xe ventilation MRI, offering a means of ventilatory assessment without breath-hold constraints. Furthermore, the dynamic PREFUL VDP may offer new insight into ventilatory dynamics, making it a powerful complement to Xe MRI.



YIA-6 Volume doubling time of solid components in lung cancer: distinct implications vs. whole tumor

Yura Ahn, Sang Min Lee, Joon Beom Seo

Asan Medical Center

Purpose

To investigate whether the volume doubling time (VDT) of the solid component in lung adenocarcinomas has distinct clinical implications compared to the VDT of the whole tumor

Methods

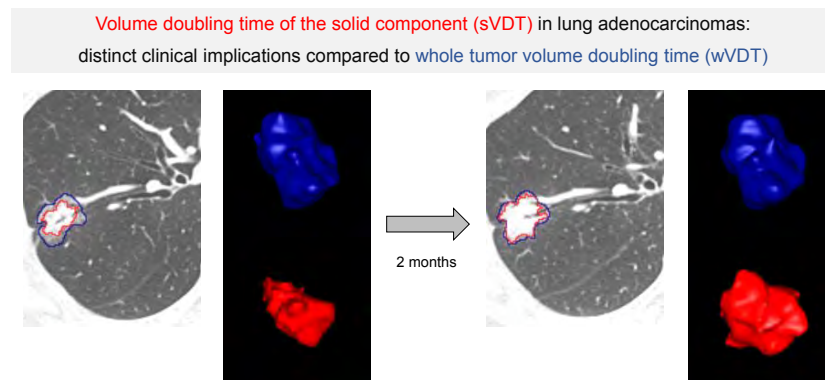
Patients who underwent at least two serial chest CT scans prior to lobectomy for lung adenocarcinoma between July 2010 and December 2020 were retrospectively included. VDT was measured using three-dimensional volumetric segmentation for both the solid component (sVDT) and the whole tumor (wVDT). The prognostic value for recurrence-free survival (RFS) and the predictive value of each VDT for nodal-positive disease (pN1 or pN2) was evaluated in total population and part-solid group.

Result

We studied 224 patients, of whom 123 (54.9%) had part-solid lesions and 101 (45.1%) had solid lesions. sVDT was longer in part-solid lesions (455 vs. 299 days, $p=0.003$). In part-solid lesions, sVDT was faster than wVDT (455 vs. 926 days, $p<0.001$). Both sVDT and wVDT (<400 days) were independent risk factors for poor RFS (hazard ratio, 2.39 [$p=0.005$] and 2.01 [$p=0.016$], respectively); however, only sVDT was significant in the part-solid group (hazard ratio 3.39 [$p=0.013$]). sVDT (<400 days) was an independent predictor of nodal positive disease in part-solid lesions (odds ratio 5.61, $p=0.038$) but not for wVDT ($p=0.288$), and sVDT (<400 days) was also significant in the total group (odds ratio 2.77 [$p=0.008$]).

Conclusion

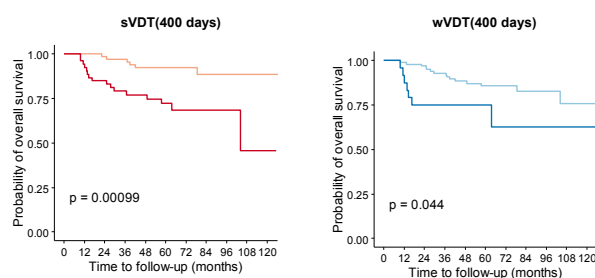
The sVDT is more effective than wVDT for predicting pathologic nodal positive disease and outcomes, particularly in part-solid lesions.



- The solid component (sVDT) grows more rapidly than the whole tumor volume (wVDT) (455 vs. 926 days, $p<0.001$)
- The solid component (sVDT) grows more slowly in part-solid lesions (455 vs. 299 days, $p=0.003$).

In part-solid lesions,

- Only sVDT (<400 days) was a significant risk factor for RFS (HR, 3.39 $p=0.013$).
- Only sVDT (<400 days) was a predictor of nodal positive disease (OR, 5.61, $p=0.038$).



Poster

(English)

COPD-1

PE1-1 Hybrid Evaluation with MRI Series of Multi-direction Diaphragm Motion and CT Images on COPD Patients

Xingyu Zhou¹⁾, Chen Ye^{2,3)}, Takayuki Okamoto³⁾, Yuma Iwao^{3,4)}, Naoko Kawata^{1,5)}, Ayako Shimada^{5,6)}, Hideaki Haneishi³⁾,

1) Graduate School of Science and Engineering, Chiba University, Chiba, Japan

2) School of Communications and Information Engineering, Nanjing University of Posts and Telecommunications, Nanjing, China

3) Center for Frontier Medical Engineering, Chiba University, Chiba, Japan

4) National Institutes for Quantum and Radiological Science and Technology, Chiba, Japan

5) Department of Respiriology, Graduate School of Medicine, Chiba University, Chiba, Japan

6) Department of Respiriology, Shin-Yurigaoka General Hospital, Kawasaki, Japan

Purpose: Chronic obstructive pulmonary disease (COPD), which results in pulmonary airflow limitation and breathing difficulty, is highly prevalent in people who often explore toxic substances and have a long smoking history. As is known, medical imaging is commonly used to detect morphological abnormalities. Our study aims to analyze the 2-D multi-direction respiratory diaphragm motion using magnetic resonance image (MRI) series and the low attenuation volume (LAV) distribution using thoracic computer tomography (CT) images.

Materials and Methods: 10 normal subjects and 24 patients with COPD were investigated in the study. First, the diaphragm profiles in the MRI series are extracted using U-net. Second, a learning-based registration method called VoxelMorph is applied to find out the displacement of all positions on the diaphragm, so that we can track the motion of these positions in the 2-D plane. Besides, the CT images corresponding to the region of interest (ROI) of MRI are re-sliced to calculate the LAV distribution. Finally, the characteristics of the diaphragm motion such as the motion similarity or direction of different positions on the diaphragm, and the correlation with the LAV distribution are further analyzed.

Results: Compared with the normal subjects, the patients with COPD had significant differences in the vertical motion direction, also the abnormal motion was observed in the 2-D sagittal plane. The LAV distribution of anterior and posterior lower lung regions showed a relatively high correlation with the motion asynchronization.

Conclusion: Our proposed evaluation method may assist in the diagnosis and therapy planning for patients with COPD.

PEI-2 Comparison Of Ventilation Imaging Threshold Techniques For Determining Non-Ventilated Volume

Edward Moon Kyu Jeagal^{1,2)}, Hooria Alowiwi¹⁾, Katherine Willowson⁴⁾, Dale Baily⁴⁾, Elizabeth Baily⁴⁾, Kaj Blokland¹⁾, Kim Prisk¹⁾, David G Chapman^{1,2,3)}, Gregory G King^{1,3,5)}

- 1) Airway Physiology and Imaging Group, The Woolcock Institute of Medical Research, Macquarie University and The University of Sydney.
- 2) Faculty of Life Sciences, University of Technology Sydney,
- 3) Department of Respiratory Medicine, Royal North Shore Hospital,
- 4) Department of Nuclear Medicine, Royal North Shore Hospital,
- 5) Northern Clinical School, University of Sydney

Introduction

Ventilation imaging allows for quantification of the extent and distribution of airway closure. However, current analysis methods to distinguish ventilated from non-ventilated lung regions have not been validated.

Aim

To compare non-ventilated lung volume calculated using three published threshold methods and a novel threshold method using 1) lung phantom models and 2) images from patients with chronic obstructive pulmonary disease (COPD).

Method

10 lung phantom models were constructed from containers of varied volumes packed with foam beads. Ventilating and non-ventilating lung regions were simulated by filling containers with a solution of Technetium-99m and non-radioactive water, respectively. Lung phantoms underwent single-photon emission computed tomography/computed tomography (SPECT/CT) according to usual methods. Additionally, 22 COPD participants underwent SPECT/CT. Non-ventilated (VentNon) volume was calculated using four threshold methods; 15% of the maximal voxel activity count (Thr_15%Max); 50% of the average voxel activity between 5 and 80% of maximal voxel activity (Thr_50%Mean5-80); using the Otsu threshold tool in the Fiji software (Thr_Otsu); a novel curve-fitting method (Thr_Slope).

Results

The mean difference \pm SD between true VentNon and calculated VentNon using Thr_15M, Thr_50%Mean5-80, Thr_Otsu, and Thr_Slope were -0.196 ± 0.653 , 0.160 ± 0.316 , -0.006 ± 0.168 , 0.02 ± 0.129 % of total lung volume, respectively. There was a positive proportional bias using Thr_50%Mean5-80, Thr_Otsu, and Thr_Slope, with the bias lowest in Thr_Slope. In people with COPD, Ventnon was significantly increased using Thr_Slope compared to the other three methods ($p < 0.05$).

Conclusion

Our novel threshold method is more accurate and robust than current methods and leads to increased non-ventilated volumes in images from COPD participants.

Table 1

	Agreement (pc)	Absolute bias (L)	Proportional bias (gradient)
Thr_15%Max	0.77	-0.20	*
Thr_50%Mean5-80	0.90	0.16	0.32
Thr_Otsu	0.98	-0.01	0.13
Thr_Slope	0.99	0.02	0.09

* There was no proportional bias for Thr_15%Max

Thr_15M and Thr_50%Mean5-80 possessed poor strength of agreement for VentNon (pc = 0.774 and 0.897, respectively). Both Thr_Otsu and Thr_Slope possessed substantial strength of agreement for VentNon (pc = 0.980 and 0.988, respectively). The mean difference \pm SD between true VentNon and Thr_15M, Thr_50%Mean5-80, Thr_Otsu, and Thr_Slope VentNon were -0.196 ± 0.653 , 0.160 ± 0.316 , -0.006 ± 0.168 , 0.02 ± 0.129 , respectively.

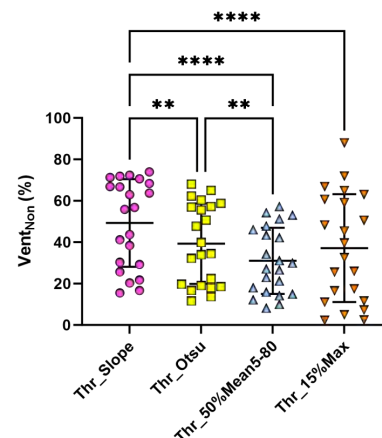


Figure 1: VentNon measurements in people with COPD as measured with Thr_Slope, Thr_Otsu, Thr_50%Mean5-80, and Thr_15%Max. **p < 0.01, ****p < 0.0001.

PE1-3 Estimating Small Airways Disease from a Single Inspiratory Chest Computed Tomography Scan

Joseph M Reinhardt, Muhammad Faizyab Chaudhary, Hira A Awan, Sarah E Gerard, Alejandro P Comellas, Eric A Hoffman

The University of Iowa

Obstruction of the small airways is a major source of resistance in chronic obstructive pulmonary disease (COPD) and is known to precede emphysema. Currently, the CT-based method for estimating functional small airways disease (fSAD) uses parametric response mapping (PRM) to classify air trapped voxels into emphysema or fSAD subtypes, which requires image registration of inspiratory and expiratory scans. However, expiratory chest CT scans are not routinely protocolled, limiting the examination of PRM-based small airways disease. In addition, adequate expiratory coaching is required to have reproducible results. We propose to use deep learning to estimate a synthetic expiratory chest CT scan from an available inspiratory CT scan, use that image pair to estimate functional small airways disease (denoted as fSAD^{Deep}), and study the associations between fSAD^{Deep} and important clinical outcomes in COPD. CT data from the SubPopulations and InteRmediate Outcome Measures in COPD Study (SPIROMICS) was used to train and validate a three-dimensional artificial intelligence generative adversarial network (GAN) with perceptual and voxel consistency regularization. Once trained on 1055 subjects from SPIROMICS, the model was applied to 31 separate subjects from SPIROMICS and 473 subjects from the Genetic Epidemiology of COPD (COPDGene) study. In SPIROMICS, fSAD^{Deep} is associated with post-bronchodilator FEV1 ($\beta=-0.048$, $P<0.001$) and FEV1/FVC ($\beta=-0.009$, $P<0.001$). Similarly, in COPDGene, fSAD^{Deep} is associated with post-bronchodilator FEV1 ($\beta=-0.030$, $P<0.001$), FEV1/FVC ($\beta=-0.007$, $P<0.001$), and Saint George Respiratory Questionnaire ($\beta=0.209$, $P=0.01$). The multivariable models were adjusted for age, race, sex, body mass index, smoking pack years, percent emphysema, and smoking status.

PE1-4 Determination of sound source of wheezes in COPD based on 4D-CT images and CFD simulation study

Hiroko Kitaoka¹⁾, Takashi Kijima²⁾

1) Dept. of Biomedical Engineering, Tokyo University of Agriculture and Technology

2) Dept. of Respiratory Medicine and Hematology, Hyogo College of Medicine

[Backgrounds] Wheezes in pulmonary emphysema are continuous musical sounds during expiration with 400 Hz or more. The textbook tells that expiratory airflow limitation in emphysema occurs at the small airways and that wheezes are generated there. However, wheezes are the strongest at the anterior cervical part and often audible without stethoscope. Those clinical features are not consistent with the textbook knowledge.

[4D-CT images] Five emphysema patients and a normal subject underwent 4D-CT during maximum forced expiration at supine posture. The intra-mediastinal airways of all emphysema patients were extremely narrowed just after the beginning of forced expiration. The membranous part in the thoracic trachea were protruded inside, meanwhile those in the cervical tracheas kept convex shapes.

[Airflow simulation through the airway] We performed expiratory airflow simulation (solver: AcuSolve, Altair Inc., USA) by the use of a 4D finite element lung model, and found periodical pressure fluctuation with 300-900Hz at the end of protrusion of the tracheal posterior wall. Relationship between the peak frequency of pressure fluctuation and airflow velocity was in agreement with Strahal's law, that was strongly suggested that the source of wheezes was periodic vortex release at the end of membranous part in the thoracic trachea. Contrarily, airflow simulation in a small bronchus (1.8 mm in diameter) indicated no apparent periodic pressure fluctuations.

[Conclusion] The present study indicated that the sound source of expiratory wheezes in pulmonary emphysema was at the end of protrusion of the tracheal posterior wall.

PE1-5 4D-CT images have solved the mystery of hilar hot spots in COPD on aerosol inhalation scintigraphy

Hiroko Kitaoka¹⁾, Takashi Kijima²⁾

1) Dept. of Biomedical Engineering, Tokyo University of Agriculture and Technology

2) Dept. of Respiratory Medicine and Hematology, Hyogo College of Medicine

[Objective] Radioaerosol inhalation lung scintigraphy was powerfully investigated around 1980s as a tool for detecting sites of airway narrowing, where abnormally deposited aerosols generated hot spots. In emphysema, bilateral hilar hot spots were observed although there were no organic stenoses in the central airways. Since 1990s, the aerosol inhalation scintigraphy has not been performed for clinical purpose because of application of X-ray CT to lung diseases, and the hilar hot spots in emphysema has been forgotten. Now we evaluated dynamic behavior of intra-mediastinal airway (IMA) by 4D-CT, and investigated the mystery of hilar hot spots.

[Method] Five emphysema patients and a normal subject underwent 4D-CT during maximum forced expiration at supine posture. Volumes of intra-thoracic trachea and bilateral main bronchi were measured, and the relative volume to the volume just before the beginning of forced expiration was calculated for each frame.

[Results] The IMA of all emphysema patients were extremely narrowed just after the beginning of forced expiration. The membranous part was invaginated throughout the IMA. There was no apparent shape change in the normal subject. The relative volume at one second after were highly correlation to FEV_{1.0} ($r^2= 0.93$).

[Discussion and Conclusion] The 4D-CT images revealed that the cause of hilar hot spots in emphysema patients were dynamic collapse of IMA during expiration where aerosols in the expired air were deposited on the protruded membranous parts at the hiluses. They also revealed that the site of airflow limitation in COPD was not small airways but IMA.

COPD-2/Airway Diseases

PE2-1 AI-based quantification of small pulmonary artery and vein volume on CT and mortality in smokers

Natascha Kwee¹⁾, Eleni-Rosalina Andrinopoulou^{2,3)}, Tjeerd van der Veer⁴⁾, Leticia Gallardo-Estrella⁵⁾, Jean-Paul Charbonnier⁵⁾, Stephen M. Humphries⁶⁾, David A. Lynch⁶⁾, Harm A. W. M. Tiddens^{4,7)}, Pim A. de Jong¹⁾, Esther Pompe^{1,8)}

- 1) University Medical Center Utrecht - Department of Radiology
- 2) Erasmus Medical Center - Department of biostatistics
- 3) Erasmus Medical Center - Department of epidemiology
- 4) Erasmus Medical Center - Department of pulmonology
- 5) Thirona
- 6) National Jewish Health - Department of radiology
- 7) Erasmus Medical Center-Sophia Children's Hospital - Department of paediatric pulmonology and allergology
- 8) Meander Medical Center - Department of radiology

Background

In chronic obstructive pulmonary disease (COPD), vascular alterations have been shown to contribute to hypoxia and pulmonary hypertension, but the independent contribution of small vessel abnormalities to mortality remains unclear.

Methods

With a novel artificial intelligence based method (LungQ, Thirona) we quantified artery and vein dimensions on computed tomography (CT) down to 0.2 millimeter. Small vessel volumes (<1 mm \varnothing) were normalized by body surface area. In 7903 current and former smokers (COPDGene study) the independent contribution of small artery and small vein volume to all-cause mortality was tested in multivariable Cox models. Additionally, we calculated the 95th percentile of small arteries and veins in 374 never smokers to create two groups: normal and high small artery or small vein volume. We describe clinical, physiological and imaging characteristics of subjects with a high small artery and high small vein volume.

Results

Both high small artery and high small vein volumes were independently associated with mortality, with an adjusted hazard ratio of 1.07 [1.01, 1.14] and 1.34 [1.21, 1.49] per mL/m² increase, respectively. In COPDGene, 447 (5.7%) subjects had high small artery volumes and 519 (9.1%) subjects had high small vein volumes and both had more emphysema, more air trapping and more severe coronary calcium.

Conclusions

In smokers, abnormally high volumes in small pulmonary arteries and veins are both relevant for mortality, which urges investigations into the etiology of small pulmonary vessels and cardiac function in smokers.

Table 1. Clinical, physiological and imaging characteristics of current and former smokers with normal and high small pulmonary arterial volumes, corrected for BSA (mL/m²)

	Normal small artery volume (N=7456)	High small artery volume (N=447)
Age (yr)	60.0 ± 9.1	62.1 ± 8.1
Packyears (yr)	44.3 ± 25.1	52.1 ± 27.0
Current smokers (n,%)	3738 (50.1%)	280 (62.6%)
FEV ₁ (% predicted)	75.5 ± 25.6	76.1 ± 26.5
CT quantified parameters		
Emphysema (%)	2.2 (0.6-7.4)	5.2 (1.7-12.3)
mAgatston score	15 (0-186)	47.5 (0-253)
Mean small arterial volume (mL/m ²)	3.72 ± 0.74	5.91 ± 0.52
5-year mortality	858 (12.4%)	65 (15.0%)
10-year mortality	1838 (30.6%)	126 (31.7%)
Total mortality	2267 (30.4%)	152 (34.0%)

Legend: Data given are mean ± standard deviation or median and interquartile range in parentheses or number and percentage in parenthesis, depending on the data distribution. FEV₁ is Forced Expiratory Volume in one second, CT is computed tomography.

Table 2. Clinical, physiological and imaging characteristics of current and former smokers with normal and high small pulmonary venous volumes, corrected for BSA (mL/m²)

	Normal small vein volume (N=7384)	High small vein volume (N=519)
Age (yr)	59.9 ± 9.0	63.9 ± 8.3
Packyears (yr)	44.0 ± 24.8	55.3 ± 28.5
Current smokers (n,%)	3795 (51.4%)	223 (43.0%)
FEV ₁ (% predicted)	76.7 ± 24.9	59.3 ± 30.5
CT quantified parameters		
Emphysema (%)	2.0 (0.6-6.7)	13.6 (4.2-27.8)
mAgatston score	15 (0-182)	86 (0-372)
Mean small venous volume (mL/m ²)	2.60 ± 0.43	3.83 ± 0.31
5-year mortality	787 (11.5%)	136 (26.9%)
10-year mortality	1714 (28.9%)	250 (53.1%)
Total mortality	2133 (28.9%)	286 (55.1%)

Legend: Data given are mean ± standard deviation or median and interquartile range in parentheses or number and percentage in parenthesis, depending on the data distribution. FEV₁ is Forced Expiratory Volume in one second, CT is computed tomography.

PE2-2 Quantitative CT Analysis based on Smoking and COPD in Normal Looking Chest CT

Gong Yong Jin

Chonbuk National University Medical School and Hospital

Purpose: To assess normal looking chest CT scans with quantitative CT (QCT) analysis based on smoking habits and chronic obstructive pulmonary disease (COPD).

Materials and Methods: 90 male patients with normal looking chest CT and quantification analysis results were enrolled in our study [normal never-smokers (n = 38) and smokers (n = 45), COPD smokers (n = 7)]. In addition, an age-matched cohort study was performed for seven smokers with COPD. The square root of the wall area of a hypothetical bronchus of internal perimeter 10 mm (Pi10), skewness, kurtosis, mean lung attenuation (MLA), and percentage of low attenuation area (%LAA) were evaluated.

Results Among patients without COPD, the Pi10 of smokers (4.176 ± 0.282) was about 0.1 mm thicker than that of never-smokers (4.070 ± 0.191 , $p = 0.047$), and skewness and kurtosis of smokers (2.628 ± 0.484 and 6.448 ± 3.427) were lower than never-smokers (2.884 ± 0.624 , $p = 0.038$ and 8.594 ± 4.944 , $p = 0.02$). The Pi10 of COPD smokers (4.429 ± 0.435 , $n = 7$) was about 0.4 mm thicker than never-smokers without COPD (3.996 ± 0.115 , $n = 14$, $p = 0.005$). There were no significant differences in MLA and %LAA between groups ($p > 0.05$).

Conclusion Even on normal looking chest CT scans, QCT showed that the airway walls of smokers are thicker than never-smokers regardless of COPD and it preceded lung parenchymal changes.

PE2-3 NOVA-CT: a novel artificial intelligence-driven volumetric CT outcome score for airway diseases

Gael Dournes, Amel Imene Hadj Bouzid, Stephanie Bui, Julie Macey, Patrick Berger

University Hospital of Bordeaux

Objectives. Holistic segmentation of CT structural alterations with 3D deep learning has recently been described in cystic fibrosis (CF), allowing the measurement of Normalized Volumes of Airway Abnormalities (NOVA-CT) as an automated quantitative outcome. Clinical validations are needed, including longitudinal and multicenter evaluations.

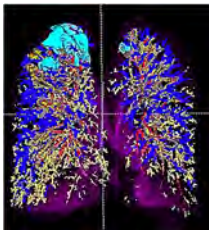
Material and Methods. The validation study was retrospective between 2010 and 2023. CF patients undergoing Elexacaftor/Tezacaftor/Ivacaftor (ETI) or corticosteroids for allergic broncho-pulmonary aspergillosis (ABPA) composed the monocenter ETI and ABPA groups, respectively. Patients from six geographically-distinct Institutions composed a multicenter External group. All patients had completed CT and pulmonary function test (PFT), with a second assessment at one year in case of ETI or ABPA treatment. NOVA-CT quantified bronchiectasis, peribronchial thickening, bronchial mucus, bronchiolar mucus, collapse/consolidation volumes, and Total Abnormal Volume (TAV) as their sum. Two observers evaluated the visual Bhalla score.

Results. 139 patients (median age, 15 years [interquartile range: 13-25]) were evaluated. All correlations between NOVA-CT to both PFT and Bhalla score were significant in the ETI (n=60), ABPA (n=20), and External groups (n=59), such as the normalized TAV ($\rho \geq 0.76$; $p < 0.001$). In both ETI and ABPA groups, there were significant longitudinal improvements in peribronchial thickening, bronchial mucus, bronchiolar mucus and collapse/consolidation ($p \leq 0.001$). An additional reversibility in bronchiectasis volume was quantified with ETI ($p < 0.001$). Intraclass correlation coefficient of reproducibility was >0.99 .

Conclusion. NOVA-CT automated scoring demonstrates validity and responsiveness for monitoring CF severity over an entire lung, and quantifies therapeutic effects on lung structure at CT, such as the volumetric reversibility of airway abnormalities with ETI.

NOVA-CT: a novel artificial intelligence-driven volumetric CT outcome score for airway diseases

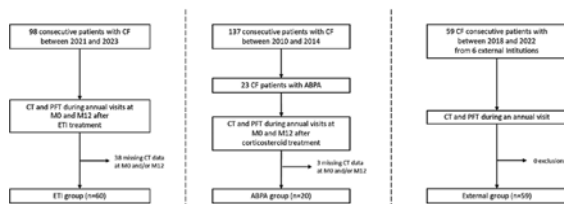
Pr. Gael DOURNES
University Hospital of Bordeaux, France



INTRODUCTION

- Visual scoring methods lack sensitivity and reproducibility to assess longitudinal bronchial changes in cystic fibrosis.
- Holistic segmentation of CT structural alterations with 3D deep learning has recently been described in cystic fibrosis (CF), allowing the measurement of Normalized Volumes of Airway Abnormalities (NOVA-CT) as an automated quantitative outcome. Clinical validations are needed, including longitudinal and multicenter evaluations.

Study flow chart



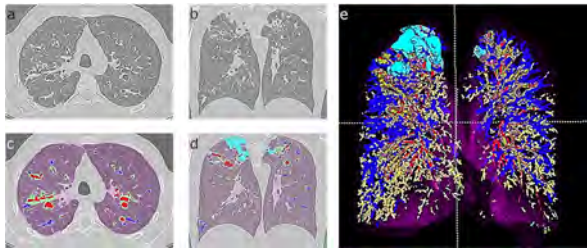
Study flow chart. CF=cystic fibrosis; CT=computed tomography; PFT=pulmonary function test; ETI=Elexacaftor/Tezacaftor/Ivacaftor; ABPA=allergic broncho-pulmonary aspergillosis; M0=initial evaluation; M12=second evaluation at 1 year.

Table 1. Characteristics of CF patients in three independent groups.

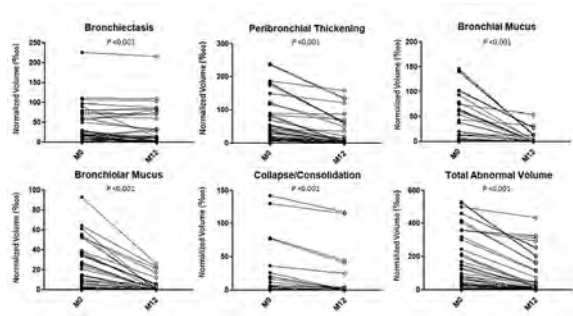
		ETI group (n=60)	ABPA group (n=20)	External group (n=59)
Age	Median [IQR]	14.6 [13-18]	16.1 [13-18]	21 [18-31]
Sex	Male [Female]	32 [28]	11 [9]	29 [30]
Height	Age M ± SD [IQR]	1.61 [1.59-1.71]	1.68 [1.61-1.71]	1.71 [1.62-1.82]
Demographic variables				
	Non-caucasian	42	12	13
	Non-caucasian	2	0	11
	Other	0	0	1
Demographics	Treatment (CT/No)	60 [2/58]	20 [0/20]	-
Pulmonary Function Test				
	FEV1% _{pred}	42.3 [39-41]	41 [39-46]	72 [60-82]
	FEV1/FVC	74 [69-80]	78 [69-86]	84 [80-91]
	BDZ ₅₀	137 [101-188]	141 [104-198]	121 [85-151]
	TLC ₅₀	136 [98-193]	93 [64-134]	108 [59-148]
Covered Demographics	Bhalla score	11 [13-18]	12 [10-18]	12 [11-13]

Factors: Data are median with [interquartile range] for continuous data and absolute numbers for categorical data.

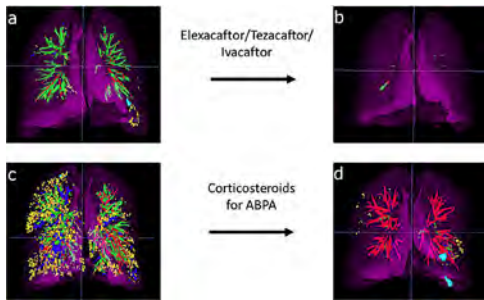
Legend: CF=cystic fibrosis; ETI=Elexacaftor/Tezacaftor/Ivacaftor; ABPA=allergic broncho-pulmonary aspergillosis; IQE=immunoglobulin E; BMI=body mass index; FEV1=forced expiratory volume in 1-second percentage predicted; FVC=forced vital capacity; RV=residual volume; TLC=total lung capacity; %p=percentage predicted.



Example of NOVA-CT quantitative measurements. CT of the chest in a 21-year-old male with cystic fibrosis, in axial (a) and coronal reformation (b). On corresponding (c) and (d) images, holistic three-dimensional segmentation by deep learning is displayed, with automated labeling of bronchiectasis (red color), peribronchial thickening (green color), bronchial mucus (blue color), bronchiolar mucus (yellow color), collapse/consolidation (cyan color), and the lung parenchyma (purple color). 3D volume rendering of lesions is displayed in (e), showing the ability to calculate the volume of airway lesions over the full CT dataset. This patient had a severe disease status, with a FEV1% of 56% and a total abnormal volume of 508 ml.



Longitudinal changes of NOVA-CT measurements in cystic fibrosis patients undergoing Elexacaftor/Tezacaftor/Ivacaftor treatment. Black circles indicate normalized volume measurements at the initiation of treatment (M0) and white circles the corresponding values at one year (M12). A significant reduction in all label volumes was noticed at paired analysis between M0 and M12, including a reduction in bronchiectasis.



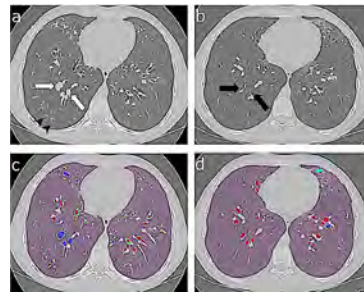
Examples of NOVA-CT holistic segmentations of displayed in 3D, demonstrating volumetric modifications of cystic fibrosis-related airway lesions in a 14-year-old female (a, b) and a 16-year-old male (c, d). Volumes in red, green, blue, yellow, cyan, and purple colors indicate bronchiectasis, peribronchial thickening, bronchial mucus, bronchiolar mucus, collapse/consolidation, and the lung parenchyma, respectively. Using Elexacaftor/Tezacaftor/Ivacaftor (ETI) (a, b), there was an improvement of FEV1% from 81 to 102% and using corticosteroids for allergic broncho-pulmonary aspergillosis (ABPA) (c, d), there was an improvement in FEV1% from the 89% to 92%. Note the most reduction in all labels' volumes with ETI (a, b), including a reversibility in bronchiectasis (red volume). Conversely, using corticosteroids for ABPA (c, d), there was a reduction in mucus but a lack of change in bronchiectasis volume.

Table 2. Correlation between quantitative CT measurement, pulmonary function test and the visual BSA score.

NOVA-CT	ETI group (n=6)				ABPA group (n=6)				Elexacaftor (n=6)			
	Walls Area	FEV1%	SAI	SAI2	Walls Area	FEV1%	SAI	SAI2	Walls Area	FEV1%	SAI	SAI2
Bronchiectasis	0.18	0.12	0.01	0.19	-0.17	-0.01	0.01	0.16	0.14	0.01	0.01	0.01
Peribronchial thickening	0.12	0.11	0.19	0.19	0.11	0.01	0.01	0.12	0.11	0.01	0.01	0.01
Bronchial mucus	0.19	0.17	0.19	0.19	0.11	0.01	0.01	0.12	0.11	0.01	0.01	0.01
Bronchiolar mucus	0.12	0.17	0.17	0.19	0.11	0.01	0.01	0.12	0.11	0.01	0.01	0.01
Collapse/Consolidation	0.19	0.17	0.17	0.19	0.11	0.01	0.01	0.12	0.11	0.01	0.01	0.01
Total Abnormal Volume	0.11	0.11	0.11	0.19	0.11	0.01	0.01	0.12	0.11	0.01	0.01	0.01

Footnote: Correlations were assessed per each segmented ETI, ABPA, and Elexacaftor group and interpreted with the coefficients of Spearman or rank. A p-value<0.05 was considered significant as indicated in bold characters.

Legend: NOVA-CT-normalized volume of airway abnormalities; CT-scanogram segmentation; 3D-normal evaluation; M0=baseline evaluation at 1 year after treatment; ETI=Elexacaftor/Tezacaftor/Ivacaftor; ABPA=allergic broncho-pulmonary aspergillosis; FEV1%=forced expiratory volume in 1 second percentage predicted.



Axial CT slice of the chest in a 16-year-old male with cystic fibrosis and undergoing corticosteroid for allergic broncho-pulmonary aspergillosis treatment at initiation (a) and after one year (b). Low dose CT (1.4 mSv) was done on a Siemens Definition648 CT scan, reconstructed with a B40s kernel and displayed with a parenchymal window width and level (width, 1500 Hounsfield Unit; level -450 Hounsfield Unit). White arrows indicate bronchiectases (a), black arrowhead small bronchiolar impactions (a) and black arrows indicate mucus-free dilatation of the bronchial lumen (b). In corresponding (c) and (d) images, NOVA-CT fully automated and holistic segmentations are shown. Red, green, blue, yellow, and purple colors indicate bronchiectasis, peribronchial thickening, bronchial mucus, bronchiolar mucus, and lung parenchyma, respectively. Note the resolution of peribronchial thickening, bronchial, and bronchiolar mucus but not bronchiectasis after treatment.

CONCLUSION

NOVA-CT automated scoring demonstrates validity, reliability and responsiveness for monitoring CF disease severity over an entire lung, and quantifies therapeutic effects on lung structure at CT, such as the volumetric reversibility of airway abnormalities with ETI.

PE2-4 Respiratory function evaluation using CT airway analysis in thoracic scoliosis surgery

Nanae Tsuchiya, Kume Matsushita, Yukari Tomori, Akira Yogi, Gyo Iida, Akihiro Nishie

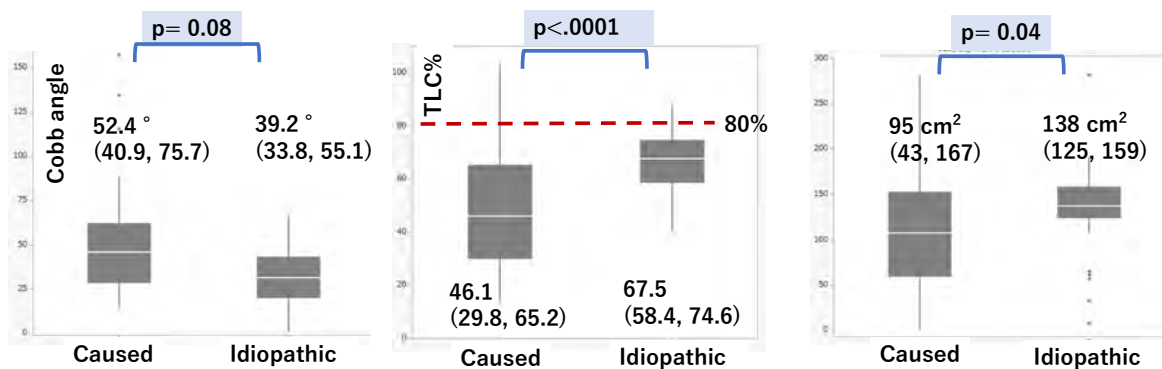
University of the Ryukyus

Purpose: To investigate whether surgical treatment improves airway deformity and respiratory dysfunction by pre- and post-operative CT airway analysis for thoracic scoliosis.

Methods: 52 thoracic scoliosis patients with pre- and post-operative CT scans: idiopathic scoliosis group (23 patients) and causative scoliosis group (29 patients) were included. From CT images, spinal thoracic deformation parameters: Cobb angle, apical vertebral translation, apical vertebral body-rib ratio, rotation angle, and respiratory function parameters: lung capacity, predicted total lung capacity (TLC%), maximum and minimum airway diameters, cross-sectional area, left and right main bronchial length ratio, were measured. Comparison between two groups of scoliosis classification, correlation between spinal deformation parameters and respiratory function parameters, and changes in parameters before and after surgery were statistically investigated.

Results: Respiratory function parameters were significantly decreased in the causative scoliosis than in the idiopathic scoliosis (TLC%: 46.1% vs 67.5%, $p < 0.0001$, tracheal stenosis area: 95cm² vs 138 cm², $p = 0.04$). In the causative scoliosis, a significant negative correlation was observed between Cobb angle and TLC% ($r = -0.57$, $p < 0.002$). There was a significant improvement in the Cobb angle after scoliosis surgery in both the idiopathic scoliosis (39.2 degrees vs 52.4 degrees, $p < 0.0001$) and the causative scoliosis (33.3 degrees vs 52.4 degrees, $p < 0.0001$). On the other hand, no significant improvement was observed in respiratory function parameters.

Conclusion: CT airway analysis was able to assess airway deformity and respiratory dysfunction in thoracic scoliosis, but there was no significant improvement in respiratory function parameters after surgical treatment.



PE2-5 Correlation of dynamic chest radiograph (DCR) with respiratory function: a study of asthma cases

Masahiro Kaneko, Koudai Miyamoto, Yu Kobayashi, Masamichi Li, Masaaki Iwabayashi, Makoto Yokota, Yuu Matsuoka, Hisanori Amimoto, Jyunji Takiguchi, Hiroshi Fujii, Hiromi Tomioka
Kobe City West Hospital

OBJECTIVE: To investigate the correlation between lung area change rate measured by dynamic chest radiography (DCR), symptoms, and respiratory function in asthma patients.

SUBJECTS: Asthma patients who were evaluated for DCR and respiratory function during the stable period from April 2023 to March 2024.

METHODS: We analyzed asthma 158 cases (ACO 38 cases, asthma excluding ACO 120 cases), the correlation lung area (at maximal inspiratory position, change rate) and height, BMI, CAT score and respiratory function tests (VC, IC, FEV1, FEV1/FVC, MMF, PEF, RV, FRC, TLC, RV/TLC) with the statistical software JMP14. The diagnosis of ACO was made according to the Guide to the Overlap Diagnosis and Treatment of Asthma and COPD, 2nd edition.

RESULTS: Lung area change was correlated with BMI, VC, IC, FEV1, %FEV1, MMF, PEF, RV/TLC, and IC/TLC in all asthma cases, with BMI, ACT, CAT, VC, IC, FEV1, PEF, and IC/TLC in ACO cases, and with VC, IC, FEV1, MMF, and IC/TLC in asthma cases except for ACO. PEF, and IC/TLC in asthma cases except ACO.

CONCLUSION: In asthma patients, lung area change correlates with indexes of obstructive impairment and IC/TLC. of obstructive impairment and IC/TLC.

	対象症例の背景 characteristics			
	asthma total	ACO	asthma without ACO	p-value
n	158	38	120	-
age [y.o.]	70 [56-78]	74 [67-79]	68 [52-77]	0.0197
male/female	78/80	25/13	53/67	0.0194x
height [m]	161 [153-169]	163 [157-169]	160 [152-168]	0.2835
BMI [kg/m ²]	23.22 [20.74-256.93]	23.2 [21.04-26.30]	22.62 [19.05-25.15]	0.0799
ACT [score]	24 [19-25]	20 [16-24]	24 [20-25]	0.0009
CAT [score]	11 [5-24]	19 [10-25]	9 [4-18]	0.0077
lung area (maximal) [cm ²]	41594±7844	44636±7835	40631±7629	0.0057
%change of lung area [%]	31.58±8.80	25.52±8.06	33.19±8.44	<0.0001
VC [L]	2.798±0.912	2.722±0.954	2.822±0.902	0.5567
ATI [%]	4.03 [0.59-8.32]	6.14 [2.09-13.6]	3.63 [0-7.65]	0.0104
IC [L]	2.015±0.686	1.852±0.729	2.067±0.666	0.0923
FEV ₁ [L]	1.86 [1.36-2.53]	1.41 [0.93-1.86]	2.045 [1.49-2.72]	<0.0001
FEV ₁ [%]	75.1 [64.5-81.6]	56.7 [50.2-64.8]	78.2 [72.5-83.1]	<0.0001
MMF [L]	1.35 [0.93-2.54]	0.62 [0.36-1.00]	1.73 [1.17-2.78]	<0.0001
PEF [L]	5.22 [3.59-7.00]	3.51 [2.81-5.02]	5.65 [4.13-7.47]	<0.0001
RV [L]	1.77 [1.42-2.25]	2.03 [1.66-2.57]	1.72 [1.38-2.10]	0.0043
FRC [L]	2.57 [2.06-3.17]	3.13 [2.37-3.68]	2.45 [2.02-2.94]	0.0066
TLC [L]	4.716±1.242	4.884±1.268	4.660±1.234	0.3446
RV/TLC	39.7 [32.6-47.5]	44.3 [38.1-49.7]	37.8 [30.6-57.3]	0.0059
IC/TLC	43.21±10.34	37.91±10.57	44.98±9.69	0.0003

肺面積変化率と身体計測・症状スコア・呼吸機能の相関

Correlation between lung area change rate and symptom score and respiratory function

	r	p
age [y.o.]	-0.2452	0.0144
height [m]	0.2983	0.0016
BMI [kg/m ²]	0.4288	0.0028
ACT [score]	0.2778	0.2160
CAT [score]	-0.2536	0.5922
VC [L]	0.4255	0.0003
IC [L]	0.5366	<0.0001
FEV ₁ [L]	0.5525	<0.0001
FEV ₁ [%]	0.4294	0.0174
MMF [L]	0.4366	<0.0001
PEF [L]	0.6240	<0.0001
RV [L]	-0.1271	0.4862
FRC [L]	-0.1155	0.5459
TLC [L]	0.2205	0.0014
RV/TLC	-0.4182	<0.0001
IC/TLC	0.5554	<0.0001

肺面積変化率と症状スコア・呼吸機能の相関：喘息(除 ACO)

Correlation between lung area change rate and symptom score and respiratory function : asthma excluding ACO

	r	p
age [y.o.]	-0.2821	0.0171
height [m]	0.3686	0.0016
BMI [kg/m ²]	0.3496	0.0028
ACT [score]	0.1486	0.2160
CAT [score]	-0.0646	0.5922
VC [L]	0.4176	0.0003
IC [L]	0.5094	<0.0001
FEV ₁ [L]	0.4834	<0.0001
FEV ₁ [%]	0.2814	0.0174
MMF [L]	0.4582	<0.0001
PEF [L]	0.5888	<0.0001
RV [L]	-0.0840	0.4862
FRC [L]	-0.0729	0.5459
TLC [L]	0.2344	0.0491
RV/TLC	-0.3728	0.0014
IC/TLC	0.5166	<0.0001

肺面積変化率と症状スコア・呼吸機能の相関：ACO

Correlation between lung area change rate and symptom score and respiratory function: ACO

	r	p
age [y.o.]	-0.1257	0.5239
height [m]	0.2759	0.1553
BMI [kg/m ²]	0.5614	0.0019
ACT [score]	0.4212	0.0256
CAT [score]	-0.4241	0.0245
VC [L]	0.4887	0.0083
IC [L]	0.5810	0.0012
FEV ₁ [L]	0.5287	0.0038
FEV ₁ [%]	0.3689	0.0534
MMF [L]	-0.0429	0.8284
PEF [L]	0.5159	0.0050
RV [L]	-0.0209	0.9159
FRC [L]	0.0212	0.9148
TLC [L]	0.3476	0.0699
RV/TLC	-0.3882	0.0412
IC/TLC	0.4839	0.0091

Lung Cancer

PE3-1 Incidental Findings in the HANSE LCS Trial - Preliminary Report

Rimma Kondrashova^{1,2}, Katharina May³, Susanne Stiebeler⁴, Sabine Dettmer^{1,2}, Benjamin-Alexander Bollmann¹, Anton Faron⁴, Gerald Schmid-Bindert⁵, Joerg Barkhausen³, Sabine Bohnet³, Martin Reck⁶, Jens Vogel-Claussen^{1,2}

- 1) Institute of Diagnostic and Interventional Radiology, Hannover Medical School, Hannover, Germany
- 2) Biomedical Research in Endstage and Obstructive Lung Disease Hannover (BREATH), German Center for Lung Research (DZL), Hannover, Germany
- 3) Universitätsklinikum Schleswig-Holstein, Campus Lübeck, Lübeck, Germany
- 4) Radiologische Allianz | LungenClinic Großhansdorf, Großhansdorf, Germany
- 5) University Medical Center Mannheim, Heidelberg University, Mannheim, Germany
- 6) LungenClinic Grosshansdorf, Großhansdorf, Germany

Purpose: To investigate the prevalence of incidental findings (IF) in the HANSE lung cancer screening (LCS) population.

Background & Methods: The implementation of LCS-programs has highlighted the evaluation of IFs - while the vast majority require no-action, others necessitate diagnostic follow-up or treatment. Overall, 9546 low-dose-CTs (LDCT) from the HANSE-Trial (baseline and one-year follow-up) were evaluated regarding IFs at three participating sites (Hannover (H), Lübeck (L) and Grosshansdorf (G)), other than coronary calcium and emphysema.

Results: Across three centers, a total of 1159 IFs were reported in 956/5191 (18.4%) subjects in the first, and 444 new IFs in 397/4356 (9.1%) subjects in the second round. In 682/5191 (13.1%) participants (baseline) and 154/4356 (3.5%) participants (new IF at one-year follow-up) follow-up imaging procedures or further downstream work-up were recommended in the LDCT-report. The IF reporting frequency varied between centers. Baseline: H: reported/downstream procedures recommended 194/159/1770 (11.0%,9.0%), L: 456/298/1772 (25.7%,16.8%), G: 509/225/1659 (30.7%,13.6%). One-year follow-up: H: reported/downstream procedures recommended 53/46/1527 (3.5%,3.0%), L: 92/34/1467 (6.3%,2.3%), G: 299/74/1362 (16.8%,5.4%). Overall, 13 IFs (<1%) uired operative treatment: aortic aneurism, atrial lipoma with upper inflow congestion, implant loosening, abscess, 2 goiters with tracheal narrowing and 4 malignances (typical carcinoid, sarcoma, thymic and renal cell carcinoma).

Conclusion: Less than 1% of participants required treatment of IFs in the HANSE-Trial. Only IFs warranting definite follow-up or treatment should be reported to reduce harm and healthcare costs of unnecessary downstream procedures. The HANSE-Trial showed that quality control is needed in an LCS-program to ensure accurate reporting of clinically relevant IFs. NSE-Trial showed that quality control is needed in an LCS-program to ensure accurate reporting of clinically relevant IFs.

A. Baseline	Hannover	Lübeck	Großhansdorf
Total exams	1770	1772	1659
Reported IFs	194	456	509
Recommended DPs	159	298	225
B. One-year follow-up	Hannover	Lübeck	Großhansdorf
Total exams	1527	1467	1362
Reported IFs	53	92	299
Recommended DPs	46	34	74
IF = incidental finding; DP = downstream procedure			

PE3-2 Characteristics of Ground-Glass Nodules in Female Never-Smokers with a Family History of Lung Cancer

Soon Ho Yoon¹⁾, Ji Young Lee¹⁾, Seung Ho Choi,²⁾ Hyungjin Kim¹⁾, Jin Mo Goo¹⁾

1) Department of Radiology, Seoul National University Hospital

2) Department of Internal Medicine and Healthcare Research Institute, Healthcare System Gangnam Center

Purpose: This study aimed to investigate the characteristics of ground glass nodules (GGNs) in female never-smokers with a family history of lung cancer (FHLC).

Methods: This retrospective study included 10,151 female never-smokers who underwent baseline low-dose chest CT scans for health check-ups from 2011 through 2015. The clinico-radiologic characteristics of GGNs were analyzed at baseline and follow-up. The prevalence of persistent GGNs and multiple GGNs, GGN growth, and lung cancer incidence were compared in participants with and without an FHLC. Multivariate logistic and Cox regression analyses explored associations between FHLC and GGN prevalence and growth.

Results: Of the 10,151 participants, 694 (6.8%) reported an FHLC. Among these, 515 (5.1%) had persistent GGNs, 199 (2.0%) had multiple GGNs, 49 (0.5%) experienced GGN growth, and 31 (0.3%) were diagnosed with lung cancer. Participants with an FHLC had higher prevalence rates of persistent GGN (8.2% vs. 4.8%), multiple GGNs (3.7% vs 1.8%), GGN growth (1.3% vs 0.4%), and lung cancer incidence (0.9% vs 0.3%). FHLC was associated with an increased prevalence of persistent GGN (odds ratio [OR] 1.686; 95% CI, 1.260-2.255; $p < 0.001$) and multiple GGNs (OR 2.015; 95% CI, 1.320-3.075; $p = 0.001$). It was also an independent risk factor for GGN growth over a 10-year period (HR 2.117; 95% CI, 1.019-4.399; $p = 0.044$), after adjusting for total size and the solid proportion of baseline GGNs.

Conclusions: Female never-smokers with an FHLC had a higher risk for developing persistent, multiple, and growing GGNs, highlighting the need for targeted screening.

PE3-3 Interobserver Variability in Lung-RADS Categorization: Tertiary Hospital vs. Non-tertiary Hospitals

You Na Kim, Seulgi You, Joo Sung Sun, Kyung Joo Park

Ajou University School of Medicine

Objectives

To evaluate interobserver agreement and diagnostic performance for Lung-RADS categorization between a tertiary hospital and non-tertiary hospitals.

Material and Methods

We retrospectively reviewed low-dose lung cancer screening CT images performed at 24 non-tertiary hospitals from August 2018 to October 2023, which were referred to a tertiary hospital. A thoracic radiologist re-interpreted these CT images. We assessed the variability in Lung-RADS categorization among non-tertiary and tertiary hospital readings, and the thoracic radiologist's reading. Modified Korean versions of Lung-RADS 1.0 and 1.1 were used. Interobserver agreement was analyzed using Cohen's kappa statistics. The diagnostic performance for predicting lung cancer was compared using the McNemar test.

Results

Fifty patients (mean age, 62 ± 7.6 years; 49 men and 1 woman) with 33 confirmed final diagnoses (15 lung cancers and 18 benign nodules) were included. There was fair agreement in Lung-RADS categorization between the tertiary and non-tertiary hospital reports ($\kappa = 0.30$, 95% CI 0.13-0.47), and fair agreement between non-tertiary hospital reports and the thoracic radiologist's interpretation ($\kappa = 0.33$, 95% CI 0.16-0.50). Almost perfect agreement was observed between the tertiary hospital report and the thoracic radiologist's interpretation ($\kappa = 0.89$, 95% CI 0.80-0.98). Specificity was significantly higher in the tertiary hospital reading (72.2%, 13/18) than in non-tertiary hospital readings (16.7%, 3/18; $p = 0.002$). Sensitivity did not differ significantly between the tertiary hospital and non-tertiary hospital readings (100% vs. 93.3%, respectively).

Conclusion

Interobserver agreement for Lung-RADS categorization between the tertiary and non-tertiary hospitals was low, with non-tertiary hospitals showing more false-positive results in lung cancer screening.

PE3-4 Real world impact of DL supported CAD for routine chest CT on management of incidental lung nodules

Edwin J.R. van Beek¹⁾, Rishi Ramaesh²⁾, Maurits Engbersen³⁾, Malihe Javidi¹⁾, David King³⁾, Jonathan Rodrigues⁴⁾, Miguel Bernabeu¹⁾

- 1) University of Edinburgh
- 2) NHS Lothian Health Board
- 3) DeepHealth
- 4) University of Bath

Purpose or Learning Objective: Incidental lung nodules at CT provide an opportunity for the timely detection of early-stage lung cancer. Computer-aided detection (CAD) supported by deep-learning aims to assist radiologists in the detection and further assessment of nodules. This study investigates the effect of CAD on agreements in management recommendations between the reporting radiologist and an expert peer reviewer.

Methods or Background: In this multicenter prospective, ethics approved study, participating radiologists from 4 centers reported on chest CTs in adult patients without a history of malignancy or nodules, during routine practice with the CAD as 'second reader.' The reporters documented management recommendations concerning lung nodules sequentially, without CAD and with CAD. All cases with nodules found either by CAD or the reporter were independently reviewed by a thoracic radiologist with at least 8 years experience (range 8 – 25 years). Recommendations of the reporter, with and without CAD, were compared to the recommendations of the reviewer. Agreement between recommendations were assessed with quadratic weighted kappa, and the difference was tested with a William's test.

Results or Findings: Nineteen percent (237/1264) of CTs had lung nodules detected and confirmed by the reviewer. In 11.4% (27/237) of nodule cases, the reporting radiologist had changed their recommendation after CAD. The most frequent reason given for this change was an initially missed nodule (8.4%; 20/237). The weighted kappa between the reporters' and the reviewers' recommendations was 0.49 and 0.55, unaided and aided by CAD ($p = 0.04$).

Conclusion: Aided by CAD, reporting radiologists found more incidental lung nodules and provided management recommendations which are more in agreement with an expert reviewer, suggesting a significant contribution of CAD to the clinical management of incidental nodules.

Demographics and changes due to CAD use

n	1264	
Age (sd)	65.02 (15.84)	
Sex		
- male	639 (50.6%)	
- female	617 (48.8%)	
- missing	8 (0.6%)	
	Unaided assessment	Aided assessment
CT scans reported with lung nodules	219/1264 (17.3%)	256/1264 (20.2%)
CT scans reported with indeterminate lung nodules	153/1264 (12.1%)	176/1264 (13.9%)

Management decision before and after CAD

	Reader without VLN	Reader with VLN
n (<i>de novo</i>)	1266	1266
value (%)		
No follow-up/discharge	1077 (85.1)	1054 (83.3)
12m	6 (0.5)	7 (0.6)
6m	4 (0.3)	5 (0.4)
3m	92 (7.3)	114 (9.0)
Workup	51 (4.0)	50 (4.0)
NA or missing	36 (2.8)	36 (2.8)

PE3-5 Application of Fractal Analysis to Chest CT of NSCLC Patients Undergoing Radiotherapy for Prognosis

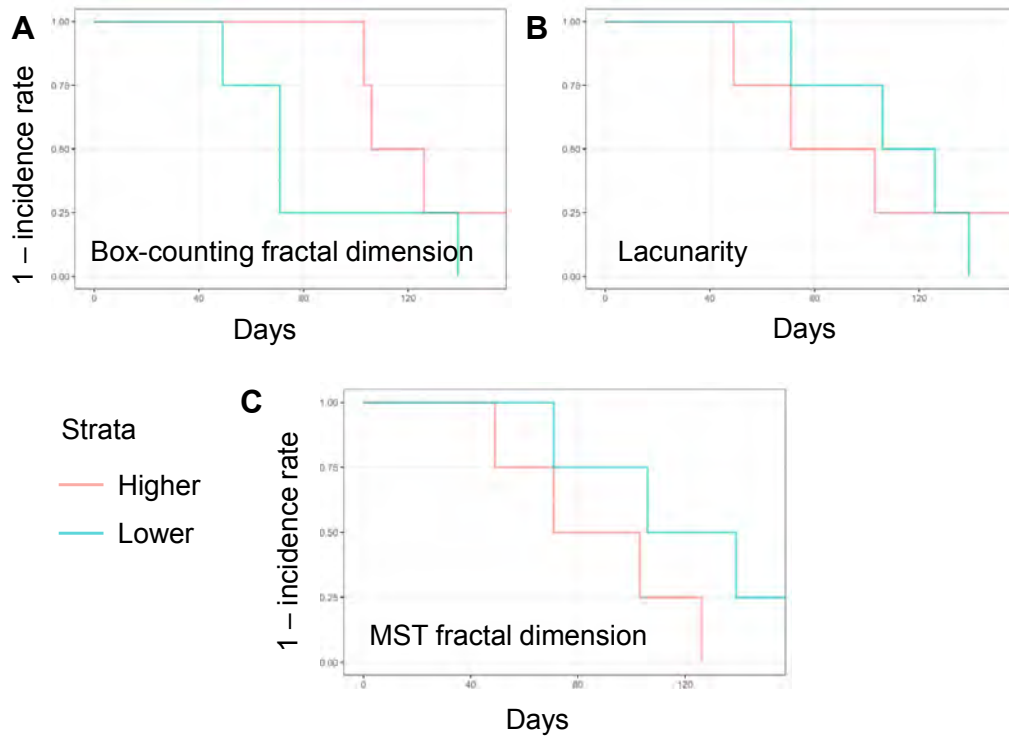
Jeongeun Hwang, Hakyoung Kim, Joon-Young Moon

Soonchunhyang University

For NSCLC patients undergoing radiotherapy, underlying IPF are more vulnerable to pulmonary toxicity following radiotherapy [1]. Our previous study [2] demonstrated that the morphometric complexity in the lung parenchyma could be measured by a box-counting fractal dimension (FD) method, and it could be utilized as a prognostic indicator for severe pulmonary toxicity. Given this, we compared it with lacunarity and minimum-spanning tree (MST) FD in terms of their prognostic performance and assessed the correlations among these methods.

Twelve IPF patients treated with definitive radiotherapy were enrolled and underwent CT scans. Normal attenuation areas (NAA) were defined and binarized at lung voxels between ≥ 950 HU and < -700 HU. Box-counting FD, lacunarity, and MST FD were measured on the NAA masks by using in-house MATLAB scripts.

Incidence curves for severe pulmonary toxicity are shown in Figure 1, where all the p-values of the log-rank tests exceeded 0.05, indicating that the small sample size of 12 hindered the discovery of statistically significant predictors that could distinguish the incidence curves along them. Further studies with more patients would be needed to find out statistical significance. Nevertheless, the results qualitatively show the potential of the morphometric complexity features as prognostics for pulmonary toxicity.



Interstitial Pneumonia

PE4-1 Quantitative computed tomography assessment of lung volumes in interstitial lung diseases

Yi Xian Cassandra Yang, Min On Tan, Kai Chin Poh, Srujana Ganti,
Uppaluri Srinivas Anandswaroop

Sengkang General Hospital

Background

The assessment of lung function via pulmonary function tests (PFT) is important in patients with interstitial lung disease (ILD), as they provide information on disease activity and progression. However, performing PFTs requires active participation by patients, which may be challenging for some.

This study aims to assess the reliability of volumetric measurements on routine chest computed tomography (CT) scans using a post-processing quantitative analysis tool, which can act as an adjunct to PFTs in the follow-up of ILD patients.

Methods

This is a retrospective single-centre cohort study. 24 sets of chest CT studies and PFTs from 11 adult patients with a diagnosis of ILD were included in the study. Lung volumes were calculated from serial chest CTs using a volumetric software.

Results

There is a good correlation between CT-derived total lung volumes (TLV) with forced vital capacity (FVC) ($p < 0.05$) and total lung capacity (TLC) ($p < 0.05$) measurements obtained via PFTs.

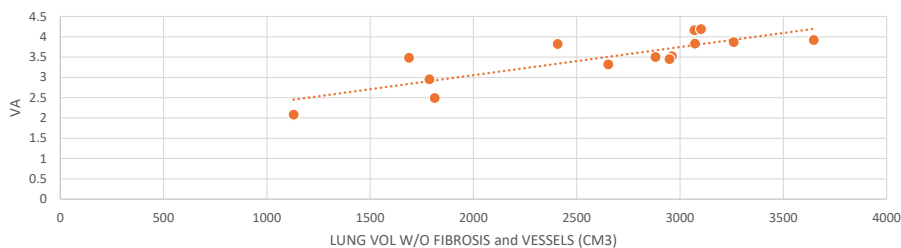
Conclusion

Automated CT-derived total lung volume may be considered as an alternative or adjunct to PFTs for the assessment of lung volumes in ILD patients.

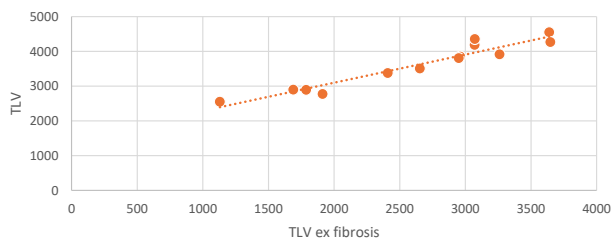
Key words

Lung function, lung volumetry, computed tomography

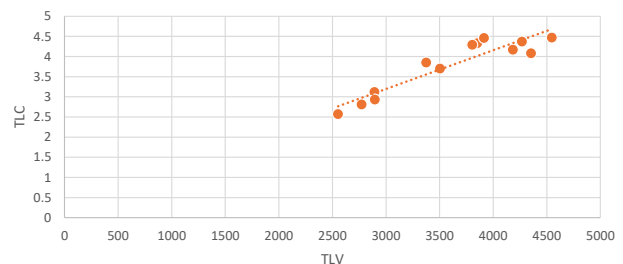
Field: LUNG VOL W/O FIBROSIS and VESSELS (CM3) and Field: VA appear highly correlated.



Field: TLV ex fibrosis and Field: TLV appear highly correlated.



Field: TLV and Field: TLC appear highly correlated.



VA= alveolar volume
TLV= total lung volume
TLC= total lung capacity

PE4-2 Automated Quantification of ILA and emphysema on CT: A Predictive Marker for PPC after Esophagectomy

You Jin Oh^{1,2)}, Seong Yong Park³⁾, Yunjoo Im⁴⁾, Hye Yoon Park⁵⁾, Ho Yun Lee^{1,2)}

1) Department of Health Sciences and Technology, SAIHST, Sungkyunkwan University,

2) Department of Radiology and Center for Imaging Science, Samsung Medical Center, Sungkyunkwan University School of Medicine,

3) Department of Thoracic and Cardiovascular Surgery, Samsung Medical Center, Sungkyunkwan University School of Medicine,

4) Division of Pulmonology and Allergy, Department of Internal Medicine, Kyung Hee University Medical Center,

5) Division of Pulmonary and Critical Care Medicine, Department of Medicine, Samsung Medical Center, Sungkyunkwan University School of Medicine

Objective: Postoperative pulmonary complications (PPC), including pneumonia, acute lung injury, and acute respiratory distress syndrome, are common morbidities and significant causes of mortality following esophagectomy. This retrospective study was conducted to assess the impact of pattern analysis of preoperative chest CT on PPC following esophagectomy.

Methods: Between 2016 and 2022, 795 patients who underwent upfront esophagectomy analyzed. We used deep learning-based automatic quantification of interstitial lung abnormality (ILA) and emphysema by chest CT. Logistic regression analyses were performed to identify risk factors for PPC.

Results: Mean age was 64.72 ± 8.27 with 698 (91.2%) male patients. PPC was developed in 129 (16.2%) patients. Current smokers were more prevalent in the PPC group, which also showed worse pulmonary function than their counterparts. The patients with PPC were more likely to have undergone open esophagectomy and intrathoracic anastomosis PPC patients exhibited larger extent of emphysema (0.123% vs. 0.236%, $p=0.005$) and ILA (0.149% vs. 0.342%, $p<0.001$) on chest CT scan. Multivariable logistic analysis demonstrated that extent of emphysema (odds ratio [OR] 1.158, $p=0.004$) and ILA (OR 1.364, $p<0.001$) were risk factors for PPC after adjusting for other confounding factors.

Conclusions: The extent of emphysema and ILA, quantified by automated software, was significantly associated with PPC. Future research should focus on perioperative management strategies for patients with emphysema / ILA and esophageal cancer.

Tables

Table 1. Basic characteristics of patients (n=765)

	No PPC (n=636)	PPC (n=129)	p
Age	64.48 ± 8.09	65.84 ± 9.02	0.089
Male	576 (90.6%)	122 (94.6%)	0.142
Smoking status			<0.001
Never smoker	81 (12.7%)	6 (4.7%)	
Ex-smoker	300 (47.2%)	43 (33.3%)	
Current smoker	255 (40.1%)	80 (62.0%)	
FEV1%	90.69 ± 14.28	85.74 ± 16.40	0.0005
DLC0%	87.25 ± 17.91	78.04 ± 15.14	<0.001
FEV1/FVC	73.53 ± 8.54	69.70 ± 10.25	<0.001
Pathology			0.325
Squamous cell carcinoma	598 (94.03%)	125 (96.9%)	
Adenocarcinoma	31 (4.87%)	4 (3.10%)	
Others	7 (1.10%)	0	
Location of lesion			0.476
Cervical	5 (0.79%)	0	
Upper	81 (12.74%)	15 (11.63%)	
Mid	271 (42.61%)	50 (38.76%)	
Lower	244 (38.36%)	59 (45.73%)	
EG junction	35 (5.5%)	5 (3.88%)	
pT			0.167
Tis	7 (1.1%)	0	
T1a	92 (14.5%)	14 (10.9%)	
T1b	348 (54.7%)	67 (51.9%)	
T2	84 (13.2%)	27 (20.9%)	
T3	100 (15.8%)	21 (16.3%)	
T4a	4 (0.7%)	0	
pN			0.164
N0	399 (62.8%)	82 (63.6%)	
N1	162 (25.6%)	25 (19.4%)	
N2	54 (8.5%)	19 (14.7%)	
N3	18 (2.8%)	3 (2.3%)	
Nx	2 (0.3%)	0	
Minimally invasive esophagectomy	237 (37.3%)	25 (19.4%)	<0.001
Level of anastomosis			<0.001
Intrathoracic anastomosis	380 (59.8%)	100 (77.5%)	
Cervical anastomosis	256 (40.3%)	29 (22.5%)	

Table 2. Parameters measured by automated quantification. All parameters were described with median (interquartile range).

	No PPC (n=636)	PPC (n=129)	p*
Whole lung volume (mL)	4920.561 (4247.186–5629.445)	4794.276 (4106.011–5608.299)	0.804
Ground glass opacity (%), unit: $\times 10^{-3}$	98.837 (41.056–289.550)	211.111 (69.399–588.326)	<0.001
Reticulation (%), unit: $\times 10^{-3}$	39.094 (11.932–131.261)	96.273 (29.302–272.917)	<0.001
Honeycombing (%), unit: $\times 10^{-3}$	0.098 (0–0.533)	0.313 (0.028–1.333)	<0.001
Extent of ILA (%)	0.149 (0.062–0.502)	0.342 (0.126–0.821)	<0.001
Extent of emphysema (%)	0.123 (0.036–0.462)	0.236 (0.033–1.367)	0.005

* Mann-Whitney U test.

Table 3. Univariable and multivariable analysis for postoperative pulmonary complications.

	Univariable analysis		Multivariable analysis	
	Odds ratio (95% confidence interval)	P	Odds ratio (95% confidence interval)	P
Sex	0.551 (0.246–1.234)	0.147
Age	1.020 (0.997–1.044)	0.090
Age (< 65, 1 year increase)	0.988 (0.935–1.045)	0.674	0.967 (0.912–1.025)	0.258
Age (≥ 65, 1 year increase)	1.044 (0.993–1.097)	0.0906	1.054 (0.997–1.114)	0.062
Smoking status				
Ex-smoker (vs. non-smoker)	1.935 (0.795–4.705)	0.145	1.680 (0.667–4.236)	0.271
Current smoker (vs. non-smoker)	4.235 (1.780–10.073)	0.001	4.887 (1.962–12.169)	0.001
Open thoracotomy (vs. minimally invasive esophagectomy)	0.430 (0.276–0.670)	<0.001	0.485 (0.304–0.775)	0.003
FEV1 (%)	0.977 (0.965–0.990)	0.001	0.981 (0.966–0.997)	0.019
Extent of ILA (%), log scale	1.049 (1.002–1.097)	0.039	1.364 (1.182–1.573)	<0.001
Extent of emphysema (%), log scale	1.114 (1.045–1.189)	0.001	1.158 (1.049–1.279)	0.004

PE4-3 Temporal volumetric concordance between bronchi and lung field on dynamic ventilation CT

Yukihiro Nagatani, Hiroaki Nakagawa, Ryo Uemura, Kentaro Fukunaga, Yoko Tsunoda, Yasutaka Nakano, Yoshiyuki Watanabe

Shiga University of Medical Science

Purpose

To compare the temporal concordance of trachea-bronchial volumes to global lung volumes during respiration between IPF and non-IPF patients and to investigate their associations with pulmonary functions

Materials and methods

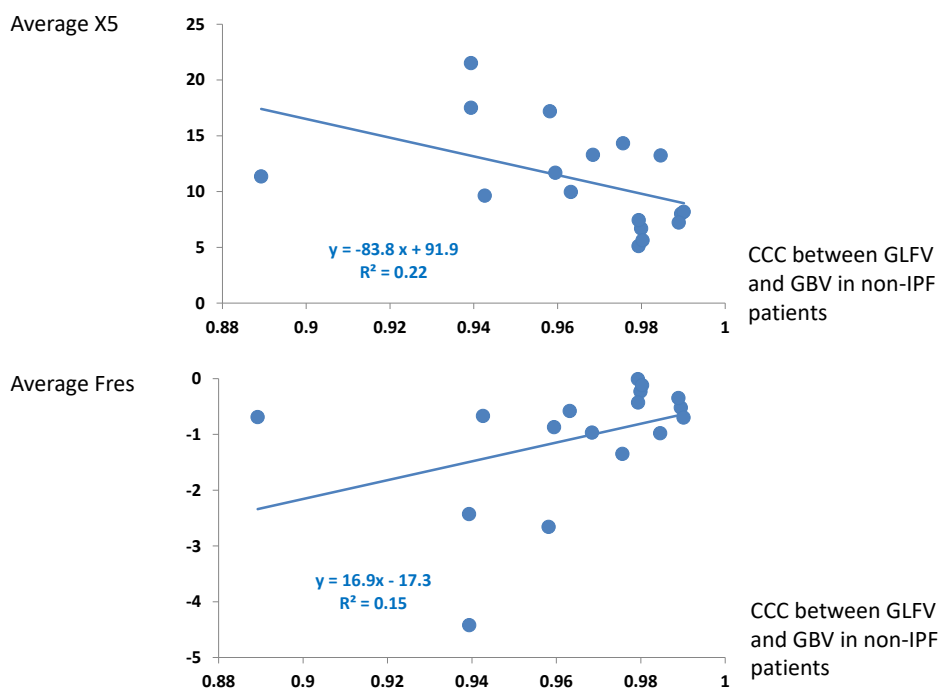
Twenty-eight patients including 11 IPF/UIP and 17 non-IPF/UIP patients underwent both DVCT by using 320-row scanner during single respiration for upper and lower lung fields (4.8 mSv) and pulmonary function test (PFT) in a single visit. In each of the included phases, global lung field volumes (GLFVs), global bronchial volumes (GBVs) and tracheal volumes were measured based on automatic segmentation by the dedicated software. Cross-correlation coefficients as concordance indices among GLFVs, GBVs and tracheal volumes were compared between IPF and non-IPF patients, and correlated with PFT parameters including measured values by forced oscillation technique. Phase delay of GBV against GLFV for the maximal and minimal measured values was also compared between IPF and non-IPF patients.

Results

CCCs in IPF patients (0.942 ± 0.062) were equivalent to those in non-IPF patients (0.965 ± 0.025), whereas the phase delay for the maximal measured values in IPF patients (0.45 ± 0.52) was larger than that in non-IPF patients (-0.12 ± 0.49). CCCs between GLBV and GBV in non-IPF patients demonstrated positive correlations with inspiratory average X5 ($r=0.498$, $p=0.042$), and negative correlations with average Fres ($r=-0.645$, $p=0.005$).

Conclusion

DVCT demonstrated that elevated respiratory reactance under rest breathing can be reflected in the discordance between GLFV and GBV in non-IPF patients and late inspiratory GBV increase compared with GLFV was delayed in IPF patients.



PE4-4 Prediction of antifibrotic therapy response for idiopathic pulmonary fibrosis by quantitative CT

Hidetake Yabuuchi¹⁾, Kouji Sagiyama²⁾, Yuzo Yamasaki²⁾, Tomoyuki Hida²⁾, Takuya Hino²⁾, Kazuya Tsubouchi³⁾, Tomotsugu Takano³⁾, Kousei Ishigami³⁾

1) Department of Health Sciences, Graduate School of Medical Sciences, Kyushu University

2) Department of Clinical Radiology, Graduate School of Medical Sciences, Kyushu University

3) Department of Respiratory Medicine, Graduate School of Medical Sciences, Kyushu University

Background: The %FVC decline following antifibrotic therapy is a significant prognostic factor for idiopathic pulmonary fibrosis (IPF) treated with antifibrotic drugs; however, imaging features, including quantitative parameters have not yet been investigated.

Purpose: To determine whether quantitative CT parameters can predict therapeutic response after antifibrotic drug therapy for IPF.

Materials and Methods: Thirty-one IPF patients (27 men, 4 women; mean age, 72.0 years) treated with antifibrotic drugs for more than one year were examined. Seven type lesions (air space, consolidation, consolidation with bronchiectasis i.e. fibrosis, ground-glass opacity, honeycombing, reticular opacity, traction bronchiectasis, normal lung, and emphysema) ratio and pulmonary vascular volume ratio were extracted from 3D volume CT using the software (QZIP-ILD, Ziosoft) and compared between responders and non-responders. Clinical parameters at baseline (age, sex, smoking index, KL-6 level, %FVC, and %DLCO) were also compared between the two groups. Non-responders were defined as patients with a 10% or more decrease in %FVC one year after the initiation of antifibrotic therapy. The predictive capability was evaluated using the receiver operating characteristic curve.

Results: Mean fibrotic lesion ratio was significantly higher in non-responder group than that of responder group (3.65 ± 2.49 vs. 2.12 ± 2.03 , $P < 0.05$), whereas there were no significant differences in other parameters. The diagnostic capability of the fibrotic lesion ratio (AUC, 0.78) was superior to that of other parameters.

Conclusion: The fibrotic lesion ratio derived from 3D volume CT data seems to be a promising tool to help predict therapeutic response in patients with IPF treated with antifibrotic drugs.

PE4-5 Quantitative Risk Thresholds for Interstitial Lung Abnormalities and Prognostic Associations

Yeon Joo Jeong¹⁾, Jong Eun Lee²⁾, Yun-Hyeon Kim³⁾, Kum Ju Chae⁴⁾

1) Pusan National University Yangsan Hospital

2) Asan Medical Center

3) Chonnam National University Hospital

4) Jeonbuk National University Hospital

Purpose

To define quantitative risk thresholds for ILAs with correlation to long-term prognostic outcomes using deep learning-based ILA quantification at CT scans.

Materials and Methods

This study included participants aged 50+ who had chest CT scans at two health centers over 7 years. ILA status was classified as none, equivocal ILA, and ILA, assessed visually. The extent of ILA was quantitatively assessed using a deep learning-based approach for ILA quantification. Multivariable Cox proportional hazards models were utilized to evaluate the association between the extent of ILA and the hazards of disease-related adverse events and all-cause mortality.

Results

A total of 2427 participants were included in this study. ILAs were found in 55 individuals (2%) and equivocal ILAs in 63 (3%). The mean ILA extent was 3.3% in the ILA group and 0.5% in the equivocal ILA group. When dividing the groups by setting thresholds of 0-1%, 1-3%, 3-5%, and 5% or more according to ILA extent, the groups with 5% or more ILA and 3-5% ILA were independently associated with disease-related adverse events (HR, 28.2; 95% CI: 8.2, 96.6; $P < .001$, and HR, 5.8; 95% CI: 1.7, 20.0; $P = 0.005$, respectively) and all-cause mortality (HR, 5.2; 95% CI: 1.6, 16.9; $P = 0.005$, and HR, 5.4; 95% CI: 2.3, 12.7; $P < .001$, respectively) compared with those having no ILA.

Conclusion

The threshold for ILA extent associated with long-term outcomes, determined by deep learning-based quantification, was 3% or more of the total lung volume.

Table A. Hazard ratios for disease-related adverse events¹

Variable	Univariable analysis		Multivariable analysis ²	
	Unadjusted HR	P value	Adjusted HR	P value
Disease-related adverse events (N=53)				
ILA Extent				
No ILA	Reference		Reference	
0-1% ILA	3.1 (1.4-6.5)	<.001	1.23 (0.5-2.6)	.588
1-3% ILA	8.1 (3.3-19.3)	<.001	2.7 (1.1-6.8)	.03
3-5% ILA	16.7 (5.1-54.5)	<.001	5.8 (1.7-20.0)	.005
5% or more ILA	59.2 (17.9-195.8)	<.001	28.2 (8.2-96.6)	<.001

Note.- Data in parentheses are 95% confidence intervals. HR = hazard ratio, ILA = Interstitial Lung abnormality. The analysis was performed using a Cox proportional hazards model.

¹ Disease-related adverse events lung cancer development, interstitial lung disease development, and lung cancer mortality, and respiratory cause mortality.

² Multivariable analysis adjusted for age, sex, smoking history, hypertension, diabetes, obesity, and chronic obstructive lung disease.

Table B. Hazard ratios for all-cause mortality

Variable	Univariable analysis		Multivariable analysis ²	
	Unadjusted HR	P value	Adjusted HR	P value
All-cause mortality (N=144)				
ILA Extent				
No ILA	Reference		Reference	
0-1% ILA	2.1 (1.3-3.5)	<.001	1.0 (0.6-1.7)	.86
1-3% ILA	3.8 (1.9-7.7)	<.001	1.5 (0.7-3.0)	.22
3-5% ILA	12.4 (5.4-28.3)	<.001	5.4 (2.3-12.7)	<.001
5% or more ILA	18.2 (5.7-57.4)	<.001	5.3 (1.6-16.9)	.005

Note.- Data in parentheses are 95% confidence intervals. HR = hazard ratio, ILA = Interstitial Lung abnormality. The analysis was performed using a Cox proportional hazards model.

² Multivariable analysis adjusted for age, sex, smoking history, hypertension, diabetes, obesity, and chronic obstructive lung disease.

Figure A. Representative Case 1: A 69-year-old female with ILA. When evaluated by deep learning-based ILA quantification, the total extent of the ILA corresponded to 17% of the total lung volume, and all 6 lung zones showed involvement of more than 5%.

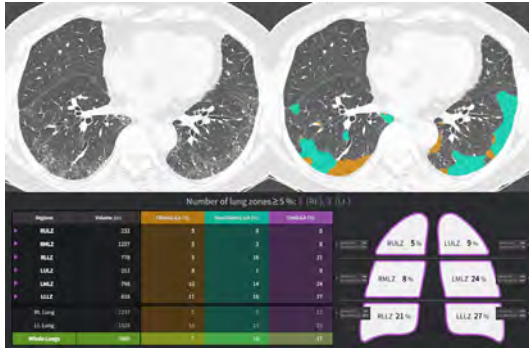


Figure B. Representative Case 2: A 64-year-old male with ILA. When evaluated by deep learning-based ILA quantification, the total extent of the ILA was found to be 13% of the total lung volume, with 4 out of 6 lung zones showing involvement of more than 5%.

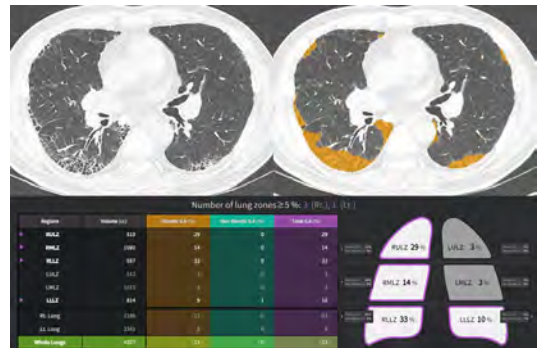


Figure C. Representative Case 3: A 57-year-old male with ILA. When evaluated by deep learning-based ILA quantification, the total extent of the ILA was found to be 3% of the total lung volume, with 1 out of 6 lung zones showing involvement of more than 5%.

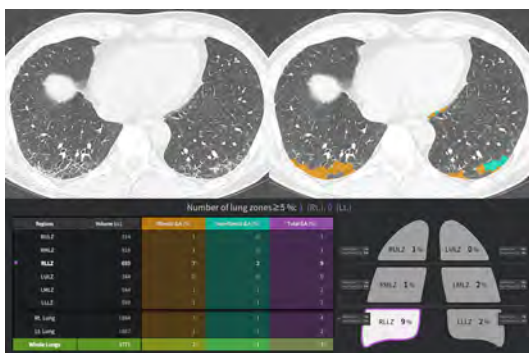
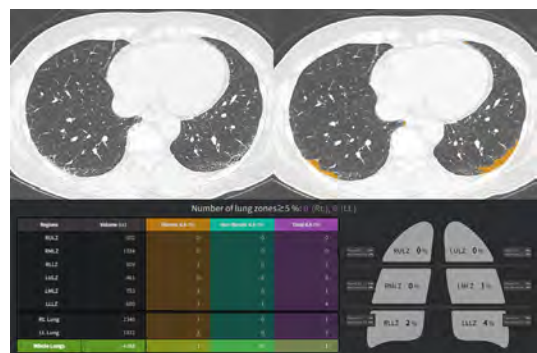


Figure D. Representative Case 4: A 65-year-old male with equivocal ILA. When evaluated by deep learning-based ILA quantification, the total extent of the ILA was found to be 1% of the total lung volume, with none of the 6 lung zones showing involvement of more than 5%.



CT

PE5-1 Pulmonary small vessel dimensions on CT in pulmonary hypertension: association with ^{99m}Tc -MAA uptake

Yukihiro Nagatani, Kazumasa Kobashi, Hiroshi Sakai, Ryo Uemura, Harumi Iguchi, Keita Sugie, Tatsuya Oki, Yoshiyuki Watanabe

Shiga University of Medical Science

Purpose

To assess the association of pulmonary small vessel configurational change on CT with both right heart pressure burden and ^{99m}Tc -MAA uptake

Materials and methods

Forty patients underwent chest CT, ^{99m}Tc -MAA and right heart catheterization within 1 month of one another. The ratio of cross-sectional areas of pulmonary small vessels less than 5 mm² to total lung field area (%CSA<5) and its vessel-based mean values (mCSA) in a coronal plane including tracheal bifurcation were measured based on binarization with the optimal threshold of -720 HU of chest CT. Metabolic arterial volumes (MAVs) on ^{99m}Tc -MAA were measured in the corresponding coronal plane. Diameter ratio of main pulmonary artery to ascending aorta ($D_{\text{MPA}/\text{AA}}$) was measured a trans-axial plane including pulmonary trunk on chest CT. Associations among the measured values and systolic pulmonary arterial pressure (sPAP) were assessed with in total as well as 12 chronic thromboembolic pulmonary hypertension (CTEPH) patients and 18 non-CTEPH PH patients

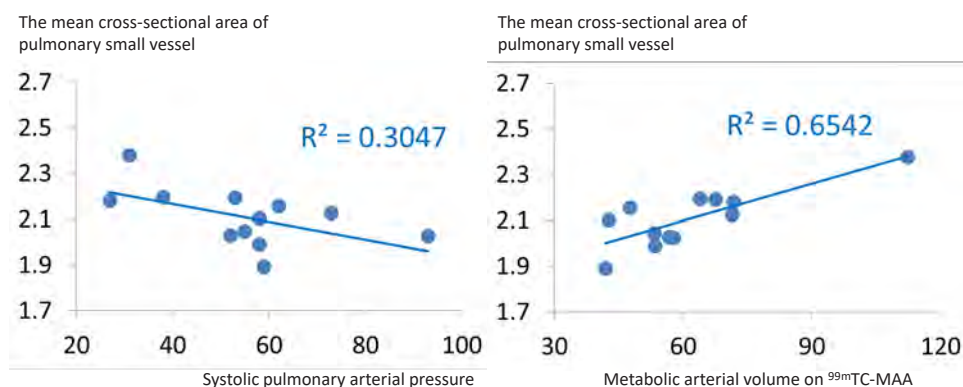
Results

In total, sPAP correlated negatively with both mCSA<5 ($r=-0.342$, $p=0.031$) and MAVs ($r=-0.424$, $p=0.006$), and positively with %CSA<5 ($r=0.322$, $p=0.043$), whereas $D_{\text{MPA}/\text{AA}}$ did not correlate with sPAP ($r=0.103$, $p=0.531$). For the CTEPH patients, mCSA<5 as well as MAVs showed a negative association with sPAP ($r=-0.609$, $p=0.047$), moreover, mCSA<5 tended to have positive association with MAVs ($r=0.573$, $p=0.066$). Similar results were not obtained for non-CTEPH PH patients.

Conclusion

The mean dimension of CSA<5 can reflect pulmonary peripheral arterial volume and predict the severity of pulmonary hypertension in the CTEPH patients.

CTEPH cases



PE5-2 Association between low-attenuation area on computed tomography and severity of COVID-19

Sadatomo Tasaka^{1,2)}, Tomoko Miura²⁾, Yoshie Ohashi²⁾, Hisanori Ebina²⁾, Shuichi Murakami²⁾

1) Hirosaki University Graduate School of Medicine

2) Murakami Shinmachi Hospital

Although COPD is a factor that aggravates COVID-19, there have been few reports on the relationship between the spread of emphysematous changes and the severity of the disease. In this study, we investigated the relationship between emphysematous changes on CT and the severity of the disease in 400 consecutive patients (204 men, mean age 74.6 years) who underwent CT scans after being diagnosed with COVID-19. The severity of the disease at the time of diagnosis was mild in 221 patients, moderate I in 101 patients, moderate II in 73 patients, and severe in 5 patients. The percentage of low-attenuation areas (%LAA) with CT values less than -950 HU was calculated from the chest CT images using image analysis software (VINCENT). The %LAA in both lungs for mild, moderate I, and moderate II/severe cases was 4.46 +/- 0.28, 5.30 +/- 0.46, and 6.52 +/- 0.94, respectively, and was significantly higher in moderate II/severe cases compared to mild cases (p=0.011). Additionally, while there were no patients with mild cases with a %LAA of 25 or more, there was one patient with moderate I and three patients with moderate II/severe cases, with a tendency for this to be more prevalent in the latter. Host factors such as underlying diseases are involved in the severity of COVID-19, and this study suggests that the risk of worsening of the disease should be considered in patients with significant emphysematous changes on CT scans.

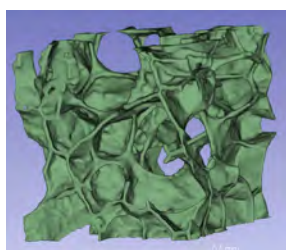
PE5-3 Analysis of alveolar walls in 3D lung micro images from large-field synchrotron radiation CT

Ryuki Ono¹⁾, Yoshiki Kawata²⁾, Keiji Umetani³⁾, Yasutaka Nakano⁴⁾, Tsuyoshi Koguma⁵⁾, Hiroaki Sakai⁶⁾, Toshihiro Okamoto⁷⁾, Noboru Niki⁸⁾

- 1) Program of Science and Technology, Graduate School of Creative Science, Tokushima University
- 2) Graduate School of Social Science and Technology, Tokushima University
- 3) Registered Institution for Facilities Use Promotion Japan Synchrotron Radiation Research Institute
- 4) Shiga University of Medical Science
- 5) Kyoto City Hospital
- 6) Hyogo Prefectural Amagasaki General Medical Center
- 7) Cleveland Clinic Heart and Vascular Institute
- 8) Medical Engineering Institute

Extraction of the alveolar wall is important to elucidate the three-dimensional microstructure of the lung. The purpose of this study is to improve the accuracy of alveolar wall extraction using SwinUNTER and to contribute to the analysis of the three-dimensional lung microstructure. In our experiments, we (1) created teacher data by extracting alveolar walls from micro-CT images of lung specimens and interactively modifying them, and (2) used this data for the analysis of lung microstructure. (2) We trained SwinUNTER on this teacher data and evaluated the accuracy of alveolar wall extraction. (3) Candidate regions of capillaries were extracted from the original image and the extraction results by applying a line enhancement filter. (4) Persistent homology was applied to the original and line-enhanced images to quantitatively evaluate the characteristics of alveolar walls and capillary pores. The evaluation results showed that the use of SwinUNTER almost eliminated artifact mis-extraction and enabled the extraction of areas with low CT values. In addition, quantitative comparison was possible by applying persistent homology not only to adult lungs but also to pediatric lungs and emphysema lungs.

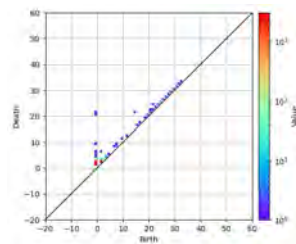
肺胞壁抽出の精度評価



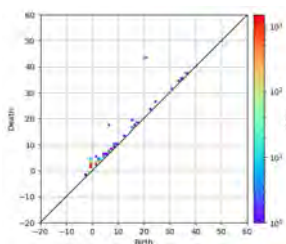
	正解率	適合率	再現率	Dice
従来法	0.975	0.868	0.903	0.885
SwinUNTER	0.983	0.940	0.968	0.950

正解率：全画素数のうち、正解画像とテスト結果の分類結果が一致する数の割合
 適合率：陽性と予測した画素のうち、正解した割合
 再現率：陰性と予測した画素のうち、正解した割合
 Dice：適合率と再現率の調和平均

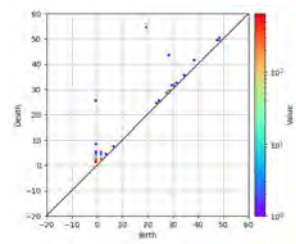
成人肺(線強調後)：パーシステント図(1次)



小児肺(線強調後)：パーシステント図(1次)



気腫肺(線強調後)：パーシステント図(1次)



PE5-4 Increased adiposity to muscle ratio and sinusitis affect quality of life in asthma—CT analysis—

Kaoruko Shimizu^{1,2)}, Hirokazu Kimura²⁾, Naoya Tanabe³⁾, Kazuya Tanimura⁴⁾, Shotaro Chubachi⁵⁾, Hiroaki Iijima⁶⁾, Susumu Sato³⁾, Nobuyasu Wakazono²⁾, Yuji Nakamaru⁷⁾, Kazufumi Okada⁸⁾, Hironi Makita^{2,9)}, Houman Goudarzi²⁾, Masaru Suzuki²⁾, Masaharu Nishimura^{2,9)}, Satoshi Konno²⁾

- 1) Division of Emergent Respiratory and Cardiovascular Medicine, Hokkaido University Hospital
- 2) Department of Respiratory Medicine, Faculty of Medicine
- 3) Department of Respiratory Medicine, Graduate School of Medicine, Kyoto University
- 4) Department of Respiratory Medicine, Nara Medical University
- 5) Division of Pulmonary Medicine, Department of Medicine, Keio University School of Medicine
- 6) Department of Respiratory Medicine, Tsukuba Medical Center Hospital, Tsukuba
- 7) Department of Otolaryngology-Head and Neck Surgery, School of Medicine, Hokkaido University
- 8) Data Science Center, Promotion Unit, Institute of Health Science Innovation for Medical Care, Hokkaido University
- 9) Hokkaido Medical Research Institute for Respiratory Diseases

Background: Deteriorated sinusitis and increased adiposity relative to muscle mass may affect the quality of life(QoL) in patients with asthma. However, whether these effects are observed regardless of intra-pulmonary pathology is unknown.

Objectives: To evaluate the correlation of the cross-sectional ratio of abdominal visceral fat (VF) to erector spinae muscle (ESM) and sinus findings based on Lund-Mackey scoring system (LMS) on computed tomography (CT) with the impaired score of the Asthma Quality of Life Questionnaire (AQLQ), regardless of airway and parenchymal disease, in patients with asthma.

Methods: Participants from the Hokkaido-based severe asthma cohort who had completed AQLQ and CT examination at the entry. The participants were divided into high (highest) and low (other quartiles) groups based on the extra-pulmonary indices. The multivariate analysis examined the association of VF/ESM for the adiposity-to-muscle ratio, LMS with AQLQ, after adjusting for the airway fractal dimension for airway index, %low attenuation volume for parenchymal index.

Results: No significant differences were observed in VF/ESM and LMS in terms of sex. The AQLQ score in the high VF/ESM group and high LMS group was lower than those in low VF/ESM group and low LMS group (N:Male/Female, 63/100). High VF/ESM (estimate [95% confidence interval], (-0.43[-0.61,-0.25])) and high LMS scores (-0.22(-0.41, -0.03)) were associated with low AQLQ scores, adjusted for age, body mass index, smoking status, blood eosinophil counts, and intra-pulmonary CT indices.

Conclusions: Increased VF relative to ESM mass and high LMS may deteriorate asthma related QoL, regardless of intra-pulmonary disease.

PE5-5 Evaluations of pulmonary function for the separated right/left lungs and five lobes by dynamic-ventilation CT

Tsuneo Yamashiro¹⁾, Hiroshi Moriya²⁾

1) Department of Radiology, Yokohama City University Graduate School of Medicine

2) Department of Radiology, Ohara General Hospital

Dynamic-ventilation CT is a scanning technique that has been utilized in recent years, when 'super multi-row CT scanners' with 320 or 256 rows have been commercially available and low-exposure technology, such as iterative reconstruction, has been implemented. While general chest CT scanning is performed with breath holdings (at full inspiration and expiration), dynamic-ventilation CT visualizes the respiratory motion of the lungs and airways by scanning during patient's free breathing. Since the scan range is 160 mm in the craniocaudal direction, in order to reproduce and analyze the respiratory motion of the entire lungs and airways, some extra techniques are required to merge the data from the upper and lower lung fields and to synchronize respiratory phases.

In this presentation, we would like to share our initial experiences of the 4-dimensional dynamic-ventilation CT of the entire lungs and to demonstrate correlations with CT-based measured lung volumes of the results from conventional pulmonary functional rests. Our results may be a clue to proceed to the next stage of pulmonary functional imaging, which estimates separated pulmonary function of the right and left lungs, also of the five lung lobes or multiple segments.

MRI/AI

PE6-1 Estimating Physiological Values of Membrane and RBC Conductance Using ^{129}Xe Gas Exchange MRI

David Mummy, Bastiaan Driehuys

Duke University

Rationale. ^{129}Xe gas exchange MRI can be used to estimate the carbon monoxide transfer coefficient KCO using the Roughton-Forster equations (1957). Previously, ^{129}Xe -based predictions of KCO were generated using statistical curve-fitting in a population with known clinical KCO (Wang 2021). However, that empirical approach does not provide physiologically valid values for the volume-independent specific conductance coefficients of the individual membrane and RBC compartments. Here, we begin with estimates of membrane and RBC conductance calculated from recently published reference equations based on patient age, sex, and height (Munkholm 2018). We then adjust these reference values based on observed patient-specific ^{129}Xe measurements to estimate KCO.

Methods. Healthy subjects (N=43, 16F/27M, age 42 ± 18 yrs) with no history of pulmonary disease underwent ^{129}Xe MRI. Imaging-based estimates of KCO were derived for each subject by calculating the reference conductance estimates for each compartment and adjusting those metrics by the observed ^{129}Xe signal. These KCO estimates were compared to clinical KCO using the Pearson correlation.

Results. Xenon-based estimates of KCO were significantly correlated with clinical measured values of KCO ($p < 0.001$, $r = 0.52$; Figure, left) with no evidence of bias (Figure, right).

Conclusion. We used ^{129}Xe measurements of the RBC and membrane signal to estimate KCO. By grounding our approach on reference equations for membrane and RBC conductance rather than building a model using empirical curve fitting, we now estimate specific conductance coefficients with physiologically meaningful values. ^{129}Xe MRI may thus enable patient-specific quantitative assessment of the independent contributions of the membrane and RBC compartments to gas exchange abnormalities.

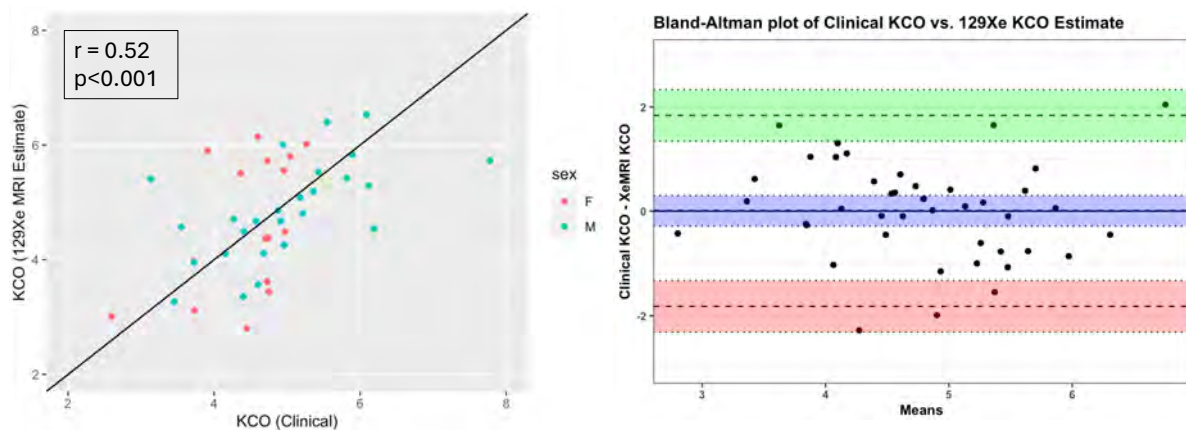


Figure. Left: scatterplot of clinical KCO vs. XeMRI estimate of KCO. The XeMRI estimates were correlated with known clinical KCO ($r = 0.52$, $p < 0.001$). The diagonal line represents $y = x$, i.e. perfect agreement between the two measurements. Right: Bland-Altman plot shows no bias between the two methods. The 95% confidence interval (top and bottom bands) is within 2 mL/min/mm Hg/L in both directions.

PE6-2 Lung normal strains in free, diaphragmatic, and thoracic breathing using 3D MR Spirometry

Adrien Duwat¹⁾, Nathalie Barrau¹⁾, Anna Reitmann¹⁾, Angeline Nemeth¹⁾, Antoine Beurnier²⁾, Thomas Similowski³⁾, Tanguy Boucneau⁴⁾, Claire Pellot-Barakat¹⁾, Vincent Lebon¹⁾, Xavier Maitre¹⁾

- 1) Université Paris-Saclay, CEA, CNRS, Inserm, BioMaps,
2) Hôpital Bicêtre, APHP,
3) Sorbonne Université, Inserm UMRS 1158 & APHP,
4) GE Healthcare

With a 10-minute dynamic lung MRI, 3D MR spirometry derives flow-volume maps from the deformation fields computed over 32 respiratory phases. From the deformation fields, dynamic normal strains can be inferred in the anatomical directions to describe the biomechanical behaviour of the lung. They were characterised in a healthy volunteer for free, diaphragmatic, and thoracic breathing at the local and lobar levels to differentiate strain driving axes along the cephalocaudal (ϵ_{CC}) and dorsoventral (ϵ_{DV}) axes (Figure 1).

During diaphragmatic breathing, normal strains show expected CC negative gradients with tensile strain in the basal regions. They are found compressive at the junction of the upper and the lower rib cage (ϵ_{CC}). Major elongations support the diaphragm as main respiratory driving force along CC during both diaphragmatic and free breathing. During free breathing, it is supplemented mainly by ϵ_{DV} in the apical regions. During thoracic breathing, ϵ_{DV} rules over ϵ_{CC} everywhere.

The strain components increase at different times during the respiratory cycles but simultaneously for the lobes (Figure 2). During free diaphragmatic breathing, lungs deform first along CC and then DV, whereas in thoracic breathing it is the other way round. During diaphragmatic breathing, ϵ_{CC} reaches a plateau due to compensating compressions in each lobe except the right upper lobe (Figure 2).

Lung dynamic normal strains (elongations or compressions) can be markers of respiratory muscle activation and recruitment. Lung compression during diaphragmatic breathing may indicate a localised expiratory effect consistent with the rib cage distortion that characterises this breathing pattern.

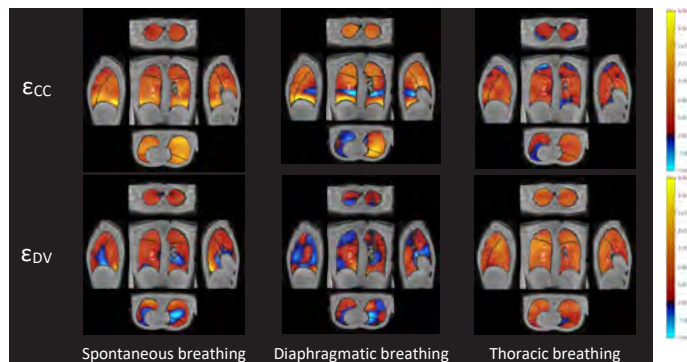


Figure 1: Exploded view of the normal strain maps for a healthy volunteer (24 years old) during free breathing (left), diaphragmatic breathing (centre) and thoracic breathing (dimensionless) at the end of inspiration along the cephalocaudal direction (top row) and along the anterior-posterior direction (bottom). At the end of inspiration, the inhaled volume is maximal and reaches the tidal volume so normal strains are mostly tensile (elongations in warm yellow) but, in some regions, they are found compressive (compressions in cold blue).

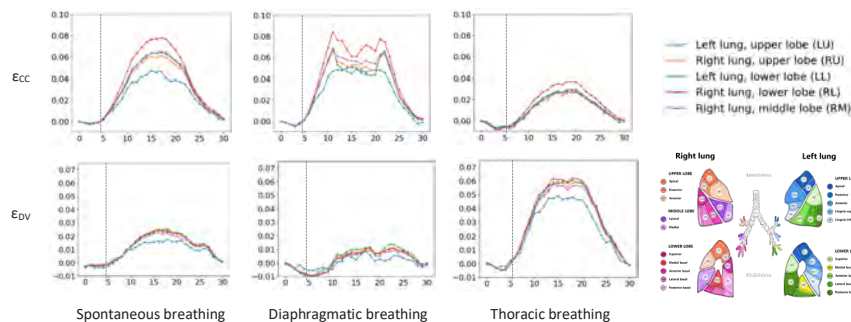


Figure 2: Normal strains along the cephalocaudal direction, ϵ_{CC} , (top) and the dorsoventral direction, ϵ_{DV} , (bottom) for the five lobes during free (left), diaphragmatic (centre) and thoracic breathing as a function of the reconstructed 32 phases over the corresponding respiratory cycle integrated over the 10-minute MRI acquisition. Dashed lines indicate the start of tensile strains at the beginning of the inspiration.

PE6-3 Vendor-Independent Simultaneous Multislice sequence for accelerated PREFUL MRI - A Proof of Concept

Sonja Luediger^{1,2)}, Filip Klimes^{1,2)}, Marius Wernz^{1,2)}, Robin Mueller^{1,2)}, Frank Wacker^{1,2)}, Jens Vogel-Claussen^{1,2)}, Andreas Voskrebenev^{1,2)}

1) Institute of Diagnostic and Interventional Radiology, Hannover Medical School,

2) Biomedical Research in Endstage and Obstructive Lung Disease (BREATH), Member of the German Center for Lung Research (DZL)

Introduction

Phase-resolved Functional Lung (PREFUL) MRI provides dynamic ventilation (V) and perfusion (Q) without the need for ionizing radiation, contrast media, or additional equipment. A whole lung acquisition (~12 slices) in slice-by-slice fashion results in a comparably long scan time (1 Minute/Slice). A more time-efficient 3D acquisition is feasible (3D PREFUL), but lacks perfusion information. Using simultaneous multislice (SMS) acquisition, a total scan time reduction can be achieved, while preserving perfusion information.

Methods

Using the vendor-independent Pulseseq sequence programming framework, a spoiled gradient echo sequence (SPGRE) with two-slice sinc excitation, asymmetric cartesian k-space trajectory with controlled aliasing (CAIPIRINHA) RF-cycling and in-plane TGRAPPA (R=2) acceleration was implemented and tested at 1.5T in one volunteer and compared with conventional SPGRE acquisition. SMS-Reconstruction was performed with the BART package. V/Q results were generated with PREFUL pipeline.

Results

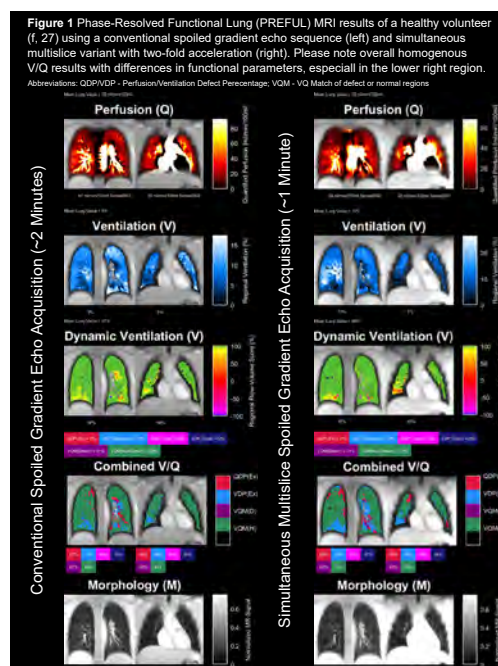
Visual inspection showed homogenous ventilation and perfusion for both sequence variants and slices. The functional parameters were similar (see Figure 1), but SMS displayed higher ventilation defect percentage (mainly in the lower right region) and reduced perfusion.

Discussion

Differences in results might originate from remaining aliasing and slice profile or reconstruction algorithm deviations. After further optimization and statistical evaluation in a healthy volunteer cohort and patient cohort, the presented sequence could be used in multi-center multi-vendor context and may reduce variability introduced by sequence variations.

Conclusion

The feasibility of a vendor-independent SMS sequence for PREFUL was demonstrated. This may facilitate the further dissemination of PREFUL by reducing scan time and vendor-dependent sequence/protocol optimizations in the future.



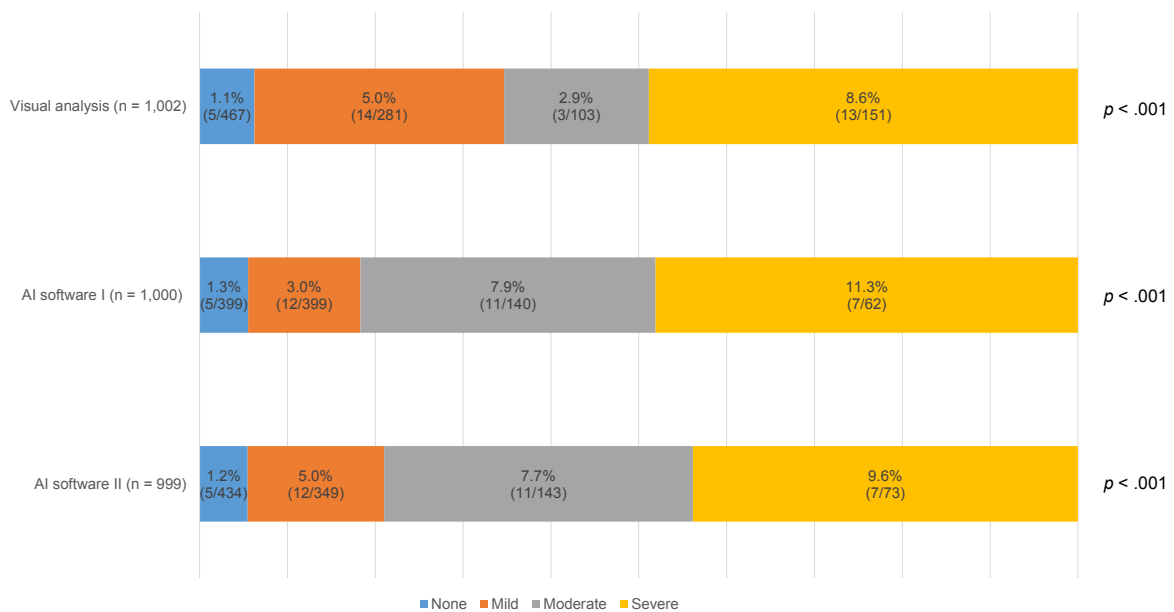
PE6-4 Coronary Artery Calcification on Low-Dose Lung Cancer Screening CT in South Korea

Won Gi Jeong

Department of Radiology, Chonnam National University Hwasun Hospital and Chonnam National University Medical School

Coronary artery calcification (CAC), detected via low-dose chest CT (LDCT) during lung cancer screening, serves as a cardiovascular risk indicator. South Korea, the first Asian nation to adopt a national LDCT lung cancer screening program, has not extensively explored CAC-related outcomes. This retrospective study evaluates the prevalence and severity of CAC using both visual analysis and artificial intelligence (AI) methods, and assesses the association with major adverse cardiovascular events (MACEs) among participants in Korea's program. The study included 1002 patients (mean age 62.4 ± 5.4 ; 994 men, 8 women) from two medical centers, covering April 2017 to May 2023. CAC assessments were conducted independently by two radiologists, with a third consulted for discrepancies. Two AI applications also evaluated CAC. MACE occurrences were tracked through electronic medical record review, with an interreader agreement kappa of 0.793 for CAC presence and 0.671 for severity. CAC was found in 53.4% of patients by visual consensus, 56.6% by AI I, and 60.1% by AI II. Severity distribution was classified as mild, moderate, and severe. The incidence of MACEs, tracked over a median of 1108 days, escalated with increasing CAC severity across all assessment methods ($p < .001$). This study underscores the significant link between CAC severity and MACE incidence in the context of Korea's national screening program, providing valuable reference for healthcare professionals involved in such initiatives and highlighting the critical need for routine CAC evaluations.

Association of coronary artery calcification severity and subsequent adverse cardiovascular events



PE6-5 Deep learning-based CAD for pulmonary nodule detection in the coronary artery calcium-scoring CT

Jung Im Jung, Suyon Chang, Kyongmin Sarah Beck

Department of Radiology, Seoul St. Mary's Hospital, College of Medicine, The Catholic University of Korea

Purpose: To evaluate the feasibility and utility of deep learning-based computer-aided diagnosis (DL-CAD) for the detection of pulmonary nodules on coronary artery calcium (CAC)-scoring CT.

Materials and Methods: This retrospective study included 273 patients (63.9 ± 13.2 years [standard deviation]; 129 men) who underwent CAC-scoring CT. A DL-CAD system was used for pulmonary nodule detection, and two independent junior readers reviewed the scans with and without DL-CAD assistance. A reference standard was established through the consensus of two experienced radiologists. Sensitivity, positive predictive value (PPV), and F1-score were assessed on a per-nodule and per-patient basis. The patients' medical record was followed up until November 2023.

Results: A total of 269 nodules were identified in 129 patients. DL-CAD alone achieved a sensitivity of 62%, PPV of 75%, and F1-score of 0.68. With DL-CAD assistance, the readers' sensitivity significantly improved (65% vs. 80% for reader 1, 82% vs. 86% for reader 2, all $p < 0.001$), without a notable increase in number of false-positives per case (0.11 vs. 0.013, $p = 0.078$ for reader 1; 0.11 vs. 0.11, $p > 0.999$ for reader 2). Per-patient analysis also enhanced sensitivity with DL-CAD assistance (73% vs. 84%, $p < 0.001$ for reader 1; 89% vs. 91%, $p = 0.250$ for reader 2). During follow-up, lung cancer was diagnosed in four patients (1.5%). Among them, two had lesions detected on CAC-scoring CT, both of which were successfully identified by DL-CAD.

Conclusion: DL-CAD demonstrated successful automation in detecting lung nodules on CAC-scoring CT, aiding less-experienced readers. Its use improved detection sensitivity without a significant increase in false-positives.

PE6-6 Octafluorocyclobutane: A new Fluorine-19 MRI agent for Pulmonary Imaging

Mitchell Albert

Lakehead University/Thunder Bay Regional Research Institute

Inert fluorinated gases are prominent novel inhalation agents for pulmonary functional magnetic resonance imaging (MRI)¹. Numerous studies demonstrated feasibility of fluorine-19 (¹⁹F) MRI of the lungs using perfluoropropane (PFP)² and sulfur hexafluoride (SF₆)³ for diagnostics and the study of various lung disorders. The short T₁ relaxation times of fluorinated gases allow a high number of signal averages yielding sufficient lung image signal-to-noise ratio (SNR). Moreover, ¹⁹F has a high natural abundance (~100%), a large gyromagnetic ratio, and is absent naturally in the living organism. These advantages result in the maximization of the ¹⁹F MRI signal. In addition, inert fluorinated gases can be premixed with oxygen (O₂) and be used for imaging during continuous breathing.

Despite most of the research being performed using PFP and SF₆, it is feasible to explore other inert fluorinated gases that can enhance the SNR level of ¹⁹F pulmonary MRI. In this study, we explored the performance of octafluorocyclobutane (OFCB) as an inhalation agent for ¹⁹F pulmonary MRI in healthy rats⁴. OFCB contains eight chemically equivalent fluorine atoms per molecule (which is a greater number of equivalent ¹⁹F atoms compared to other fluorinated gases), and has a longer spin-spin relaxation time. We have also compared OFCB to PFP in order to determine the feasibility of using OFCB as a fluorinated gas for ¹⁹F lung MRI by comparing its SNR to the SNR of PFP scans.

In vivo T₁ and T₂* relaxation times of OFCB-O₂ mixture were measured to be equal to 17.77 ± 1.5 ms and 3.4 ± 0.4 ms respectively. The gradient echo (GRE) lung images acquired in axial orientation using 70° Ernst flip angle (FA) condition (TR = T₁) and averaged over either 11s (single breath-hold) or 185 s (continuous breathing) demonstrated the SNR of 9.72 ± 2.1 and 14.48 ± 4.51 respectively. The same images acquired using PFP gas demonstrated smaller SNR of 9.72 ± 2.0 for single breath-hold protocol and of 12.68 ± 4.09 for continuous breathing. OFCB images acquired using continuous breathing protocol and full longitudinal magnetization recovery condition (FA = 90°, TR = 5T₁) showed the SNR equal to 10.23 ± 0.7 , whereas PFP images acquired using the protocol demonstrated lower SNR of 8.81 ± 0.46 .

OFCB significantly outperformed PFP in all three different imaging protocols ($p < 0.05$). The observed normalized SNR (normalized for the number of signal averages) advantage of OFCB agreed well with theoretical predictions for single breath-hold protocol and for continuous breathing with 90° excitation FA. A slight deviation from theoretical values was observed for continuous breathing protocol with 70° Ernst angle. This was potentially caused by slight mismatch between the OFCB T₁ *in vivo* and the TR value used during the scan. In addition, it could be explained by the absence of respiratory gating.

Overall, OFCB substantially outperforms PFP and the image quality of OFCB scans was significantly higher.

1. Couch, M. J. *et al.* 19F MRI of the Lungs Using Inert Fluorinated Gases: Challenges and New Developments. *J. Magn. Reson. Imaging* **49**, 343–354 (2018).
2. Couch, M. J. *et al.* Pulmonary ultrashort echo time 19F MR imaging with inhaled fluorinated gas mixtures in healthy volunteers: feasibility. *Radiology* **269**, 903–9 (2013).
3. Adolphi, N. L. & Kuethe, D. O. Quantitative mapping of ventilation-perfusion ratios in lungs by 19F MR imaging of T1 of inert fluorinated gases. *Magn. Reson. Med.* **59**, 739–746 (2008).
4. Shepelytskyi, Y. *et al.* Evaluation of fluorine - 19 magnetic resonance imaging of the lungs using octafluorocyclobutane in a rat model. *Magn. Reson. Med.* **85**, 987–994 (2021).

Poster

(Japanese)

COPD-1

PJ1-1 Diaphragm dome height on chest radiography as a predictor of dynamic lung hyperinflation in COPD

Masashi Shiraishi¹⁾, Yuji Higashimoto¹⁾, Ryuji Sugiyama¹⁾, Hiroki Mizusawa¹⁾, Yu Takeda¹⁾, Masaya Noguchi¹⁾, Osamu Nishiyama²⁾, Ryo Yamazaki²⁾, Tamotsu Kimura¹⁾, Yuji Tohda²⁾, Hisako Matsumoto²⁾

1) Department of Rehabilitation Medicine, Kindai University School of Medicine

2) Department of Respiratory Medicine and Allergology, Kindai University School of Medicine

Background and objective: Dynamic lung hyperinflation (DLH) can play a central role in exertional dyspnoea in patients with chronic obstructive pulmonary disease (COPD). Chest X-ray is the basic tool for assessing static lung hyperinflation in COPD. However, the predictive capacity of DLH using chest X-ray remains unknown. This study was conducted to determine whether DLH can be predicted by measuring the height of the right diaphragm (dome height) on chest X-ray.

Methods: This single-centre, retrospective cohort study included patients with stable COPD with pulmonary function test, cardiopulmonary exercise test, constant load test, and pulmonary images. They were divided into two groups according to the median of changes of inspiratory capacity ($\Delta IC = IC_{\text{lowest}} - IC_{\text{at rest}}$). The right diaphragm dome height and lung height were measured on plain chest X-ray.

Results: Of the 48 patients included, 24 were classified as having high DLH ($\Delta IC \leq -0.59$ L from rest; -0.59 L, median of all) and 24 as having low DLH. Dome height correlated with ΔIC ($r = 0.66, p < 0.001$). Multivariate analysis revealed that dome height was associated with high DLH independent of %low attenuation area on chest computed tomography and %FEV₁. Furthermore, the area under the receiver operating characteristic curve of dome height to predict high DLH was 0.86, with sensitivity and specificity of 83% and 75%, respectively, at a cutoff of 20.5 mm. Lung height was unrelated to ΔIC .

Conclusion: Diaphragm dome height on chest X-ray may adequately predict high DLH in patients with COPD.

慢性閉塞性肺疾患患者における動的肺過膨張と胸部単純 X 線による横隔膜ドーム高との関連

白石 匡¹⁾, 東本 有司¹⁾, 杉谷 竜司¹⁾, 水澤 裕貴¹⁾, 武田 優¹⁾, 野口 雅矢¹⁾, 神吉 健吾¹⁾, 西山 理²⁾, 山崎 亮²⁾, 木村 保¹⁾, 東田 有智²⁾, 松本 久子²⁾

1) 近畿大学病院 リハビリテーション部

2) 近畿大学病院 呼吸器・アレルギー内科学

【はじめに】

慢性閉塞性肺疾患 (COPD) 患者における肺過膨張の評価には胸部 X 線検査による評価が基本的である。しかし、胸部 X 線画像を用いた DLH の予測能は明らかになっていない。そこで本研究では、胸部 X 線における右横隔膜の高さ (Dome 高) を測定することで、DLH を予測可能か明らかにすることを目的とした。

【方法】

本研究は後ろ向きコホート研究で、2018 年 4 月～2022 年 12 月までに外来呼吸リハビリテーションを実施し、呼気ガス分析装置を用いた定常運動負荷試験 (PeakW の 70% 負荷) にて DLH の指標となる ΔIC (Peak 時 IC- 安静時 IC)、胸部 X 線画像による右 Dome 高と肺過膨張所見、超音波診断装置による横隔膜移動距離、肺機能検査 (FVC, FEV₁)、胸部 CT による低吸収域 (% LAA) を測定できる安定期 COPD 患者を対象とした。

【結果】

48 名が解析対象となり、24 名が low DLH ($\Delta IC \leq -0.59$ L)、24 名が high DLH ($\Delta IC > -0.59$ L) と分類した。Dome 高は ΔIC ($r = 0.66, p < 0.001$) と横隔膜移動距離 ($r = 0.76, p < 0.001$) に正の相関を認めた。ロジスティック回帰分析では、Dome 高は、胸部 CT の % LAA や FEV₁ とは独立して、high DLH の予測因子であった (調整済み Odd 比 0.67, 95% CI ; 0.520-0.857, $p < 0.01$)。

【結論】

胸部 X 線画像による横隔膜評価は、超音波検査が実施できない施設でも、DLH 予測において有用である可能性が示唆された。

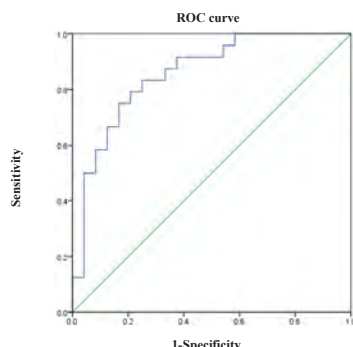
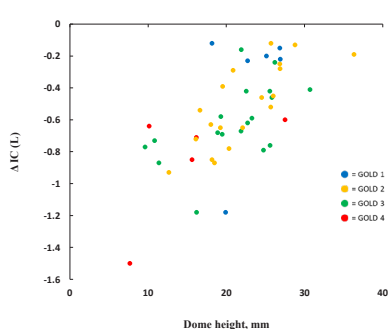


Table 1. Multivariate analysis for high DLH (AIC from rest ≤ -0.59 L)

Index	Odd ratios	95%CI	p value
Right dome height, mm	0.67	0.516-0.862	0.002
%LAA, %	0.59	1.002-1.123	0.044
%predicted FEV ₁ , %	0.97	0.929-1.012	0.161

DLH = dynamic lung hyperinflation; FEV₁ = forced expiratory volume in 1 s; AIC = change of inspiratory capacity from rest during exercise; LAA: low attenuation area.

PJ1-2 Correlation of DCR with symptoms, physical function, and respiratory function: A Study of COPD cases

Masahiro Kaneko, Yuu Kobayashi, Kodai Miyamoto, Masaaki Iwabayashi, Masamitsu Li, Yuu Matsuoka, Makoto Yokota, Hisanori Amimoto, Junji Takiguchi, Hiroshi Fujii, Hiromi Tomioka
Kobe City West Hospital

OBJECTIVE: To investigate the correlation between lung area change rate measured by dynamic chest radiography (DCR), symptoms, and respiratory function in COPD patients.

subjects: COPD patients who underwent DCR, CT, respiratory function tests, 6-minute walk test, walking speed, and SMI(BIA) assessment during the stable period from April 2023 to March 2024.

Methods: We analyzed 64 COPD cases (ACO 31cases, COPD cases excluding ACO 33cases), the correlation lung area change rate and height, BMI, SMI (InBody: bioelectrical impedance [BIA] method), mMRC, CAT score, 6-minute walking distance, walking speed (m/sec), and respiratory function tests (VC, IC, FEV1, FEV1/FVC, MMF, PEF, RV, FRC, TLC, RV/TLC) with the statistical software JMP14. ACO diagnosed according to the Guide to Overlap Diagnosis and Treatment of Asthma and COPD, 2nd ed.

Result: In all COPD patients, lung area change rate correlated with BMI, mMRC, CAT, 6MWD, gait speed, Goddard score, VC, IC, FEV1, %FEV1, MMF, PEF, RV/TLC, and IC/TLC. In ACO patients, lung area change rate correlated with BMI, SMI, gait speed, Goddard score, VC, IC, FEV1, %FEV1, MMF, PEF, RV/TLC, and IC/TLC. In COPD patients excluding ACO, lung area change rate correlated with BMI, mMRC, CAT, 6MWD, gait speed, Goddard score, IC, FEV1, %FEV1, MMF, PEF, RV/TLC, and IC/TLC.

Conclusions: In COPD patients, changes in lung area correlate with symptoms, exercise capacity, physical function, obstructive impairment index, residual air fraction, IC/TLC, and other parameters.

胸部 X 線動態画像 (DCR) と症状, 運動耐用量・身体機能, 呼吸機能の相関: COPD 症例における検討

金子 正博, 小林 裕, 宮本 滉大, 岩林 正明, 李 正道, 松岡 佑, 横田 真, 網本 久敬, 瀧口 純司, 藤井 宏, 富岡 洋海
神戸市立医療センター西市民病院 呼吸器内科

目的: COPD 症例における, 胸部 X 線動態撮影 (DCR) で測定した肺面積 (最大吸気位, 変化率) と症状・運動耐用量・筋肉量・身体機能・呼吸機能の相関を検討する。

対象: 2023 年 4 月~2024 年 3 月の期間, 安定期に DCR・呼吸機能検査・6 分間歩行試験・歩行速度・InBody を評価した COPD 症例。

方法: COPD 64 症例について, 肺面積 (最大吸気位) および肺面積変化率と身長・BMI・SMI, mMRC・CAT score, 6 分間歩行距離・歩行速度 (m/秒), 呼吸機能検査 (VC, IC, FEV1, FEV1/FVC, MMF, PEF, RV, FRC, TLC, RV/TLC) との Spearman の順位相関係数を統計ソフト JMP14 にて算出した。結果: 肺面積 (最大吸気位) は, 身長・VC・RV・FRC・TLC と, 肺面積変化率は, BMI・SMI・mMRC・CAT・6MWD・歩行速度・Goddard score・VC・IC・FEV1・%FEV1・MMF・PEF・RV/TLC・IC/TLC と相関を認めた。

結論: COPD 症例において肺面積変化率は症状や運動耐用量・身体機能, 閉塞性障害の指標や残気率・IC/TLC 等と相関する。

対象症例の背景 characteristics	COPD total		ACO	COPD without ACO	p-value
	n		n	n	
age [yr]	64	74.3(8.4)	31	33	0.4703
male/female	75/15/1	48/15	21/10	27/6	0.2524
height [m]	1.62(0.05)	1.62(0.05)	1.61(0.02)	1.63(0.07)	0.3444
BMI [kg/m ²]	21.2 (19.3-24.6)	23.4 (19.6-25.2)	20.1 (18.7-22.0)	0.0267	
SMI [kg/m ²]	6.27(1.07)	6.21(1.40)	6.31(0.80)	0.7596	
mMRC []	1.9(0.2)	1.7(0.3)	1.9(0.3)	0.5402	
CAT [score]	18.9(9.2)	18.9(8.6)	17.0(8.5)	0.0530	
6MWD	375 (195-496)	259 (185-460)	384 (201-462)	0.3305	
walking speed	1.02(0.02)	1.02(0.02)	1.10(0.02)	0.2456	
Goddard score [score]	8 (3-11)	8 (2-11)	9 (4-13)	0.3073	
lung area [mm ² (cm ²)]	462.77(81.67)	443.52(80.58)	480.48(79.86)	0.0733	
%change of lung area [%]	25.38(4.69)	26.91(6.47)	23.90(6.16)	0.1864	
VC [L]	2.675(0.869)	2.692(0.975)	2.699(0.772)	0.8780	
IC [L]	6.14 (1.72-11.92)	6.91 (2.85-14.20)	4.51 (1.10-9.92)	0.1672	
FEV1 [L]	1.82(0.67)	1.86(0.73)	1.79(0.62)	0.6112	
FEV1/FVC [%]	1.38(0.04)	1.34(0.03)	1.41(0.08)	0.0202	
MMF [L]	56.13(13.26)	53.45(12.02)	56.72(14.33)	0.5282	
PEF [L]	6.02(0.38(0.96)	5.94(0.30(0.96)	6.04(0.40(0.99)	0.3190	
RV [L]	3.36 (2.90-4.98)	3.66 (2.71-5.00)	3.32 (2.96-4.60)	0.3104	
FRC [L]	2.32(0.704)	2.24(0.704)	2.42(0.893)	0.3623	
TLC [L]	3.29(0.921)	3.69(0.918)	3.29(0.910)	0.2606	
RV/TLC [%]	5.02(1.275)	4.95(1.338)	5.09(1.233)	0.6630	
RV/IC [%]	46.57(10.60)	45.20(10.09)	47.71(11.16)	0.6447	
IC/TLC [%]	36.44(4.86)	37.70(5.25)	35.29(10.38)	0.3374	

	r	p
age [yr]	0.1829	0.0957
height [m]	-0.1502	0.4735
BMI [kg/m ²]	0.3504	0.0059
SMI [kg/m ²]	0.6671	0.0013
mMRC []	-0.4728	0.0170
CAT [score]	-0.4054	0.0421
6MWD	0.4886	0.0132
walking speed	0.4349	0.0298
Goddard score [score]	-0.4043	0.0253
VC [L]	0.3855	0.0542
IC [L]	0.4397	0.0279
FEV1 [L]	0.6578	0.0004
FEV1/FVC [%]	0.4918	0.0125
MMF [L]	0.3379	0.0905
PEF [L]	0.5802	0.0024
RV [L]	-0.4836	0.0143
FRC [L]	-0.3836	0.0584
TLC [L]	-0.0204	0.8695
RV/TLC [%]	-0.5883	0.0020
IC/TLC [%]	0.6317	0.0012

肺面積変化率と身体計測・症状スコア・身体機能・呼吸機能の相関: COPD全体	r	p
age [yr]	0.1308	0.4462
height [m]	0.0764	0.6306
BMI [kg/m ²]	0.4768	0.0014
SMI [kg/m ²]	0.5504	<0.0001
mMRC []	-0.4487	0.0028
CAT [score]	-0.4691	0.0076
6MWD	0.4654	0.0019
walking speed	0.4239	0.0052
Goddard score [score]	-0.5061	0.0006
VC [L]	0.4408	0.0035
IC [L]	0.5413	0.0002
FEV1 [L]	0.6531	<0.0001
FEV1/FVC [%]	0.5191	0.0004
MMF [L]	0.5245	0.0004
PEF [L]	0.6327	<0.0001
RV [L]	-0.3270	0.0346
FRC [L]	-0.2511	0.2087
TLC [L]	0.0918	0.5631
RV/TLC [%]	-0.5460	0.0002
IC/TLC [%]	0.6574	<0.0001

肺面積変化率と症状スコア・身体機能・呼吸機能の相関: ACO	r	p
age [yr]	0.1351	0.0951
height [m]	0.3375	0.1852
BMI [kg/m ²]	0.5885	0.0130
SMI [kg/m ²]	0.6589	0.0040
mMRC []	-0.4502	0.0698
CAT [score]	-0.4026	0.1081
6MWD	0.4798	0.0513
walking speed	0.5077	0.0375
Goddard score [score]	-0.5661	0.0178
VC [L]	0.3708	0.0982
IC [L]	0.4464	0.0050
FEV1 [L]	0.6973	0.0019
FEV1/FVC [%]	0.6363	0.0000
MMF [L]	0.6059	0.0005
PEF [L]	0.7407	0.0007
RV [L]	-0.0950	0.8219
FRC [L]	-0.0287	0.9130
TLC [L]	0.3279	0.1989
RV/TLC [%]	-0.4884	0.0487
IC/TLC [%]	0.7045	0.0016

PJ1-3 CT imaging indices to predict COPD in smokers

Fumi Mochizuki¹⁾, Naoya Tanabe²⁾, Hiroaki Iijima¹⁾, Takafumi Shimada¹⁾, Hiroichi Ishikawa¹⁾, Takashi Naito¹⁾, Yusuke Shiraishi²⁾, Tomoki Maetani²⁾, Ryo Sakamoto³⁾, Tsuyoshi Oguma⁴⁾, Susumu Sato²⁾, Megumi Kanasaki⁵⁾, Izuru Masuda⁶⁾, Toyohiro Hirai²⁾, Nobuyuki Hizawa⁷⁾

- 1) Department of Respiratory Medicine, Tsukuba Medical Center Hospital.
- 2) Department of Respiratory Medicine, Graduate School of Medicine, Kyoto University,
- 3) Department of Diagnostic Imaging and Nuclear Medicine, Graduate School of Medicine, Kyoto University.
- 4) Department of Respiratory Medicine, Kyoto City Hospital,
- 5) Medical Examination Center, Takeda Hospital,
- 6) Clinical Research Institute, National Hospital Organization, Kyoto Medical Center,
- 7) Department of Pulmonary Medicine, Faculty of Medicine, University of Tsukuba

Background: Visually-diagnosed centrilobular emphysema (CLE), and quantification of airway wall thickness and emphysema severity on computed tomography (CT) are associated with airflow limitation in smokers. The aim of this study was whether these indices can be used for accurate detection of chronic obstructive pulmonary disease (COPD) in smokers.

Methods: We retrospectively included male subjects aged 40 years or older with a smoking history of at least 10 pack-years who participated health checkup and underwent lung cancer screening CT and spirometry at two Japanese hospitals. The percentage of low-attenuation area < -950 HU (%LAA) was quantified. CLE and paraseptal emphysema (PSE) were visually assessed according to the Fleischner Society guidelines. Airway wall thickness was calculated as the mean percentage of wall area of one selected segmental or subsegmental bronchus from each lung lobe (segmental or subsegmental WA%). Logistic regression models were used to develop diagnostic prediction for COPD and receiver operating characteristic (ROC) curves were used to detect the area under the curve (AUC).

Results: Among 513 smokers included in this study, 55 had COPD. In multivariable regression analysis models using the stepwise backward variable selection method, CLE presence, high %LAA, and high subsegmental WA% were independently associated with COPD. A logistic regression model using CLE, %LAA, and subsegmental WA% predicted COPD with a sensitivity of 84%, specificity of 88%, and AUC of 0.908.

Conclusions: A model using quantification of airway wall thickness and emphysema, and visually-identified CLE may allow for detecting COPD in smokers..

健診受診喫煙者における COPD 診断と関連する CT 指標の検討

望月 芙美¹⁾, 田辺 直也²⁾, 飯島 弘晃¹⁾, 嶋田 貴文¹⁾, 石川 博一¹⁾, 内藤 隆志¹⁾, 白石 祐介²⁾, 前谷 知毅²⁾, 坂本 亮³⁾, 小熊 毅⁴⁾, 佐藤 晋²⁾, 金崎 めぐみ⁵⁾, 榊田 出⁶⁾, 平井 豊博²⁾, 檜澤 伸之⁷⁾

- 1) 筑波メディカルセンター病院呼吸器内科
- 2) 京都大学大学院医学研究科呼吸器内科学
- 3) 京都大学大学院医学研究科放射線医学講座
- 4) 京都市立病院呼吸器内科
- 5) 武田病院健診センター
- 6) 京都医療センター臨床研究センター
- 7) 筑波大学医学医療系呼吸器内科

【目的】喫煙者において、CT で定量的に評価した気道壁肥厚と肺気腫の重症度、視覚的に検出した小葉中心性肺気腫 (CLE) の存在は、気流閉塞との関連が報告されている。これらの指標による COPD 予測能を検討した。【方法】2 施設の健診センターを受診し、スパイロメトリー、胸部 CT を施行された、10pack-years 以上の喫煙歴を有する 40 歳以上の男性 513 例を対象とした。肺気腫は、全肺容積に対する -950HU 未満の低吸収域割合 (%LAA) と、Fleischner Society 分類による視覚的肺気腫 (CLE, 傍壁在性肺気腫 [PSE]) を評価した。気道壁面積比 (WA%) は右 B1, 右 B4, 右 B10, 左 B1, 左 B10 の 3,4 次気管支の平均値を算出した。ロジスティック回帰分析を用いて COPD (1 秒率 <70%) と関連する因子を検討した。【結果】55 例が COPD に該当した。ステップワイズ法を用いた多変量ロジスティック回帰分析では、CLE あり、% LAA 高値、4 次気管支の WA% 高値はそれぞれ独立して COPD と関連し、これらを用いたモデルの COPD 予測は感度 84%、特異度 88%、ROC 曲線の AUC は 0.908 であった。【結語】健診受診男性喫煙者において、CT 上の定量的かつ視覚的な肺気腫評価と、気道壁肥厚評価の組み合わせは、高精度で COPD を予測できることが示唆された。

PJ1-4 Association of gut microbiome and CT measured indices in patients with COPD

Daisuke Kinose¹⁾, Satoru Kawashima¹⁾, Seiko Ohno^{3,6)}, Yasumitsu Ueki¹⁾, Aya Ooka¹⁾, Keiko Narumiya¹⁾, Wataru Shigemori¹⁾, Tomoko Iriyama¹⁾, Shinya Yokoe¹⁾, Yoko Tsunoda¹⁾, Ruriko Yukimura^{1,4)}, Akio Yamazaki¹⁾, Yasuki Uchida¹⁾, Hiroaki Nakagawa¹⁾, Makoto Osawa⁴⁾, Masafumi Yamaguchi¹⁾, Akira Andoh²⁾, Emiko Ogawa⁵⁾, Yasutaka Nakano^{1,4)}

- 1) Division of Respiratory Medicine, Department of Internal Medicine, Shiga University of Medical Science
- 2) Division of Gastroenterology, Department of Internal Medicine, Shiga University of Medical Science
- 3) Division of Cardiovascular Medicine, Department of Internal Medicine, Shiga University of Medical Science
- 4) Division of Infection Control and Prevention, Shiga University of Medical Science
- 5) Health Administration Center, Shiga University of Medical Science
- 6) Medical Genome Center, National Cerebral and Cardiovascular Center

Previous studies have demonstrated that the composition of the gut microbiota in patients with COPD undergoes changes as the disease progresses.

Uptodate, there is no information regarding how they relate to the CT image index such as Pi10 or LAV%.

This is a single center observational study to see the association of gut microbiota with Pi10 and LAV% in patients with COPD.

We recruited 94 participants from the outpatient clinic of our institution, including 81 patients with COPD and 13 non-COPD ever smokers.

Neither Pi10 nor LAV% demonstrated an association with alpha-diversity index of gut microbiome. Similarly, these CT indices did not exhibit an association with beta-diversity index.

The findings of this study indicate that lung structure changes in COPD may not be influenced by the gut microbiota or vice versa.

COPD 患者における腸内細菌叢と CT 指標の関連について

黄瀬 大輔¹⁾, 河島 暁¹⁾, 大野 聖子^{3,6)}, 植木 康光¹⁾, 大岡 彩¹⁾, 成宮 慶子¹⁾, 重森 度¹⁾, 入山 朋子¹⁾, 横江 真弥¹⁾, 角田 陽子¹⁾, 行村 瑠里子^{1,4)}, 山崎 晶夫¹⁾, 内田 泰樹¹⁾, 仲川 宏昭¹⁾, 大澤 真⁴⁾, 山口 将史¹⁾, 安藤 朗²⁾, 小川 恵美子⁵⁾, 中野 恭幸^{1,4)}

- 1) 滋賀医科大学内科学講座 (呼吸器内科)
- 2) 滋賀医科大学内科学講座 (消化器内科)
- 3) 滋賀医科大学内科学講座 (循環器内科)
- 4) 滋賀医科大学感染制御部
- 5) 滋賀医科大学保健管理センター
- 6) 国立循環器病研究センター・メディカルゲノムセンター

腸内細菌叢の構成は、COPD の進行に伴い変化することが報告されている。

現在までのところ、Pi10 や LAV% と腸内細菌叢との関連についての報告はない。

今回我々は、単施設観察研究において、COPD 患者の腸内細菌叢と Pi10 や LAV% との関連について調べた。

滋賀医科大学附属病院呼吸器内科外来通院中の 94 名 (81 名の COPD 患者、13 名の非 COPD 喫煙者) を対象とした。

Pi10 や LAV% と腸内細菌叢の α 多様性指標や β 多様性指標との関連は認めなかった。

COPD 患者の肺構造変化は腸内細菌叢による影響は受けず、また腸内細菌叢への影響もないのかもしれない。

PJ1-5 Longitudinal analysis of fibrotic lesions in COPD using Persistent Homology

Yusuke Shiraishi¹⁾, Naoya Tanabe¹⁾, Shizuo Kaji²⁾, Tomoki Maetani¹⁾, Ryo Sakamoto³⁾, Tomohiro Handa^{1,4)}, Susumu Sato^{1,5)}, Shigeo Muro⁶⁾, Toyohiro Hirai¹⁾

- 1) Department of Respiratory Medicine, Kyoto University
- 2) Kyusyu University, Institute of Mathematics for Industry
- 3) Department of Diagnostic Imaging and Nuclear Medicine, Kyoto University
- 4) Department of Advanced Medicine for Respiratory Failure, Kyoto University
- 5) Respiratory Care and Sleep Control Medicine, Kyoto University
- 6) Respiratory Medicine, Nara Medical University

[Rationale] COPD sometimes coexists with fibrotic changes known as interstitial lung abnormalities (ILAs). However, their natural course and clinical impacts remain unknown. A recent study showed that the topological analysis using persistent homology allows for segmenting fibrosis and emphysema three-dimensionally (J Appl Physiol. 2021;131:601). This study aimed to examine the longitudinal changes in interstitial lesions quantified using persistent homology and their clinical impacts on patients with COPD.

[Methods] This study was retrospective analysis of prospective observational COPD cohort at Kyoto university hospital. Persistent homology was applied for segmented lung field CT images to obtain a pair of CT numbers at which homological feature corresponding to voids appeared (birth) and disappeared (death) by sweeping the CT number threshold from high to low values. Based on a previous report, fibrotic voxels were defined as those whose neighboring regions are rich in voids cycles with larger difference between birth and death (lifetime), and the volume percentage of fibrotic volume ratio to total lung volume (PHfibrosis%) were calculated. 5-year changes in pulmonary function, PHfibrosis%, and 10-year mortality were assessed.

[Results] 124 patients (70 ± 7.7years old, 93% male) completed baseline and follow-up CT scans. There was a weak correlation between changes in PHfibrosis% and Kco decline ($r=-0.2$, $p=0.03$). When divided by the median of changes in PHfibrosis%, the number of exacerbations was not different, but the large change group showed poorer mortality.

[Conclusion] Longitudinal changes in PHfibrosis% were associated with diffusing capacity decline and mortality.

パーシステントホモロジーを用いた COPD における線維化病変の評価

白石 祐介¹⁾, 田辺 直也¹⁾, 鍛冶 静雄²⁾, 前谷 知毅¹⁾, 坂本 亮³⁾, 半田 知宏^{1,4)}, 佐藤 晋^{1,5)}, 室 繁郎⁶⁾, 平井 豊博¹⁾

- 1) 京都大学大学院医学研究科呼吸器内科学
- 2) 九州大学マス・フォア・インダストリ研究所
- 3) 京都大学大学院医学研究科放射線医学講座
- 4) 京都大学大学院医学研究科呼吸不全先進医療講座
- 5) 京都大学大学院医学研究科呼吸管理睡眠制御学講座
- 6) 奈良県立医科大学 呼吸器内科

【背景】 COPD に併存する線維化病変の経時変化と臨床経過に及ぼす影響は十分に明らかにされていない。位相学の一つであるパーシステントホモロジー (PH) を胸部 CT に応用し、線維化領域の定量が可能である。

【方法】 前向き観察研究に参加した COPD 患者で、登録時と 5 年後に胸部 CT を撮影した 124 例を対象とした。胸部 CT 画像で、CT 値を連続的に変化させ、0.1, 2 次元の PH 特徴量を抽出した (特徴量が出現、消失する CT 値を birth, death とした)。既報に基づき、2 次元のパーシステント図で、 $-1260 < \text{birth} < -380$, $\text{birth} - \text{death} > 360$ を満たす領域を線維化と定義した。5 年間の線維化領域の体積割合変化 (Δ PHfibrosis%) と肺機能経年低下、10 年間の予後との関連を検討した。

【結果】 Δ PHfibrosis% と Δ Kco に弱い相関を認めた ($r=-0.2$, $p=0.03$)。 Δ PHfibrosis% の中央値で群分けすると、増悪頻度に差はなかったが、 Δ PHfibrosis% が大きい群で予後不良であった。

【結語】 PH を用いて定量した線維化領域の経時変化は拡散能の経年低下および予後と関連する。

COPD-2/Airway-CT

PJ2-1 Examination of the effects of smoking in healthy subjects using medical examination images

Takahiro Ibaraki¹⁾, Masanori Iizuka¹⁾, Takanori Fujihara¹⁾, Izumi Satoh¹⁾, Yusuke Inui¹⁾, Masahide Ueda¹⁾, Fumitaka Mitoh¹⁾, Asuka Okada¹⁾, Hideaki Takenaka¹⁾, Sumito Choh¹⁾, Masayuki Mizuno²⁾, Shigeo Muro³⁾

1) Respiratory Medicine, Osaka Saiseikai Suita Hospital

2) Osaka Saiseikai Suita Medical Welfare Center Kento Health Management Center

3) Department of Respiratory Medicine, Nara Medical University

Background and Purpose: It has been reported that fractal dimension (D) is decreased in patients with chronic obstructive pulmonary disease (COPD), but few reports have evaluated D in healthy smokers. We evaluated the impact of smoking on D from an imaging perspective in subjects undergoing health checkups.

Subjects and Methods: 310 men aged 40 years or older who underwent CT health examinations at the Kento Health Care Center of this hospital from April 1, 2019 to March 31, 2022 were included in the study, and the results were examined retrospectively. Those with respiratory diseases (COPD, bronchial asthma, etc.) were excluded. Results: Subjects were 53 (40-75) years old, Brinkman Index (BI) 200 (0-2250), LAA% 28.1% (4.5%-44.2%), D 1.52 (1.29-2.01). BI showed a significant correlation with both LAA% and D (LAA%: $p=8.43 \times 10^{-3}$, D: $p=1.16 \times 10^{-4}$). Conclusion: Smoking decreased LAA% and D even in lungs that had not yet developed COPD. The results also suggest that the decrease in D may assess lung structural destruction more acutely than the worsening of emphysematous lesions (LAA%) or respiratory function.

健診画像を用いた健常者における喫煙の影響の検討

茨木 敬博¹⁾, 飯塚 正徳¹⁾, 藤原 隆徳¹⁾, 佐藤 いずみ¹⁾, 乾 佑輔¹⁾, 上田 将秀¹⁾, 美藤 文貴¹⁾, 岡田 あすか¹⁾, 竹中 英昭¹⁾, 長 澄人¹⁾, 水野 雅之²⁾, 室 繁郎³⁾

1) 大阪府済生会吹田病院 呼吸器内科

2) 大阪府済生会吹田医療福祉センター 健都健康管理センター

3) 奈良県立医科大学 呼吸器内科学講座

背景・目的：慢性閉塞性肺疾患（COPD）患者において、フラクタル次元（D）が低下することが報告されているが、健常喫煙者においてDを評価した報告は少ない。健診受診者を対象に、喫煙による影響を画像的な観点から評価した。対象・方法：2019年4月1日～2022年3月31日当院健都健康管理センターでCT健診を受診した40歳以上の男性310名を対象とし、後方視的に検討を行った。尚、呼吸器疾患（COPD、気管支喘息等）を指摘されている方は除外とした。結果：対象群の年齢は53歳（40歳-75歳）、Brinkman Index（BI）は200（0-2250）、LAA% 28.1%（4.5%-44.2%）、D 1.52（1.29-2.01）であった（いずれも中央値）。BIはLAA%とDいずれも有意な相関を認めた（LAA%： $p=8.43 \times 10^{-3}$ 、D： $p=1.16 \times 10^{-4}$ ）。結語：COPDに至っていない肺でも喫煙によりLAA%、Dの低下が認められた。また、Dの低下は気腫性病変の悪化（LAA%）や呼吸機能の低下よりも鋭敏に肺の構造破壊を評価する可能性が示唆された。

PJ2-2 The relationships between FEV1 and inspiratory and expiratory CT measurements

Emiko Ogawa^{1,2)}, Tomoko Iriyama²⁾, Yoko Tsunoda²⁾, Akio Yamazaki²⁾, Yumiko Matsuo²⁾,
Yasuki Uchida²⁾, Hiroaki Nakagawa²⁾, Daisuke Kinose²⁾, Masafumi Yamaguchi²⁾, Yasutaka Nakano²⁾

1) Health Administration Center, Shiga University of Medical Science

2) Division of Respiratory Medicine, Department of Medicine, Shiga University of Medical Science

Background and Aims: Chronic obstructive pulmonary disease (COPD) is characterized by the decrease in expiratory flow and its pathophysiology has been mainly evaluated by the parameters of inspiratory CT. The aim of this study is the evaluation of the parameters of expiratory CT on COPD pathophysiology.

Methods: This is the part of the Shiga University of Medical Science (SUMS) COPD Cohort study. A total of 268 subjects (47 non-COPD subjects and 220 COPD patients) were enrolled from May, 2011 to January, 2023. Pulmonary function tests and both inspiratory and expiratory chest CT were performed at the entry of the cohort. The percentage of low attenuation volume (LAV%) as emphysematous lesions and the square root of the wall area of a hypothetical airway with an internal perimeter of 10 mm ($\sqrt{\text{Aaw at Pi10}}$) as an index of airway lesions, were quantitatively measured using the inspiratory and expiratory chest CT. The relationships between FEV₁ (%predicted) and the imaging parameters were determined.

Results: All of the CT parameters, such as $\sqrt{\text{Aaw at Pi10}}$ and LAV% at -950HU of inspiratory CT and $\sqrt{\text{Aaw at Pi10}}$ and LAV% at -856HU and -950HU of expiratory CT were significantly correlated with FEV₁ (%predicted) ($\rho=-0.26$ ($p<0.0001$), $\rho=-0.40$ ($p<0.0001$), $\rho=-0.20$ ($p=0.0008$), $\rho=-0.47$ ($p<0.0001$), and $\rho=-0.47$ ($p<0.0001$) respectively). In multivariate regression analysis, FEV₁ (%predicted) was independently contributed by LAV% at -950HU of inspiratory CT, $\sqrt{\text{Aaw at Pi10}}$ and LAV% at -856HU of expiratory CT.

Conclusion: Using both parameters of inspiratory and expiratory CT may predict the severity of COPD precisely.

一秒量と吸気・呼気 CT 測定の関係

小川 恵美子^{1,2)}, 入山 朋子²⁾, 角田 陽子²⁾, 山崎 晶夫²⁾, 松尾 裕美子²⁾, 内田 泰樹²⁾, 仲川 宏昭²⁾,
黄瀬 大輔²⁾, 山口 将史²⁾, 中野 恭幸²⁾

1) 滋賀医科大学保健管理センター

2) 滋賀医科大学内科学講座呼吸器内科

背景と目的: 慢性閉塞性肺疾患 (COPD) は、呼気流量の減少を特徴とし、病態は、通常、吸気 CT で測定された指標を用いて評価される。本研究の目的は、呼気 CT で測定された指標と COPD 病態生理の関係を評価することである。

方法: 滋賀医科大学の COPD コホート研究に、2011 年 5 月から 2023 年 1 月までに参加した合計 268 人 (non-COPD 47 人、COPD 患者 220 人) を対象とした。コホートのエントリー時に呼吸機能検査と吸気および呼気 CT 検査を実施した。CT の画像解析は、低吸収域体積割合 (LAV%) を気腫性病変の指標として、内周が 10mm の仮想気道の壁面積の平方根 ($\sqrt{\text{Aaw at Pi10}}$) を気道病変の指標として定量測定した。FEV₁ (%predicted) と画像指標との関係を検討した。

結果: FEV₁ (%predicted) は、吸気 CT で測定した $\sqrt{\text{Aaw at Pi10}}$ (Ins-Pi10) と -950HU をカットオフとした LAV% (Ins-LAV%-950) 及び、呼気 CT で測定した $\sqrt{\text{Aaw at Pi10}}$ (Exp-Pi10) と -856HU と -950HU をカットオフとした LAV% (Exp-LAV%-856 と Exp-LAV%-950) と有意な相関を認めた (それぞれ $\rho = -0.26$ ($p < 0.0001$), $\rho = -0.40$ ($p < 0.0001$), $\rho = -0.20$ ($p = 0.0008$), $\rho = -0.47$ ($p < 0.0001$), および $\rho = -0.47$ ($p < 0.0001$))。多変量回帰分析では、FEV₁ (%predicted) には、Ins-LAV%-950, Exp-Pi10, および - Exp-LAV%-856 が独立して寄与している事が示された。

結論: 吸気 CT と呼気 CT の両方の指標を使用すると、COPD の重症度を正確に予測できる可能性が示唆された。

PJ2-3 Clinical significance of airway to lung ratio in asthma patients

Takafumi Shimada¹⁾, Hiroaki Iijima¹⁾, Kaoruko Shimizu²⁾, Hirokazu Kimura²⁾, Fumi Mochizuki¹⁾, Kazuya Tanimura³⁾, Shotaro Chubachi⁴⁾, Naoya Tanabe⁵⁾, Susumu Sato⁵⁾, Satoshi Konno²⁾, Nobuyuki Hizawa⁶⁾

- 1) Department of Respiratory Medicine, Tsukuba Medical Center Hospital, Tsukuba, Japan
- 2) Department of Respiratory Medicine, Faculty of Medicine, Hokkaido University, Sapporo, Japan
- 3) Department of Respiratory Medicine, Nara Medical University, Kashihara, Japan
- 4) Division of Pulmonary Medicine, Department of Medicine, Keio University School of Medicine, Tokyo, Japan
- 5) Department of Respiratory Medicine, Graduate School of Medicine, Kyoto University, Kyoto, Japan
- 6) Department of Pulmonary Medicine, Faculty of Medicine, University of Tsukuba, Tsukuba, Japan

Introduction/Aims : Dysanapsis is a size mismatch between the airways and the lung, and can be quantitatively assessed as the airway to lung ratio (ALR) using computed tomography (CT). Dysanapsis has been implicated in the deposition and sensitization of inhaled airborne substances and is assumed to be involved in the pathology of asthma. This study aimed to examine whether ALR affects inhaled antigen sensitization in asthmatic patients independent of bronchial tree morphology (airway fractal dimension; AFD).

Methods: We studied 161 asthma patients (57 males/104 females) without abnormal lung shadows or visual emphysema on CT in the Hokkaido refractory asthma cohort. ALR was calculated as the ratio of geometric mean extrapulmonary airway diameter to CT lung volume. Σ iMAST, which is the sum of each class of inhaled antigens in MAST33, was calculated as an index of inhaled antigen sensitization. Factors associated with high Σ iMAST, including ALR and AFD, were investigated.

Results: Univariate analysis showed that ALR was significantly lower in the high Σ iMAST group compared to the low Σ iMAST group (0.078 vs. 0.085, $p < 0.001$). Multivariate logistic regression analysis showed that low ALR was associated with high Σ iMAST independent of factors such as AFD, sex, age, and smoking history.

Conclusions: Dysanapsis, or low ALR is associated with the degree of inhaled antigen sensitization in asthmatic patients, suggesting that it is involved in the pathology of asthma.

喘息患者における Airway to lung ratio の臨床的意義

嶋田 貴文¹⁾, 飯島 弘晃¹⁾, 清水 薫子²⁾, 木村 孔一²⁾, 望月 芙美¹⁾, 谷村 和哉³⁾, 中鉢 正太郎⁴⁾, 田辺 直也⁵⁾, 佐藤 晋⁵⁾, 今野 哲²⁾, 檜澤 伸之⁶⁾

- 1) 筑波メディカルセンター病院
- 2) 北海道大学大学院医学研究院呼吸器内科学教室
- 3) 奈良県立医科大学呼吸器内科学講座
- 4) 慶応義塾大学医学部呼吸器内科
- 5) 京都大学大学院医学研究科呼吸器内科学
- 6) 筑波大学医学医療系呼吸器内科

【背景】 気道と肺のサイズミスマッチは dysanapsis と呼ばれ、CT 画像を用いて Airway to lung ratio(ALR) として定量的評価が可能である。Dysanapsis は吸入物質の沈着と感作に関与することが示唆され、喘息病態に関与している可能性がある。**【目的】** ALR が気管支樹形態 (気道フラクタル次元; AFD) と独立して、喘息患者の吸入抗原感作に影響するかを検証する。**【方法】** 北海道難治性喘息コホートにおいて CT で肺野異常影や肉眼的気腫のない 161 名 (男 57/ 女 104) の喘息患者を検討した。CT で肺外気道径の幾何平均と CT 肺容積の比として ALR を算出した。吸入抗原感作の指標として MAST33 の各吸入抗原のクラスを総計した Σ iMAST を算出した。 Σ iMAST 高値に影響する因子について ALR, AFD を含め検討した。**【結果】** 単変量解析では Σ iMAST 高値群は低値群に比し ALR が有意に低値であった (0.078 vs. 0.085, $p < 0.001$)。多変量ロジスティック回帰分析では ALR 低値が AFD や性別、年齢、喫煙歴等の因子と独立して Σ iMAST 高値に関連した。**【結論】** Dysanapsis=ALR 低値は喘息患者の吸入抗原感作の強さと関連し、喘息病態に関与していることが示された。

PJ2-4 Development of the method for CT imaging evaluation of the airways in bronchiectasis

Tomoki Maetani¹⁾, Naoya Tanabe¹⁾, Atsuyasu Sato¹⁾, Yusuke Shiraishi¹⁾, Ryo Sakamoto²⁾, Shizuo Kaji³⁾, Motonari Fukui⁴⁾, Susumu Sato^{1,5)}, Toyohiro Hirai¹⁾

1) Department of Respiratory Medicine, Graduate School of Medicine, Kyoto University

2) Department of Diagnostic Imaging and Nuclear Medicine, Graduate School of Medicine, Kyoto University

3) Institute of Mathematics for Industry, Kyushu University

4) Respiratory Disease Center, Kitano Hospital, The Tazuke Kofukai Medical Research Institute

5) Department of Respiratory Care and Sleep Control Medicine, Graduate School of Medicine, Kyoto University

[Background]Bronchiectasis has been focused in recent years due to the increasing number of patients. Although the airway-to-artery diameter ratio is frequently used in radiological evaluation, there are few reports on quantitative evaluation focusing on airway morphology. In this study, we developed a method to quantitatively evaluate bronchiectasis from CT images in order to clarify the pathogenesis of bronchiectasis.

[Methods]17 cases with bronchiectasis and 16 cases from health checkups were analyzed. Airway mask images were created from CT images using SYNAPSE VINCENT. A custom python script was used to extract the centerline of the airway, identify the lobe bronchi, and quantify the degree of airway taper from the lobe bronchi to the peripheral branches descending four generations. The X-axis was the length from the origin of the lobe bronchi and Y-axis was inner diameter of the airway. The linear regression was performed for each pathway. The mean Tapering index of each pathway was calculated for each patient.

[Results]The mean (standard deviation: SD) of the Tapering index for patients who underwent medical checkup was -0.19 (0.02). The averaged percentage of pathways with a Tapering index greater than the mean value +1 SD was 35.5% in cases of bronchiectasis. Airways with a particularly high Tapering index were visually bronchiectatic.

[Conclusion]Quantification of the degree of airway taper can be a useful imaging metric of bronchiectasis.

気管支拡張症における気道の画像的評価手法の開発

前谷 知毅¹⁾, 田辺 直也¹⁾, 佐藤 篤靖¹⁾, 白石 祐介¹⁾, 坂本 亮²⁾, 鍛冶 静雄³⁾, 福井 基成⁴⁾, 佐藤 晋^{1,2)}, 平井 豊博¹⁾

1) 京都大学大学院医学研究科 呼吸器内科学

2) 京都大学大学院医学研究科 放射線医学講座 画像診断学・核医学

3) 九州大学 マス・フォア・インダストリ研究所

4) 公益財団法人田附興風会 医学研究所北野病院呼吸器内科

5) 京都大学大学院医学研究科呼吸管理睡眠制御学講座

【背景】気管支拡張症は患者数が増加傾向で注目されている。画像的評価では気管支動脈比が頻用されるが気道形態に注目し評価した報告は乏しい。今回、気管支拡張症の病態解明のため CT 画像から気管支拡張を定量的に評価する手法を開発した。

【方法】気管支拡張症を認める 17 例、健診受診症例 16 例を用いた。SYNAPSE VINCENT を用いて CT 画像から気道マスク画像を作成した。自作 python スクリプトにて気道の中心線を抽出し、葉気管支を同定、葉気管支から末梢 4 分岐下までの気道の先細りの程度を定量化した。具体的には中心線上の各点ごとに、葉気管支起始部からの経路長・その断面における気道内径を計算した。X 軸を経路長、Y 軸を気道内径とし経路ごとに直線回帰を行いその傾きを Tapering index とした。さらに患者ごとに各経路の Tapering index の平均を計算した。

【結果】健診受診症例の Tapering index の平均 (標準偏差 SD) は -0.19 (0.02) であった。この平均 +1SD を超える経路の割合を気管支拡張各症例で算出し、その平均は 35.5% であった。Tapering index が特に高い気道は視覚的にも気管支拡張が見られた。

【結語】気道先細りの程度の定量化は気管支拡張の画像指標となる可能性がある。

PJ2-5 Clinical Remission and Chest Computed Tomography Findings with Biologics in Severe Asthma

Shinya Tsukamoto¹⁾, Naoya Tanabe¹⁾, Satoshi Marumo²⁾, Yu Hara³⁾, Atsushi Funauchi²⁾, Shota Takahashi⁴⁾, Yusuke Hayashi¹⁾, Kyohei Morita⁴⁾, Moon Hee Hwang⁴⁾, Motonari Fukui²⁾, Takeshi Kaneko³⁾, Toyohiro Hirai¹⁾

1) Department of Respiratory Medicine, Graduate school of Medicine Kyoto University

2) Respiratory Disease Center, Kitano Hospital

3) Respiratory Medicine, Yokohama City University

4) Respiratory Medicine, Osaka Red Cross Hospital

Background and aims: The achievement of clinical remission (CR) has been proposed to determine the efficacy of biologics for severe asthma; however, it is unclear whether CR reflects structural changes. In this study, we investigated the association between CR and CT findings.

Method: We performed a retrospective analysis of patients who underwent chest CT after receiving the same biologics for at least 1 year at 4 domestic institutions from 2013 to 2023. CR was defined as 3-way (1-year ACT \geq 23, no exacerbations, no systemic steroids) and as 4-way (1-year ACT \geq 20, no exacerbations, no systemic steroids, %FEV1 \geq 80%). The patients were divided into CR and non-CR groups. The differences in chest CT findings and clinical background were examined.

Results: 59 patients were included. The CR rate was 25.4% in 3-way and 30.5% in 4-way. In 3-way, the 3rd bronchial external diameter, lumen area, and wall area were significantly higher in the non-CR group, suggesting no association with structural abnormalities. In 4-way, the 4th bronchial wall thickness and area were significantly higher in the non-CR group. There was no significant difference in mucus plugs. Dividing into %FEV1 \geq 80% or not, Airway fractal dimension and total airway count were significantly higher in the higher group, reflecting structural abnormalities more clearly.

Conclusion: In severe asthma using biologics, CR was associated with 4th bronchial wall thickness/area in the 4-way criteria. Further prospective studies on the significance of chest CT findings in clinical remission are warranted.

重症喘息に対する生物学的製剤による Clinical Remission と胸部 CT 所見の検討

塚本 信哉¹⁾, 田辺 直也¹⁾, 丸毛 聡²⁾, 原 悠³⁾, 船内 敦司²⁾, 高橋 祥太⁴⁾, 林 優介¹⁾, 森田 恭平⁴⁾, 黄 文禧⁴⁾, 福井 基成²⁾, 金子 猛³⁾, 平井 豊博¹⁾

1) 京都大学大学院医学研究科呼吸器内科学

2) 北野病院呼吸器内科

3) 横浜市立大学呼吸器内科学

4) 大阪赤十字病院呼吸器内科

【背景・目的】重症喘息に対する生物学的製剤 (BIO) の効果判定に臨床的寛解 (CR) の達成が提唱されているが、CR が構造的変化を反映するかは不明である。本研究では CR と CT 指標の関連を検討した。【方法】2013～2023 年に国内 4 施設で同一 BIO を 1 年以上投与した後に胸部 CT を施行した症例を後方視的に解析した。CR の定義は 3-way (1 年間 ACT \geq 23, 増悪・全身ステロイド投与なし) と 4-way (1 年間 ACT \geq 20, 増悪・全身ステロイド投与なし, 1 秒量 \geq 予測量の 80%) の 2 つを用いた。対象患者を CR 達成の有無で CR 群・非 CR 群に分け、CT 所見の差異を検討した。【結果】解析対象は 59 例、CR 率は 3-way 25.4%、4-way 30.2% だった。3-way では非 CR 群で第 3 次気管支外径、管腔面積、壁面積が有意に大きく、構造的異常との関連は示唆されなかった。4-way では非 CR 群で第 4 次気管支壁厚・面積が有意に高値だった。粘液栓は有意差を認めなかった。肺機能項目の達成・非達成で評価すると、達成群で Airway fractal dimension, Total airway count が有意に高値であり、より構造的異常を反映した。【結論】BIO を用いた重症喘息患者では、4-way では CR と構造的異常が関連した。CR での意義につき更なる検討が必要である。

Interstitial Pneumonia/Vascular Diseases

PJ3-1 4DCT study of regional lung mobility in patients with interstitial lung disease

Yoko Tsunoda¹⁾, Hiroaki Nakagawa¹⁾, Yukihiro Nagatani²⁾, Shinya Yokoe¹⁾, Tomoko Iriyama¹⁾, Wataru Shigemori¹⁾, Akio Yamazaki¹⁾, Daisuke Kinose¹⁾, Masafumi Yamaguchi¹⁾, Emiko Ogawa¹⁾, Yoshiyuki Watanabe²⁾, Yasutaka Nakano¹⁾

1) Division of Respiratory Medicine, Department of Internal Medicine, Shiga University of Medical Science

2) Department of Radiology, Shiga University of Medical Science

Aims: Several studies using inspiratory and expiratory CT have reported limited lung mobility in the lower lung in patients with interstitial lung disease (ILD). These may represent the progressive fibrosis and limited lung mobility. However, there are few reports on lung mobility using 4-dimensional computed tomography (4DCT). We investigated how the degree of local lung fibrosis affects regional lung mobility.

Methods: A total of 73 patients with chronic ILD were enrolled. 4DCT images were acquired using automated voice guidance. Five points were placed on the right midclavicular line from the apex to diaphragm (point 1 at the apex and point 5 at the diaphragm) at maximal inspiration. The movement of the lung was analyzed using the automatic tracking system. We measured the moving distance of each point for one respiratory cycle, and defined the distance corrected for lung volume as the Regional Lung Mobility (RLM) index.

Results: The %FVC was positively correlated with the RML index of point 5 ($\rho = 0.26$, $p = 0.029$), but not with points 2 and 3. The degree of fibrosis in the lower lung was negatively correlated with the RML index of point 5 ($\rho = -0.24$, $p = 0.044$), while it was positively correlated with the RML index of points 2 and 3 ($\rho = 0.24$, $p = 0.038$, $\rho = 0.26$, $p = 0.029$, respectively).

Conclusion: The increase of fibrosis in the lower lung had the positive influence on the mobility of the middle lung and negative influence on the lower lung.

4DCT を用いた間質性肺炎患者における肺局所の可動性についての検討

角田 陽子¹⁾, 仲川 宏昭¹⁾, 永谷 幸裕²⁾, 横江 真弥¹⁾, 入山 朋子¹⁾, 重森 度¹⁾, 山崎 晶夫¹⁾, 黄瀬 大輔¹⁾, 山口 将史¹⁾, 小川 恵美子¹⁾, 渡邊 嘉之²⁾, 中野 恭幸¹⁾

1) 滋賀医科大学医学部附属病院呼吸器内科

2) 滋賀医科大学医学部附属病院放射線科

目的：吸気・呼気 CT の研究で間質性肺炎において下肺の可動性が制限されることが報告されている。しかし、4DCT を用いた肺の可動性に関する報告は少ない。4DCT を用いて肺局所の動きを定量化し、呼吸機能検査や肺の線維化の程度との関係について検討した。

対象：当院通院中の間質性肺炎患者で研究の同意を得た 73 症例。

方法：自動音声案内に従って 4DCT 画像を撮影、画像解析ソフト (Ziostation[®], Ziosoft) の自動追跡システムを用いて、以下の解析を行った。

最大吸気時に右鎖骨中線上で肺尖部～横隔膜までの距離を 4 分割し、得た 5 点を肺尖部から点 1～5 とした。各点が 1 呼吸サイクルで移動した距離 (Regional Lung Mobility; RLM) を、呼気体積 3 乗根で補正したものを RML index と定義し、肺内の各点の動きの指標とした。

結果：% FVC は点 5 の RML index と正の相関があった ($\rho = 0.26$, $p = 0.029$) が、点 2・3 とはなかった。下肺の線維化の程度は点 5 の RML index と負の相関があった ($\rho = -0.24$, $p = 0.044$) 一方、点 2・3 の RML index と正の相関があった (それぞれ $\rho = 0.24$, $p = 0.038$, $\rho = 0.26$, $p = 0.029$)。

結論：下肺の線維化の程度が強いと下肺の可動性は抑制されたが、中肺の可動性は保たれていた。

PJ3-2 Factors in lung volume reduction in RA-related ILD by quantitative chest CT

Masahiro Tahara¹⁾, Takako Kawaguchi¹⁾, Kei Yamasaki¹⁾, Yoshiya Tanaka²⁾, Kazuhiro Yatera¹⁾

1) Department of Respiratory Medicine, University of Occupational and Environmental Health,

2) The First Department of Internal Medicine and Graduate School of Medical Science, University of Occupational and Environmental Health

Background: The evaluation of interstitial lung disease associated with rheumatoid arthritis (RA-ILD) heavily relies on imaging and pulmonary function tests (PFTs). However, clinical challenges arise when pulmonary function cannot be adequately assessed due to symptoms such as coughing.

Objective: This study aimed to explore the feasibility of using lung volume measurements from an imaging analysis system as a substitute for PFTs in patients with RA-ILD. Additionally, the study investigates factors associated with reduced lung volume.

Methods: The study included patients diagnosed with RA-ILD at our hospital in 2017 and 2018, for whom both imaging and pulmonary function test data were available. Lung volume (LV) and lung density were measured using an imaging analysis system (VINCENT, FUJIFILM). The percentage change in lung volume (%LV) over two years from diagnosis was analyzed using multiple regression to identify associated factors.

Results: Among the 48 patients with RA-ILD (median age of 55.5 years), the median %FVC and %LV were 88.0% and 105.8%, respectively. There was a positive correlation between changes in %FVC and %LV ($r=0.403$, $P < 0.01$). Multiple regression analysis revealed that the change in the -750 to -500 Hounsfield unit (HU) range ($\beta = -2.99$, $P < 0.01$) was an independent factor associated with the percentage change in lung volume.

Conclusion: For patients with RA-ILD, lung volume measurements obtained from imaging analysis systems can serve as a viable alternative to traditional pulmonary function tests. Additionally, an increase in the -750 to -500 HU range is associated with a decrease in lung volume.

関節リウマチ関連間質性肺疾患における胸部 CT 定量評価での肺容積減少因子の解析

田原 正浩¹⁾, 川口 貴子¹⁾, 山崎 啓¹⁾, 田中 良哉²⁾, 矢寺 和博¹⁾

1) 産業医科大学 医学部 呼吸器内科学

2) 産業医科大学 医学部 第1内科学

【背景】関節リウマチ関連間質性肺疾患 (RA-ILD) の評価は画像や肺機能が重要だが、咳嗽等で肺機能評価が不十分になることが臨床的に問題である。【目的】RA-ILD 患者における画像解析システムによる肺容積での肺機能検査代用の可能性と肺容積減少の関連因子を探索する。【方法】2017, 2018 年に当院で RA-ILD と診断され画像や肺機能検査が利用可能な患者を対象とした。画像解析システム (VINCENT, FUJIFILM) で肺容積 (lung volume: LV) と肺野濃度を測定し、診断から 2 年間の %LV 変化量 (Δ %LV) に関連する因子を重回帰分析で評価した。【結果】RA-ILD 患者 48 例 (年齢中央値 55.5 歳) の内、%FVC, %LV 中央値は 88.0%, 105.8% であった。 Δ %FVC と Δ %LV は正の相関を示し ($r=0.403$, $P < 0.01$)、 Δ %LV の重回帰分析では Δ -750-500HU 領域 ($\beta = -2.99$, $P < 0.01$) が独立した相関を認めた。【結論】RA-ILD 患者では、画像解析システムによる肺容積で肺機能検査の代用が可能で、-750-500HU 領域の増加が肺容積減少に関連する。

PJ3-3 Lung volume changes by lung lobe in patients with interstitial lung disease

Masashi Zenta^{1,2)}, Kenji Tsushima³⁾, Tomohiro Hattori⁴⁾, Jin Kubo⁵⁾, Natsuko Yuzuguchi²⁾,
Minami Akama²⁾, Satoshi Kido²⁾

1) Department of Rehabilitation, International University of Health and Welfare (IUHW) Ichikawa Hospital

2) Department of Health and Social Services, Course of Health and Social Services, Graduate School of Saitama Prefectural University

3) Department of Pulmonary Medicine, Tokyo Medical University Hachioji Medical Center

4) Department of Respiratory Medicine, IUHW Ichikawa Hospital

5) Department of Rehabilitation Medicine, IUHW Ichikawa Hospital

Background: Although there have been reports on lung volume and asymmetry by lung lobe in imaging findings of interstitial lung disease (ILD), to the best of our knowledge, no reports have followed changes over time.

Purpose: This study evaluated lung volume loss by lung lobe over a 2-year period in patients with ILD.

Methods: Patients diagnosed with ILD at our hospital from 2017 to 2021 and undergoing 2-year CT evaluation were included. Lung volumes were evaluated using CT image analysis software (ziostation2, ziosoft) to calculate lung volumes by lung lobe. Bonferroni method was used for repeated measures one-way ANOVA and post-hoc test for lung volumes per lung lobe at the time of diagnosis, 1 year after diagnosis, and 2 years after diagnosis.

Results: Seventy-seven patients with ILD were analyzed, and the right and left lower lobes were significantly decreased (right lower lobe: $P < 0.01$, left lower lobe: $P < 0.01$). On the other hand, the right middle lobe showed no decrease over time ($P = 0.08$), while the upper lobe showed a significant decrease on the left side (right upper lobe: $P = 0.56$, left upper lobe $P < 0.01$).

Conclusion: Lung volumes calculated from CT in patients with ILD showed a decrease over time in the lower lobe, but not in the middle lobe. As for the upper lobe, asymmetry was observed, with a greater decrease in lung volume on the left side.

間質性肺疾患患者における肺葉別の肺容積の変化

善田 督史^{1,2)}, 津島 健司³⁾, 服部 知洋⁵⁾, 久保 仁⁴⁾, 袖口 菜津子²⁾, 赤間 美波²⁾, 木戸 聡史²⁾

1) 国際医療福祉大学市川病院リハビリテーション室

2) 埼玉県立大学大学院保健医療福祉学研究所

3) 東京医科大学八王子医療センター呼吸器内科

4) 国際医療福祉大学市川病院リハビリテーション科

5) 国際医療福祉大学市川病院呼吸器内科

【背景】 間質性肺疾患 (ILD) の画像所見において、肺葉別の容積や非対称性に関する報告はあるが、我々の知り限り経時的変化を追った報告はない。

【目的】 本研究は、ILD 患者における 2 年間の肺葉別の肺容積低下を評価した。

【方法】 2017 年から 2021 年に当院で ILD と診断され、2 年間の CT 評価を行っている患者を対象とした。肺容積の評価は CT 画像解析ソフトウェア (ziostation2, ziosoft) を用い、肺葉ごとの肺容積を算出した。診断時、診断から 1 年後、2 年後の肺葉ごとの肺容積に対し、反復測定一元配置分散分析と事後検定に Bonferroni 法を行った。

【結果】 ILD 患者 77 名を解析し、左右下葉は有意に低下していた (右下葉: $P < 0.01$ 、左下葉: $P < 0.01$)。一方、右中葉は経時的減少が見られず ($P = 0.08$)、上葉では左側で有意な低下を認めた (右上葉: $P = 0.56$ 、左上葉 $P < 0.01$)。

【結論】 ILD 患者における CT から算出された肺容積は、下葉では経時的に低下していたが、中葉では低下を認めなかった。上葉については非対称性を認め、左側の肺容積がより低下していた。

PJ3-4 Pulmonary hypertension associated with systemic sclerosis: utility of pulmonary artery volume ratio

Hidetake Yabuuchi¹⁾, Kouji Sagiyama²⁾, Yuzo Yamasaki²⁾, Tomoyuki Hida²⁾, Takuya Hino²⁾, Kazuya Tsubouchi³⁾, Hiroaki Niiro⁴⁾, Kousei Ishigami²⁾

- 1) Department of Health Sciences, Graduate School of Medical Sciences, Kyushu University
- 2) Department of Clinical Radiology, Graduate School of Medical Sciences, Kyushu University
- 3) Department of Respiratory Medicine, Graduate School of Medical Sciences, Kyushu University
- 4) Department of Medicine and Biosystemic Science, Graduate School of Medical Sciences, Kyushu University

Background: Pulmonary hypertension (PH) is a major cause of death in patients with systemic sclerosis (SSc) as well as interstitial lung disease (ILD), and early detection and treatment are important.

Purpose: To determine whether pulmonary artery (PA) volume ratio can predict PH in patients with SSc.

Materials and Methods: Twenty patients with SSc (5 men, 15 women; mean age, 61.0 years), including 10 with PH were examined. Pulmonary artery volume ratio, PA-to-aorta ratio, and ILD volume ratio were extracted from non-contrast enhanced 3D volume CT using the software (Ziostation2, Ziosoft) and compared between the PH and non-PH groups. PH was defined as a mean pulmonary artery pressure (mPAP) of >20 mmHg. The diagnostic capability was evaluated using the receiver operating characteristic curve.

Results: Mean PA volume ratio was significantly higher in PH group than that of non-PH group (18.59 ± 3.49 vs. 12.9 ± 3.75 , $P < 0.01$), whereas there was no significant difference in PA-to-aorta ratio (1.08 ± 0.08 vs. 0.91 ± 0.14 , $P = 0.10$). The diagnostic capability of the PA volume ratio (AUC, 0.85) was superior to that of other parameters.

Conclusion: PA volume ratio derived from non-contrast 3D volume CT data seems to be a promising tool for the detection of PH in patients with SSc.

全身性強皮症合併肺高血圧症：3D-CT 肺動脈容積比の有用性

藪内 英剛¹⁾, 鷺山 幸二²⁾, 山崎 誘三²⁾, 樋田 知之²⁾, 日野 卓也²⁾, 坪内 和哉³⁾, 新納 宏昭⁴⁾, 石神 康生²⁾

- 1) 九州大学大学院医学研究院保健学部門
- 2) 九州大学大学院医学研究院臨床放射線科学分野
- 3) 九州大学病院呼吸器内科
- 4) 九州大学病院 免疫・膠原病・感染症内科

背景：肺高血圧症（PH）は間質性肺疾患（ILD）と同様に、全身性強皮症（SSc）患者の主な死因であり、早期発見と治療が重要である。目的：肺動脈容積比がSSc患者のPHを予測できるかどうかを調べる。対象と方法：SSc患者20名（男性5、女性15、平均年齢61.0歳）（うちPH患者10名）を対象とした。肺動脈容積比、ILD病変容積比は、非造影3D-CTからソフトウェア（Ziostation2、Ziosoft）を用いて、肺動脈-大動脈比は2D-CT上で計測し、PH群と非PH群で比較した。PHは、平均肺動脈圧（mPAP）が20mm Hg以上と定義した。診断能は、ROC曲線を用いて評価した。結果：平均肺動脈容積比はPH群で非PH群より有意に高かったが（ 18.59 ± 3.49 vs 12.9 ± 3.75 , $P < 0.01$ ）、肺動脈-大動脈比には有意差を認めなかった（ 1.08 ± 0.08 vs 0.91 ± 0.14 , $P = 0.10$ ）。肺動脈容積比の診断能（AUC, 0.85）は他のパラメータよりも優れていた。結論：非造影3D-CTデータから得られる肺動脈容積比は、SSc患者におけるPHの検出に有用と考えられる。

PJ3-5 Quantitative assessment of heterogeneity of lung density in patients with CTEPH

Naoko Kawata^{1,2)}, Toshihiko Sugiura¹⁾, Yuma Iwao^{3,4)}, Akira Nishiyama⁵⁾, Keiichi Ishida⁶⁾,
Takuji Suzuki¹⁾, Hideaki Haneishi³⁾, Nobuhiro Tanabe^{1,7)}

- 1) Department of Respiriology, Graduate School of Medicine, Chiba University
- 2) Graduate School of Science and Engineering, Chiba University
- 3) Center for Frontier Medical Engineering, Chiba University
- 4) Institute for Quantum Medical Science, National Institutes for Quantum Science and Technology
- 5) Department of Radiology, Chiba University Hospital
- 6) Department of Cardiovascular Surgery, Chibaken Saiseikai Narashino Hospital
- 7) Department of Respiratory Medicine, Chibaken Saiseikai Narashino Hospital

Purpose: In recent years, the degree of heterogeneity in the lung region of interest has been reported to be associated with disease severity and prognosis in a variety of diseases. The aim of this study was to investigate whether lung density analysis on non-contrast chest CT images before and after pulmonary artery endarterectomy (PEA) in chronic thromboembolic pulmonary hypertension (CTEPH) could reflect pulmonary circulation dynamics.

Materials and Methods: Fifty-one patients with CTEPH who underwent PEA were retrospectively enrolled. CT texture analysis (CTTA) was performed after lung fields were extracted from chest CT images using thresholding and deep learning methods. The association between radiomic parameters and right heart catheterization and other clinical items before and after PEA was investigated.

Results: Mean lung density and entropy, which indicate heterogeneity of lung field density, were higher in the group with mean pulmonary artery pressure of 25 mm Hg or higher one year after PEA (n=19) than in the group with mean pulmonary artery pressure of less than 25 mm Hg (n=32), while uniformity, which indicates homogeneity of density, skewness, and kurtosis showed lower values.

Conclusion: Heterogeneity of lung density reflects pulmonary circulation dynamics and CTTA may be a minimally invasive method to assess and predict postoperative pulmonary circulation dynamics after PEA in patients with CTEPH.

慢性血栓塞栓性肺高血圧症患者における肺野濃度の不均一性の評価

川田 奈緒子^{1,2)}, 杉浦 寿彦¹⁾, 岩男 悠真^{3,4)}, 西山 晃⁵⁾, 石田 敬一⁶⁾, 鈴木 拓児¹⁾, 羽石 秀昭³⁾,
田邊 信宏^{1,7)}

- 1) 千葉大学大学院医学研究院 呼吸器内科学
- 2) 千葉大学大学院融合理工学府 基幹工学専攻 医工学コース
- 3) 千葉大学フロンティア医工学センター
- 4) 量子科学技術研究開発機構
- 5) 千葉大学大学院医学研究院画像診断・放射線腫瘍学
- 6) 千葉県済生会習志野病院心臓血管外科
- 7) 千葉県済生会習志野病院呼吸器内科

目的: 近年、様々な疾患で、画像から得られる注目領域の濃度不均一性の程度が疾患重症度や予後と関連することが報告されている。今回の研究は、慢性血栓塞栓性肺高血圧症 (CTEPH) における術前後での胸部単純 CT での肺野 (体積) 濃度が肺循環動態を反映しているか検討することを目的とした。

対象と方法: 肺動脈内膜摘除術 (PEA) を施行した CTEPH 患者 51 名について後方視的に登録した。しきい値処理と深層学習を用いて胸部 CT から肺野を抽出した後に CT texture analysis (CTTA) を行った。画像評価項目と PEA 前後での右心カテーテル項目や他の臨床項目との関連を検討した。

結果: CTTA 術後 1 年に平均肺動脈圧 25mm Hg 以上を認める群 (n=19) では、25mmHg 未満群 (n=32) に比して mean lung density (平均肺野濃度) や濃度の不均一性を示す entropy が高く、濃度の均一性を示す uniformity が低かった。Skewness (歪度) や kurtosis (尖度) が低かった。

結論: 肺野濃度の不均一性は肺循環動態を反映し、CTTA は CTEPH 患者の PEA 術後の肺循環動態を評価、予測する低侵襲な手法となる可能性がある。

PJ3-6 Dual-Energy CT Thoracic Imaging: Late-Phase Can Replace Unenhanced and Early-Phase Scans.

Shuhei Doi, Masahiro Yanagawa, Daiki Nishigaki, Keisuke Ninomiya, Kazuki Yamagata, Ryo Ogawa, Yuriko Yoshida, Akinori Hata, Yukiko Tokuda, Noriyuki Tomiyama
Osaka University Graduate School of Medicine

Purpose:

To assess the feasibility of generating contrast-enhanced early phase and non-contrast CT images from contrast-enhanced late phase images using dual-energy CT by adjusting the keV energy.

Methods and Materials:

45 patients underwent dual-energy CT scans with fast kV switching mode. Various CT images including unenhanced and enhanced CT (early and late phases) were acquired. Contrast material dosage was determined based on patient weight. Additionally, images at different keV levels were created from the late phase, and virtual non-contrast CT (VNC) was generated from both early and late phases. ROIs were placed on the aorta, pulmonary artery (PA), and superior vena cava (SVC), and each CT value was measured. Statistical comparisons were made between the 6 groups in the early (70keV) and late phases (50-, 55-, 60-, 65-, and 70-keV), and between the 3 groups in the true non-contrast CT (TNC) and VNC created from the early and late phases (70keV), respectively, using the repeated measures analysis of variances test. P values < 0.05 were significant.

Results:

No significant differences of CT values were shown as follows (P=1.00): in the aorta and PA between early phase-70 keV and late phase-55 keV; in the SVC between early phase-70 keV and late phase-65 keV. VNC image of early- and late-phase 70 keV and TNC showed no significant differences (p>0.05).

Conclusions:

Late phase images at 55 keV may serve as alternatives to early phase images at 70 keV. Caution is advised regarding contrast effects, particularly in the SVC. VNC images effectively replicated true non-contrast CT images.

デュアルエネルギー CTによる胸部画像の後期相の検討：単純および早期相の代替可能性の評価

土居 秀平, 梁川 雅弘, 西垣 大毅, 二宮 啓輔, 山形 和樹, 小川 遼, 吉田 悠里子, 秦 明典,
徳田 由紀子, 富山 憲幸

大阪大学大学院医学系研究科放射線統合医学講座放射線医学教室

目的：デュアルエネルギー CT (DECT) の keV エネルギーを変化させ、造影後期相から早期相及び単純 CT 画像を生成できるかを検討すること。

方法と材料：45 人の患者に DECT を施行した。造影剤の投与量は患者体重に応じて調整し、後期相から異なる keV レベルの画像を生成した。大動脈、肺動脈、上大静脈に ROI を設定し、それぞれの CT 値を測定した。早期相 (70keV) と後期相 (50、55、60、65、70keV) の 6 群間、および早期相と後期相 (70keV) からそれぞれ作成した仮想単純 CT (VNC) と真の単純 CT (TNC) との 3 群間で、反復測定分散分析検定を用いて統計的比較を行った。P 値 < 0.05 を有意とした。

結果：早期相 70 keV と後期相 55 keV 間で、大動脈と肺動脈の CT 値に有意差がなく、早期相 70 keV と後期相 55 keV 間で、上大静脈の CT 値に有意差がなかった (p=1.00)。早期相および後期相 70 keV の VNC 画像と TNC 画像には有意差がなかった (p>0.05)。

結論：後期相の 55keV 画像は早期相の 70keV 画像を代替できる。ただし、SVC における造影効果については注意が必要である。また、VNC 画像は真の単純 CT 画像を代替できる。

CT

PJ4-1 Micro-nodule analysis of pneumoconiosis using 3D CT images

Rento Nii¹⁾, Yoshiki Kawata²⁾, Yoshinori Ohtsuka³⁾, Takumi Kishimoto⁴⁾, Kazuto Ashizawa⁵⁾, Noboru Niki⁶⁾

- 1) Tokushima University
- 2) Institute of Post LED Photonics, Tokushima University
- 3) Hokkaido Chuo Rosai hospital
- 4) Okayama Rosai Hospital
- 5) Department of Clinical Oncology Unit of Translational Medicine, Nagasaki University
- 6) Medical Science Institute Inc

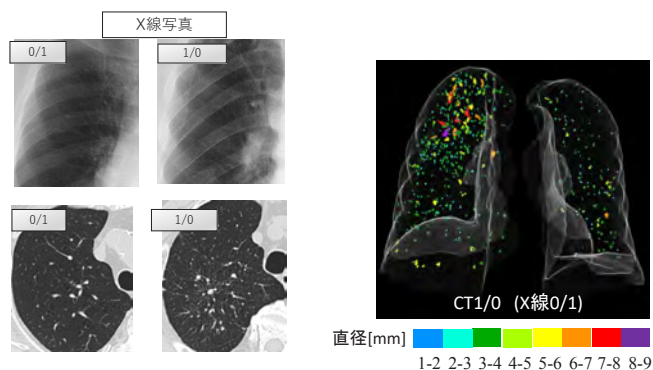
Pneumoconiosis is an occupational respiratory disease caused by inhaling mineral dust into the lungs. In our country, the diagnosis of pneumoconiosis is conducted using chest radiography, and it is pathologically classified into Types 0 through 4. Types 1 and above are eligible for workers' compensation claims. However, there are discrepancies in diagnosis between Type 0 (0/1) and Type 1 (1/0) in the boundary area as interpreted by radiologists. Recently, there has been anticipation for more accurate diagnosis using three-dimensional CT images, which can evaluate lesions more precisely compared to X-ray images. Therefore, this study aims to develop a diagnostic support manual for pneumoconiosis using three-dimensional CT images. We extract micro-nodules manually from CT images to create a dataset and analyze the number, size, and distribution of micro-nodules. Furthermore, we aim to elucidate the differences in micro-nodules among different types of pneumoconiosis.

3次元CT画像によるじん肺の粒状影解析

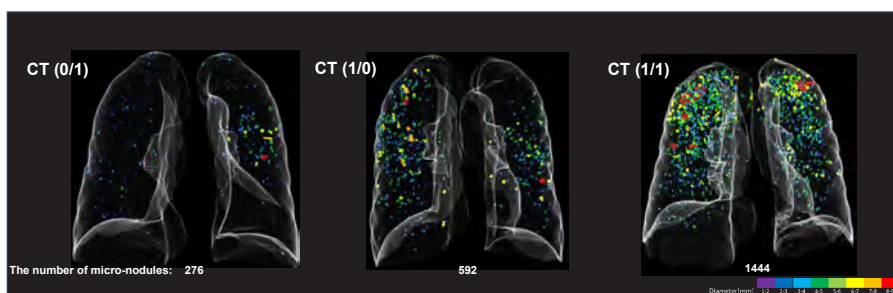
新居 蓮叶¹⁾, 河田 佳樹²⁾, 大塚 義紀³⁾, 岸本 卓巳⁴⁾, 芦澤 和人⁵⁾, 仁木 登⁶⁾

- 1) 徳島大学
- 2) 徳島大学ポストLED研究所
- 3) 北海道中央労災病院
- 4) 岡山ろうさい病院
- 5) 長崎大学医歯(薬)学総合研究科
- 6) 株式会社医用科学研究所

じん肺は、鉱物の粉塵を肺に吸入することによって生じる職業性呼吸器疾患である。我国において、じん肺の診断は胸部単純X線写真を用いて行われており、第0型から第4型に病理区分される。第1型以上から労災認定の対象となる。しかし、第0型の0/1と第1型の1/0の境界領域では読影医によって診断に差が生じる。近年、X線写真に比べて正確に病変を評価できる3次元CT画像を用いた高精度な診断が期待されている。そこで、本研究では3次元CT画像を用いたじん肺の診断支援マニュアル作成を目指す。CT画像よりマニュアルで粒状影を抽出しデータセットを作成し、粒状影の個数、大きさ、分布を解析する。そして病型ごとの粒状影の差を明らかにする。



粒状影のマニュアル抽出結果



PJ4-2 Lung and airway dynamics using respiratory 4DCT including the whole respiratory system

Hiroshi Moriya, Motoharu Hakozaki, Mika Hoshino, Ken-ichirou Hirai
Ohara general hospital

Introduction: Respiratory dynamic CT including the whole respiratory system can be obtained by scanning 2 or 3 volumes with a 16 cm ADCT while breathing continuously. This method allows for respiratory dynamic images of the nasal cavity, larynx, trachea, bronchi, and entire lungs. Advances in segmentation technology allow for the acquisition of the volume and CT value of any structure, which can then be displayed as a time curve.

Subjects: Lung cancer cases (whole lung respiratory dynamic imaging for evaluation of adhesions before resection)

Devices used: 320-row ADCT (AquilionONE), Ziostation2

Results: The airway and lungs could be depicted, and preoperative adhesions could be determined. The volume and CT value of each lung lobe, as well as the tracheal volume and cross-sectional area, could be measured. Segmentation was good for extracting the left and right lungs, but there were few cases where lung lobe extraction was good, and manual correction was required. This was due to the deterioration of image quality due to the ultra-low dose and blurring due to breathing. Extraction of the trachea and main bronchi was good, but peripheral bronchi was poor. In COPD, differences in peak phase were sometimes observed in the time curve for each lung lobe. Compared with healthy subjects, a reduction in cross-sectional area was sometimes observed during expiration in COPD.

Summary: This method makes it possible to determine the respiratory phase from the total lung volume. It is possible to display the fluctuations of any structure involved in respiration.

呼吸器系全体を含む呼吸動態 4DCT による肺・気道動態の可視化 一定量化と技術的課題一

森谷 浩史, 箱崎 元晴, 星野 実加, 平井 健一郎
大原総合病院

はじめに:呼吸を継続しながら 16cm ADCT で 2~3 ボリュームをスキャンすることで、呼吸器系全体を含む呼吸動態 CT が得られます。この方法では、鼻腔、喉頭、気管、気管支、肺全体の呼吸動態画像が得られます。セグメンテーション技術の進歩により、任意の構造の体積と CT 値を取得でき、それを時間曲線として表示できます。

対象: 肺癌症例 (切除前の癒着評価のための全肺呼吸動態画像)

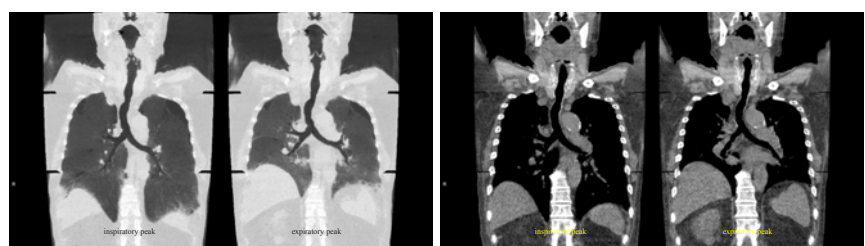
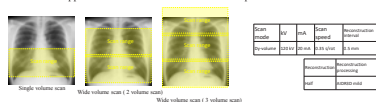
使用機器: 320 列 ADCT (AquilionONE)、Ziostation2

結果: 気道と肺を描写でき、術前の癒着を判定できました。各肺葉の体積と CT 値、気管の体積と断面積を測定できました。セグメンテーションは左右の肺の抽出には適していましたが、肺葉の抽出が良好な症例は少なく、手動での修正が必要でした。これは、極低線量による画質の劣化と呼吸によるぼやけによるものです。気管と主気管支の抽出は良好でしたが、末梢気管支の抽出は不良でした。COPD では、各肺葉の時間曲線にピーク位相の違いが見られることがありました。健康者と比較して、COPD では呼気時に断面積の減少が見られることがありました。

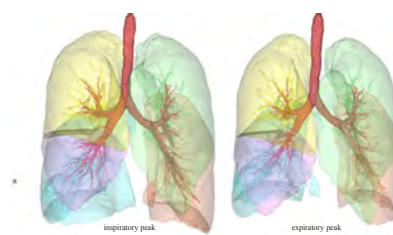
要約: この方法により、全肺容量から呼吸位相を判定することが可能です。呼吸に関与するあらゆる構造の変動を表示することができます。

Method of step&shoot whole-lung respiratory dynamic CT

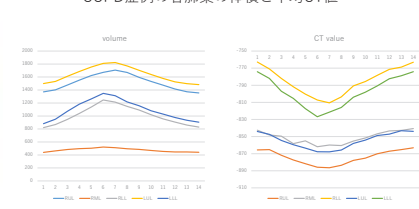
1. Consistent respiratory cycles by recorded voice guidance.
2. Dynamic volume scanning using 320-row ADCT (reconstruction interval: 0.35 s).
Two or three volumes of respiratory dynamic CT with 1-cm overlap.
3. Body-surface marker placed on the precordial body surface.
4. Selection of the inspiratory peak phase and expiratory peak phase of the scanned dynamic data.
5. After the phases of the two or three volumes were matched, they were joined together and the overlapped cross sections in the dataset of each phase were deleted.



呼吸曲線と胸腔内気管断面積



COPD症例の各肺葉の体積と平均CT値



PJ4-3 Association Between The Cross-sectional Area Of Erector Spinae Muscles And Mortality in CPFE Patients

Tatsuhiro Furuyama, Kazuki Ota, Shin Furutaka, Nobuhiro Fujioka, Kazuya Tanimura, Yukio Fujita, Yoshifumi Yamamoto, Shigeto Hontsu, Shigeo Muro

Department of Respiratory Medicine, Nara Medical University

Background: The cross-sectional area of erector spinae muscle (ESM_{CSA}), which can be measured by chest CT, is considered a significant prognostic factor that correlates with various clinical parameters in patients with COPD and those with idiopathic pulmonary fibrosis. On the other hand, its usefulness in patients with combined pulmonary fibrosis and emphysema (CPFE), which has features of both diseases, has not been fully investigated.

We conducted a retrospective cohort study of adult patients with CPFE who visited our hospital from February 1, 2011, to December 31, 2023. ESM_{CSA} was measured on a single axial chest CT image at the initial visit, and the association with each clinical parameter and prognosis (all-cause mortality) was evaluated.

Results: We included 137 patients (male/female=130/7, age 72.7 ± 8.2 years, BMI 23.4 ± 3.2 kg/m²) in the analysis. ESM_{CSA} showed a significant negative correlation with age, RV/TLC, and degree of emphysema, and a significant positive correlation with weight, BMI, %FEV1, and %DLCO, and no correlation with mMRC, %VC, %FVC, degree of fibrosis. In prognostic analysis, patients with low ESM_{CSA} (<26.3 cm²) had a significantly worse prognosis ($p=0.0003$). Low ESM_{CSA} and mMRC were independent significant prognostic factors in multivariate Cox proportional hazards models. Conclusion: ESM_{CSA} was a significant prognostic factor in CPFE patients as well. ESM_{CSA} suggested to be more closely associated with COPD than interstitial pneumonia.

気腫合併肺線維症患者における脊柱起立筋横断面積と臨床パラメータや予後との関連

古山 達大, 太田 和輝, 古高 心, 藤岡 伸啓, 谷村 和哉, 藤田 幸男, 山本 佳史, 本津 茂人, 室 繁郎

奈良県立医科大学附属病院呼吸器内科

【背景】胸部CTで測定可能な脊柱起立筋横断面積 (ESM_{CSA}) は COPD 患者、特発性肺線維症患者において複数の臨床指標と相関する有意な予後関連指標とされる。一方、両疾患の特徴を有する気腫合併肺線維症 (CPFE) 患者において、その有用性についての検討は十分ではない。

【方法】2011年2月1日から2023年12月31日までに当院通院歴のある成人 CPFE 患者を対象とする後ろ向きコホート研究を行った。初診時の胸部CTで ESM_{CSA} を測定し、各臨床パラメータと予後 (全死因死亡) との関連を評価した。

【結果】137例 (男性/女性=130/7、年齢 72.7 ± 8.2 歳、BMI 23.4 ± 3.2 kg/m²) を解析対象とした。 ESM_{CSA} は年齢、RV/TLC、気腫の程度と有意な負の相関、体重、BMI、%FEV1、%DLCOと有意な正の相関を示したが、mMRC、%VC、%FVC、線維化の程度とは相関を認めなかった。予後解析において ESM_{CSA} 低値 (<26.3 cm²) の患者では有意に予後が不良 ($p=0.0003$) で、多変量 Cox 比例ハザードモデルでは ESM_{CSA} 低値と mMRC は独立した有意な予後関連因子であった。

【結語】CPFE 患者においても ESM_{CSA} は有意な予後関連因子であった。 ESM_{CSA} 低下は間質性肺炎よりも COPD の要素との関連が深いことが示唆された。

PJ4-4 Experimental analysis of usefulness of ultra-high-resolution scanning on dynamic ventilation CT

Ryo Uemura¹⁾, Yukihiro Nagatani¹⁾, Jun Matsubayashi²⁾, Hiroaki Nakagawa³⁾, Kentaro Fukunaga^{3,4)}, Yoko Tsunoda³⁾, Yasutaka Nakano³⁾, Yoshiyuki Watanabe¹⁾

1) Department of Radiology, Shiga University of Medical Science

2) Center for Clinical Research and Advanced Medicine, Shiga University of Medical Science

3) Division of Respiratory medicine, Department of Internal Medicine, Shiga University of Medical Science

4) Department of Respiratory medicine, Kohka Public Hospital

Purpose

To compare normal resolution scanning (NRS) and ultra-high-resolution scanning (UHRS) in the detection rates and the dimensional measurements accuracy compared with smart phone images as a reference standard (RS) of simulating peripheral air space (SPAS) on dynamic computed tomography (DCT)

Materials and methods

For 14 surface cross sections (SCS) in 6 cellulose sponge phantoms, 8 sets of images, a combination of 4 phases (from uncompressed to moderately- compressed), and 2 compression cycle durations (CCD): 4 and 5 seconds, were obtained based on DCT. In the 112 SCSs, following 3 items were compared between NRS and UHRS; 1) SPAS count on binarized images using the Moment function, 2) its association with compression rate of the sponge phantom with linear mixed model, and 3) measurement agreement against the RS for SPAS area by Bland-Altman plot.

Results

UHRS depicted more total SPAS for 4-second CCD as well as 5-second one (32.3) than NRS (14.2) ($p < 0.001$). The decrease ratio of SPAS in UHRS demonstrated stronger correlation with the compression rate as compared with NRS (0.43 in UHRS vs 0.22 in NRS) ($p = 0.004$). The measurement agreement in UHRS by an observer as well as another observer was closer to RS than that in NRS, as the bias and limit of agreement was 0.9 and -2.8 to 4.5 for UHRS, and 1.7 and -1.7 to 5.0 for NRS ($p < 0.05$).

Conclusion

DCT by UHRS demonstrated higher detection rate, stronger correlation to the compression rate, and higher accuracy in the SPAS dimensional measurement than that by NRS.

動態 CT における超高精細スキャンの有用性の実験的解析

上村 諒¹⁾, 永谷 幸裕¹⁾, 松林 純²⁾, 仲川 宏明³⁾, 福永 健太郎^{3,4)}, 角田 陽子³⁾, 中野 恭幸³⁾, 渡邊 嘉之¹⁾

1) 滋賀医科大学 放射線科

2) 滋賀医科大学 臨床研究開発センター

3) 滋賀医科大学 呼吸器内科

4) 公立甲賀病院 呼吸器内科

目的

動態 CT におけるスポンジファントム (SF) 内の末梢気腔構造 (SPAS) の描出能と、スマートフォン画像を参照基準 (RS) とした SPAS の面積測定誤差を超高精細スキャン (UHRS) と通常解像度スキャン (NRS) で比較するため

方法

動態 CT により、6つの SF の各 14 断面に対し、4 段階の圧縮率、2 種類の圧縮間隔 (4 秒と 5 秒) の 8 組の画像が UHRS と NRS で得られた。得られた 112 画像において、次の 2 種類の解析で UHRS と NRS を比較した。1) 2 値化処理を用いてサイズ分布別の SPAS の数を測定、圧縮率との線形混合モデルで解析した。2) RS に対する面積測定誤差を Bland-Altman 法で解析した。

結果

1) いずれの圧縮間隔においても、UHRS(32.3)の方がNRS(14.2)と比べて描出されるSPASの数が大きかった ($p < 0.001$)。また、SPAS数と圧縮率との相関関係はUHRS($r = 0.43$)において、NRS($r = 0.22$)と比べて強かった ($p = 0.004$)。2) 観察者による測定は別の観察者と同様にUHRSの方がNRSよりもRSと一致、bias, limit of agreementはそれぞれ、UHRSで0.9, -2.8から4.5、NRSで1.7, -1.7から5.0であった ($p < 0.05$)。

結論

UHRSによる動態CTは、NRSと比べ、多くのSPASを検出可能、SPAS数と圧縮率の相関関係が強く、面積測定はRSと良く一致した。

PJ4-5 Correlation between CT findings and pulmonary function parameters in NTM disease

Nobuyoshi Hamao, Isao Ito, Kensuke Nishioka, Masahiro Shirata, Issei Oi, Seiichiro Imai, Toyohiro Hirai

Department of Respiratory Medicine, Graduate School of Medicine, Kyoto University

Background: Nontuberculous mycobacterial pulmonary disease (NTM-PD) often exhibits pulmonary function impairment, such as obstructive or restrictive impairment, with variation among patients according to the damaged lesions in the lung.

Methods: Patients with NTM-PD were consecutively enrolled between September 2019 and December 2020 at the Respiratory Infection Clinic of our hospital. Patients' data were comprehensively collected through laboratory examinations, pulmonary function test, chest computed tomography, and questionnaires for the assessment of subjective symptoms and health-related quality of life.

Results: There were correlations between bronchiectasis score and FEV1/FVC, bronchiolitis score and FEF25-75%, and consolidation score and %DLCO.

Conclusion: In NTM-PD, pulmonary function parameters were useful to assess the degree of radiological findings quantitatively.

肺非結核性抗酸菌症における画像所見と呼吸機能検査の相関について

濱尾 信叔, 伊藤 功朗, 西岡 憲亮, 白田 全弘, 大井 一成, 今井 誠一郎, 平井 豊博
京都大学大学院医学研究科 呼吸器内科学

【背景・目的】肺非結核性抗酸菌症は細気管支炎や気管支拡張などさまざまな気道所見が認められる疾患である。肺非結核性抗酸菌症における呼吸機能検査所見が自覚症状やCT所見などどのように相関するかを検討した。【方法】2019年9月から2020年12月までに京都大学医学部附属病院に肺非結核性抗酸菌症で外来受診した104例を対象とした。それぞれの症例でCT、呼吸機能検査を実施し、問診票を用いて自覚症状や健康関連QOLについて調査した。画像所見は気管支拡張、細気管支炎、空洞、結節、浸潤影についてスコアリングを行い、各陰影と呼吸機能検査所見の相関を検討した。【結果】FEV1/FVCは気管支拡張スコアと正の相関を認め、FEF25-75%は細気管支炎スコアと、%DLcoは浸潤影スコアと負の相関を認めた。【考察】各陰影のスコアは特定の呼吸機能の項目との相関を認めていた。肺非結核性抗酸菌症における呼吸機能検査は、各病変の進行の程度を定量的に評価するのに有用であると考えられた。

Table 1. Spearman's rank correlation coefficient between CT score and other parameters

	Bronchiectasis		Bronchiolitis		Cavity		Nodules		Consolidation		Total score	
	p	P-value	p	P-value	p	P-value	p	P-value	p	P-value	p	P-value
BMI	-0.34	<0.001	-0.05	0.55	-0.16	0.11	0.08	0.43	-0.20	0.038	-0.24	0.013
VAS cough	0.35	<0.001	0.28	0.004	0.25	0.012	0.23	0.021	0.09	0.39	0.43	<0.001
VAS sputum	0.36	<0.001	0.21	0.029	0.10	0.33	0.24	0.013	0.15	0.14	0.34	<0.001
VAS difficulty of expectoration	0.22	0.028	0.20	0.040	0.05	0.64	0.24	0.015	-0.02	0.86	0.25	0.012
VAS hemoptysis	0.13	0.20	0.29	0.003	0.12	0.23	0.32	0.001	0.10	0.31	0.27	0.006
VAS fatigue	0.13	0.19	0.15	0.13	0.11	0.28	0.27	0.007	0.07	0.46	0.18	0.06
VAS fever	0.15	0.12	0.30	0.003	0.17	0.079	0.30	0.002	0.13	0.20	0.31	0.002

VAS dyspnea	0.15	0.13	0.24	0.014	0.20	0.045	0.29	0.003	0.01	0.92	0.29	0.003
VAS anorexia	0.13	0.18	0.08	0.43	0.10	0.29	0.16	0.11	0.16	0.11	0.19	0.056
mMRC	0.18	0.068	0.21	0.030	0.26	0.009	0.13	0.18	0.16	0.10	0.33	<0.001
Hb	-0.05	0.62	0.14	0.17	0.00	0.99	0.15	0.13	-0.29	0.002	0.01	0.93
WBC	0.19	0.051	0.23	0.018	0.11	0.26	0.14	0.15	-0.04	0.69	0.23	0.018
CRP	0.31	0.002	0.25	0.009	0.42	<0.001	0.14	0.16	0.19	0.053	0.47	<0.001
Total protein	0.16	0.09	0.27	0.006	0.18	0.072	0.07	0.51	-0.06	0.55	0.24	0.012
Albumin	-0.19	0.055	-0.20	0.037	-0.16	0.10	-0.01	0.90	-0.29	0.003	-0.29	0.003
%VC	-0.45	<0.001	-0.35	<0.001	-0.39	<0.001	-0.10	0.31	-0.29	0.003	-0.56	<0.001
%FVC	-0.46	<0.001	-0.34	<0.001	-0.32	<0.001	-0.08	0.45	-0.29	0.003	-0.52	<0.001
%FEV ₁	-0.25	0.012	-0.33	<0.001	-0.22	0.028	-0.13	0.17	-0.08	0.42	-0.34	<0.001
FEV ₁ /FVC	0.23	0.021	-0.13	0.18	0.16	0.11	-0.10	0.29	0.19	0.056	0.16	0.10

FEF _{25-75%}	0.08	0.43	-0.20	0.041	0.11	0.28	-0.08	0.43	0.08	0.45	0.05	0.62
%FRC	-0.17	0.083	-0.16	0.10	-0.26	0.008	-0.12	0.22	-0.00	0.99	-0.26	0.008
%RV	-0.07	0.47	-0.15	0.14	-0.13	0.20	-0.22	0.022	0.14	0.17	-0.13	0.19
%TLC	-0.41	<0.001	-0.33	<0.001	-0.33	<0.001	-0.19	0.051	-0.20	0.042	-0.50	<0.001
RV/TLC	0.35	<0.001	0.15	0.14	0.20	0.040	-0.12	0.24	0.35	<0.001	0.35	<0.001
%D _{CO}	-0.15	0.14	-0.09	0.36	-0.12	0.23	-0.00	0.99	-0.34	<0.001	-0.20	0.040
%D _{CO} /VA	0.19	0.060	0.17	0.08	0.12	0.24	0.12	0.22	-0.23	0.020	0.17	0.050

p, Spearman's rank correlation coefficient; BMI, body mass index; VAS, visual analog scale; Hb, hemoglobin; mMRC, modified British Medical Research Council; WBC, white blood cell; CRP, C-reactive protein; FEV₁, forced expiratory volume in one second; VC, vital capacity; FVC, forced vital capacity; FEF_{25-75%}, forced expiratory flow between 25% and 75% of vital capacity; FRC, functional residual capacity; RV, residual volume; TLC, total lung capacity; D_{CO}, diffusing capacity of lung for carbon monoxide; D_{CO}/VA, D_{CO} per unit of alveolar volume.

Nuclear/AI

PJ5-1 A case of Sjögren's syndrome in whom thymic MALT lymphoma was detected by gallium scintigraphy

Nanae Tsuchiya, Gyo Iida, Yukari Tomori, Akira Yogi, Akihiro Nishie
University of the Ryukyus

A woman in her 50s with a history of Sjögren's syndrome was referred to our hospital due to numbness in her extremities. She had lost weight (6 kg/6 months) and had increased erythrocyte sedimentation, and we suspected neuropathy associated with a tumor or inflammation, and imaging exams were performed. Contrast-enhanced CT showed a flat, contrast-enhanced soft tissue structure in the anterior mediastinum, and contrast-enhanced MRI showed microcystic structures and dot areas of reduced diffusion within the lesion. Although the size seem to be large for a thymus gland, the shape was maintained. Gallium scintigraphy showed accumulation to the anterior mediastinal lesion, and a malignant tumor including MALT lymphoma was strongly suspected. FDG-PET showed increased FDG uptake in the lesion (SUVmax 11.9). She underwent anterior mediastinal tumor resection using video-assisted thoracic surgery, and histological diagnosis was MALT lymphoma. MALT lymphoma is a low-grade B-cell lymphoma that occurs in mucous membranes and glandular tissues. It accounts for 7% to 9% of all malignant lymphomas and is more common in middle-aged women. Thymic MALT lymphoma is rare and associated with autoimmune diseases such as Sjögren's syndrome. When abnormal accumulation is found in the anterior mediastinum on gallium scintigraphy in patients with autoimmune diseases, thymic MALT lymphoma must be considered.

ガリウムシンチにて胸腺 MALT リンパ腫を指摘出来たシェーグレン症候群の一例

土屋 奈々絵, 飯田 行, 友利 由香理, 與 儀彰, 西江 昭弘
琉球大学病院放射線科

シェーグレン症候群の既往のある 50 代女性。四肢のしびれの精査目的に当院受診となった。半年で 6kg の体重減少、血沈亢進があり腫瘍や炎症に伴う神経障害を疑い、画像検査を行った。CT にて前縦隔に造影増強される扁平な軟部構造があり、MRI では病変内に小嚢胞構造と点状の拡散低下域を伴っていた。胸腺としてややサイズが大きい形態は保たれていた。ガリウムシンチでは前縦隔病変に一致して強い集積を認め、MALT リンパ腫を含む悪性腫瘍を強く疑った。FDG-PET でも SUVmax 11.9 と高集積を認めた。胸腔鏡下前縦隔腫瘍摘出術を施行され、組織学的にて MALT リンパ腫と診断された。MALT リンパ腫は粘膜、腺組織に発生する B 細胞系の低悪性度リンパ腫で、全悪性リンパ腫に占める割合は 7～9%、中年女性に好発する。胸腺発生は稀だが、シェーグレン症候群のような自己免疫性疾患との関連が報告されている。今回、ガリウムシンチにて胸腺 MALT リンパ腫を指摘出来たシェーグレン症候群の一例を経験した。自己免疫疾患症例のガリウムシンチにて前縦隔に異常集積が認められた場合、胸腺 MALT リンパ腫を考慮する必要がある。

PJ5-2 Effectiveness of prior PET/CT fusion imaging using CT-guided trans thoracic biopsy

Fumiyasu Tsushima, Sho Maruyama, Soichiro Tatsuo, Shinya Kakehata, Hiroyuki Miura,
Shingo Kakeda

Hirosaki University School of Medicine & Hospital

Purpose

To compare computed tomography (CT)-guided percutaneous biopsy with and without registration of prior positron emission tomography (PET)/CT images in the diagnosis of thoracic tumors.

Methods

We performed clinically indicated percutaneous biopsy in 11 patients with thoracic large (>6cm) tumors. The final diagnosis was based on pathological outcomes, or clinically findings and the results of at least 6-month follow-up. The patients underwent CT-guided percutaneous biopsy with prior PET/CT images obtained no more than 60 days earlier. The registered images were used to plan the procedure and help target the tumors. After biopsy, puncture points were classified as low (group 1, n=2) or high (group 2, n=9) on PET.

Results

CT-guided percutaneous needle biopsy yielded adequate samples in all patients. Diagnosis was confirmed by specific histomorphometry: no cancerous tissue was obtained in 1 of 2 patients in the PET low-intensity group (group 1, 1 of 2 patients; group 2, 9 of 9 patients).

Conclusion

CT-guided percutaneous biopsy is a simple and safe technique that provides an accurate diagnosis in the majority of thoracic tumors; PET/CT-guided biopsy may be a means to prevent biopsy failure.

胸部 CT ガイド下生検における術前 PET/CT の有用性

対馬 史泰, 丸山 翔, 辰尾 宗一郎, 掛端 伸也, 掛田 伸吾

弘前大学医学部放射線診断学講座

目的

CT ガイド下経皮生検における術前 FDG-PET/CT 画像の有用性とその条件について検討した。

方法

対象は術前の造影 CT、PET/CT が行われ、臨床的適応のある経皮的 CT ガイド下生検が実施された 11 例の大型 (>6cm) 胸部腫瘍患者。腫瘍サイズ、PET/CT を加えることによる穿刺部位変更の有無と実際の穿刺部位、病理結果を検討した。

結果

CT ガイド下経皮針生検により全例で検体が得られた。FDG 高集積部位が穿刺されたもの 9 例、低集積部位が穿刺されたもの 2 例で、うち 1 例は癌細胞が得られず、後に小細胞癌と診断された。造影 CT に PET/CT を加えることで穿刺部位が変更となる症例は 6 例あり、特に腫瘍径 8cm 以上の腫瘍は 4 例全例で変更となった。

結論

CT ガイド下経皮生検における術前 PET/CT はサイズの大きな腫瘍において有用な可能性がある。

PJ5-3 A Case of Pulmonary MALT Lymphoma that was Difficult to Differentiate from Inflammatory Changes

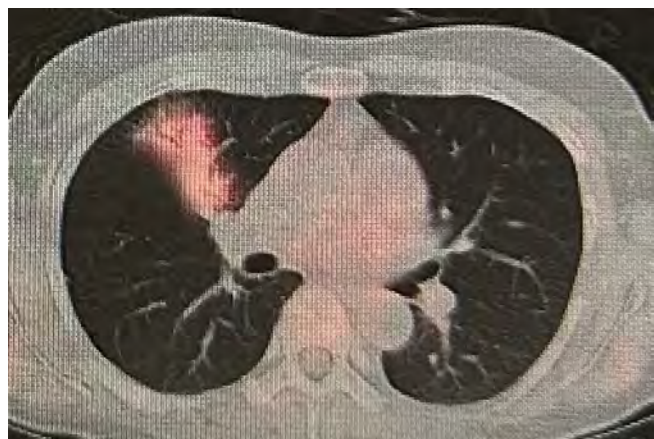
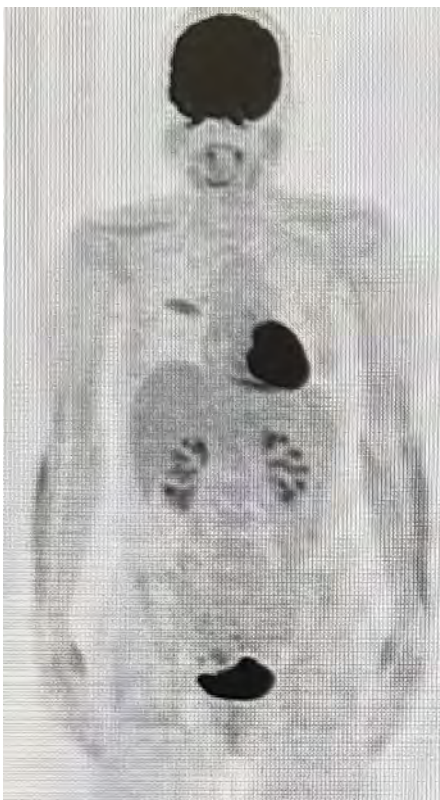
Tsuyoshi Komori, Hiroki Matsutani, Hiroshi Jyuri, Akira Higashiyama, Fumitoshi Aga, Fumihiko Soeda, Kazuhiro Yamamoto, Keigo Osuga
Osaka Medical and Pharmaceutical University

A tumor that differentiates into extranodal B cells from the marginal zone of reactively formed lymphoid follicles to the interfollicular region is called MALT lymphoma. MALT lymphoma is a low-grade B-cell lymphoma that occurs in mucosal and glandular tissues, found in the stomach and other parts of the gastrointestinal tract, lungs, thyroid, salivary glands, and lacrimal glands. A 40 years old woman who, during a routine chest X-ray, was found to have an abnormal shadow in the right hilar region. A chest CT suggested bronchopneumonia, but despite treatment and follow-up, the shadow did not disappear, raising suspicion of a malignant lesion. However, a bronchoscopy did not reveal any malignant findings. FDG-PET showed accumulation in the shadow, leading to a surgical biopsy, and pathological diagnosis confirmed pulmonary MALT lymphoma. Here, we report a case of pulmonary MALT lymphoma that was difficult to differentiate from inflammatory disease, along with a brief literature review.

FDG-PET で炎症性変化と鑑別困難であった肺 MALT リンパ腫の一例

小森 剛, 松谷 裕貴, 重里 寛, 東山 央, 安賀 文俊, 添田 文彦, 山本 和宏, 大須賀 慶悟
大阪医科薬科大学

反応性に形成されたリンパ濾胞の辺縁帯から濾胞間領域にかけて存在する節外性 B 細胞への分化を示す腫瘍を MALT リンパ腫という。MALT リンパ腫は、粘膜や腺組織に発生する低悪性度の B 細胞リンパ腫で、胃やその他の消化管、肺、甲状腺、唾液腺、涙腺などに認められる。症例は 40 歳代女性、定期検診の胸部レントゲンで、右肺門部に異常影を指摘され、胸部 CT で気管支肺炎を疑われ、加療および経過観察するも、陰影消失せず悪性病変が疑われるも、気管支鏡では悪性所見は認めなかった。FDG-PET で陰影に集積が見られたため、外科的生検を施行し、病理診断の結果、肺 MALT リンパ腫であった。今回、炎症性疾患との鑑別が困難であった肺 MALT リンパ腫の 1 例を経験したので、若干の文献的考察を加えて報告する。



PJ5-4 Automatic extraction of PA and PV in the mediastinum / pulmonary hilum from non-contrast 3DCT images

Manato Akatsuka¹⁾, Yoshiki Kawata²⁾, Seiyuu Ootani³⁾, Keiju Aokage³⁾, Noboru Niki⁴⁾

- 1) Graduate School of Integrated Science and Technology, Department of Engineering, University of Tokushima
2) Tokushima University Post-LED Photonics Research Institute
3) National Cancer Center Hospital East
4) Medical Science Research Institute Co., Ltd.

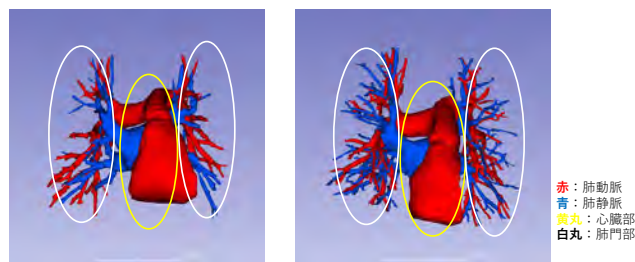
In clinical practice, there is a need to accurately extract pulmonary arteries and veins from non-contrast CT images. In particular, extracting these vessels near the pulmonary hilum is a difficult task. The objective of this study is to automatically extract pulmonary arteries and veins in the mediastinal and hilar regions from non-contrast 3D CT images with high accuracy. The extraction procedure is as follows: (1) Manually extract pulmonary arteries and veins at the pulmonary hilum and generate supervised data. (2) Create teacher data for 10 cases using 3D U-Net. (3) Manually modify the created teacher data and create teacher data for another 20 cases using 3D U-Net. (4) Repeat these steps to create highly accurate teacher data for a total of 40 cases. We also evaluated the teacher data and extraction results using the 10-Fold method. The evaluation results showed that the Dice coefficient was higher than 0.90, indicating that the extraction results using the teacher data created in this study were quite accurate, although there were some erroneous extractions. Future work will require the development of extraction methods with higher accuracy. Particular emphasis should be placed on methods that minimize false positives.

非造影 3 次元 CT 画像の縦隔部・肺門部の肺動脈・肺静脈の自動抽出

赤塚 真人¹⁾, 河田 佳樹²⁾, 大谷 正侑³⁾, 青景 圭樹³⁾, 仁木 登⁴⁾

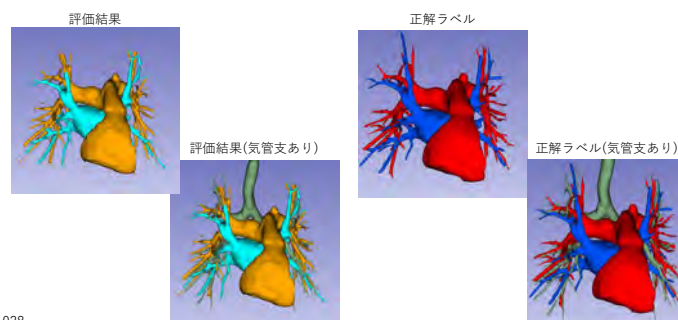
- 1) 徳島大学大学院 創成科学研究科 理工学専攻
2) 徳島大学 ポスト LED フォトニクス研究所
3) 国立がん研究センター東病院
4) 株式会社 医用科学研究所

臨床現場では、非造影 CT 画像から肺動脈と肺静脈を正確に抽出することが求められています。特に、肺門部付近のこれらの血管を抽出するのは難しい課題です。この研究の目的は、非造影 3 次元 CT 画像から縦隔部と肺門部の肺動脈と肺静脈を高い精度で自動的に抽出することです。抽出手順は以下のとおりです：(1) 肺門部での肺動脈と肺静脈を手動で抽出し、教師データを作成する。(2) 3D U-Net を使用して 10 症例の教師データを作成する。(3) 作成した教師データを手動で修正し、3D U-Net を用いてさらに 20 症例の教師データを作成する。(4) これらの手順を繰り返して、合計 40 症例の高精度な教師データを作成する。また、10-Fold 法を用いて教師データと抽出結果を評価しました。評価の結果、Dice 係数は 0.90 よりも高くなり、この研究で作成した教師データを用いた抽出結果は誤抽出があるものの、かなりの精度で抽出されていることが分かりました。今後は、より高い精度を持つ抽出手法を開発することが求められます。特に、誤抽出を最小限に抑える方法に重点を置く必要があります。



縦隔部・肺門部の肺動脈・肺静脈の抽出例

症例番号	027	028	031	038
Dice値	0.912	0.945	0.908	0.926



028

Sponsored Seminar

Luncheon Seminar 1 Sponsored by CANON MEDICAL SYSTEMS CORPORATION

August 23 (Fri) 11:20-12:20

State of the Art CT and MRI for Pulmonary Functional Imaging

Yoshiharu Ohno, M.D., Ph.D. ^{1,2)}

¹Department of Diagnostic Radiology, Fujita Health University School of Medicine, ²Joint Research Laboratory of Advanced Medical Imaging, Fujita Health University School of Medicine

Over the past few decades, pulmonary imaging technologies have advanced from chest radiography and nuclear medicine methods to CT and MRI. It is nowadays possible to identify and measure pulmonary pathologies before these are obvious even to patients or detected on conventional morphologic images. Key technological advances including multi-parametric CT image processing methods, inhaled hyperpolarized and fluorinated gas MRI as well as four-dimensional free-breathing CT and MRI methods have been suggested to measure ventilation and perfusion. While there remain some technical limitations and reimbursement and access issues, these technical advances are now ready for clinical use. Moreover, Canon Medical Systems Corporation is continuously providing new area-detector CTs (ADCTs), upright ADCT, new 1.5T and 3T MR systems with sophisticated MR sequences and image reconstructions as well as image analysis software for pulmonary functional imaging.

In this lecture, state of the art CT and MR techniques for pulmonary functional imaging are presented based on the following key issues: 1) new ADCT and MR systems provided by Canon Medical Systems, 2) techniques and derived functional biomarkers from ventilation, perfusion, gas exchange, and biomechanics imaging; and 3) recent clinical evidence by these techniques and systems in patients with various pulmonary diseases.

Luncheon Seminar 2

共催：アストラゼネカ株式会社

August 23 (Fri) 11:20-12:20

COPD と ACO ～最新のガイドライン・手引きを踏まえた治療介入

室 繁郎

奈良県立医科大学 呼吸器内科学講座 教授

健康日本 21（第 3 次）で COPD の死亡率減少が目標となり、そのために増悪抑制は重要な治療ターゲットである。長時間作用型吸入気管支拡張薬（LABDs）やそれらと吸入ステロイド製剤（ICS）との配合薬に増悪抑制の豊富なエビデンスがある。COPD（慢性閉塞性肺疾患）診断と治療のためのガイドライン第 6 版では頻回の増悪かつ末梢血好酸球増多（ $300/\mu\text{L}$ 以上）の場合において ICS/LAMA/LABA によるトリプル療法が推奨されている。一方、昨今のエビデンスの後解析等では増悪歴や末梢血好酸球増多が比較的軽微であってもトリプル療法の増悪抑制率等が報告されており、今後のトリプル療法の処方機会が増加していくかもしれない。また、ICS は喘息合併例（Asthma-COPD overlap: ACO）には併用必須であり、トリプル療法の位置付けが日本呼吸器学会の“ACO の手引き改訂版（2023）”で明確にされている。本講演では健康日本 21 の話題と上記二つのガイドライン・手引きをそれぞれ概説する。

■ Luncheon Seminar 3-1

Sponsored by Corelinesoft Co., Ltd.

August 24 (Sat) 12:00-13:00

Implementation of Artificial Intelligence in LDCT lung cancer screening - the HANSE Study

Jens Vogel-Claussen

Hannover Medical School

The radiologists in the HANSE Study are supported by state-of-the-art artificial intelligence (AI)-based lung nodule detection software (Coreline Soft, Seoul, South Korea) with automated volume analysis, integrated Lung-RADS 1.1 classification, volume doubling time (VDT) calculation, and nodule risk calculation using the PanCan (Brock University) nodule malignancy probability calculator (2b) for lung nodules. HANSE integrates cardiac calcium and pulmonary emphysema scoring in a holistic screening approach.

■ Luncheon Seminar 3-2

Sponsored by Corelinesoft Co., Ltd.

August 24 (Sat) 12:00-13:00

Role of artificial intelligence in the clinical practice of interstitial lung disease

Gong Yong Jin

Jeonbuk National University Medical School and Hospital

The efficacy of antifibrotic agents has been confirmed in several clinical trials for progressive fibrotic interstitial lung disease (ILD). The inclusion criteria for these trials included fibrosis greater than 10% on chest HRCT and an increase in the extent of fibrosis on HRCT over time, highlighting the importance of quantitative assessment of fibrosis on chest CT. Visual evaluation of HRCT has poor inter-reader consistency and limited sensitivity to changes in disease severity over time. To address this limitation, several technologies have emerged in recent years to quantify parenchymal lesions on chest HRCT using texture analysis or deep learning. These techniques are now being applied in clinical trials of novel antifibrotic agents. Additionally, AI-based quantitative CT technologies for ILD have been developed and are expected to be applied clinically to a wide variety of ILD cases. However, when using AI software, understanding the type of training data used to develop the technology is crucial. AI systems may be influenced by the specific physicians who provided the diagnoses included in the training data. Therefore, it's important to validate AI against different imaging conditions and patient populations. Although the currently developed AView by Coreline Software company has both advantages and disadvantages mentioned above, I would like to share my experiences in quantifying ILD using this program.

Luncheon Seminar 4

Sponsored by United Imaging Healthcare Japan K.K.

August 24 (Sat) 12:00-13:00

Advancing Pulmonary CT Imaging: AI Integration with the uCT 960+ System

Adam G. CHANDLER, Ph.D.

UIH America, Inc., Houston, TX, USA

AI-driven image reconstruction and post-processing are trending focuses in medical imaging, promising enhanced diagnostic accuracy and reduced radiation exposure, essential for widespread clinical adoption.

This presentation highlights the latest AI features and cutting-edge technologies integrated into United Imaging's family of Computer Tomography (CT) scanners, including our premium 16-cm system, the uCT 960+, designed for clinical and research pulmonary applications. Our solutions address current clinical challenges in CT imaging, offering optimized scanning workflows with intelligent patient positioning using our in-house developed uAI Vision 3D camera. AI-empowered scanning optimizes dose and scan ranges while maintaining peak image quality.

United Imaging's CT systems incorporate innovative detector materials for high resolution and ultra-low noise, as well as our next-generation image reconstruction technique, AI-IR.

This world's first combined AI and model-based iterative reconstruction technique allows for high-quality CT images at previously unattainable dose levels.

Our suite of AI-enabled thoracic post-processing applications is fully optimized for accurate detection of pulmonary diseases, including nodule detection, malignancy prediction, pneumonia identification, quantitative analysis, and lymph node detection. These features facilitate robust follow-up evaluations and intelligent follow-up mechanisms.

By providing comprehensive CT solutions, we open the door to unique thoracic applications, including ultra-low dose lung screening protocols, free-breathing thoracic scanning, and one-click disease detection and follow-up determination.

United Imaging's advancements ensure our CT systems excel in both clinical and research settings, addressing the evolving needs of medical imaging practices.

Luncheon Seminar 5

共催：サノフィ株式会社 / リジェネロン・ジャパン株式会社

August 25 (Sun) 12:00-13:00

多角的に捉える閉塞性肺疾患の治療

福永 興壱

慶應義塾大学医学部 呼吸器内科 教授

喘息は吸入ステロイドを中心とした抗喘息薬の普及により年間死亡者数は明らかに減少の一途をたどり、多くの患者のコントロールは良好となった。しかし、臨床において治療反応性が得られない難治性喘息がいまだ存在する。一方で、そのような難治性喘息に大きなパラダイムシフトをもたらした薬剤が生物学的製剤である。わが国では2009年のIgE抗体を皮切りに、IL-5抗体、IL-5受容体 α 抗体、IL-4/IL-13受容体抗体、そして最近ではTSLP抗体と次々に生物学的製剤が上市され、その治療効果のエビデンスが蓄積されつつある。これらの生物学的製剤の使い分けは、好酸球、IgE、FeNOといったタイプ2バイオマーカーを用いて検討されているが、明確な基準はいまだなく、患者さんにとっての適切な薬剤選択のためにより多くの情報が今後必要と考える。本講演では難治性喘息を中心に閉塞性肺疾患の病態を多角的な視点でとらえた今後の治療戦略について概説したいと思う。

Morning Seminar

共催：日本ベーリンガーインゲルハイム株式会社

August 25 (Sun) 8:00-9:00

間質性肺疾患診療における AI 応用の現状と可能性

半田 知宏

京都大学大学院医学研究科 呼吸不全先進医療講座

インターネットの普及や深層学習技術の開発によって人工知能の技術革新が進み、近年では大規模言語モデルの開発と生成 AI の実用化を伴って、人工知能は社会に大きな変革をもたらしている。間質性肺疾患の領域においても、画像解析や組織診断などの分野で AI の臨床応用が進んでおり、近年では AI 技術を用いた in silico の創薬も実用化されている。進行性の肺線維症における抗線維化薬の有効性が示され、肺の炎症や線維化を定量化する技術が求められており、AI 技術を用いた定量的画像解析ソフトウェアへの期待も大きい。本講演では、間質性肺疾患診療における AI 応用の現状と、AI を用いた定量的ソフトウェアの応用例を示し、間質性肺疾患診療における AI の展望や課題についても触れたい。

We thank the following companies for their valuable support of Joint Meeting of JSPFI and IWPF1 2024

Subsidies

Shiga Prefecture

Otsu City

General Foundation WAJINKAI

Takateru Izumi Commemorative Subsidy of Kyoto Health Management Research Foundation

Sponsors

The Federation of Pharmaceutical Manufacturers' Associations of JAPAN

Asahi Kasei Pharma Corporation

AstraZeneca K.K.

Bayer Yakuhin, Ltd

CANON MEDICAL SYSTEMS CORPORATION

CHEST M.I., INC.

Chugai Pharmaceutical Co., Ltd.

Corelinesoft Co., Ltd.

DAIICHI SANKYO COMPANY, LIMITED

ELI LILLY JAPAN K.K.

Fuji Pharma Co., Ltd.

FUJIFILM Medical Co., Ltd.

FUKUDA LIFETECH KEIJI CO., LTD.

GlaxoSmithKline K.K.

Insmmed GK

Kracie Pharmaceutical, Ltd

KYORIN Pharmaceutical Co., Ltd.

Merck Biopharma Co., Ltd.

Moderna Japan Co., Ltd.

MSD K.K.

Nihon Medi-Physics Co., Ltd.

Nippon Boehringer Ingelheim Co., Ltd.

NIPPON KAYAKU Co., Ltd.

NIPRO CORPORATION

NOVARTIS PHARMA K.K.

PDRadiopharma Inc.

Philips Japan, Ltd.

Regeneron Japan KK

Sanofi K.K.

Shionogi & Co., Ltd.

TAIHO PHARMACEUTICAL CO., LTD.

TSUMURA & CO.

United Imaging Healthcare Japan K.K.

Ziosoft, Inc.

(alphabetical order)

Kyorin 



薬価基準収載

選択的P2X3受容体拮抗薬/咳嗽治療薬



リフヌア[®]錠45mg

LYFNUA[®] Tablets 45mg

ゲーファピキサントクエン酸塩錠

処方箋医薬品（注意－医師等の処方箋により使用すること）

効能又は効果、用法及び用量、禁忌を含む注意事項等情報等については電子添文をご参照ください。

発売元

杏林製薬株式会社

東京都千代田区大手町一丁目3番7号

〈文献請求先及び問い合わせ先：くすり情報センター〉

東京都新宿区左門町20番地

製造販売元

MSD株式会社

東京都千代田区九段北1-13-12

作成年月:2024.5



あしたの感染症と、 たたかっている。

感染症がこの世からなくなることはない。
パンデミックも、きっとまた起こる。
だからこそ、SHIONOGIは逃げずに向き合い続けます。
その時私たちの創るワクチンが、治療薬が、
強く、強く、ひとつでも多くのいのちを守れるように。
薬ができることの、その先へ。



insmed®



アミノグリコシド系抗生物質製剤

薬価基準収載



アリケイス® 吸入液 590mg

ARIKAYCE®

アミカシン硫酸塩 吸入用製剤

処方箋医薬品[※]

注) 注意 - 医師等の処方箋により使用すること

効能又は効果、用法及び用量、禁忌を含む使用上の注意等については電子化された添付文書をご参照ください。

製造販売元

インスメッド合同会社
東京都千代田区永田町二丁目10番3号
東急キャピトルタワー13階

<https://insmed.jp>

〔文献請求先及び問い合わせ先〕
メディカルインフォメーションセンター
電話：0120-118808

insmed®, insmed logo, インスメッド®, ARIKAYCE® and アリケイス® are registered trademarks of insmed Incorporated.

All other trademarks referenced herein are the property of their respective owners.

2023年7月作成

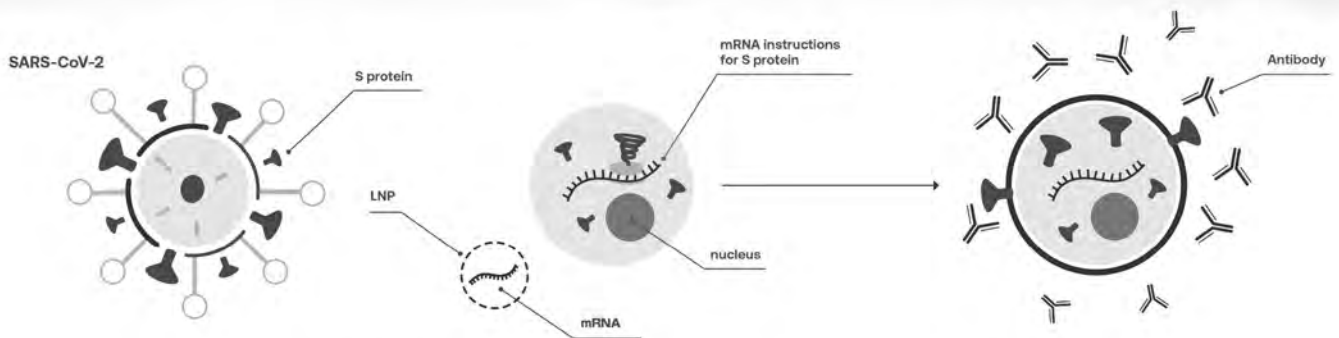
PP-ARIK-JP-00697

© 2023 Insmed GK. All Rights Reserved.

© 2023 PARI GmbH. All Rights Reserved.

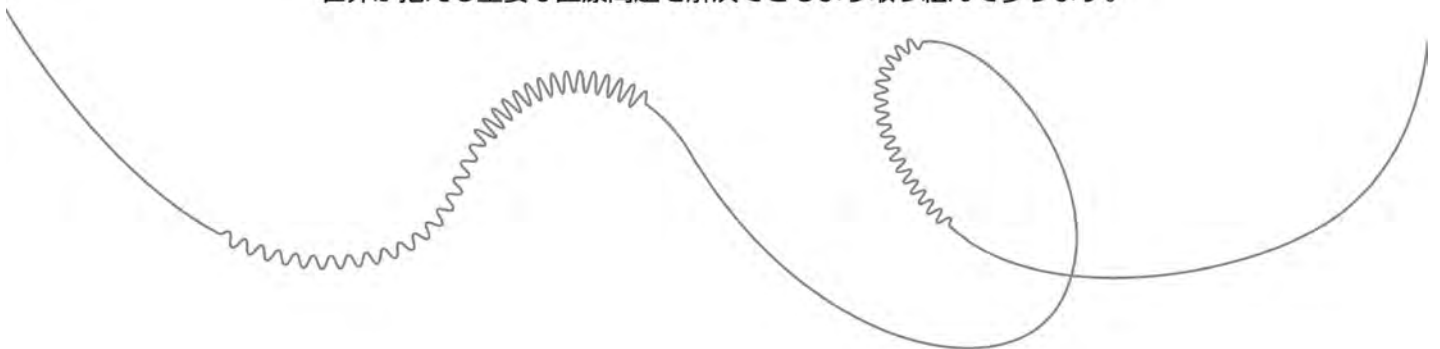
moderna®

this changes everything



**モデルナは、患者さんのために革新的な次世代型の新薬を生み出し、
mRNAサイエンスの約束を果たします。**

私たちの mRNA プラットフォームによって、何百万人もの人々を苦しめる疾患から、
数十人を苦しめる超希少疾患まで、そして個人レベルの疾患まで、
世界が抱える重要な医療問題を解決できるよう取り組んで参ります。





非イオン性尿路・血管造影剤

イオプロミド 300注 20mL・50mL・100mL 370注 20mL・50mL・100mL 300注シリンジ 50mL・80mL・100mL 「BYL」 370注シリンジ 50mL・80mL・100mL

処方箋医薬品（注意—医師等の処方箋により使用すること） **薬価基準収載**

※ 効能又は効果、用法及び用量、警告、禁忌、原則禁忌を含む使用上の注意につきましては、
製品添付文書をご参照ください。



Bayer

製造販売元【文献請求先及び問い合わせ先】

バイエル薬品株式会社

大阪市北区梅田2-4-9 〒530-0001

<https://pharma.bayer.jp>

【コンタクトセンター】

0120-106-398

<受付時間> 9:00～17:30（土日祝日・当社休日を除く）

Clear Direction. ➤ From Diagnosis to Care.

Iopromide「BYL」

会員制
画像診断情報サイト

ラジサポ「F」

Radiology support website by Fuji Pharma

ご登録およびすべてのコンテンツのご利用は無料です。



https://www.fuji-pharma.jp/contents_user/auth/login



イオパミドール注「F」

非イオン性尿路・血管造影剤 イオパミドール注射液
処方箋医薬品^{注)} 薬価基準収載

イオパミドール150注「F」
50mL/200mL

イオパミドール300注「F」
20mL/50mL/100mL

イオパミドール370注「F」
20mL/50mL/100mL

イオパミドール300注シリンジ「F」
50mL/80mL/100mL/150mL

イオパミドール370注シリンジ「F」
50mL/65mL/80mL/100mL



イオヘキソール注「F」

非イオン性造影剤 イオヘキソール注射液
処方箋医薬品^{注)} 薬価基準収載

イオヘキソール300注「F」
20mL/50mL/100mL

イオヘキソール350注「F」
20mL/50mL/100mL

イオヘキソール240注シリンジ「F」
100mL

イオヘキソール300注シリンジ「F」
50mL/80mL/100mL/110mL/125mL/150mL

イオヘキソール350注シリンジ「F」
70mL/100mL

注)：注意—医師等の処方箋により使用すること。

■効能・効果、用法・用量、警告・禁忌を含む使用上の注意等につきましては添付文書をご参照ください。

製造販売元
(資料請求先)



富士製薬工業株式会社

〒939-3515 富山県富山市水橋辻ヶ堂1515番地
<https://www.fujipharma.jp/>

Smart Imaging

“みる”をシンプル、スマートに。

独自の技術性能 Revorability で
より高度な認識、解析、描写を実現する REVORAS。
高機能・高性能でありながらシンプルな操作性で
驚異的なイメージングを可能にします。

 Revorability



イメージングインテリジェンス / ziostation
REVORAS

一般的名称：汎用画像診断装置ワークステーション 販売名：ザイオステーション レヴォラス R L 認証番号 304ABBZX00001000

 ziosoft ザイオソフト株式会社

〒108-0073 東京都港区三田一丁目4番28号 三田国際ビル
Tel:03-5427-1903 Fax:03-5427-1907
www.zio.co.jp



www.zio.co.jp/revoras

ADJP-2165



世界中の人々の
健康で豊かな生活に貢献する

イノベーションに情熱を。ひとに思いやりを。



Daiichi-Sankyo

第一三共株式会社

お客様の声をカタチにして、モストグラフ®が待望のアップデート!
3Dカラーグラフィックの見やすさと、
使いやすさを追求しました。

総合呼吸抵抗測定装置

MostGraph®-03

- 23インチワイド液晶モニターで3Dカラーグラフィック波形や数値を表示
- 2Dカラーグラフ、3Dカラーグラフィックを組み合わせた7パターンの画面表示
- 測定値の時系列グラフ、3Dカラーグラフィックの時系列表示・印刷*
- 小児測定に対応した3Dカラーグラフィックのキッズスケール
- キャリブレーションチェック履歴表示、精度管理レポート印刷*
- 測定補助アニメーションなどを採用したスパイロメトリ機能(オプション)

*印刷するにはオプションのプリンタセットが必要です。



一般名称:呼吸機能測定装置
管理医療機器:特定保守管理医療機器
認証番号:304ALBZX00022000

先進の医療機器で健やかな呼吸をサポート

本社/〒113-0033 東京都文京区本郷3-25-11

TEL.(03) 3813-7200 (代)

大阪営業所/〒537-0022 大阪府大阪市東成区中本2-11-5 森之宮シルクビル4F TEL.(06) 6975-7071 (代)

CHEST チェスト 株式会社

ホームページ <https://www.chest-mi.co.jp>

営業所 / 札幌・秋田・仙台・新潟・さいたま・東京・西東京・横浜・名古屋・金沢・大阪・広島・松山・福岡・大分



生薬には、
個性がある。

漢方製剤にとって「良質」とは何か。その答えのひとつが「均質」である、とツムラは考えます。自然由来がゆえに、ひとつひとつに個性がある生薬。漢方製剤にとって、その成分のばらつきを抑え、一定に保つことが「良質」である。そう考える私たちは、栽培から製造にいたるすべてのプロセスで、自然由来の成分のばらつきを抑える技術を追求。これからもあるべき「ツムラ品質」を進化させ続けます。現代を生きる人々の健やかな毎日のために。自然と健康を科学する、漢方のツムラです。

良質。均質。ツムラ品質。



株式会社ツムラ <https://www.tsumura.co.jp/> 資料請求・お問合せは、お客様相談窓口まで。
医療関係者の皆様 tel.0120-329-970 患者様・一般のお客様 tel.0120-329-930 受付時間 9:00~17:30(土・日・祝日は除く)

2021年4月制作 (審)



薬価基準収載



ドライパウダー吸入式喘息・COPD治療配合剤 処方箋医薬品^注

ブデソニド・ホルモテロールフマル酸塩水和物吸入剤

ブデホル[®]吸入粉末剤30吸入・60吸入「ニプロ」

(先発・代表薬剤：シムビコートタービュヘイラー30吸入・60吸入)

^注 注意—医師等の処方箋により使用すること [®]:登録商標

●「効能・効果」、「用法・用量」、「禁忌」を含む注意事項等情報等の詳細は、電子添文をご参照ください。

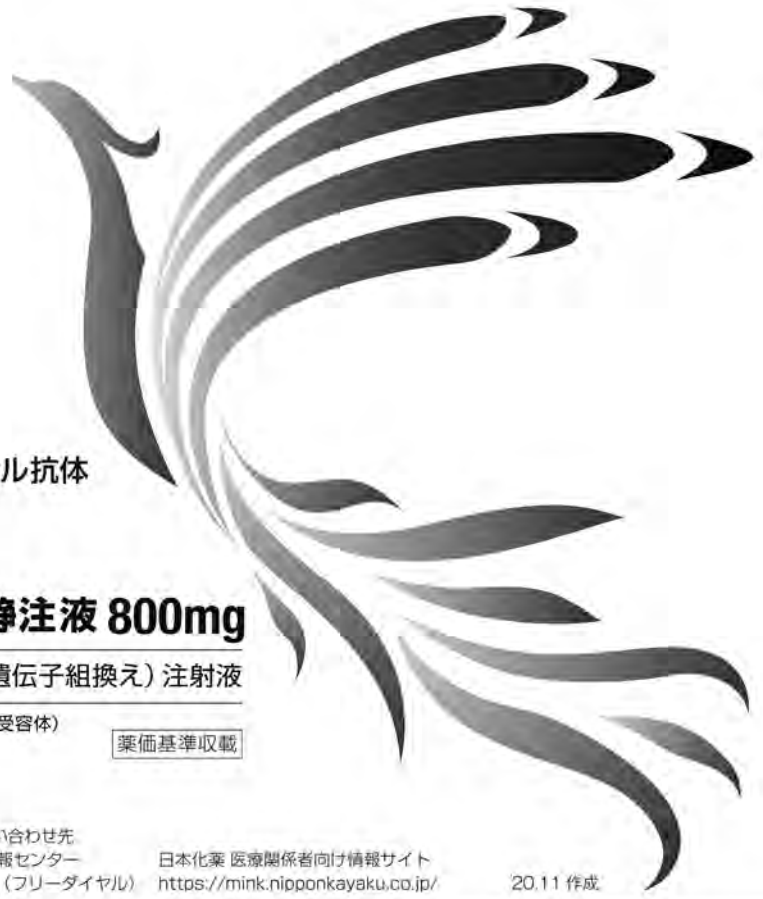
製造販売元
(資料請求先)

ニプロ株式会社

大阪府摂津市千里丘新町3番26号
<https://www.nipro.co.jp/>

医薬品についてのお問い合わせ(医薬品情報室)
0120-226-898 FAX 050-3535-8939

2024年3月作成 (KI)
【審2403257811】



抗悪性腫瘍剤 ヒト型抗EGFR^注モノクローナル抗体
生物由来製品、劇薬、処方箋医薬品*

ポトラザ[®]点滴静注液 800mg

Portrazza[®] Injection ネシツムマブ (遺伝子組換え) 注射液

注) EGFR: Epidermal Growth Factor Receptor (上皮細胞増殖因子受容体)
*注意—医師等の処方箋により使用すること

薬価基準収載

製造販売元  **日本化薬株式会社**
東京都千代田区丸の内二丁目1番1号

文献請求先及び問い合わせ先
日本化薬 医薬品情報センター
0120-505-282 (フリーダイヤル)

日本化薬 医療関係者向け情報サイト
<https://mink.nipponkayaku.co.jp/>

20.11 作成

※効能又は効果、用法及び用量、警告・禁忌を含む使用上の注意等については、添付文書をご参照ください。



CURIOSITY 発見はいつも 好奇心から。

メルクバイオフーマ株式会社

〒153-8926 東京都目黒区下目黒 1-8-1 アルコタワー 4F
www.merckgroup.com/jp-ja

MERCK

いつもを、いつまでも。

あたり前のようにつづく毎日ほど、

かけがえのないものはない。

私たちは、“いつも”を支える力になりたい。

大切な“いつも”が失われた時、

強く取り戻す力を届けたい。

いつもを、いつまでも。

私たち大鵬薬品ひとりひとりの願いです。

 大鵬薬品



AsahiKASEI

Creating for Tomorrow



旭化成ファーマ株式会社



がんに勝ちたい、もっと。



家族と一緒にいたい、もっと。



患者さんを笑顔にしたい、もっと。



革新的な薬を届けたい、もっと。



がんと向き合う
一人ひとりの想いに
応えたい。

私たちMSDは、革新的ながん治療薬を
開発する情熱を抱き、
一人でも多くの患者さんに
届けるという責任をもって
がん治療への挑戦を続けています。

WINNING
MORE
AGAINST
CANCER

MSD株式会社

〒102-8567 東京都千代田区九段北 1-13-12 北の丸スクエア
<http://www.msd.co.jp/>



RetevmoTM
selpercatinib

抗悪性腫瘍剤 / RET[®] 受容体型チロシンキナーゼ阻害剤
腫瘍、がん治療薬

レットガイモ[®] カプセル40mg
カプセル80mg
セルベルカチニブカプセル

※ RET (rearranged anaplastic lymphoma kinase) 阻害剤として承認された最初の薬剤

CYRAMZA[®]
(ramucirumab)

抗悪性腫瘍剤 ヒト型抗VEGFR-2[®]モノクローナル抗体
生物由来製品、腫瘍、がん治療薬

サイラムザ[®] 点滴静注液 100mg
点滴静注液 500mg

CYRAMZA[®] Intravenous Injection ラムシルマブ(遺伝子組換え)注射液

※ VEGFR-2 (Vascular Endothelial Growth Factor Receptor-2) 阻害剤として承認された最初の薬剤
* 腫瘍-血管新生の抑制により効果を発揮する

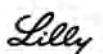
効能又は効果、用法及び用量、警告・禁忌を含む注意事項等情報等については電子添文をご参照ください。

製造販売元 (文献請求先及び問い合わせ先)
日本イーライリリー株式会社
〒651-0086 神戸市中央区福上通5丁目1番28号

Lilly Answers リリーアンサーズ (医療関係者向け)
日本イーライリリー 医薬情報問合せ窓口
www.lillymedical.jp

0120-360-605^{※1}
受付時間 月曜日～金曜日 9:45～17:30^{※2}
※1 通話料は別件です。携帯電話からのご利用はできません。
※2 中国語・英語・フランス語・ドイツ語で対応できる場合があります。
※3 転送は47日以内に行われます。

PP-SE-JP-1083
2024年4月作成



Reimagining Medicine

医薬の未来を描く

NOVARTIS



抗悪性腫瘍剤 / 抗PD-L1^{注1}ヒト化モノクローナル抗体

生物由来製剤、創薬、処方箋医薬品^{注2}

テセントリク 点滴静注 1200mg

TECENTRIQ

【薬価標準収載】

アテゾリズマブ (遺伝子組換え) 注
※: ノブアソラ ロソサドビル (L) 製剤

抗悪性腫瘍剤 抗VEGF^{注2}ヒト化モノクローナル抗体

生物由来製剤、創薬、処方箋医薬品^{注3}

アバスタン 点滴静注用 100mg/4mL
400mg/16mL

AVASTIN

【薬価標準収載】

パニツマブ (遺伝子組換え) 注

抗悪性腫瘍剤 / ALK^{注3}阻害剤

創薬、処方箋医薬品^{注4}

アレセンサ カプセル 150mg

ALECENSA アレクシニブ塩酸塩カプセル

【薬価標準収載】

アレクシニブ塩酸塩カプセル

抗悪性腫瘍剤

上皮増殖因子受容体 (EGFR) チロシンキナーゼ阻害剤

創薬、処方箋医薬品^{注5}

タルセバ錠 25mg
100mg
150mg

Tarceva

エリロシニブ塩酸塩

注1) PD-L1: Programmed Death-Ligand 1 注2) VEGF: Vascular Endothelial Growth Factor (血管内皮増殖因子)
注3) ALK: Anaplastic Lymphoma Kinase (未分化リンパ腫キナーゼ) 注4) ※: 注意-医師等の処方箋により使用すること

「効能又は効果、用法及び用量、警告・禁忌を含む注意事項等情報」等については、電子化された添付文書をご参照ください。

製造販売元



中外製薬株式会社

〒103-8324 東京都中央区日本橋室町2-1-1

【文献請求先及び問い合わせ先】 メディカルインフォメーション部
TEL.0120-189-706 FAX.0120-189-705

【販売情報提供活動に関する問い合わせ先】
<https://www.chugai-pharm.co.jp/guideline/>

Roche ロシュ グループ

2024年4月作成

Kracie

twice or three times a day 選べるやさしさ



スティックで、健やかな暮らしへ

クラシエ 薬品株式会社

【資料請求先】 〒108-8080 東京都港区海岸3-20-20

医療用医薬品ウェブサイト 「漢・方・優・美」 <http://www.kampoyubi.jp>

■各製品の「効能・効果」、「用法・用量」、「使用上の注意」等については製品添付文書をご参照ください。

Canon

私たちは、 「いのち」から 始まる。

激動する世界で「いのち」の輝きこそが未来への
希望であり、前へ進む力であると

キヤノンメディカルシステムズは信じています。

医療機器メーカーである私たちの使命は、
尊い「いのち」を守る医療への貢献。

創業以来、つねに医療関係者の方々と手を携え、
数々の技術開発に挑んできました。その想いは、
経営スローガン「Made for Life」として、
世界中の社員一人ひとりの胸に変わることなく
息づいています。

医療の現場を全力で支え、
健康と「いのち」を守る臨床価値を創出するために。
私たちはこれからも“いま”を拓き続けてまいります。

患者さんのために、
あなたのために、
そして、
ともに歩むために。

Made For life



GSK



3成分配合 喘息・COPD治療剤 薬価基準収載

処方箋医薬品(注意-医師等の処方箋により使用すること)

テリルジー 100エリプタ
14・30吸入用

TRELEGY ELLIPTA

フルチカゾンフランカルボン酸エステル・
ウメクリジニウム臭化物・ピランテロール
トリフェニル酢酸塩ドライパウダーインヘラー



3成分配合 喘息治療剤 薬価基準収載

処方箋医薬品(注意-医師等の処方箋により使用すること)

テリルジー 200エリプタ
14・30吸入用

TRELEGY ELLIPTA

フルチカゾンフランカルボン酸エステル・
ウメクリジニウム臭化物・ピランテロール
トリフェニル酢酸塩ドライパウダーインヘラー

※「効能又は効果」、「用法及び用量」、「禁忌を含む注意事項等情報」等については電子添文をご参照ください。

専用アプリ「添文ナビ」で
GS1バーコードを読み取ることで、
最新の電子添文等を閲覧できます。



(01)14987246783023

(テリルジー100エリプタ14・30吸入用、
テリルジー200エリプタ14・30吸入用)

製造販売元

グラクソ・スミスクライン株式会社

〒107-0052 東京都港区赤坂1-8-1

文献請求先及び問い合わせ先

TEL:0120-561-007(9:00~17:45/土日祝日及び当社休業日を除く)

FAX:0120-561-047(24時間受付)

PM-JP-FVU-ADVT-210001

改訂年月2023年9月(MK)